Characterising human gametogenesis arrest from gene to protein

Marie Christou-Kent

Communauté
UNIVERSITÉ Grenoble Alpes

THÈSE

Pour obtenir le grade de

DOCTEUR DE LA COMMUNAUTE UNIVERSITE GRENOBLE ALPES

Spécialité : **BIOLOGIE DU DEVELOPPEMENT/ONCOGENESE**

Arrêté ministériel : 25 mai 2016

Présentée par

Marie CHRISTOU-KENT

Thèse dirigée par **Christophe ARNOULT,** DR, IAB/UGA

préparée au sein du **Laboratoire GETI**
« Génétique, Epigénétique et Thérapies de l'Infertilité »
Institut pour l'Avancée des Biosciences
dans **l'École Doctorale Chimie et Sciences du Vivant**

Caractérisation de l'arrêt de la gamétogenèse chez l'homme du gène à la protéine

Thèse soutenue publiquement le **« 21 Novembre 2019 »**,
devant le jury composé de :

Pr. Pierre RAY
Professeur des Universités, UGA/IAB, Président

Dr. Véronique DURANTHON
Directeur de Recherche INRA, Jouy en Josas, Rapporteur

Dr. Dominique WEIL
Directeur de Recherche CNRS, Sorbonne Université, Rapporteur

Dr. Marie-Hélène VERLHAC
Directeur de Recherche CNRS, Collège de France, CIRB, Examinateur

Dr. Rémi DUMOLLARD
Chargé de Recherche CNRS, UPMC, Station Marine de Villefranche-sur-Mer, Examinateur

Dr. Christophe ARNOULT
Directeur de Recherche, UGA/IAB, Directeur de Thèse

Title

Characterising human gametogenesis arrest from gene to protein

Abstract

Infertility is considered a global public health issue since it affects more than 50 million couples worldwide. Current assisted reproductive technologies (ARTs) have minimal requirements for gametes that are competent for fertilisation and subsequent embryo development. In cases where genetic abnormalities lead to arrested gametogenesis and the production of immature, defective or degraded gametes, treatment is not usually possible. Identifying the molecular causes of these types of infertility is crucial for developing new strategies to treat affected couples. Moreover, these patients represent a unique opportunity to discover new actors of oogenesis and spermatogenesis and to decipher the molecular pathways involved in the production of competent gametes.

Genetic analysis of cohorts of infertile patients with shared ancestry can allow the identification of inherited genetic variants as possible causal factors. Using whole exome sequencing, we identified a homozygous pathogenic variant of the gene PATL2 in a cohort of patients with a phenotype of arrested oogenesis due to Oocyte Maturation Deficiency (OMD). OMD is a rare pathology characterised by the recurrent ovulation of immature oocytes. PATL2 encodes an oocyte ribonucleoprotein whose amphibian orthologue had been shown to be involved in oocyte translational control and whose function in mammals was poorly characterised. We also identified a pathogenic variant of the gene SPINK2 in a familial case of azoospermia. SPINK2 encodes a serine protease inhibitor thought to inhibit acrosin activity during sperm acrosome formation.

We showed, through generation of Patl2 and Spink2 knockout (KO) mice and Patl2 tagged mice (the latter using CRISPR-Cas9), that both corresponding proteins play essential respective roles in gametogenesis. We demonstrated that Patl2 is strongly expressed in growing mouse oocytes and that its absence leads to the dysregulation of numerous transcripts necessary for oocyte growth, meiotic maturation and preimplantation embryo development. This was accompanied by a phenotype of subfertility in KO females in natural mating, a large proportion of ovulated oocytes lacking a polar body (immature) and/or displaying spindle assembly defects in

immunostaining, and a high rate of oocytes with an aberrant response to fertilisation in IVF experiments. In Spink2 KO mice, we demonstrated that absence of Spink2 protein, which is located in the acrosome of maturing and mature spermatozoa, leads to azoospermia with arrested spermiogenesis and autophagy at the round-spermatid stage. This is plausibly due to aberrant acrosin activity in the absence of its inhibitor, corroborated by fragmentation and displacement of the Golgi apparatus and absence of the acrosome as shown through immunostaining.

We have thus characterised two genetic subtypes of human infertility associated with mutation of these two genes. In doing so, we have furthered our understanding of the respective roles of these crucial actors of mammalian gametogenesis, potentially paving the way for improvement of current ARTs and development of new, personalised therapies.

Titre

Caractérisation de l'arrêt de la gamétogenèse chez l'homme du gène à la protéine

Résumé

L'infertilité est considérée comme une préoccupation majeure de santé, touchant à plus de 50 millions de couples mondialement. Les techniques actuelles d'Assistance Médicale à la Procréation (AMP) ont comme prérequis des gamètes aptes à la fécondation et au développement embryonnaire. Dans les rares cas où des anomalies génétiques mènent à un arrêt de la gamétogenèse et donc à la production de gamètes immatures, défectueux ou dégradés, un traitement n'est pas possible. Afin d'envisager de nouvelles stratégies de traitement, il est nécessaire de comprendre les bases moléculaires de ce type d'infertilité. De plus, ces patients représentent une opportunité unique nous permettant de découvrir de nouveaux acteurs de l'ovogenèse et de la spermatogenèse ainsi que de déchiffrer les voies moléculaires impliquées dans la production de gamètes compétentes.

L'analyse génétique de cohortes de patients consanguins peut permettre l'identification de variantes génétiques héritées comme causes possibles de la pathologie. Nous avons identifié, par séquençage exomique, un variant pathogène du gène PATL2 dans les patientes atteintes d'un échec de maturation ovocytaire. Cette pathologie, que nous avons appelé la Déficience Méiotique Ovocytaire (DMO), consiste en l'ovulation récurrent d'ovocytes immatures et non-fécondables. Le gène PATL2 code une ribonucléoprotéine ovocytaire qui a été impliqué dans la régulation de la traduction des ARNm maternelles chez l'amphibien. Sa fonction chez les mammifères était jusqu'à présent mal caractérisé. Nous avons aussi identifié un variant pathogène du gène SPINK2, codant un inhibiteur de protéases qui est important pour la neutralisation de l'acrosine pendant le développement de l'acrosome.

Par la génération de lignées de souris déficientes (KO) pour les gènes Patl2 et Spink2, et d'une lignée PATL2 « étiquetée » par la méthode CRISPR-Cas9, nous avons montrés que les deux protéines correspondantes jouent des rôles indispensables dans leurs gamétogénèses respectives. Nous avons démontré que Patl2 est fortement exprimé dans l'ovocyte murin en cours de croissance, et que son absence entraîne une dérégulation de nombreux transcrits essentiels pendant la phase de croissance, de maturation méiotique ou de développement pré-

implantatoire. Les femelles PATL2 KO sont sous-fertiles par accouplement naturel, et lors de la stimulation hormonale produisent une grande proportion d'ovocytes sans globule polaire (immatures) et/ou avec des défauts au niveau du fuseau méiotique, mis en évidence par immunomarquage. De plus, suite à la fécondation in vitro, un grand nombre d'ovocytes PATL2 KO ont répondu de manière aberrante à la fécondation. Concernant les mâles SPINK2 KO, nous avons montré que l'absence de la protéine SPINK2, qui se localise dans l'acrosome, entraîne une azoospermie avec un arrêt de la spermiogenèse et une autophagie au stade spermatide-ronde. Cet effet est vraisemblablement dû à une activité aberrante de l'acrosine en absence de son inhibiteur, une hypothèse soutenue par la fragmentation de l'appareil de Golgi et l'absence de l'acrosome, événements observés par immunofluorescence.

Nous avons, donc, caractérisé deux sous-types génétiques d'infertilité humaine associés à la mutation de ces deux gènes. Ce faisant, nous avons approfondi notre compréhension des fonctions respectives de ces acteurs clés de la gamétogenèse chez les mammifères, ce qui pourrait ouvrir la voie vers une amélioration des techniques d'AMP actuelles ainsi que le développement de thérapies alternatives et personnalisées.

Remerciements

Je remercie Mesdames le Docteur Dominique WEIL et le Docteur Véronique DURANTHON d'avoir accepté la charge d'être rapporteurs de ma thèse. Je remercie également Madame le Docteur Marie-Hélène VERLHAC et Messieurs le Docteur Rémi DUMOLLARD et le Professeur Pierre RAY d'avoir accepté de participer à mon jury. Je tiens à remercier tous les membres du jury pour le temps qu'ils m'ont consacré afin d'évaluer ce travail.

Je remercie toute l'équipe GETI pour leur soutien au cours de ma thèse. Je tiens à exprimer toute ma reconnaissance envers mon Directeur de Thèse, le Docteur Christophe ARNOULT, non seulement pour son investissement et son encadrement, mais aussi pour son encouragement, son enthousiasme et sa disponibilité. Je remercie à Sandra YASSINE et à Roland ABI-NAHED pour le temps qu'ils m'ont accordé lors de mon arrivée dans l'équipe. Je remercie Emeline LAMBERT et tous les étudiants de l'équipe, actuels et anciens, pour les bons moments passés ensemble au laboratoire et en dehors ! Magali, merci de ton aide et de ton enthousiasme pour le projet. Je te passe le relais en toute confiance et te souhaite plein de succès !

Je tiens à remercier Mesdames le Docteur Nathalie Beaujean et le Docteur Pascale Hoffmann pour leurs conseils lors des comités de suivi de thèse et le Docteur Nathalie Beaujean encore une fois pour les nombreuses lettres de recommandation !

Je remercie tous mes amis à l'IAB, j'ai toujours apprécié nos conversations lors de mes passages à l'institut !

A ma famille, merci de votre soutien et d'avoir toujours eu confiance en moi.

A mes amis à Grenoble, merci d'avoir été ma deuxième famille, je vous aime.

Table of contents

List of figures

List of tables

Abbreviations

ACR: acrosin
AR: acrosome reaction
ARE: AU-rich elements
ART: Assisted reproduction technologies
BMP15: bone morphogenetic protein 15
cAMP: cyclic adenosine monophosphate
CBC: cap-binding complex
CDC25: cell division cycle 25
CDK1: cyclin-dependent kinase 1
cGMP: cyclic guanosine monophosphate
COC: cumulus-oocyte complex
CPE: cytoplasmic polyadenylation element
CPEB: cytoplasmic polyadenylation element binding protein
CPSF: cleavage and polyadenylation specificity factor
CRISPR: clustered regularly interspaced short palindromic repeats
DAZL: deleted in azoospermia-like
DDX6: DEAD-Box Helicase 6
EGA: embryonic genome activation
eIF: eukaryotic translation initiation factor
EPABP: embryonic poly(A) binding protein
ESHRE: European Society of Human Reproduction and Embryology
FSH: follicle stimulating hormone
GDF9: growth and differentiation factor 9
GnRH: gonadotropin-stimulating hormone
GV: germinal vesicle
GVBD: germinal vesicle breakdown
hCG: human chorionic gonadotropin
ICMART: The International Committee for Monitoring Assisted Reproductive Technology
ICSI: intracytoplasmic sperm injection
IVF: *in vitro* fertilisation
IVM: *in vitro* maturation
LH: luteinising hormone
MAPK: mitogen-activated protein kinase
MI: metaphase I
MII: metaphase II
MPF: maturation promoting factor
MSY2: Y-box binding protein 2
MTOC: microtubule-organising centres
mTOR: mammalian target of rapamycin
MZT: maternal-zygote transition
NGS: next-generation sequencing
NOA: non-obstructive azoospermia
NSN: non-surrounded nucleolus
OATS: oligoasthenoteratozoospermia
OMD: Oocyte maturation/meiotic deficiency
PABP: poly(A)-binding protein
PAP: poly(A) polymerase
PARN: poly(A)-specific ribonuclease
PAS: polyadenylation signal
Pat1: protein associated with topoisomerase II
PATL1/2: protein associated with topoisomerase II-like 1/2
PBE: pumilio binding element
PCOS: polycystic ovary syndrome
PGC: primordial germ cell
POI: primary ovarian insufficiency
PUM: pumilio
RBP: RNA-binding protein
RINGO/Spy: rapid inducer of G2/M progression in oocytes/speedy
RNP: ribonucleoprotein
SAC: spindle assemble checkpoint
SN: surrounded nucleolus
SPINK2: serine peptidase inhibitor, Kazal type 2
UTR: untranslated region
WES: whole exome sequencing
WHO: World Health Organisation

Introduction

Chapter 1: Female gametogenesis and mRNA regulation

Part A: Oocyte and follicle development

1. The female reproductive system

The internal female reproductive organs are the ovaries, uterus and fallopian tubes. The female gametes are contained within the ovaries which are the centres of gamete storage and development as well as crucial endocrine organs. The ovaries release a mature oocyte at monthly intervals from puberty to menopause. Fertilisation occurs within the Fallopian tubes and the fertilised egg divides and forms a blastocyst which implants in the endometrium of the uterus. The uterus also produces secretions that are crucial for allowing sperm progression.

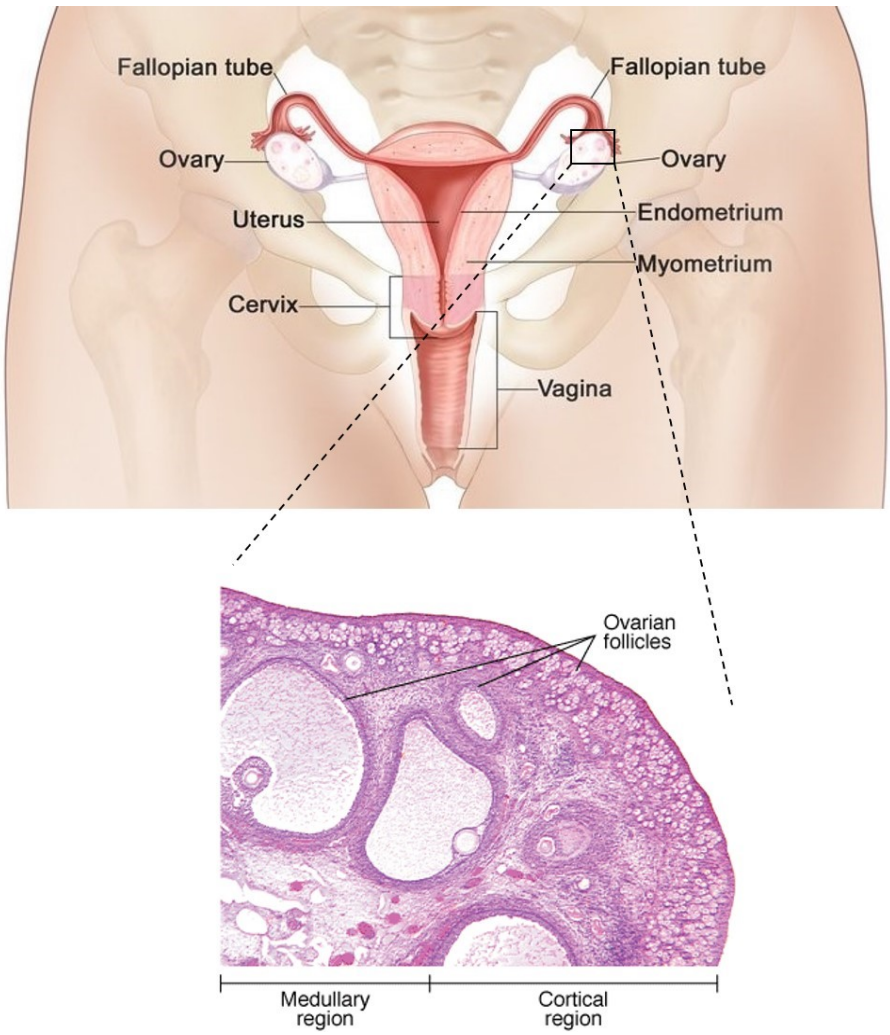

Figure 1. Anatomy of the female reproductive tract.
Source: National Cancer Institute (https://visualsonline.cancer.gov/details.cfm?imageid=8262)

Oocyte maturation takes places within ovarian follicles, which are the functional units of the ovary. The follicle forms many functions important for oocyte development, forming a protective barrier, creating an internal environment favourable to oocyte growth and co-ordinating the development of the oocyte with external signals. The somatic granulosa cells and developing oocyte are in constant cross-talk though transzonal projections or 'gap junctions' in the zona pellucida. The granulosa cells are also responsible for the production of oestrogen.

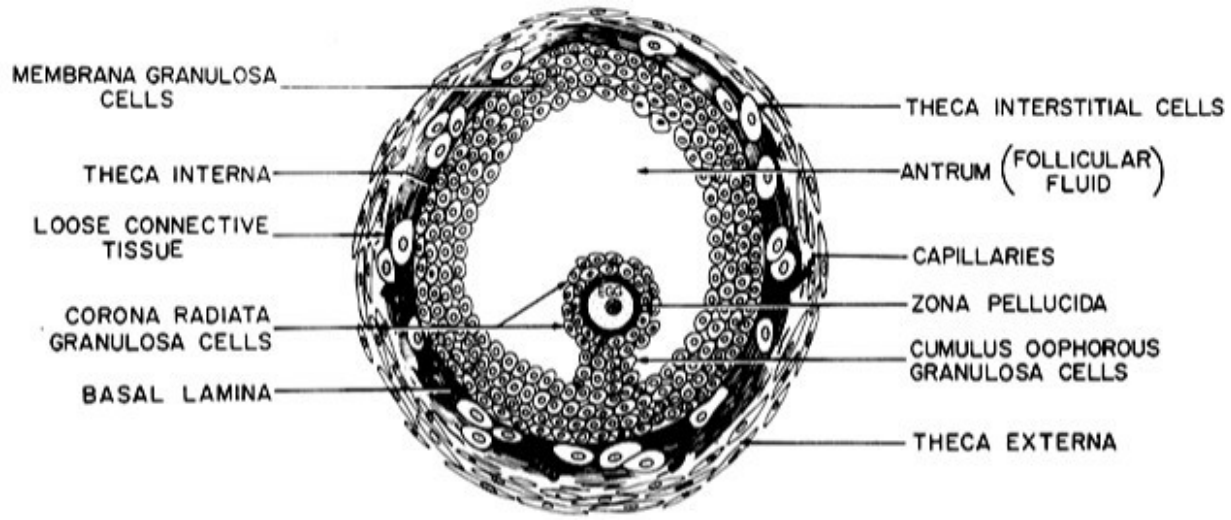

Figure 2. Anatomy of the mature (antral) ovarian follicle.
Source: Erickson, 1983 [1]

1.1. The hypothalamic-pituitary-gonadal axis

The female reproductive system is controlled by the interaction of hormones produced by the hypothalamus, pituitary gland and ovaries. The hypothalamus secretes gonadotropin-releasing hormone (GnRH) which stimulates the gonadotropic cells of the anterior pituitary gland to release follicle stimulating hormone (FSH) and luteinising hormone (LH). FSH stimulates follicular cell proliferation in the ovary and the maturing follicles in turn secrete estradiol. LH triggers ovulation and the development of the corpus luteum, which in turn secretes progesterone necessary to prepare the endometrium for implantation. The ovary also produces hormones Inhibin A and B which act at different times during the menstrual cycle to regulate secretion of FSH allowing for ovulation of a single mature oocyte [2]. This complex feedback system is summarised in Figure 3.

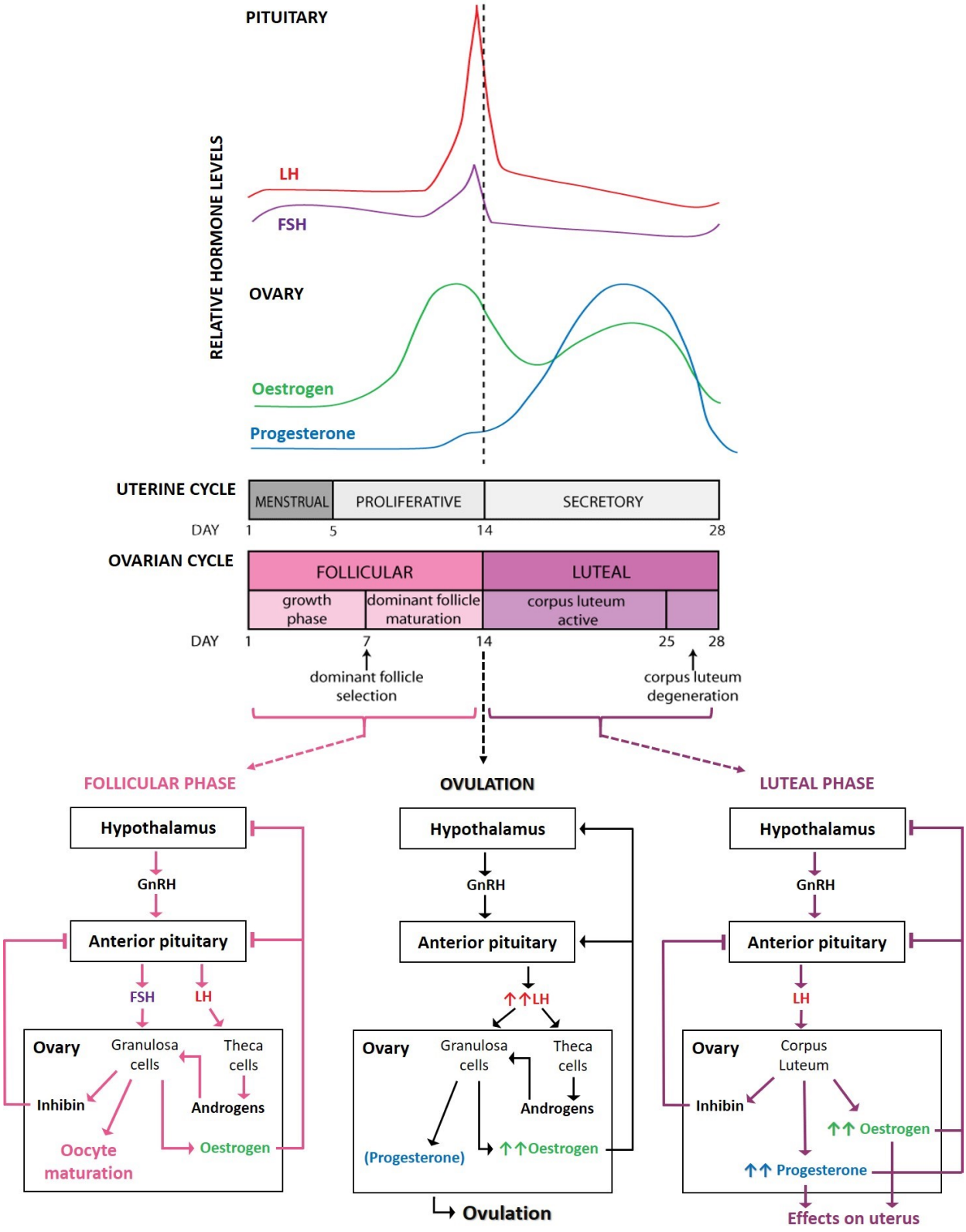

Figure 3. Hormonal control of the female reproductive cycle.

The hypothalamic-pituitary-gonadal axis and follicular phases. Arrows indicate positive feedback and bars indicate negative feedback. *Source: Adapted from University of Washington (https://courses.washington.edu/conj/bess/female/female.html)*

2. Oogenesis and folliculogenesis: co-ordinated molecular and cellular events

Folliculogenesis describes the development of the ovarian follicle. Beginning *in utero*, folliculogenesis can be divided into gonadotropin-independent and gonadotropin-dependent stages (Figure 4). The first stage is characterised mainly by oocyte growth and differentiation and the second stage by dramatic follicular growth.

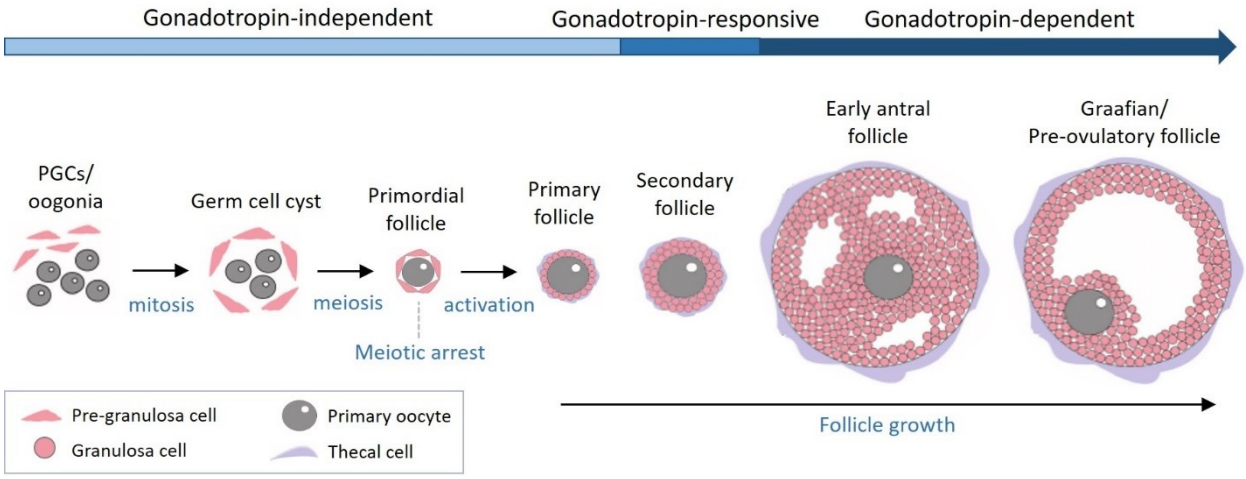

Figure 4. Ovarian follicle stages.
Stages of mammalian folliculogenesis showing gonadotropin-independent and dependent stages.
Source: Adapted from Piotrowska et al, 2013 [3]

In humans, the process of folliculogenesis from the recruitment of a primordial follicle through to the pre-ovulatory stage takes almost a year. The gonadotropin-independent stage is the slowest, taking around 290 days and giving rise to a secondary follicle (class 1, Figure 5). From here it takes around 60 days to progress to the Graafian follicle stage (classes 2-8, Figure 5) in response to gonadotropins. The dominant follicle is selected from a group of class 5 stage follicles towards the end of the luteal phase of the menstrual cycle and takes 20 days to complete its maturation before ovulation. All other follicles stimulated to mature beyond the secondary follicle (preantral) stage will undergo atresia (percentages indicated in Figure 5) [4,5]. Only around 1% (300-400) of the oocytes present in the ovary at puberty will reach ovulatory state [6].

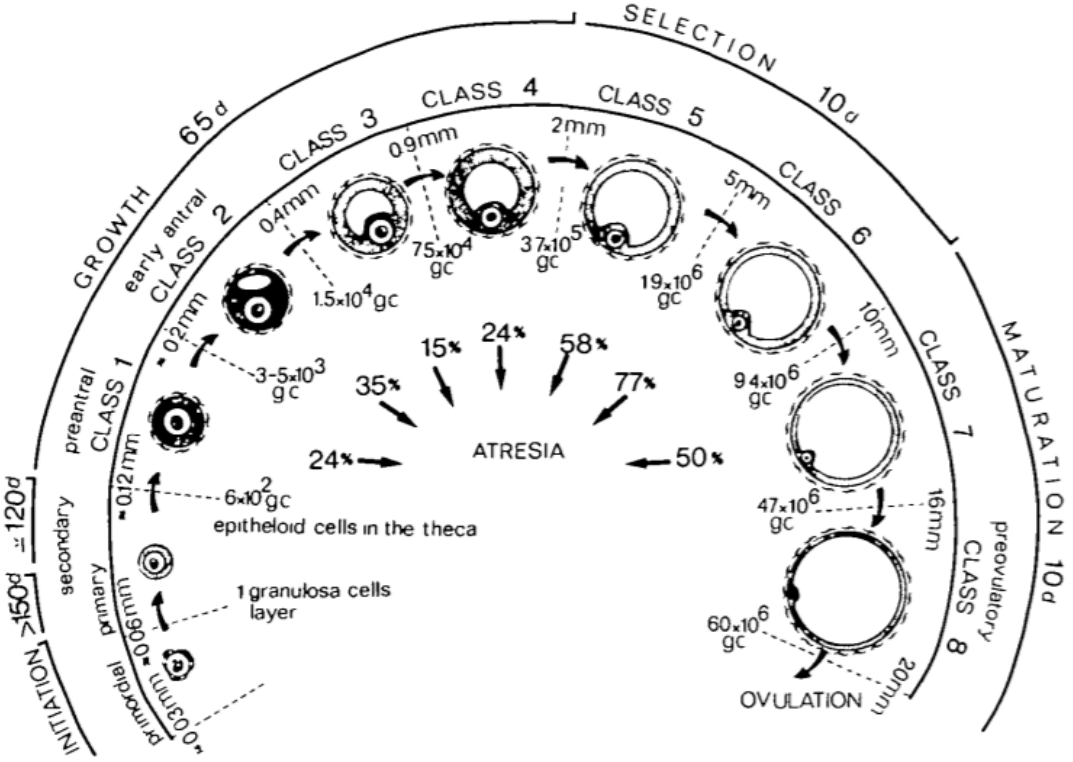

Figure 5. Chronology of human folliculogenesis.
Timeline of the steps from primordial follicle recruitment, dominant follicle selection, and ovulation. Follicles are labelled to indicate developmental stage, size, and percentage lost through atresia. D: days, gc: granulosa cell (number). *Source: Gougeon, 1986* [7]

2.1. Primordial follicle formation

In humans, oogonia form between weeks 6-10 of gestation from a cluster of ~100 primordial germ cells which migrate to the genital ridge. The oogonia proliferate exponentially via mitosis such that their number increase from ~600 000 at 8 weeks to 6-7 million at 20 weeks (Figure 6) thus colonising the ovary. After this stage, the number of oogonia begins to decrease due to depletion through apoptosis. Oogonia promptly begin to enter meiosis from around week 10, becoming oocytes. They arrest meiosis at the diplotene stage of prophase I and are encapsulated in primordial follicles from around week 15 until birth. A newborn ovary contains around 1 million oocytes, of which only around 3-400 000 remain by puberty. The reason for this large-scale depletion remains unclear, although it has been hypothesised to be a meiosis quality control mechanism or linked to insufficient growth/survival factors from neighbouring somatic cells. Germ cell survival and apoptosis have been shown to be controlled by a balance of proteins encoded by the *Bcl-2* apoptosis-regulator gene family in mice [6,8,9].

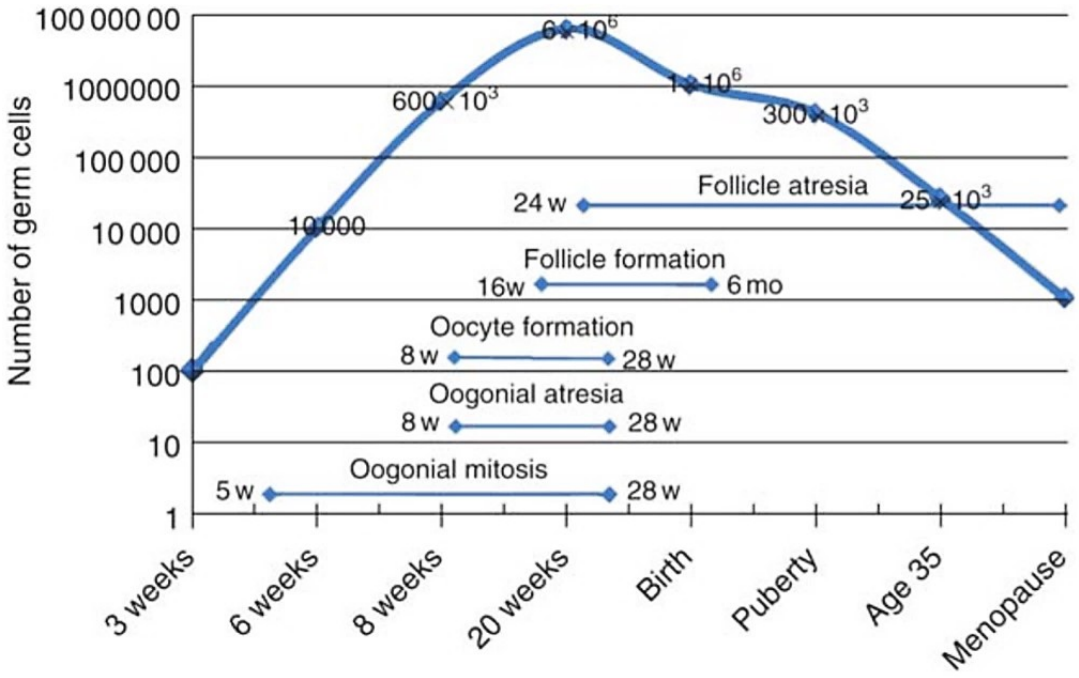

Figure 6. Germ cell number evolution from *in utero* development to menopause.
mo: month. W: week. *Source: Oktem and Urman, 2010 [6]*

As oogonia divide by mitosis they form clusters known as germline cysts, which enter meiosis in a synchronous fashion. Entry into meiosis and the end of the oogonial stage are marked by premeiotic DNA synthesis, at which time oogonia become known as primary oocytes. The gene *Stra8* (Stimulated By Retinoic Acid 8) has been shown to be crucial for this transition in mice [10]. Cyst breakdown and primordial follicle formation are co-ordinated by Notch signalling and in mammals require the oocyte-specific transcription factors FIGLA (Factor in the germline alpha), NOBOX (Newborn ovary homeobox gene) and germ-cell-specific LHX8 (LIM Homeobox 8) and SOHLH1/2 (Spermatogenesis and oogenesis specific basic helix-loop-helix 1/2), which activate transcription of numerous oocyte-specific genes including growth and differentiation factor 9 (*GDF9*), bone morphogenetic protein 15 (*BMP15*), and zona pellucida genes 1–3 (*ZP1–3*) [11–13]. In mice, FIGLA, NOBOX and LHX8 persist during oocyte growth while expression of *FOXO3*, *SOHLH1* and *2* is more confined to primordial and smaller primary follicles. FOXL2 (Forkhead box L2) is a granulosa cell transcription factor that is expressed throughout follicular development and is necessary for the organisation of somatic cells around oocytes to form primordial follicles [14,15].

2.2. Primordial follicle activation

In mammals, primordial follicles make up the ovarian reserve and consist of a primary oocyte surrounded by a single layer of flattened granulosa cells contained within a basal lamina. They have limited contact with the endocrine system since they do not have an independent blood supply [4]. Primordial follicles, which are around 25µm diameter in humans, remain in a dormant state with oocytes arrested at the diplotene stage of prophase I until being activated to grow. The recruitment of primordial follicles begins soon after their formation at the foetal stage and continues until the follicular reserve is exhausted around menopause.

The mechanism by which primordial follicles are recruited to mature remains somewhat mysterious. Only recently has light been shed on this process through the study of transgenic mouse models, and there is substantial evidence that follicular activation as well as development are to an extent governed by an intrinsic oocyte programme, and that the oocyte is likely the dominant factor in determining its own differentiation and that of its surrounding granulosa cells [16]. Dormancy and activation are likely controlled by a balance of inhibitory and stimulatory signals from the oocyte itself as well as the pre-granulosa cells, surrounding follicles and stromal cells and endocrine factors.

One of the major signalling pathways co-ordinating primordial follicle dormancy/activation in mammals is the oocyte PI3K/PTEN pathway activated by granulosa cell-secreted Kit ligand (KL) and growth factors (Figure 7). Several members of the PI3K pathway have been associated with phenotypes of premature and irreversible follicle activation and diminishment of the ovarian reserve in mouse studies including *Pten* (phosphatase and tensin homologue deleted on chromosome 10), *Foxo3a* (forkhead box O3A) and *Tsc1/2* (Tuberin/tuberous sclerosis complex) [17–20]. Granulosa cells produce KL in response to oocyte-secreted growth factors. KL activates receptor protein tyrosine kinase (RPTK) on the oocyte surface and triggers the PI3K cascade, leading to phosphorylation and inactivation of FOXO3 and TSC1/2. FOXO3 is a transcription factor that promotes transcription of cell cycle arrest genes and TSC1/2 negatively regulates the mTOR pathway. The mTOR pathway is activated, promoting protein translation and follicle activation (Figure 7) [21].

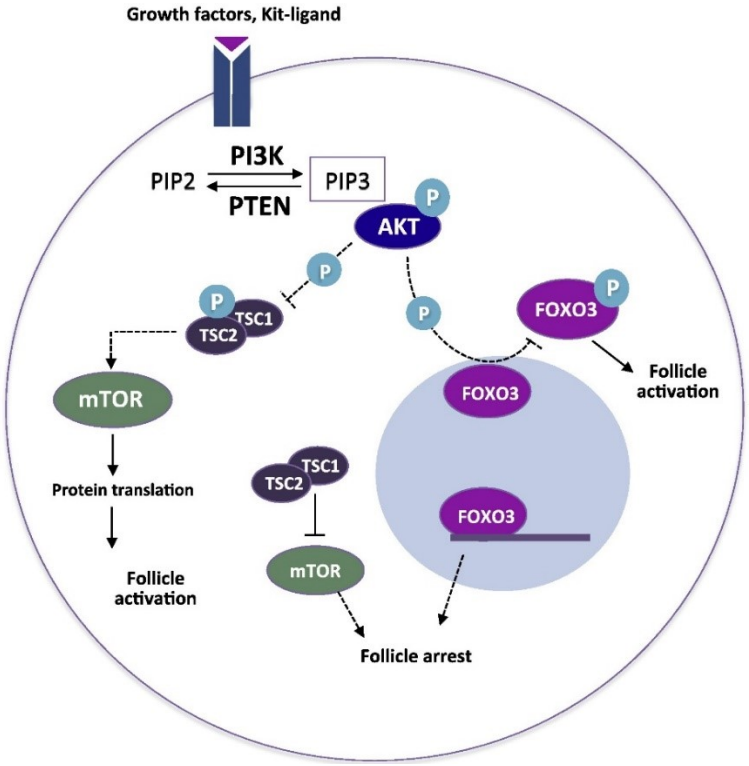

Figure 7. The PI3K/PTEN/AKT and TSC/mTOR pathways in primordial follicle arrest and activation (mouse).

Ligands (e.g. KIT) and growth factors activate membrane receptor tyrosine kinase and activate PI3K (phosphatidylinositol 3-kinase), leading to increased PIP3 (phosphatidylinositol (3,4,5)-triphosphate) levels. PIP3 recruits serine/threonine kinase AKT to the membrane which is phosphorylated and activated and in turn phosphorylates FOXO3a (forkhead box O3A) which is inactivated and translocated from the nucleus to the cytoplasm. TSC1/2 (tuberin/tuberous sclerosis complex 1,2), negative regulator of mTORC1 (mammalian target of rapamycin complex 1) also becomes phosphorylated and inactivated via AKT. PTEN (phosphatase and tensin homologue) is a negative regulator of the PI3K pathway. *Source: Sánchez and Smitz, 2012* [21]

In mammals, Anti-Mullerian hormone (AMH) secreted by growing neighbouring follicles have a negative paracrine regulatory effect on activation [4]. SOHLH1, SOHLH2, and FIGLA appear to play a role in primordial follicle survival and activation through regulation of critical downstream genes [12]. Similarly, LHX8 and NOBOX control the expression of several genes regulating follicle development, including *GDF9* and *BMP15*. GDF9 and BMP15 as well as mesenchymal-cell-secreted BMP-4 and 7 are transforming growth factor-beta (TGF-β) ligands that play an important role in follicular activation amongst other stages of folliculogenesis [22]. Lastly, androgen-promoted expression of insulin-like growth factor (IGF-I) and its oocyte receptor have been shown to promote follicle activation and growth in primates [23].

2.3. Preantral follicle development

Upon recruitment, the flattened pre-granulosa cells of the mammalian primordial follicle become cuboidal. A primary follicle is defined by the presence of at least one cuboidal granulosa cell in a single layer surrounding the oocyte. The oocyte also begins to grow and differentiate, marked by a progressive increase in mRNA synthesis. Zona pellucida genes are expressed (through action of FIGLA and NOBOX) and ZP glycoproteins are secreted, polymerising at the oocyte surface to eventually surround the oocyte, forming an extracellular coat that plays a vital role during oogenesis and in fertilisation and preimplantation development [1,24]. As the zona pellucida forms, granulosa cells extend cytoplasmic transzonal projections which connect with oocyte microvilli (as well as each other) forming gap junctions. Gap junctions are formed of connexin (Cx) proteins, with oocytes primarily synthesising Cx37 and granulosa cells synthesising Cx43 [25]. These intercellular channels intimately link the oocyte and granulosa cells by providing a substantial surface area for diffusion of metabolites, ions, and signalling molecules [26]. This communication allows for co-ordinated development of the follicle and oocyte and is essential for successful oogenesis and ovulation [27].

In humans, the granulosa cells start expressing FSH receptors from the primary follicle stage as a result of stimulation from FSH, activin, cAMP and TGF [28]. Despite this early expression of FSH receptors, primary follicles are not thought to be sensitive to cyclic FSH fluctuations within the physiological range (they lack an independent vascular system), however it is possible that they are affected by abnormally high plasma FSH levels (i.e. induced ovulation or age-related).

In response to stimulation from the oocyte-derived growth factors GDF9 and BMP15, granulosa cells proliferate to form multiple layers in a stratified epithelium [29]. At this stage the follicle is considered a secondary follicle. The theca assembles from stroma-like cells around the basal lamina, eventually forming two distinct layers: the theca interna and theca externa. Theca development is accompanied by vascularisation, connecting the follicle to nutrients and hormones and transporting waste and secreted products. Certain stromal cells in the theca interna differentiate into steroidogenic theca interstitial cells, expressing LH receptors, likely in response to LH exposure from the bloodstream. By the end of the secondary follicle stage, all granulosa cells express FSH receptors. The follicle thus becomes gonadotropin responsive.

2.4. Oocyte growth

The preantral follicle period is accompanied by dramatic oocyte growth during which the human oocyte increases from ~30 µm to ~120 µm in diameter, increasing its volume around 100-fold [30]. The oocyte genome is reactivated upon recruitment and the oocyte enters a phase of intense transcriptional, translational and metabolic activity which is thought to be promoted by the oocyte growth factors GDF9 and BMP15 and the granulosa cell Kit ligand [31,32]. During this time, maternal-specific imprints are established on a locus-by-locus basis through CpG methylation of DNA regulatory sequences [33]. In mice, this growth phase (lasting 2-3 weeks) results in a 300-fold increase in RNA content and the rate of protein synthesis increases 38-fold [34,35].

This growth phase is crucial since once the oocyte resumes meiosis, the condensed chromosome state prevents transcription of genes as they are required. The absence of transcriptional activity lasts until embryonic genome activation (EGA), occurring at the late 2-cell stage in mice and 4-8 cell stage in humans (Figure 8) [36]. The oocyte must therefore synthesise in advance all material necessary to satisfy its mRNA and protein requirements for growth and differentiation as well as for meiotic maturation, response to fertilisation, the maternal-to-zygote transition (MZT) and the first embryonic divisions.

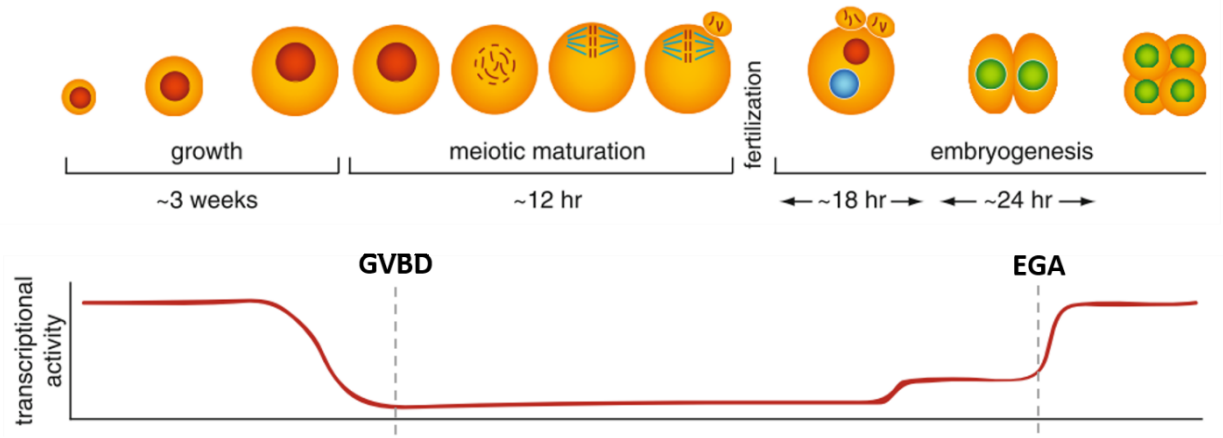

Figure 8. Transcriptional activity during the stages of oocyte growth, meiotic maturation and early embryogenesis (mouse).
GVBD: Germinal vesicle breakdown, EGA: Embryonic genome activation. *Source: Adapted from Clarke et al, 2012* [37]

The oocyte completes its growth by the end of the preantral stage and is maintained in meiotic arrest by its follicular environment [38]. It was previously believed that this negative control is achieved through entry of cAMP (cyclic adenosine monophosphate) into the oocyte from granulosa cells via gap junctions. It has since been shown in mice that cAMP is produced by the oocyte itself, stimulated by GPR3 (a constitutively active G protein-coupled receptor), and it is instead cyclic GMP that passes across the gap junctions from granulosa cells. cGMP helps maintain meiotic arrest by inhibiting phosphodiesterase 3A (PDE3A)-mediated cleavage of cAMP [39,40]. cAMP prevents meiotic resumption by blocking the cascade leading to activation of the Maturation Promoting Factor (MPF) (Figure 11) [41].

2.5. Follicle maturation and ovulation

Gonadotropin stimulation triggers the secondary follicle to develop into an antral follicle. The antral follicle is characterised by the presence of the fluid-filled cavity known as the antrum. This follicular fluid is composed of plasma exudate combined with secretions from the oocyte and granulosa cells [42]. The antrum forms by a process known as cavitation, whereby fluid-filled spaces form between granulosa cells, swelling to form a single cavity at one pole of the oocyte. This has the effect of separating the granulosa cells into mural granulosa cells that surround the antrum, and cumulus oophorus cells that surround the oocyte. Evidence in mice shows that cavitation occurs in response to intrinsic signalling, with essential roles found for granulosa-cell derived KIT ligand and activin as well as oocyte-derived Cx37 [27,43].

The further growth and differentiation of the follicle into a mature or Graafian follicle is stimulated by FSH, which diffuses into the antrum from the surrounding blood vessels. Once the antrum has formed, granulosa cells differentiate to carry out specialised functions according to their spatial organisation. In mice this differentiation is determined by a concentration gradient of oocyte-secreted proteins including GDF9 and BMP15 [44]. In monovulatory species, the continued growth and final maturation of the follicle is dependent on dominant follicle selection. This is the process a single follicle is selected from the cohort of growing follicles to undergo final differentiation and acquire the ability for ovulation. In humans, cows and mares, the postulated mechanism for dominant follicle selection is a transition from FSH to LH-dependence [45].

Selection is followed by further antral growth and follicular cell proliferation. Non-selected follicles undergo atresia.

Ovulation requires the collective actions of endocrine, immune and intraovarian paracrine signalling, including signals from the oocyte itself. Following the LH surge and shortly before ovulation, the physical integrity of the cumulus-oocyte complex (COC) is weakened and the gap junctions between the oocyte and neighbouring granulosa cells begin to retract, greatly decreasing the ionic and metabolic coupling. This phenomenon, known as cumulus cell expansion, occurs in response to LH-stimulated IL1 secretion from the thecal cells and oocyte-secreted GDF9 and BMP15 via pathways such as SMAD2/3 (Sma- and Mad-related protein 2/3) as shown in mice [46]. Amongst other effects, cumulus cell expansion facilitates the detachment of the COC from the follicle and influences the capacity of sperm to penetrate the cumulus cell barrier. In mice, LH also stimulates mural granulosa cells to secrete EGF (epidermal growth factor)-like ligands that transduce the ovulation signal to the cumulus cells, and other factors which become part of the cumulus cell matrix. Cumulus cells produce PGE2 which enhances their own signalling cascades via cAMP accumulation. The oocyte modulates the follicle's response to the ovulation signal via GDF9, BMP15 and BMP6 secretion (Figure 9) [47]. This signalling ultimately results in rupture of the follicle and release of the COC into the ampulla where it may be fertilised.

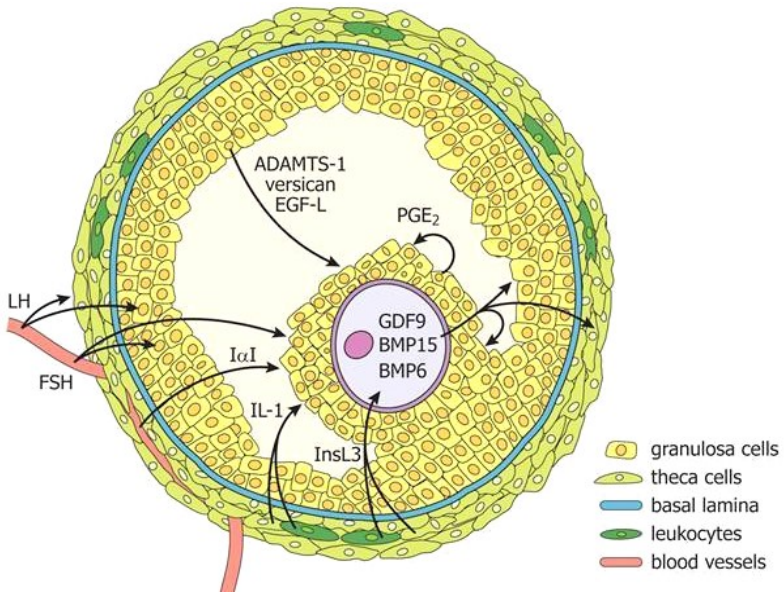

Figure 9. Signalling pathways and mediators of ovulation (mouse).
IL-1: interleukin-1, InsL3: insulin-like peptide 3, Egf-L: EGF-like ligands, II: inter--trypsin inhibitor, PGE2: prostaglandin E2 .*Source Williams and Erickson, 2012* [4]

2.6. Meiotic maturation and developmental competence

a) Final growth phase and transcriptional silencing

During follicular growth, the oocyte remains in meiotic arrest with decondensed, transcriptionally active chromosomes. In this state of meiotic arrest, it is known as a germinal vesicle (GV) oocyte, referring to its visible nucleus. In the final stages of folliculogenesis, the oocyte gains the competence to resume meiosis. This capacity is accompanied by extensive chromatin rearrangement and gradual transcriptional silencing. In many mammalian species, chromatin condenses in small heterochromatin clusters which attach to the nucleolus [33]. In mice, the decondensed chromatin state, known as NSN for non-surrounded nucleolus, is more commonly found in preantral follicle oocytes, and the condensed SN (surrounded nucleolus) state becomes more prevalent in antral follicles of increasing diameter (Figure 10). This change, correlated with transcriptional silencing, is associated with meiotic competence [48]. The mechanisms involved in this large-scale remodelling are not fully understood, however histone methylation and acetylation play a key role, and there is evidence to show that it may be modulated by the surrounding cumulus granulosa cells [49]. Acquisition of meiotic competence also involves the formation of cytoplasmic microtubule-organising centres (MTOCs) in preparation for spindle assembly [50].

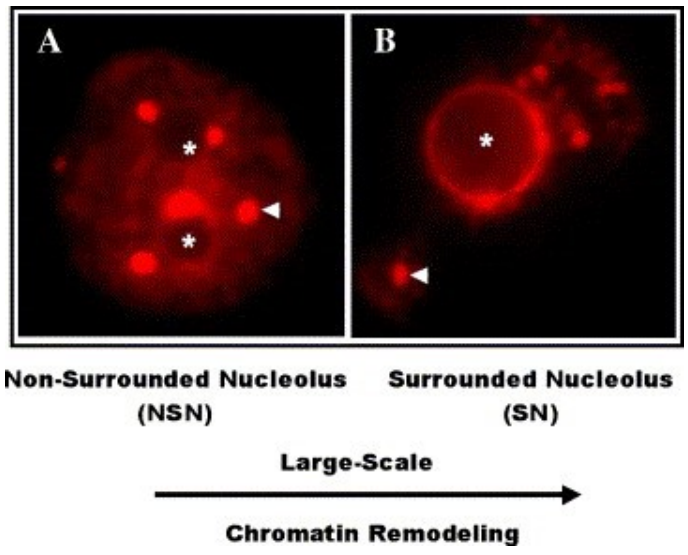

Figure 10. Chromatin configuration remodelling in mouse GV oocytes.
Representative micrograph of NSN and SN chromatin configurations. Hoechst 33248-stained DNA is shown in red. Arrowheads indicate heterochromatin and stars indicate nucleoli. *Source: De la Fuente, 2006* [33]

Despite reaching meiotic competence, oocytes will only resume meiosis if removed from the prohibitive follicular environment [51]. This inhibition of meiotic resumption acts to ensure that the oocyte completes the additional stages of maturation and differentiation required to gain full developmental competence. These final cellular events and their regulation are comparatively poorly understood; however, it is known that they must take place in a co-ordinated manner in order to support correct meiotic completion, fertilisation, genome reprogramming, DNA replication and EGA.

b) Germinal Vesicle Breakdown (GVBD) and nuclear and cytoplasmic maturation

Cumulus expansion reduces oocyte exposure to cGMP from the granulosa cells. The LH surge also induces swift changes in mural granulosa cells which ultimately lead to decreased cGMP production. This results in an outflow of cGMP from the oocyte leading to activation of PDE3A and rapid inhibition of cAMP. In mice, this consequentially inactivates Protein kinase A (PKA), dephosphorylating CDC25 and WEE2 (key regulators of CDK1) and activating the maturation promoting factor (MPF, composed of CDK1 and cyclin B1) (Figure 11) [50,52]. The oocyte therefore undergoes germinal vesicle breakdown (GVBD) and re-enters meiosis.

The mammalian oocyte meiotic spindle assembles in the absence of centrioles through a poorly understood mechanism likely driven by MTOCs. It had been demonstrated that MTOCs originate from a microtubule network that extends across the GV oocyte cytoplasm and that migrate towards the chromosomes at GVBD [53]. A recent competing theory suggest that the chromosomes themselves initiate microtubule nucleation [54]. The bipolar spindle forms over several hours by microtubule polymerisation and stabilises during metaphase progression. The chromosomes align along its equatorial plate such that homologous kinetochores are attached to microtubules from opposite poles [55]. Finally, the spindle assembly checkpoint (SAC) is activated, allowing the cycle to progress to anaphase.

In the first division, homologous chromosomes that had remained joined throughout the GV stage are finally separated while sister chromatids remain joined. This is achieved thanks to the protein Shugosin which prevents Cohesin phosphorylation between sister chromatid kinetochores [56]. Telophase ensues and the spindle migrates to (or is already located close to according to competing theories [57,58]) the oocyte cortex inducing the formation of a cortical actomyosin domain. Asymmetric division occurs in order to minimise loss of cytoplasm.

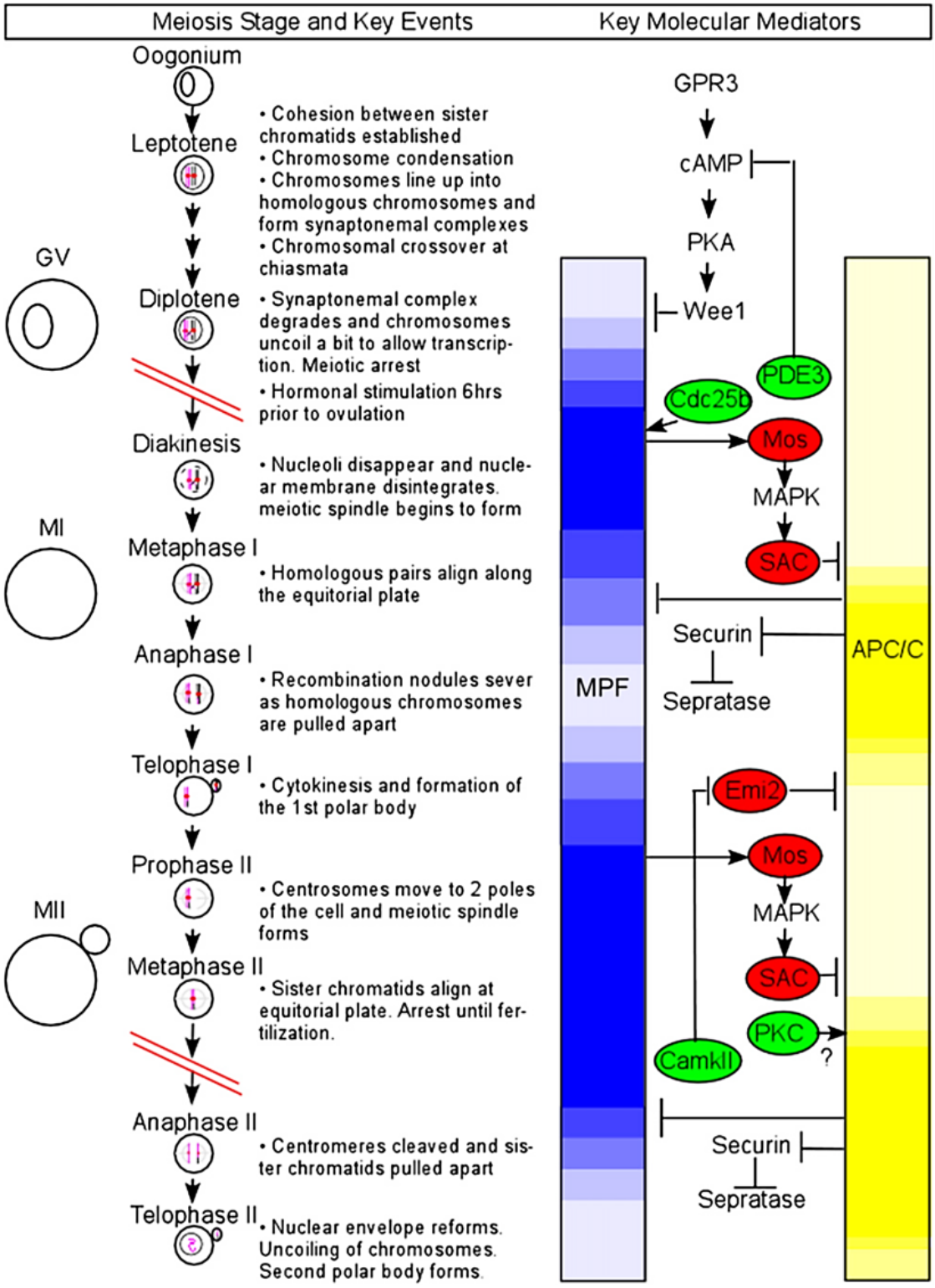

Figure 11. Oogenesis meiotic events and key mediators (mouse).

MPF (Maturation promoting factor) plays a pivotal role in meiotic progression during which its expression oscillates and is critically regulated by APC/C (anaphase-promoting complex/cyclosome). Double red lines indicate natural meiotic arrest points. GPR3: G-protein coupled-receptor 3, PKA: protein kinase A, PDE3: Phosphodiesterase 3, SAC: spindle assembly checkpoint, MAPK: Mitogen-Activated Protein Kinase. *Source: Beall et al, 2010* [52]

Polar body extrusion (PBE) represents completion of the first meiosis and the oocyte promptly enters meiosis II, forming the second meiotic spindle in a subcortical position (and a second polar actomyosin domain). At this stage (metaphase II or MII), the oocyte once again arrests meiosis until the event of fertilisation. The oocyte is ovulated at this stage and considered fully 'mature' and fertilisable (Figure 12).

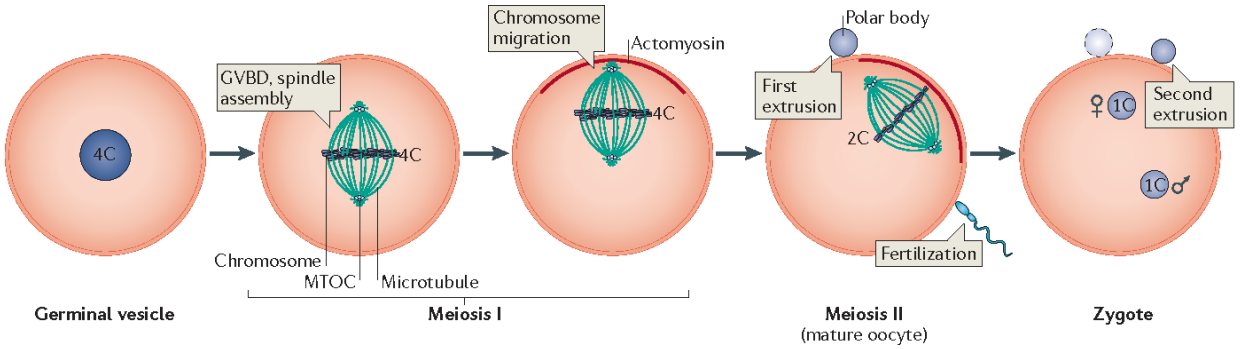

Figure 12. Mammalian oocyte nuclear maturation events.
'C' nomenclature refers to DNA content. 4C denotes 2N chromosome number and chromosomes consisting of two chromatids. 2C denotes 1N chromosome number with chromosomes consisting of two chromatids. 1C denotes 1N chromosome number with chromosomes consisting of single chromatids. The cortical actomyosin domain is shown in red. *Source: Li and Albertini, 2013* [59]

Nuclear maturation is accompanied by a dramatic reorganisation of the oocyte cytoplasm and the movement of organelles such as the Golgi apparatus, mitochondria, endoplasmic reticulum and vesicles. Mitochondria, for example, relocate around the forming spindle, which is thought to be a requirement to satisfy ATP demands for this high-energy process [60]. Despite being considered important for developmental competence, the exact functions of many of these rearrangements are not entirely understood.

To be developmentally competent, correct chromosome alignment, segregation and trafficking is crucial. For this to be possible, the molecular components of the meiotic machinery must be present in sufficient concentrations, and this relies on an undisrupted translational programme. Defects at this stage result in aneuploidy and/or developmental arrest. It is not impossible that maternal age-related increase in aneuploidy may be related to a disruption in the translational programme affecting chromosome cohesion and spindle stability.

3. Oocyte response to fertilisation and the maternal-to-zygote transition

The oocyte itself plays a significant role in fertilisation as illustrated in Figure 13. For fertilisation to be possible, the cumulus matrix/zona pellucida environment must be receptive to sperm recognition and penetration, and facilitative of the sperm acrosome reaction. Crucial roles of the mammalian oocyte include 1) mediating sperm-egg adhesion through surface receptor proteins such as CD9 [61], GPI (Glycosyl-phophatidyniositol) and Juno (sperm membrane Izumo receptor [62]), 2) drawing the sperm into the oocyte via microvilli elongation and actin polymerisation and 3) preventing polyspermy.

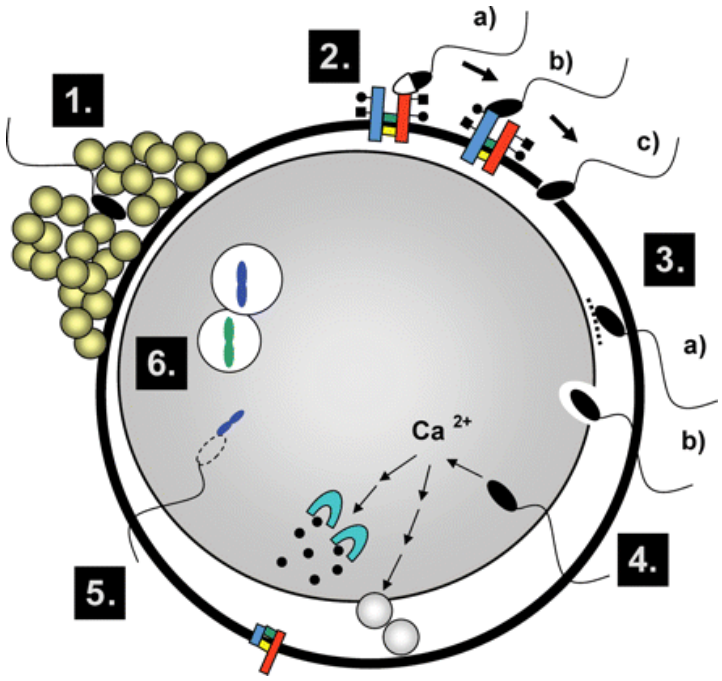

Figure 13. The 6 stages of successful fertilisation.
1) Sperm penetration of expanded cumulus cells. 2) Sperm recognition of the zona pellucida: a) sperm bind an N-terminal of ZP2, b) undergo the acrosome reaction and c) penetrate the zona pellucida. 3) Sperm-oocyte fusion: sperm bind the oolema through interactions with microvilli and membrane proteins (a) and form a fusion pore (b). 4) Oocyte activation leading to the cortical granule reaction, polyspermy block and completion of the second meiosis. 6) Pronuclei formation and migration. *Source: Swain and Pool, 2008* [63]

Polyspermy block is achieved through a combination of mechanisms. Following fertilisation, Juno is shed from the oocyte membrane and the cortical reaction occurs in which cortical granules are exocytosed leading to zona hardening (in response to calcium waves from the

endoplasmic reticulum) [64]. Cortical granules are derived from Golgi complexes during oocyte growth [65]. Ovastacin, a cortical granule metalloendoprotease encoded by *Astl*, lyses the ZP2 binding site and prevents further sperm binding the 2-cell embryo [66]. Through sperm and oocyte mediators, fertilisation activates the oocyte to reinitiate and complete meiosis 2, segregating sister chromatids and extruding the second polar body to leave a haploid maternal nucleus.

Upon fertilisation, extensive epigenetic reprogramming of the maternal and paternal genomes takes place to establish a state of zygotic totipotency. This genome-wide chromatin reprogramming is mainly due to unknown maternal factors [67]. While the paternal genome is rapidly demethylated, the maternal genome is protected and demethylated in stages [68]. This differential demethylation is regulated by maternal factors (e.g. DPPA3/Stella, Developmental Pluripotency Associated 3 [69,70]) which act to preserve the methylation of maternal imprinted regions, allowing parent-of-origin-specific gene expression. The compact protamine-associated sperm chromatin is unpacked by oocyte factors and the protamines replaced with maternal histones. *De novo* nucleosome assembly is dependent on the oocyte-derived histone variant H3.3 chaperone complex HIRA [71] and is essential for pronuclear formation and the first cleavage. The nuclear envelope reforms, incorporating nuclear pore complexes and lamins through the activity of oocyte protein kinases and phosphatases. The female pronucleus, which forms adjacent to the second polar body, migrates towards the larger, central male pronucleus and they eventually fuse [72].

These events are followed by a regulated transfer of developmental control entailing the necessary degradation of maternal transcripts and proteins and new transcription from the parental genomes, or embryonic genome activation (EGA). EGA occurs in two waves: a minor EGA during the late pronuclear stage and a major EGA at a species-dependent stage (2-cell stage in mice and 4-8-cell stage in humans) [73]. In zebrafish, it was shown that 269 genes were directly activated in the minor EGA mediated by the maternal transcription factors Nanog, Oct4 and SoxB1 [74]. In mammals, minor EGA is essential for embryo cleavage and occurs in a time-dependent manner following fertilisation according to an internal mechanism that has been called the zygotic clock (Figure 14). In mice, major EGA is dependent on both minor EGA and the first cleavage event and is necessary for progression to the 4-cell stage. Its initial repression is mediated by chromatin compaction combined with deficiency of the transcriptional machinery

at this stage [75]. Several models exist regarding the mechanism of major EGA initiation, including the 'dilution' of maternal repressive factors relative to nuclear material through subsequent divisions, or the translation of maternal activating factors according to a 'maternal clock' which accumulate to a certain threshold level [73].

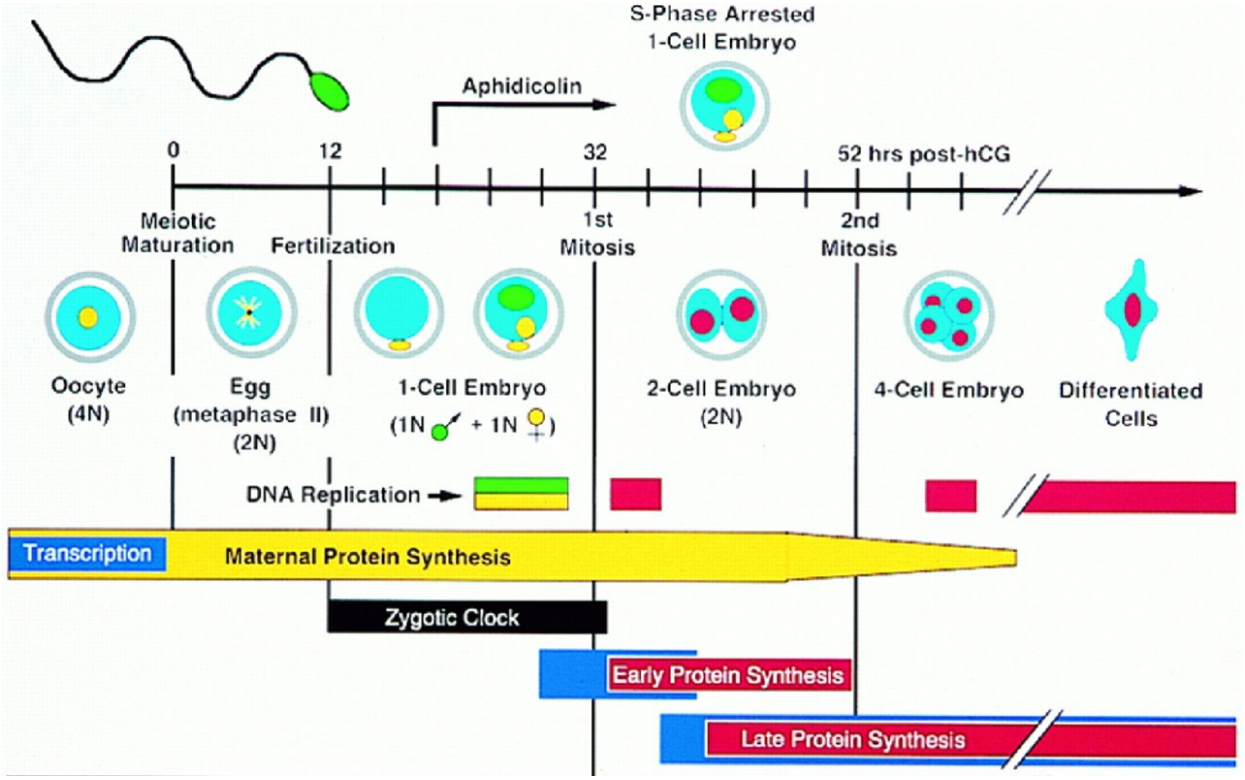

Figure 14. The maternal-to-zygote transition and minor and major EGA (mouse).
Time scale is hours post hCG-injection. Blue bars indicate transcription, events associated with the paternal pronucleus are indicated in green, the maternal pronucleus in yellow, and zygotic nuclei in red. (Aphidicolin is a specific inhibitor of replicative DNA polymerases which arrests development at the beginning of S-phase but does not prevent minor EGA). *Source: Nothias et al, 1995* [75]

This complex chain of events leading up to EGA relies heavily on maternal factors transcribed during oocyte growth. The oocyte provides the environment in which the newly formed embryonic genome activates its developmental programme and thus is an essential factor in the embryo's developmental success. It is for this reason that a truly developmentally competent oocyte must have undergone not only faithful meiotic maturation but also adequate cytoplasmic preparation.

Part B: Post-transcriptional gene regulation in the oocyte

1. Gene expression and regulatory mechanisms

For correct and timely function, each cell regulates the expression of its genes to suit its specific protein requirements at any given moment. These requirements are dictated by cell type and evolve in response to extracellular cues. A cell can execute gene regulation at a number of stages along the protein production pathway: 1) at the transcription level, via transcription factors and chromatin accessibility, 2) at the mRNA level by controlling the processing, storage, translation and degradation of transcripts and 3) at the protein level, where protein activity can be modulated via post-translational modifications or degradation (Figure 15).

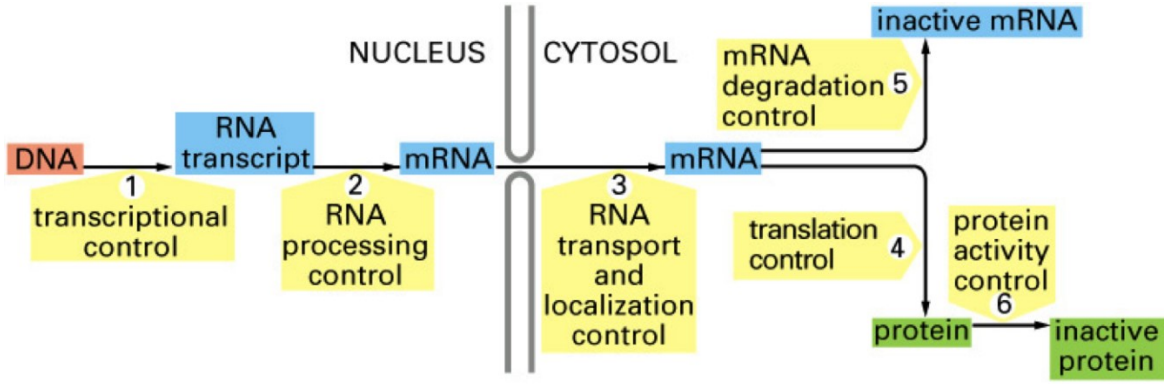

Figure 15. The eukaryotic protein production machinery and levels of gene expression control. *Source: Alberts et al, 2002* [76]

The most prominent form of regulation for the majority of genes is executed at the level of transcriptional control [76]. Transcription factors bind to accessible DNA regulatory sequences upstream of the gene near the site of transcription initiation through DNA-binding motifs and act as switches, turning on or off transcription through recruitment of the transcription machinery. Messenger transcripts then typically exist transiently, with eukaryotic transcript half-lives ranging from several minutes to several days [77]. In growing mouse fibroblast cells, the median average half-life was shown to be 9 hours for mRNA compared to 46 hours for proteins (Figure 16A) [78]. Protein expression depends on mRNA abundance (Figure 16D, and mRNA abundance is determined by the balance of rates of transcription and decay. Factors that influence mRNA synthesis, stability and association with the translation machinery thus have an important impact on protein expression.

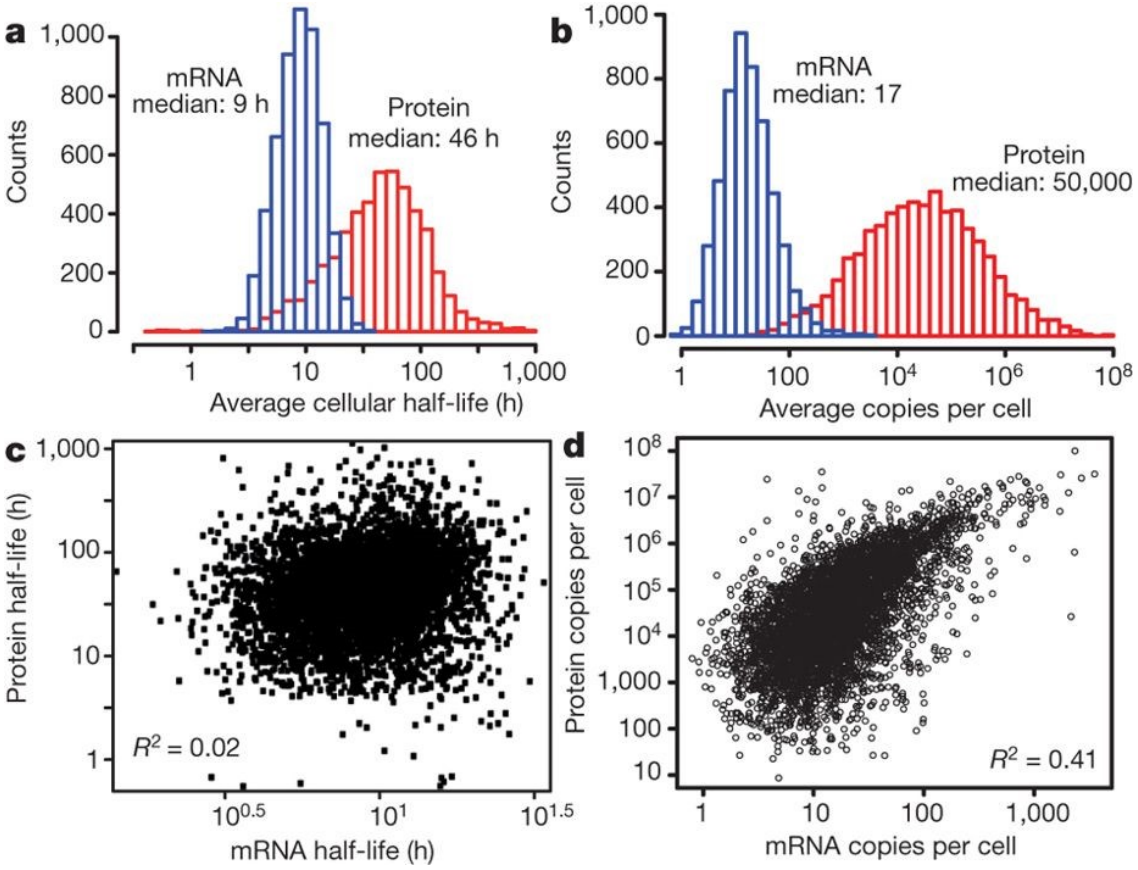

Figure 16. mRNA and protein levels and half-lives in non-synchronised NIH3T3 mouse fibroblasts. Histograms of mRNA (blue) and protein (red) half-lives (a) and levels (b). Proteins were on average 5 times more stable and 2800 times more abundant than mRNAs and spanned a higher dynamic range. c) Correlation of mRNA and protein half-lives (none) and d) levels (significant). *Source: Schwanhäusser et al, 2011* [78]

Post-transcriptional regulation is an essential component of the cell's ability to regulate protein expression as it represents a secondary layer of control that is independent from the transcription machinery. This type of regulation allows for rapid response to external stimuli [79] and becomes the prominent form of regulation in cases where transcription is not possible, i.e. due to compact/inaccessible chromatin. Post-transcriptional regulation can be global, through modulation of key components of the protein synthesis machinery, but it can also be RNA-specific, through the presence of *cis*-regulatory elements typically within the 3'UTR of the mRNA sequence. Such sequences are recognised by *trans*-acting RNA-binding proteins (RBPs) which are capable of recruiting or preventing recruitment of the key machineries.

1.1. Ribonucleoproteins and mRNA regulation

Throughout an mRNA's lifetime, its movements and fate are governed by the proteins and other molecules that bind to it. An mRNA molecule is constantly bound by a multitude of RNA-binding proteins (RBPs) that are necessary for facilitating intracellular transport, entry to and exit from translational activity, and recruitment of or protection from the cell's degradation machinery (Figure 17). For this reason, it is better to refer to the synthesis and movement of messenger ribonucleoprotein (RNP) particles. RBPs typically bind to elements within the mRNA sequence, often located in the 3' UTR, through RNA-binding domains. Several such domains have been characterised, including zinc-finger (Znf), RNA recognition motif (RRM) and K homology (KH) domains. The affinity of these binding interactions is usually relatively low and the recognised sequence variable, leading to a range of possible affinities and interactions [80].

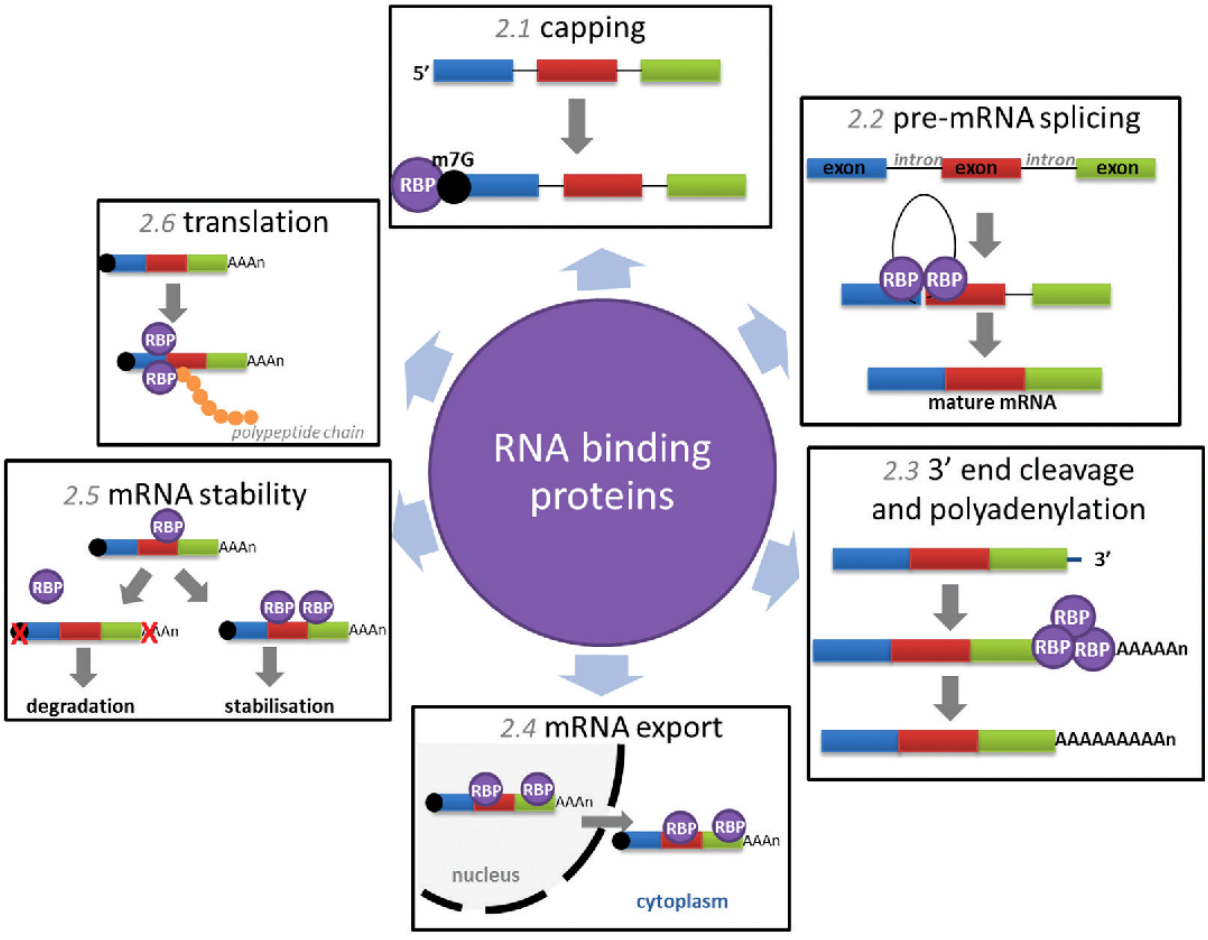

Figure 17. The diverse roles of RNA binding proteins in post-transcriptional control.
Source: Sutherland et al, 2015 [81]

1.2. The journey of a messenger RNA guided by bound proteins

a) Synthesis and processing of pre-mRNA

In eukaryotes, protein-coding genes with accessible promoter regions are transcribed by RNA polymerase II, which is recruited and bound to the promoter through transcription factors [82]. The polymerase synthesises a pre-mRNA molecule from the DNA template in the 5' to 3' direction until beyond the gene's stop codon. During elongation, the 5' end of the RNA molecule receives a 7-methylguanosine cap which prevents degradation by exonucleases and is bound by the nuclear cap-binding complex (CBC). In humans, the protein CPSF (cleavage and polyadenylation specificity factor) binds the AAUAAA sequence (also known as the polyadenylation signal or PAS) in the 3' UTR as part of a complex that includes Poly(A) Polymerase (PAP). CPSF cleaves the transcript ~10-30 nucleotides after the PAS sequence, releasing the pre-mRNA and defining its end terminus [83]. PAP catalyses the addition of adenine bases to the 3' terminus forming the 3' poly-A tail of around 200 adenine nucleotides. This serves to protect the transcript from degradation and plays a major role in the regulation of translation initiation. Poly(A)-binding protein (PABP) binds to the poly(A) tail, protecting it from exonucleases. Non-coding introns are removed in a sequence-specific mechanism by the spliceosome. The mature messenger RNA and its associated proteins, forming a ribonucleoprotein (RNP) complex, can then be exported from the nucleus to the cytoplasm through recognition of the CBC by nuclear pore complexes [84].

b) Translation and decay

Once in the cytoplasm, the nuclear CBC is replaced by the cytoplasmic cap-binding complex, eIF4F, comprising eukaryotic translation initiation factors eIF4E (cap-binding), eIF4G and eIF4A. eIF4F binds the 40S ribosomal subunit via eIF3. eIF4G associates with PABP, creating a pseudo-circular structure that favours efficient translation and protects the mRNA from degradation (Figure 18). Another initiation factor, eIF2 with bound GTP, recruits eukaryotic initiator tRNA (Met-tRNAi) to the 40S ribosomal subunit forming the pre-initiation complex. This complex locates and delivers Met-tRNAi to the AUG start codon, which with the aid of additional factors and GTP hydrolysis, recruits the 60S ribosomal subunit and assembles the full ribosome to begin translation [85,86]. mRNAs containing a premature stop codon are degraded with equal probability during each subsequent round of translation via nonsense-mediated decay [87].

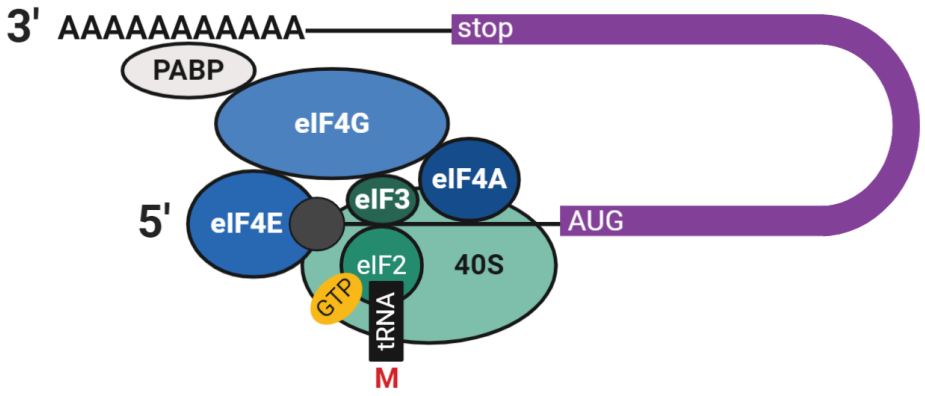

Figure 18. Translation initiation in eukaryotes.
The closed-loop, cap-dependent translation initiation model. Proteins in shades of green form the 43S complex and in blue the eIF4F complex. eIF: eukaryotic translation initiation factor. PABP: poly(A) binding protein, M: methionine, GTP: Guanosine-5'-triphosphate. *Source: Own work (created using BioRender)*

A long poly(A) tail is correlated with translational efficiency. Deadenylation slows translation and, in most cell types, initiates mRNA degradation by disrupting the translation initiation complex and exposing the 5' end to decapping enzymes. Deadenylation and exoribonuclease degradation is the pathway by which most mRNAs undergo decay. It is thought that first the PAN2/3 (poly(A)-nuclease) complex shortens the poly(A) tail to around 80 residues, after which the CCR4-NOT complex or PARN (Poly(A)-specific ribonuclease) takes over and removes most or all of the remaining tail [88]. Deadenylation is followed either by 3' to 5' degradation by the cytoplasmic exosome or association of the ring-shaped Lsm1–7 complex to the 3' end which induces decapping by Dcp1p/Dcp2p [89]. Decapping leaves the mRNA molecule vulnerable to 5' to 3' degradation by the exoribonuclease XRN1 [90]. mRNAs can also undergo decay via endonucleolytic degradation through sequence-specific cleavage by the RNA-induced silencing complex (RISC) associated with small interfering RNA (siRNA). The presence of certain AU-rich elements (AREs) in the 3' UTR signals rapid degradation through specific binding proteins [91].

c) P-bodies and stress granules

The above described mRNA decay and interference machinery as well as translationally inactive mRNAs tend to concentrate in discrete cytoplasmic foci known as P-bodies (processing bodies). P-bodies are membrane-less organelles that are sites of translational repression, mRNA degradation and also mRNA storage, since mRNAs can subsequently return to translation [92]. They are phase-separated (liquid-liquid) RNP granules that present as droplets of around 0.5 µm

(Figure 19). The role of P-bodies as sites of RNA decay or storage has been a subject of debate, however it is now thought that the primary function of P-bodies is the co-ordinated storage of regulatory mRNAs grouped by function, or 'regulons'. The group of mRNAs that locates to P-bodies is particular in that they tend to have intrinsically low translation rates (lower polysome association and protein yield) [93]. P-bodies could then act to physically separate mRNAs requiring tight control and co-ordinated expression from those that are efficiently translated [94]. Mammalian proteins that localise to P-bodies and those that are instrumental in P-body assembly or essential structural components are listed in Table 1. Another type of somatic RNP granule are stress granules, which appear in response to environmental stress and contain mRNAs that are halted in translation initiation. They have a number of proteins in common with P-bodies such as CPEB1, DDX6 and eIF4E [95].

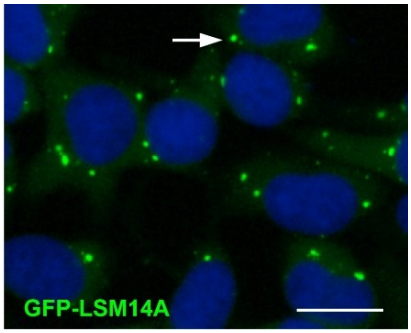

Figure 19. P-bodies labelled with GFP-LSM14A in HEK293 cells
The white arrow indicates a P-body. DAPI-stained nuclei are in blue. Scale bars: 10 µm. *Source: Hubstenburger et al, 2017* [94]

Protein	Function	Protein	Function
XRN1	5′ decay	**PAT1B***	Repression/decay
DCP2	5′ decay	**DDX6****	Repression/decay
EDC3	5′ decay	**4E-T****	Repression/decay
EDC4*	5′ decay	**LSM14A/RAP55****	Repression/decay
PAN3*	Deadenylation	**LSM14B**	Repression/decay
CCR4*	Deadenylation	**CPEB1***	Repression
LSM1*	5′ decay	**GW182***	miRNA pathway
LSM4*	5′ decay		

Table 1. Mammalian proteins that localise to P-bodies
1 star: P-bodies disappear after respective protein silencing by siRNA. 2 stars: P-bodies cannot reform after respective protein knockdown even after treatment with P-body enhancing agents. *Source: Standart and Weil, 2018* [93]

2. Regulation of gene expression and mRNA storage in the oocyte

2.1. Oocyte RNPs and the specific requirements of the oocyte

Oocytes have particular requirements when it comes to gene regulation owing to the condensed chromatin state that is established at the end of the growth phase. Regulation cannot be executed at the transcription level since transcription is effectively silenced from the late GV stage until EGA following fertilisation. Gene expression control is therefore transferred from the nucleus to the cytoplasm, from transcriptional regulation to translational regulation (Figure 20). The unique challenge of the oocyte is the synthesis and preservation of all transcripts necessary for and during the complex processes of meiotic maturation, sperm processing, nuclear reprogramming, and EGA initiation as well as their timely and selective translation and degradation. To meet these requirements, a number of specialised RNPs exist (Table 2), making up a specialised and multi-layered mRNA processing system. The fine regulation of mRNA translation combined with the controlled post-translational modification and degradation of proteins allows the oocyte to modulate the abundance of active factors in a temporal and spatial manner.

The oocyte environment is a particularly stable one, with a very low intrinsic decapping rate. Maternal oocyte mRNAs have an average half-life of around 2 weeks in growing mouse oocytes [96,97]. It is estimated that 30-45% of the mRNAs transcribed during vertebrate oocyte growth are translationally repressed until meiotic maturation or fertilisation [98]. These stored mRNAs are typically deadenylated upon export from the nucleus to the cytoplasm, leaving poly(A) tails of around 20-40 residues long that are unconducive to translation since PABP and eIF4G are unable to bind [99]. In oocytes, deadenylation is not linked with decapping in the same way as in somatic cells [95]. The deadenylated state is preserved and the mRNA stabilised by the binding of specific RBPs until translation is required, at which time the mRNA is derepressed and the poly(A) tail is restored (Figure 20). This switch is often mediated by phosphorylation of the RBP as part of a signalling cascade. Some oocyte RBPs have a dual activity, both capable of repressing and activating/enhancing translation according to their phosphorylation state (Figure 21).

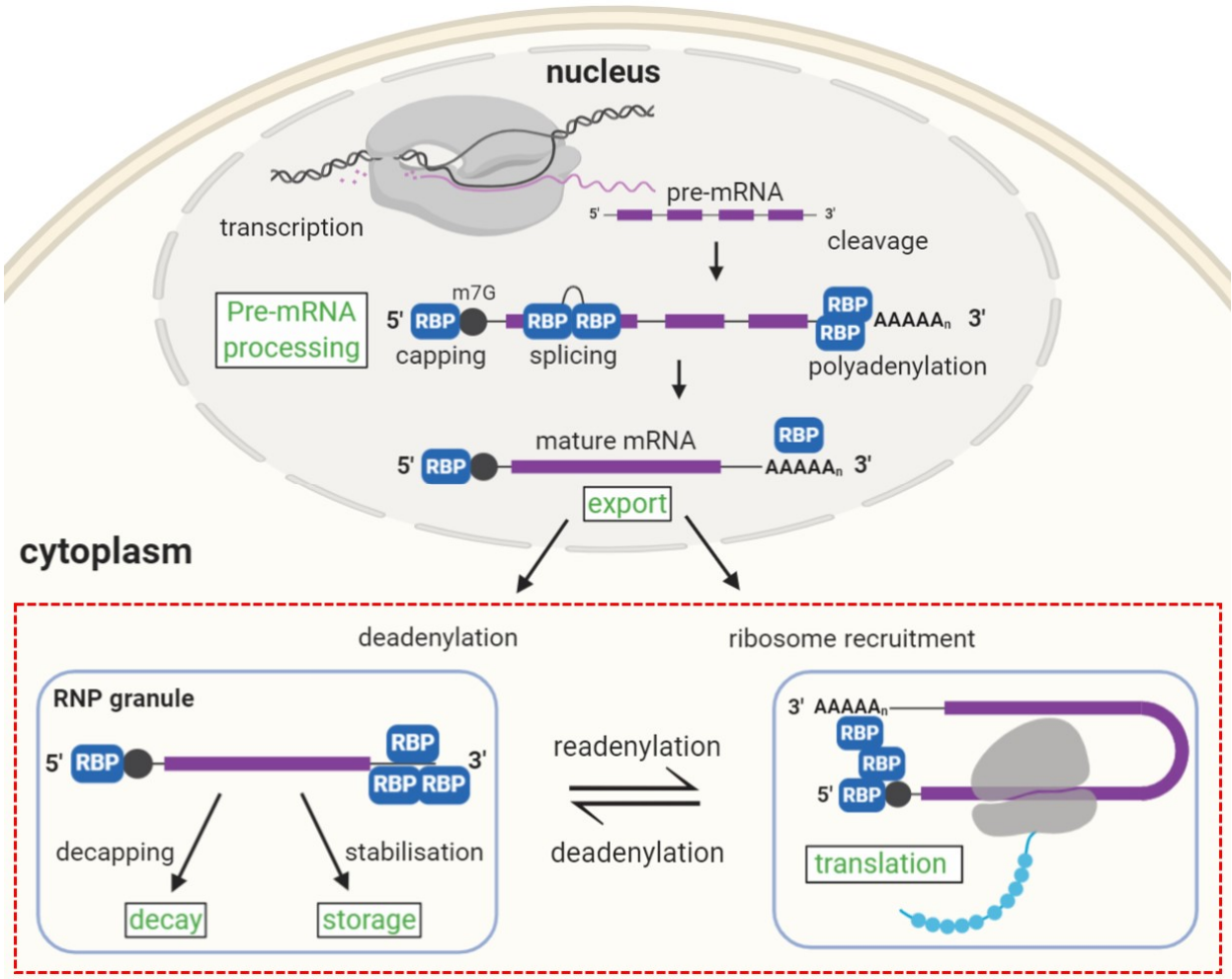

Figure 20. Nuclear and cytoplasmic post-transcriptional regulation in oocytes

The red box highlights the importance of cytoplasmic events in oocyte mRNA regulation. RBP: RNA-binding protein, RNP: ribonucleoprotein. The purple block represents coding sequence and black circle represents the 7-methylguanylate (m7G) cap. *Source: own work (created with BioRender)*

The most widely studied model for oocyte transcript dynamics is *Xenopus*, due to the quantity of oocyte material that easily be obtained in comparison with mammalian models, and this model has allowed the characterisation of many RNPs involved in translational control. RBPs whose mammalian orthologues have been shown to have important roles through mouse KO studies are listed in Table 2. The most extensively characterised mechanism involves the cytoplasmic polyadenylation element (CPE) located in the 3' UTR of many mRNAs and its binding protein CPEB1. Another involves Pumilio (PUM) proteins that recognise the PUM-binding element (PBE) [100]. Figure 21 illustrates several key 3'UTR elements and their corresponding RBPs and whether they mediate translational repression or activation. Many other oocyte RNPs

have been identified as playing important roles in oocyte mRNA regulation by mechanisms which have yet to be fully elucidated, such as Y-box-binding protein MSY2: a global regulator of mRNA stability and DAZL: which appears to be involved in translational activation by a polyadenylation-independent mechanism [97,101].

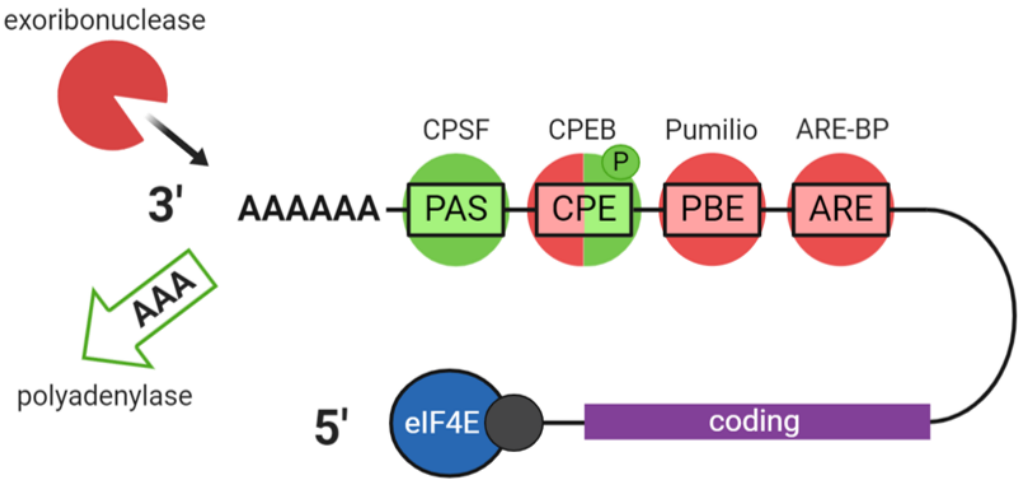

Figure 21. Key 3'UTR elements, their associated RBPs and control of poly(A) tail length.
3'UTR elements and RBPs mediating polyadenylation and translation activation are shown in green and those mediating deadenylation and translational repression in red. PAS: polyadenylation signal, CPSF: cleavage and polyadenylation specificity factor, CPE: cytoplasmic polyadenylation element, CPEB (CPEB1): CPE-binding protein, PBE: Pumilio-binding element, ARE: AU-rich element, ARE-BP: ARE-binding protein. *Source: Own work (created with BioRender)*

Gene Symbol	Full Gene Name	RNA-Binding Domain	Consensus Sequence	Associated Mouse Phenotypes	Ref
CPEB1	Cytoplasmic polyadenylation element binding protein 1	RRMx2, Znf	UUUUA(A)U	KO: females sterile. Embryonic oocyte development suspended at the pachytene stage of prophase I	[102]
CPEB4	Cytoplasmic polyadenylation element binding protein 4	RRMx2, Znf	UUUUA(A)U	KD: oocytes show impaired MI to MII transition and absence of first polar body extrusion	[103]
DAZL	Deleted in azoospermia-like	RRMx1	UUUG/CUUU	KD: oocytes showed decreased translation during late meiosis and improper spindle assembly KO: females (and males) sterile	[104]
EPABP	Embryonic poly(A)-binding protein	RRMx4	mRNA poly(A) tail	KO: females infertile. Impaired growth and lack of transcriptional silencing in GV oocytes; failed translation activation in MII oocytes	[105]
LSM14B	LSM Family Member 14B			KD: high proportion of MI-arrested oocytes	[106]
MSI2	Musashi homolog 2 (Drosophila)	RRMx2	G/AU$_{1–3}$AGU	KO: females showed impaired folliculogenesis and decrease in number of MII oocytes	[107]
MSY2	Y-box-binding protein 2	CSDx1	UCCAUCA	KO: females (and males) infertile with impaired folliculogenesis and oocyte loss.	[108]
PUM1	Pumilio 1 (Drosophila)	PUMx1	UGUAX$_{2–4}$UA	KO: diminished ovarian reserve, oocytes showed delayed meiosis	[100]
PUM2	Pumilio 2 (Drosophila)	PUMx1	UGUAX$_{2–4}$UA	KO: Females of normal fertility, possible redundancy with PUM1	[109]
ZAR1	Zygote arrest 1	PHD	A/UUUA/GUCU	KO: failed cleavage after fertilisation, some blastocysts with impaired EGA	[110]
ZAR1L	Zar1-like	PHD	A/UUUA/GUCU	KD: two-cell stage embryonic arrest	[111]
ZFP36L2	mRNA decay activator protein ZFP36L2	Znf_CCCHx2	(AUUUA)$_n$	KO (C57BL/6NTac): embryonic arrest at the two-cell stage KO (F3 strain): females anovulatory, oocytes did not mature	[112, 113]

Table 2. Mammalian oocyte RNA-binding proteins with corresponding transgenic mouse phenotypes.

Source: Adapted from Luong and Conti, 2019 [80]

RNP complexes represent spatial as well as temporal mRNA regulation, allowing for localised expression and degradation within the cell. The germ-cell equivalent of somatic P-bodies have been called 'germ granules', referring to cytoplasmic, membrane-less organelles that are unique to the germline and contain orthologues of somatic P-body proteins such as DDX6, suggesting a conserved role [114]. In many model organisms (*Xenopus*, *Drosophila*, *C. elegans* and zebrafish), germ granules are present in oocytes of all stages. In mammals, however, germ granules have been described to exist only in primordial follicle oocytes of mice under 2 weeks of age [115,116]. One study demonstrated that upon disappearance of germ cell granules or P-bodies in mammalian oocytes, a new mRNA storage region appears close to the oocyte cortex (Figure 22) [116].

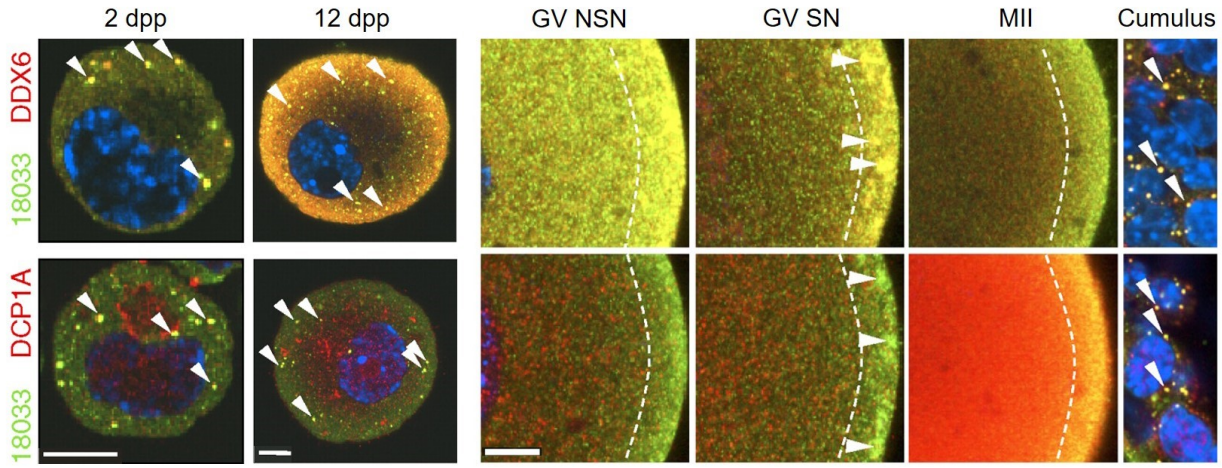

Figure 22. Germ-cell granules or 'P-bodies' in young mouse oocytes and a sub-cortical mRNA storage domain in growing/mature oocytes.
Confocal images of mouse oocytes from 2 dpp and 12 dpp females and NSN and SN GV oocytes, MII eggs and cumulus cells from adult females after staining with 18033 (stains EDC4), DCP1A, and DDX6 antibodies. Diagonal arrowheads depict P-bodies and horizontal arrowheads depict subcortical aggregates. Dashed lines border the subcortical domain. Staining with 18033 is green, other proteins are red, and DNA staining in blue. Scale bars: 10 µm. *Source: Flemr et al, 2010* [116]

Another type of RNA storage compartment identified in oocytes are Balbiani bodies: large membrane-less cytoplasmic organelles that were initially described in dormant *Xenopus* oocytes in which they were found to contain Golgi elements, mitochondria and endoplasmic reticulum as well as RNA [117]. Such structures have been reported to exist in oocytes of other vertebrate species, although in mice they have been identified only in very young oocytes, and these have not been found to contain RNA [118].

2.2. The CPEB1 mechanism

CPEB1 functions as a crucial regulator of polyadenylation and therefore of translation. Originally characterised in *Xenopus* oocytes, it has seen been shown to regulate key mRNAs in various cell types including neurons [119]. It is a zinc finger-containing protein that assembles complexes with other proteins to perform a dual functionality, capable of both translational repression and activation according to its phosphorylation state. The CPE sequence recognised by CPEB1 is UUUUA(A)U. In a computational analysis of mRNA 3' UTRs, 31% (mouse) – 36% (human) of analysed mRNAs were predicted to be involved in CPE-mediated translational regulation [98]. CPEB1 is expressed until the MI stage in mouse oocytes and controls the translation of the oocyte-specific MAP kinase-kinase-kinase c-Mos and cyclin B1, proteins crucial for the progression of meiosis [101].

In the CPEB1 mechanism, as characterised in frogs, proteins involved in poly(A) control include Symplekin (likely a platform protein), CPSF bound to the 3' UTR PAS sequence, poly(A) ribonuclease (PARN), and the poly(A) polymerase Gld2 (germ-line development factor 2). The latter two are both active with competing activities, however PARN has higher activity than Gld2, resulting in overall deadenylation of CPE-containing mRNAs. When CPEB1 is phosphorylated by the Aurora A kinase (at Ser174), its binding to Gld2 and CPSF become stronger and as a result PARN is excluded from the RNP complex, allowing Gld2 to elongate the poly(A) tail (Figure 23A) [120]. The orthologous mechanism in mammals has yet to be fully characterised, especially in light of a study in 2007 that showed that GLD2 is dispensable in mouse oocytes [121]. Polyadenylation status was unaffected in the oocytes of *Gld2* KO mice as was overall health and fertility. This indicates evolutionary divergence and the existence of an alternative source of poly(A) adenylation in the mouse.

A second mode of CPEB1-mediated translational control characterised in *Xenopus* acts through the prevention of the interaction between cap-binding eIF4E and eIF4G via an intermediary protein, thus preventing formation of the eIF4F complex (Figure 23B). This intermediary protein was long thought to be Maskin [120] and the mechanism the following: when the poly(A) tail is short, CPEB1 interacts with eIF4E via Maskin, then following Cpeb1 phosphorylation and mRNA polyadenylation, PABP binds to the poly(A) tail and binds eIF4G, which can outcompete Maskin and bind eIF4E allowing translation initiation. There is now however considerable evidence showing that the intermediary protein is more likely to be eIF4E transporter 4E-T, since Maskin

is not expressed in growing oocytes and direct evidence of Maskin and eIF4E interaction is lacking [122,123].

4E-T (or Clast4 in mice) is highly expressed in the cytoplasm of growing mouse oocytes and was identified as part of CPEB1 RNP in *Xenopus* alongside 4E-T rather than eIF4G or Maskin. It is phosphorylated during meiotic maturation in both *Xenopus* and mouse oocytes by an unknown kinase and is a partner of Xp54 (whose mammalian orthologue is DDX6) [124]. In *Xenopus* oocytes, 4E-T was shown to interact with eIF4E1b: an ovary-specific close homologue of eIF4E (70% identity) that weakly binds the 5' cap [125] and whose expression is confined to oocytes and early embryos in *Xenopus*, zebrafish and mice. A new model was proposed based on these observations for specific inhibition of translation via the eIF4E1b–4E-T–CPEB1 complex which would seem to prevent the binding of eIF4E1a to the cap structure. In this model, which requires further validation, translation is inhibited through the repressive qualities of 4E-T (and associated Xp54) bound to the 3'UTR via unphosphorylated CPEB1, which is expelled upon CPEB1 phosphorylation allowing assembly of the eIF4F complex (Figure 23B) [95].

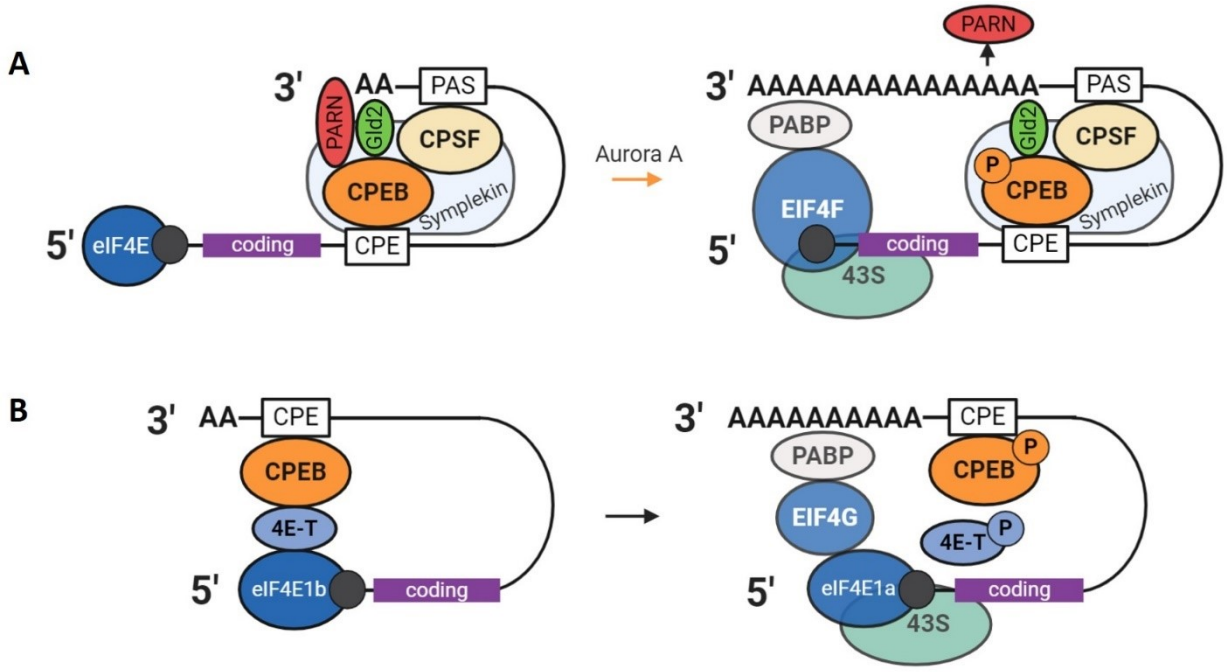

Figure 23. Models of regulation of mRNA translation by CPEB1 and associated proteins.
A) Poly(A) regulation via PARN and Gld2 as described in *Xenopus*. The transition from translational repression to activity occurs via phosphorylation of CPEB1 by the kinase Aurora A. B) Proposed model of translation regulation through binding of 4E-T with CPEB1 and eIF4E1b hindering interaction of eIF4E1a with the cap structure. *Source: Own work (BioRender), based on Kang and Han, 2011* [122]

Another member of the CPEB family, CPEB4, has also been found to play an important role in oocyte meiotic progression. CPEB1 controls the translation of CPEB4, activating it at a later stage of meiosis. CPEB4 likely replaces CPEB1, driving the transition of metaphase I to metaphase II in a positive translational loop [103].

2.3. PUM2-DAZL-EPABP

The Pumilio proteins (PUM1/2), members of the PUF protein family are involved in translational regulation in *Xenopus* oocytes. They bind to the 3' PUM-binding element (PBE: $UGUAX_{2-4}UA$) as well as the Nanos response element (NRE: UGUA) [80]. PUM1/2 are thought to mediate translational repression through interaction with the CCR4-NOT deadenylase complex [126]. PUM2 forms a complex with DAZL (Deleted in azoospermia-like) and EPABP (Embryonic poly(A) binding protein) and represses the translation of RINGO/Spy, a CDK1 activator necessary for CPEB1 and cyclin B1 activation in immature *Xenopus* oocytes [127,128]. PUM1 has recently been shown to be important in the establishment of the primordial follicle pool, meiosis and oocyte developmental competence in mice [100]. There are reports that PUM1/2 can directly bind CPEB1 [127].

DAZL and EPAPB can be considered co-repressors of translation when they are associated with PUM2. DAZL associates with uracil-rich 3' UTR sequences and is thought able to interact with a large number of oocyte RNAs as an activator of translation. In mice, DAZL is expressed until the zygote stage, plays an essential role in primordial germ cell differentiation and is thought to regulate mRNAs important for spindle assembly, meiosis and maternal mRNA degradation [104]. The proposed model for DAZL-mediated activation is via the recruitment of additional PABPs to the mRNA 3' end which facilitates additional interaction with the 5' factors and enhanced recruitment of the ribosomal subunit [129].

While PABP acts as a global translational regulator, EPABP is specific to and is the predominant poly(A)-binding protein in oocytes and early embryos in *Xenopus*, mouse and human [105]. EPABP prevents deadenylation and is required for translational activation of several key mRNAs in *Xenopus* oocytes. In *Xenopus,* EPABP is both part of the CPEB1-CPSF and DAZL-PUM2 complexes. EPABP is required for oocyte maturation and also for oocyte-granulosa cell communication in preantral follicles [126].

2.4. Other important oocyte mRNA regulators

a) MSY2/FRGY2

Germ-cell specific RNA-binding protein MSY2 (Y-box binding protein 2, in *Xenopus* Frgy2) is highly abundant in mouse oocytes until fertilisation, comprising around 2% of total oocyte protein in mice [130]. Its *Xenopus* orthologue Frgy2 is a partner of Cpeb1 and a principal component of maternal RNPs [95]. In mice, it was shown that MSY2 depletion in GV oocytes leads to aberrant oocyte growth, reduced mRNA stability, failure to halt transcription, and a dramatic disturbance of the transcriptome. 36% of oocyte transcripts were altered more than two-fold in MSY2-/- compared to WT oocytes, and there was a global decrease of 25% in mRNA quantity (despite failure to halt transcription) [97]. Since no consensus sequence was identified in the 3'UTRs of the dysregulated mRNAs, it was concluded that MSY2 likely acts as a 'master regulator' of global mRNA, conferring stability by an unknown, possibly non-sequence-specific mechanism.

b) DDX6 (Rck/p54)

DEAD-Box Helicase 6 is an RNA helicase with a diverse range of functions. It is both a decapping activator and translational repressor and is a component of all known types of RNP granules: P-bodies, stress granules and germ cell granules [131]. In *Xenopus* oocytes, its orthologue Xp54 was shown to mask maternal mRNAs as a binding partner of CPEB1, associating with mRNAs encoding proteins necessary for meiotic progression [132,133]. Xp54 localises to both the nucleus and cytoplasm, and in transcriptionally active oocytes, it binds a major set of newly transcribed mRNAs and accompanies them to the cytoplasm by an alternative export pathway. In transcriptionally quiescent oocytes (beyond GVBD), it is restricted to the cytoplasm and remains associated with mRNAs until they are required for translation, either at meiotic maturation or after fertilisation. Studies have indicated that Xp54 acts as a remodeller of RNP complexes, displacing RNA-binding proteins to accommodate others for entry into various pathways (degradation, storage or decay) and these functions are thought to be conserved in mammals, although functional studies are lacking [134].

c) Musashi (MSI)

Musashi RBPs have a double role as translational repressors and activators. They contain RNA recognition motifs in their N-terminals and bind to a Musashi binding element (MBE) in the mRNA 3' UTR. Originally described in Drosophila, Musashi has been well-characterised in *Xenopus* oocytes where it was found to be part of the Pumilio and CPEB1 pathway. RINGO/Spy-dependent CDK1 activity phosphorylates Musashi, activating translation of its target mRNAs including Mos [135]. This activation requires association of Musashi with EPABP, and interaction between Musashi and the poly(A) polymerase GLD2 has been reported [135]. Musashi proteins have been shown to be expressed in mouse GV oocytes, however their role in mammalian oocytes remains poorly studied.

d) RAP55B/LSM14B

The RAP55 (mRNA-associated protein of 55 kDa, also known as LSM14) family consists of two paralogues in vertebrates: RAP55A and RAP55B. Conserved in eukaryotes, they contain several domains (including a LSm domain) allowing for translational repression, mRNP inclusion and localisation to P-bodies and stress granules. Originally discovered as an RNA-binding in newt oocytes, xRAP55 has been found to repress translation of maternal mRNAs in *Xenopus* oocytes and interact directly with Xp54 [136]. It is expressed in *Xenopus* oocytes of all stages as well as in embryos, but was shown to be phosphorylated in matured oocytes, indicating a potential mode of action. In mouse oocytes it has been identified in Balbiani bodies and found to colocalise with Dcp1a and DDX6 [115,137]. Studies have primarily focused on RAP55A or have not made the distinction between the two paralogues, and their expression and functions have yet to be compared [138]. It was recently shown that whereas knockdown of RAP55A did not affect meiotic progression in mouse oocytes, RAP55B knockdown led to a high proportion of oocytes displaying metaphase I-arrest, chromosome misalignment, abnormal SAC and MPF activation and modified Cyclin B1 and Cdc20 mRNA levels [106].

e) Somatic cell-mediated translational regulation

As is well established, the cross-talk between the oocyte and its surrounding cumulus cells is vital for the oocyte developmental competence. It is possible that this signalling is mediated through translational regulation. Differences in the levels of certain key proteins are observed in oocytes that have matured *in vitro* to those that have matured *in vivo*. The accumulation of

certain proteins is influenced by the PI3K/PTEN/mTOR pathway (Figure 7). mTOR kinases (TORC1/2) that are downstream of cumulus cell growth factor/Kit Ligand stimulation phosphorylate 4E-BP (a cap-dependent translational repressor expressed in mammalian oocytes) during GVBD leading to its detachment from eIF4E and allowing for translational activation. Transcripts that are controlled in this way include those required for spindle assembly, chromosome alignment and segregation, such as TPX2 (Targeting Protein for the *Xenopus* kinesin xklp2) whose translation is controlled in a spatial as well as temporal manner via this pathway [139,140]. The subset of mRNAs controlled in this way may be determined by the presence of TOP (terminal oligopyrimidine) sequences in the 5' UTR of transcripts [139]. Differentially phosphorylated forms of 4E-BP have been identified on the meiotic spindle and at the spindle poles in mouse oocytes, and its phosphorylating kinases are also present on the spindle at the beginning of meiotic resumption, indicating that phosphorylation of 4E-BP promotes translation of spindle assembly components. Expression of a mutant form of 4E-BP results in spindle abnormality [141].

f) Small non-coding RNAs

Small non-coding RNAs such as microRNAs (miRNAs) and endogenous small interfering RNAs (endo-siRNAs) are important actors of post-transcriptional control and are expressed in mammalian oocytes. These small RNAs degrade or repress the expression of target mRNAs through full or partial sequence complementarity. miRNAs are transcribed by RNA polymerase III in a precursor form and processed by the Drosha/DGCR8 complex before being exported to the cytoplasm and cleaved by DICER to around 21 nucleotides. They then combine with Argonaute (AGO) proteins to form an RNA-induced silencing complex (RISC) that recognises the 3' UTR of targets. siRNAs differ to miRNAs in that they bypass Drosha/DGCR8 processing, require full sequence complementarity, and associate with AGO2 which is unique in having endonucleolytic activity.

miRNAs have been found to play a critical role in deadenylation and clearance of maternal mRNAs in zebrafish zygotes [142]. In mice however, whereas invalidation of *Dicer* or *Ago* leads to disrupted meiotic maturation and spindle formation defects in mice [126], *Dgcr8* invalidation (interfering with miRNA but not siRNA levels) did not affect oocyte or embryo development [143]. This indicates potential species-differences and a particularly important role for endo-siRNA regulation in mouse oocytes, also known to be highly active [144].

3. Waves of translation and degradation

3.1. Translational activation beyond meiotic resumption

Oocyte maturation is governed by waves of translation leading to the cascade of molecular events that are associated with meiotic resumption. CPEB1-mediated activation and polyadenylation of dormant mRNAs is thought to play a primary role. Many elements of this cascade have been elucidated in *Xenopus* oocytes, in which meiotic progression can be induced through treatment with progesterone. The chain of events leading to translational activation is not as well characterised in mammals as in amphibians due to difficulty in obtaining sufficient material. Although largely similar, certain differences, especially in the timing of events, have been reported between the amphibian and mammalian mechanisms, including later phosphorylation of CPEB1 in mammals.

Meiotic progression requires activation of kinases MAPK (mitogen-activated protein kinase) and CDK1 (cyclin-dependent kinase 1). The MAPK cascade is activated by Mos, which also combines with CDK1 to form the Maturation Promoting factor. Translation of both Mos and CDK1 is activated by CPEB1 [120]. CPEB1 activation, which occurs first near the oocyte membrane, is mediated by Aurora A kinase. The upstream events of Aurora A kinase-mediated CPEB1 activation depend on the key protein RINGO/Spy (Rapid inducer of G2/M progression in oocytes/Speedy) and its regulation via the polyadenylation-independent Pumilio-EPABP-DAZL mechanism. In *Xenopus*, this mechanism is as follows: upon progesterone stimulation, PUM2 (Pumilio) dissociates from the Pumilio Binding Element present in the 3' UTR of RINGO/Spy mRNA as well as from DAZL and EPABP. The DAZL-EPABP complex then activates RINGO/Spy translation and RINGO/Spy recruits CDK1, initiating the phosphorylation of Aurora A as well as Musashi. Aurora A kinase phosphorylates CPEB1, and Musashi induces early activation of Mos and cyclin B5 [128,135,145]. Phosphorylation of CPEB1 leads to the polyadenylation and translation of CPE-containing mRNAs by the mechanisms previously described.

One mouse oocyte study analysed polysome-bound mRNA and revealed a switch in the translation programme of mouse oocytes before and after GVBD (in MII versus GV oocytes) [104]. A third of all analysed mRNAs were recruited to the polysome (upregulated or translationally activated) or exited the polysome (downregulated or translationally repressed) by at least a two-fold factor upon meiotic maturation (Figure 24A). The 3' UTR sequences of the

translationally activated mRNAs were found to contain 2 or more CPEs, whereas those lacking CPEs were associated with downregulation (Figure 24B). The same pattern was found for DAZL-binding elements. A functional annotation of the genes with altered translation profiles during oocyte maturation is shown in Figure 24C, and shows a downregulation in genes important during oocyte growth, in particular mitochondrial transcripts, and including protein biosynthesis and ribonucleoprotein genes, and a strong upregulation in transcription regulation and cell cycle genes as well as mRNA processing. Overall these controlled pathways correspond to cell cycle and chromatin remodelling components, transcription and mRNA decay machinery as well as secreted factors.

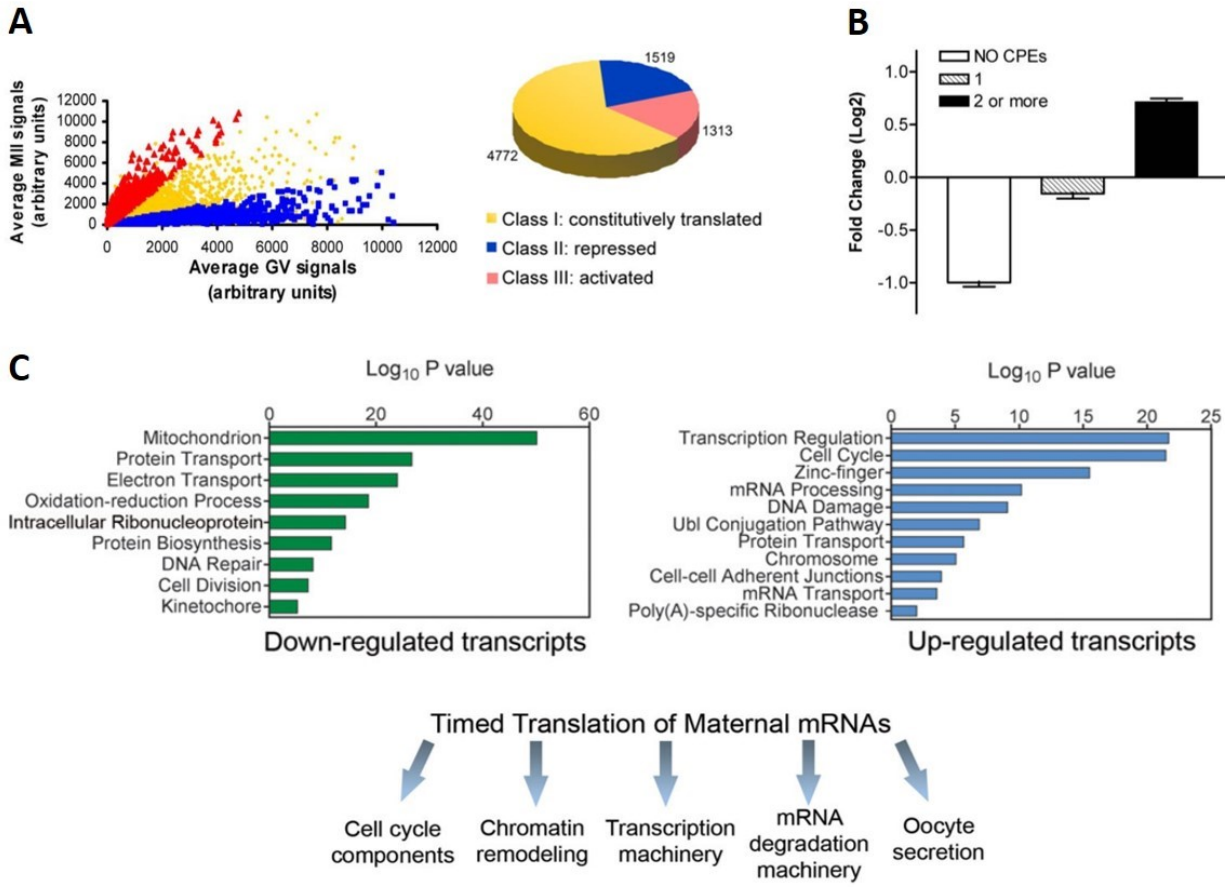

Figure 24. The oocyte translation programme.

A) Comparison of transcripts associated with the polysome in GV and MII mouse oocytes divided into three classes: constitutively translated, repressed or activated between the two stages according to a two-fold change cut-off. B) The relation between the number of CPEs in an analysis of the 3' UTRs of 4645 transcripts and log2-fold change in polysome association between GV and MII. C) Functional annotation of down-regulated (released from polysome) and up-regulated (recruited to polysome) transcripts between GV and MII. *Sources: Chen et al, 2011, Conti and Franciosi, 2018* [50,104]

Differences have been found in the timing of polyadenylation of CPE-containing mRNAs during maturation such as for Mos and Cyclin B1. Such differences could be explained by a combinatorial code of 3'UTR *cis*-elements and their *trans*-binding proteins whereby the state and timing of translational repression or activation is determined by a play-off between repressive and activating factors. Piqué et al [98] described a code based on the number and relative position of CPEs and PBEs that determined the timing of CPEB1-mediated translation in frog oocytes. A more recent study defined such a code in mouse oocyte mRNAs whereby the efficiency of translational repression and activation depended on the numbers and positions of CPEs relative to PASs [146]. Differentially timed translation activation can also be mediated by the sequential activation of RBPs, such as has been proposed for DAZL which is thought to be translationally activated during oocyte maturation by CPEB1 [104]. In this model, DAZL could be responsible for a second wave of translational activation of transcripts necessary during later stages of meiosis, in a chain that grants another layer of temporal control.

3.2. Degradation of maternal elements

The degradation of maternal mRNAs begins at meiotic resumption, during which time the quantity of poly(A) RNA decreases from 80 pg to around 50 pg per oocyte in mice. This degradation continues in the zygote and 2-cell embryo, where it drops to 10 pg [97]. As shown in Figure 25, meiotic resumption, fertilisation and EGA each trigger waves of mRNA degradation. The progressive purging of maternal mRNAs is a requirement in order to allow the embryonic genome to take control of gene expression at EGA. Disruption of the waves of mRNA degradation obstruct embryonic development [80].

Degradation of maternal transcripts is highly regulated both temporally and spatially according to a species-specific programme [147]. Generally, both maternal factors and newly transcribed zygotic factors (from the minor EGA) are involved in this process [148]. In *Xenopus*, the maternal component of the decay machinery mainly involves RNA-binding proteins that recognise 3' UTR sequences such as AREs (AU-rich element) and EDENs (embryonic deadenylation element). The EDEN binding protein (EDEN-BP) is activated and induces deadenylation upon fertilisation. Degradation of targeted maternal mRNAs then depends on the zygotic component that largely relies on small RNAs [147]. A well-characterised example in Drosophila is the maternal RBP Smaug, which deadenylates maternal mRNAs through recruitment of the CCR4-NOT complex [149].

In mice, there is a strong wave of transcript elimination that occurs shortly after fertilisation triggered by maternal factors, and a second round that coincides with the major EGA mediated by zygotic factors [73]. The programme that determines specific maternal transcript degradation in mammals is however poorly defined. One mechanism that is well characterised in mammals is the global transition to instability via MSY2 phosphorylation. MSY2, which confers stability to mRNAs during oocyte growth, is phosphorylated upon meiotic maturation by a CDK1-mediated means, such that virtually all MSY2 is phosphorylated by the MII stage [150]. The precise effect of this phosphorylation on the function of MSY2 is not clear, however the consequence is the degradation of maternal mRNAs, presumably due to loss of stability. It is likely that the phosphorylated form of MSY2 is unable to bind or otherwise protect mRNAs from the oocyte's degradation machinery [37]. MSY2 mRNA levels also drop leading to a decrease in MSY2 protein, which remains detectable at low levels until the 2-cell embryo stage.

Maternal proteins are also targeted for degradation during the maternal-to-zygote transition (MZT) by the ubiquitin–proteasome pathway [151]. The removal of germline-specific proteins and proteins involved in the MZT is an important step as many of these would interfere with the acquisition of a somatic, totipotent identity and mitotic divisions if they remained. This is another step in the erasing of the maternal legacy and handing over of control to the embryonic programme.

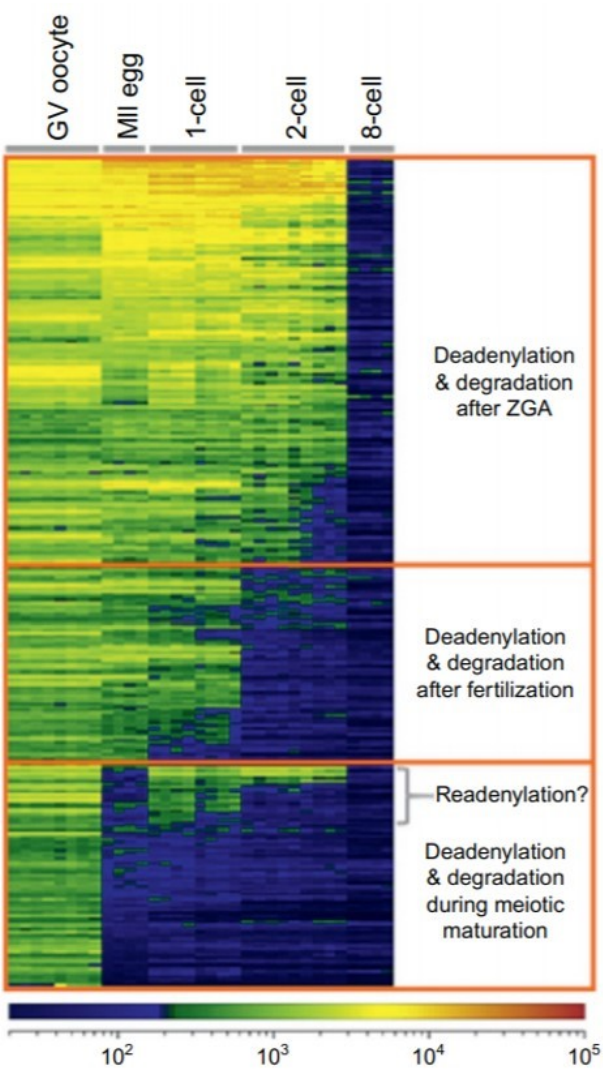

Figure 25. Microarray profiling of ~300 oocyte-specific genes during maturation.
The colour scale indicates mRNA abundance according to fluorescence intensity (arbitrary units). ZGA: Zygotic genome activation. *Source: Svoboda et al, 2015* [96]

Pat1 proteins: diverse regulators of mRNA

Pat1 (protein associated with topoisomerase II) proteins, conserved across eukaryotes, are RNA-binding proteins that have been shown to be involved in numerous aspects of mRNA metabolism. They participate in large regulatory RNP complexes and localise to P-bodies in somatic cells. A single Pat1 protein (Pat1p) exists in yeast and invertebrates, whereas in vertebrates two orthologous proteins have evolved (PatL1/Pat1b and PATL2/Pat1a) with distinct regulatory functions in the soma and germline (Figure 26A). Pat1 proteins have been implicated in mRNA decay, translational repression and, more recently, in pre-mRNA processing. Genetic invalidation studies demonstrate their importance, with phenotypes of slow growth and defective glucose starvation recovery in different yeast species and embryonic lethality in both *C. elegans* and *D. melanogaster* [152–155]. The current hypothesis is that Pat1 proteins act as scaffold or platform proteins, interacting with both mRNA and other proteins of various functions. In vertebrates, these roles appear to have been partitioned amongst the two Pat1 paralogues: somatic PATL1 appears to be primarily involved in mRNA decay and PATL2, specific to oocytes, in translational repression.

Pat1p was first identified as a protein that interacted with topoisomerase II in *Saccharomyces cerevisiae*. Topoisomerase II is an enzyme involved maintaining structural chromatin integrity by removing tangles and supercoils from the DNA helix and is essential for the separation of daughter strands after replication. Pat1p was reported to interact with a highly conserved, leucine-rich region of the Topoisomerase II protein. Pat1p-deficient *S. cerevisiae* cells had reduced viability and decreased fidelity of chromosome segregation in both mitosis and meiosis: a similar phenotype to topoisomerase II-deficient mutants [156]. However, since this original publication in 1996, there has been little mention of this aspect of Pat1p activity in the literature, with subsequent studies uncovering the post-transcriptional functions of Pat1p [157]. More recently, however, attention has returned to the possibility of a nuclear role of Pat1 in light of evidence in human cell lines that PATL1 is in fact a shuttling nucleocytoplasmic protein [158].

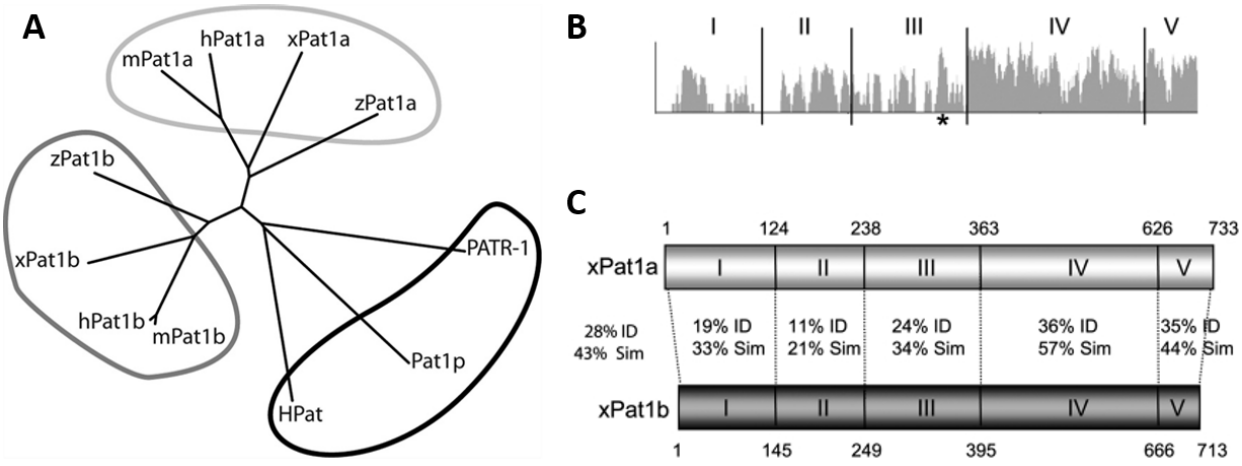

Figure 26. Phylogenetic tree of Pat1 proteins across species and sequence homology.
A) An unrooted phylogenetic tree (ClustalW). Black ring: invertebrates and yeast Pat1p. Dark grey ring: Pat1b/PATL1 proteins. Light grey ring: Pat1a/PATL2 proteins. Species nomenclature: Pat1p: *S. cerevisiae*, PATR-1: *C. elegans*, HPat: *D. melanogaster*, hPat1a/b: *Homo sapiens*, mPat1a/b: *Mus musculus*, zPat1a/b: *Danio rerio*, xPat1a/b: *X. laevis*. B) Similarity plot of the alignment of eight pairs of vertebrate Pat1 proteins (Vector NTI). The height of the peak indicates degree of similarity. C) Schematic representation of *X. laevis* Pat1a and Pat1b protein regions (not to scale). The identity (ID) and similarity (sim) scores between delineated domains of xPat1a and xPat1b are indicated (Ebi, EMBOSS pairwise alignment tool). *Source: Marnef and Standart, 2010, Marnef et al, 2010* [159,160]

Despite its known functions in mRNA regulation as part of an RNP complex, Pat1 proteins contain no recognisable motifs or features for RNA or protein interaction. Functional domains have been defined through deletion studies (Figure 27A). A consistent functional delineation is the distinction of a proline-rich N-terminal and a long C-terminal, dividing the protein roughly in half. The C-terminal is commonly subdivided into a 'Mid' region and 'Pat-C' region. The consensus is that the C-terminal, which shows the highest degree of conservation between paralogous and orthologous Pat1 proteins (Figure 26 B,C), is the domain responsible for both decapping and translational repression functions. The N-terminal shows much lower sequence conservation and is thought to be largely disordered. It has been associated with functions including deadenylation and CCR4-NOT association, contains the nuclear export sequence in PATL1 and features a region present in many, but not all Pat1 homologues that associates with DDX6/Xp54/Dhh1 (which in flies also binds Edc3 in a mutually exclusive manner) (Figure 27A) [157]. All tested Pat1 proteins have been shown to be able to bind mRNA, and the Mid domain

has been shown to bind RNA directly, although a consensus binding sequence has not been found [158,161,162].

The crystal structure of the Pat-C region of human PATL1 was resolved and published in 2010 [163] (the structure of yeast Pat-C has since also been published [164]) and was revealed to form an α-α superhelix, a feature commonly associated with scaffold structures for protein or nucleic acid interactions (Figure 27B). This structure is thought to be common to all Pat1 proteins. Full structural analysis has so far not been possible due to difficulties in purifying the full-length recombinant protein [218].

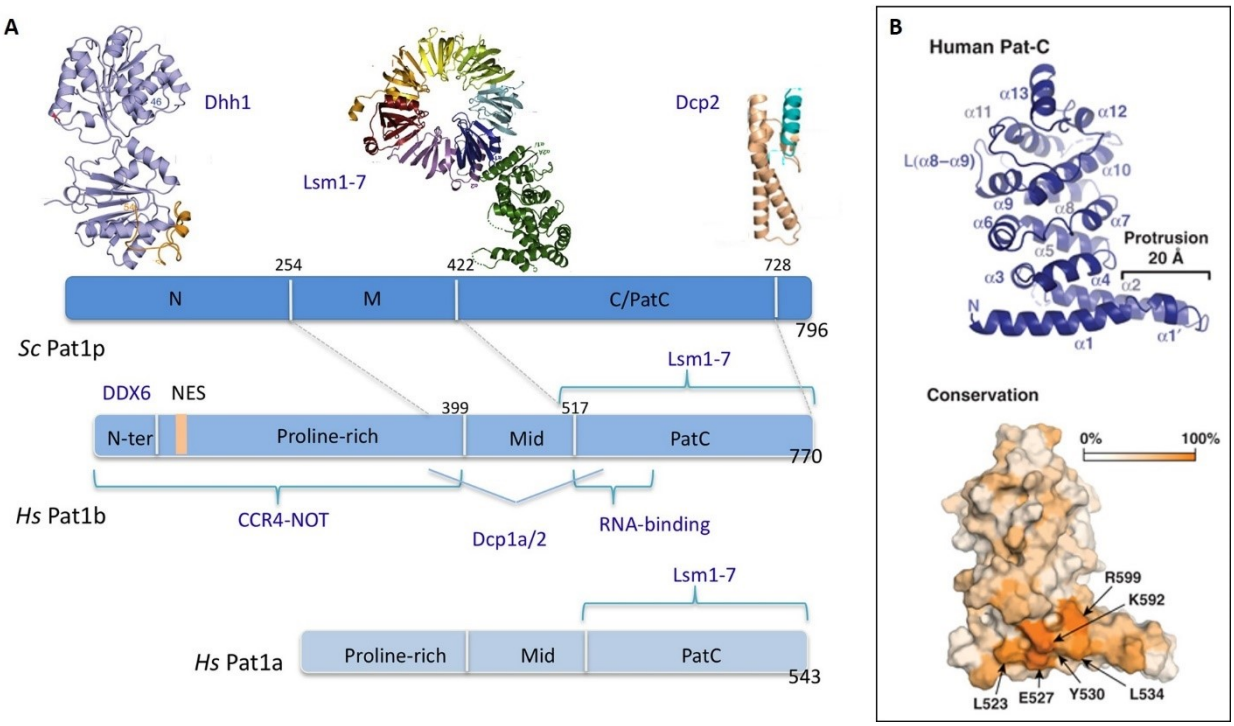

Figure 27. Pat1 functional domains and the Pat-C crystal structure.
A) Representation of domain architecture for yeast Pat1p (top), human PATL1/Pat1B (middle) and human PATL2/Pat1a (bottom) showing identified interaction sites with other proteins. B) Crystal structure of human PATL1 Pat-C domain: Ribbon diagram (top) and Surface representation (bottom), coloured by sequence conservation amongst six species. The colour reflects sequence identity: white (0%) to orange (100%). Highly conserved solvent-exposed residues are labelled (structural representations were generated using Pymol). *Sources: Vindry et al, 2019 and Braun et al, 2010* [163,165]

3.3. Pat1/PatL1 proteins in mRNA processing and decay

Pat1p was co-purified with the Lsm1-7 complex, which binds U-rich sequences near the 3' end of oligoadenylated mRNA, and the Xrn1 5'-3' exoribonuclease in yeast in a study published in 2000 [166]. They found that Pat1 deletion increased the half-lives of reporter mRNAs, which retained their 5' caps despite deadenylation, suggesting a role for Pat1p in mediating decapping and 5'-3' degradation. This role has been corroborated by many subsequent studies, and Pat1 proteins have been found to interact with a number of proteins involved in mRNA decay, including CCR4-NOT deadenylation enzymes, the DCP1/2 decapping complex and decapping co-activators Edc3 and 4 and DDX6 (Dhh1 in yeast) [162,167].

The exact mechanism by which Pat1 promotes decapping remains to be fully understood. Only recently has some light been shone on this mechanism in yeast. Co-crystallisation of Pat-C and the Lsm1-7 complex revealed conserved Pat1 residues that physically interact with Lsm2 and 3 [168,169]. Lobel et al (2019, preprint [170]) showed that, whereas the Pat-C domain alone is sufficient for Lsm-binding, short-linear motifs located within the Pat1 Mid domain are required to stabilise the binding of the complex to RNA, possibly through RNA-binding itself [163,170]. They also revealed that Pat1 binds helical leucine-rich motifs (HLMs) in the C-terminal region of Dcp2 via its own C-terminal. Charenton et al (2017 [171]) also showed that Pat1p interacted with a HLM in yeast Xrn1 via the same site (the specific site required for these interactions is however fungus-specific). Overall this implies a model by which Pat1p interacts with factors acting at both the 3' and 5' mRNA ends, providing a link between deadenylation and decapping (illustrated in Figure 28B).

The localisation of Pat1p to cytoplasmic P-bodies has been well-documented. It is thought to act as a scaffold for several P-body proteins, including those involved in 5'-3' decay and others involved in translational repression [172,173]. PATL1 also strongly localises to P-bodies in mammalian cell lines and plays an instrumental role in their assembly [174]. On top of its well-characterised and predominant cytoplasmic function, recent evidence has described a dual, nuclear function for PATL1 after the identification of a CRM1-dependent nuclear export signal (NES) [158,165]. A potentially phosphorylated form of PATL1 was found localised to several types of nuclear RNP granules in proliferating HEK293 cells as part of a complex with LSM2-8 (Figure 28), representing an estimated 15% total PATL1 protein [165]. Deletion of PATL1 in HEK293 cells followed by RNA-sequencing revealed alterations in a number of alternative splicing events

involving skipping of exons with weak donor sites [165]. These data reveal a fascinating dual role for PATL1 at the level of pre-mRNA processing. A summary of the cytoplasmic and nuclear functions of PATL1 is given in Figure 28.

Regarding the mRNA transcripts that are targeted by Pat1 proteins, transcriptomic studies in *Pat1p*, *Lsm1* and *Dhh1* yeast knockout strains revealed significant overlap between the groups of mRNAs that were upregulated in the Pat1p and Lsm1 deficient strains, which partially overlapped with that of the Dhh1 deficient strain, and it was concluded that Dhh1 and Pat1/Lsm1 target specific gene subsets through unique features [175]. Interestingly, in PatL1-deficient HEK293 cells, transcripts containing 3' AU-rich elements (AREs) were upregulated, representing a major group of mRNAs that are particularly enriched in P-bodies, in line with previous observations that Pat1p binds poly(U) sepharose beads [167]. This is in contrast with DDX6, which targets GC transcripts [165]. These results indicate that, although a specific binding sequence has not yet been identified, PATL1 controls a specific group of mRNAs.

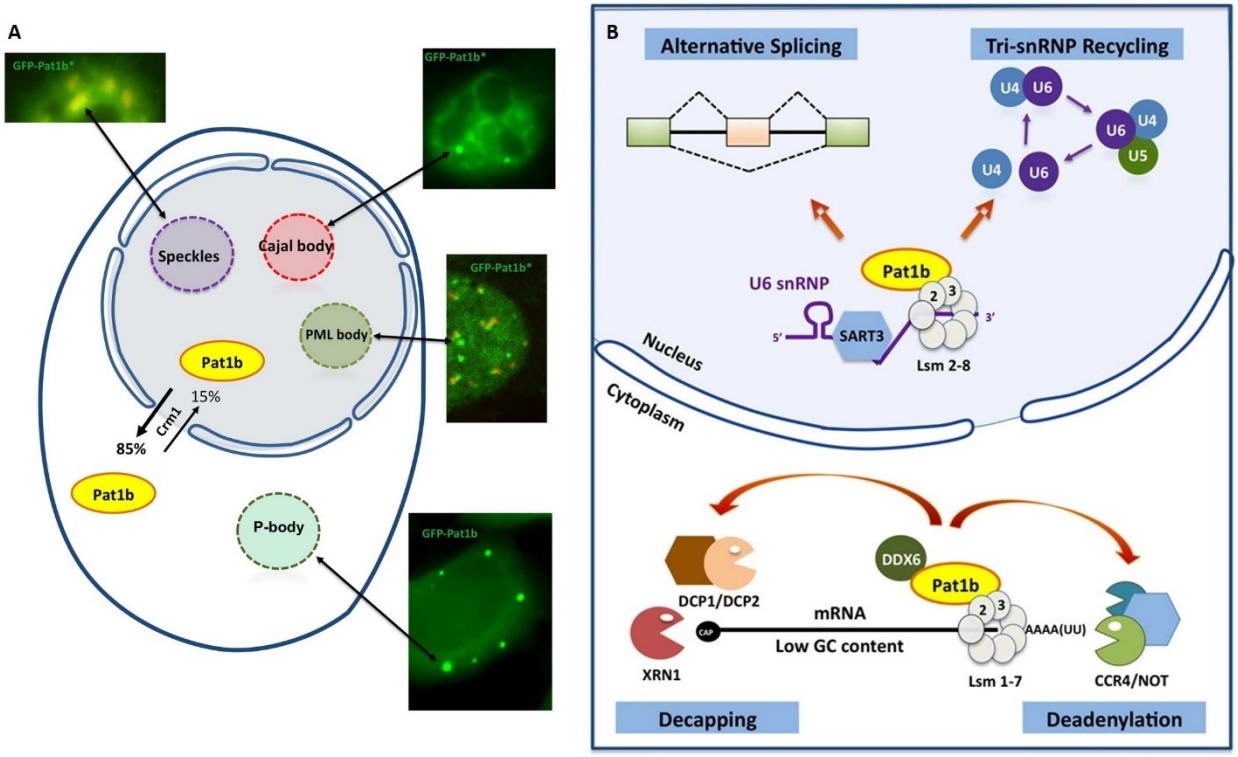

Figure 28. Dual cytoplasmic and nuclear roles of human PATL1(Pat1b).
A) Subcellular distribution of human PatL1 in cytoplasmic and nuclear granules and localisation of GFP-PatL1 and GFP-PatL1-NES* (inactivated NES) in cytoplasmic P-bodies and nuclear Cajal bodies, splicing speckles and PML bodies in HeLa cells. B) Summary model of Pat1b's functions in cytoplasmic mRNA decay and nuclear alternative splicing. *Source: Vindry et al, 2019* [176]

3.4. Pat1p and PATL2 (Pat1a) in translational repression

The translational repression aspect of Pat1 proteins appears to be specific to yeast Pat1p and vertebrate PATL2/Pat1a. In yeast, Pat1p, together with Dhh1, is required to repress translation upon glucose starvation [177]. Overexpression of Pat1p in yeast (and of Dhh1, but not of Dcp1) led to a reduced rate of translation (indicated by a decrease in ^{35}S methionine incorporation) and induced relocation of certain mRNAs from the polysome to RNP granules, without affecting overall mRNA abundance. Polysomes were also dramatically reduced and P-body abundance increased [177]. It was suggested that both Pat1p and Dhh1 relocate translating mRNAs from the polysome and assemble P-bodies, and that additional steps were required downstream to initiate decay. Pat1p also repressed translation *in vitro* in a yeast cell-free system [152].

This role in the regulation of translation is probably mediated via Pat1p's interaction with translation initiation factors such as the 40S ribosomal subunit [152] and RNA-independent interaction with Pab1p (yeast poly(A) binding protein), eIF-4E and eIF4G [178]. Nissan et al (2010) observed that the Pat1p Mid+PatC domain reduced the accumulation of 48S complexes in a translation assay whereas it did not affect formation of the 43S complex, suggesting that Pat1p limits the interaction of the 43S complex with mRNA [179]. This function appears to be mediated primarily by the Pat1 C-terminal, however an inhibitory role has also been reported for the Pat1 N-terminal, possible through its binding to Dhh1/DDX6 [179].

When tethered to an mRNA reporter, both *Xenopus* Pat1a and Pat1b (introduced experimentally) repressed translation in oocytes without decapping (likely due to the intrinsically low decapping activity of the oocyte environment), however this is not thought to reflect a true function for endogenous xPat1b, especially since it is not normally expressed in oocytes [160]. Tethering human PATL1 to reporter mRNA in human cell lines induced a drop in reporter activity correlated with the drop in mRNA levels [174,180], indicating that the role of human PATL1 is restricted to mRNA degradation. Interestingly, human PATL2 had no decay or repression effect on tethered mRNA in human cell lines, in which it is not normally expressed [173]. This indicates a high importance of cellular context in the functions of these paralogous proteins. This difference in translational repression activity between human and *Xenopus* Pat1a/PATL2 when tethered to mRNA could be due to sequence differences in the N-terminal, since human PATL2 lacks the DDX6 interaction domain which is present in *Xenopus* Pat1a [176]. Human PATL2 also does not localise to P-bodies when expressed in mammalian cells [160].

a) Vertebrate Pat1a/PATL2 and its oocyte-specific function

Xenopus Pat1a was identified as a cytoplasmic RNP in growing oocytes [181,182]. Originally named P100, xPat1a was found able to selectively bind RNA. It was later identified through mass spectrometry and co-immunoprecipitation as an abundant binding partner of CPEB1 [125,136]. In *Xenopus,* Pat1a was shown to be specific to oocytes (Figure 29A), to be expressed uniquely in the cytoplasm (Figure 29B) and to degrade rapidly after GVBD induced by progesterone and replaced by xPat1b (Figure 29C) [160,183]. This degradation pattern is also what is observed for CPEB1 in *Xenopus* oocytes. xPat1a has a 19% sequence identity with yeast Pat1p, 28% identity with xPat1b and 34% identity with human PATL2 (EMBOSS Needle).

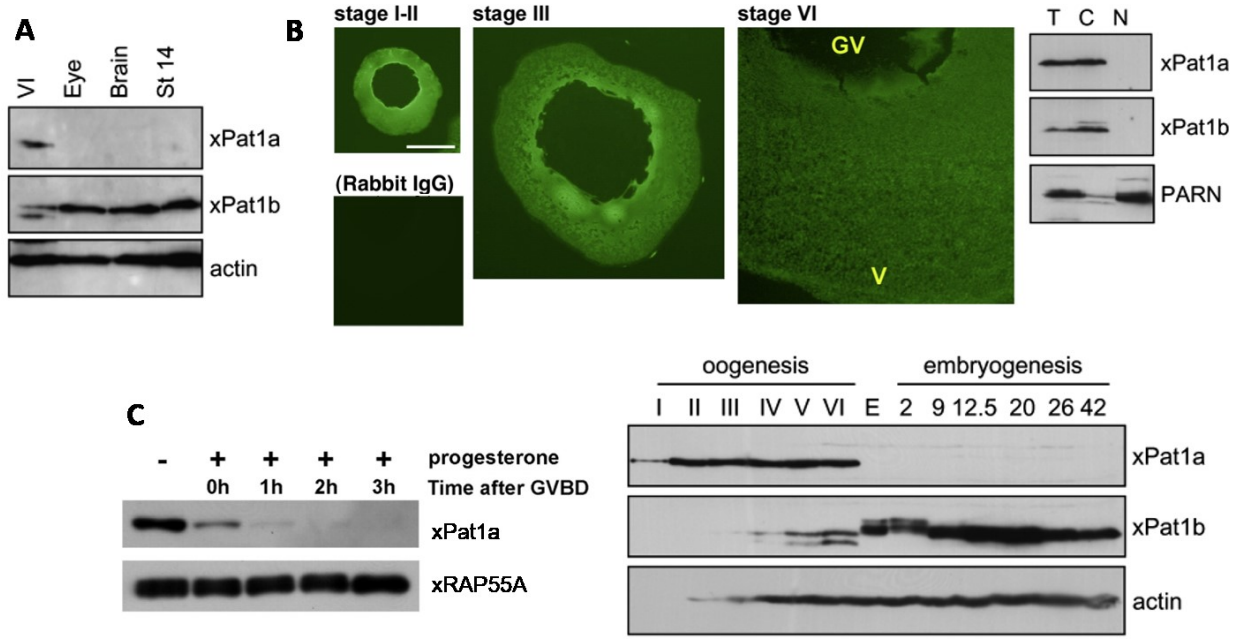

Figure 29. Expression profile of xPat1a.

A) Western blot with a single stage IV oocyte, eyes (n=10) and brains (n=5) of stage 42 embryos, and one Stage 14 embryo. B) Sections of stage I–II, III, and VI oocytes stained with anti-xPat1a antibody or rabbit IgG. GV: germinal vesicle, V: vegetal region. Scale bar: 100 µm. C) Left: Western blot showing the disappearance of xPat1a in oocytes after GVBD: stage VI oocytes were incubated in the absence (−) or presence (+) of progesterone and collected just after the appearance of a white spot (0 h), or at the indicated time points after the appearance of white spots. Right: Western blot of xPat1a and xPat1b expression levels in oocytes stages I–VI, egg, and different embryonic stages (two-cell, stage 9: midblastula, stage 12.5: gastrula, stage 20: neural fold closure, stage 26: tail-bud stage, stage 42: tadpole-like stage). *Sources: Nakamura et al, 2010, Marnef et al, 2010* [160,184]

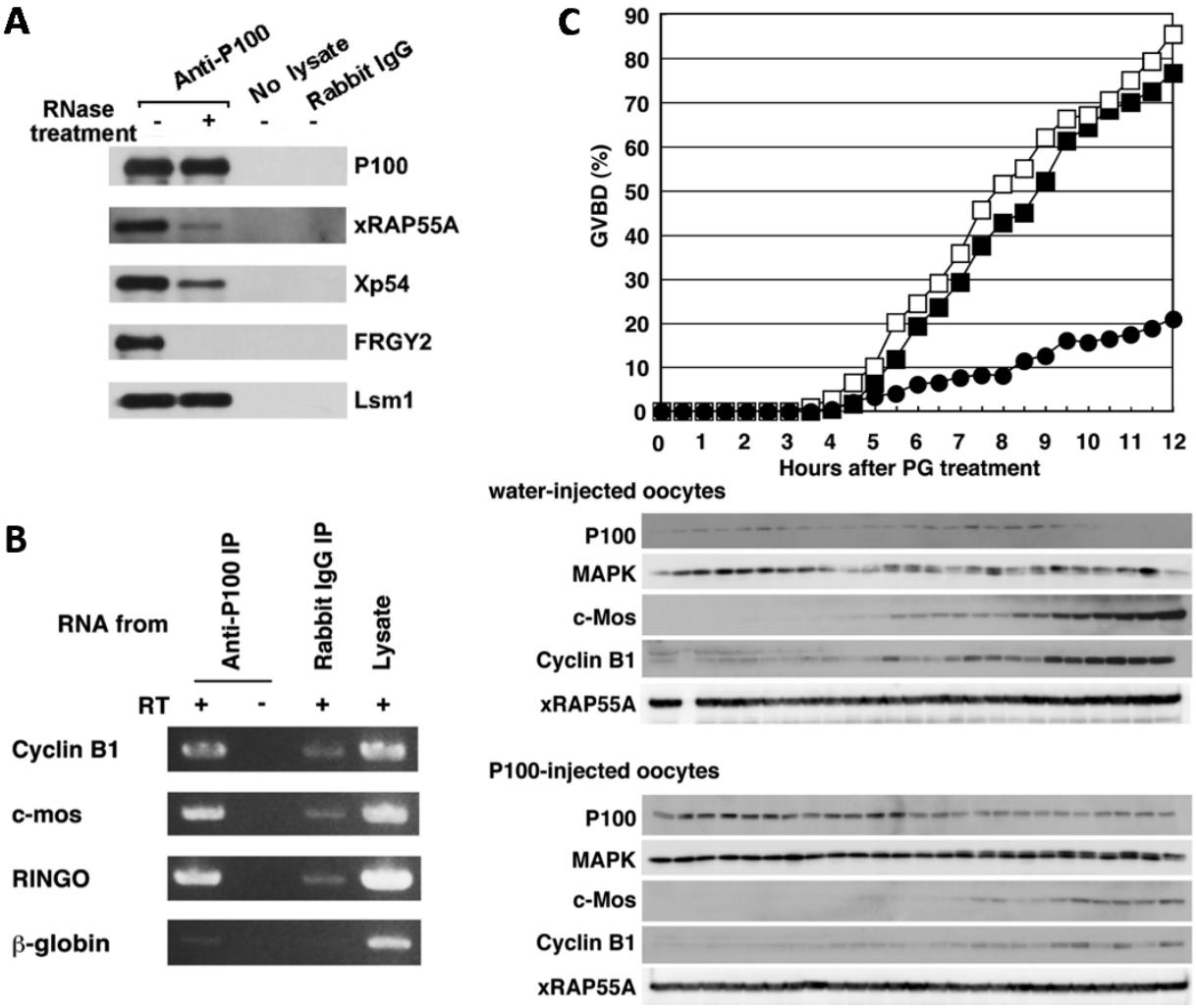

Figure 30. Characterisation the xPa1a RNP and effect of xPa1a overexpression on oocyte maturation.

A) Lysates were prepared from small oocytes (stages I–III) with (+) or without (-) RNase treatment. Anti-xPat1a antibody beads or rabbit IgG beads were incubated with (or without) oocyte lysate. Bound proteins were resolved by SDS-PAGE. xPat1a(P100), xRAP55A, Xp54, FRGY2 and Lsm1 were detected by immunoblotting. B) RNA immunoprecipitated with anti-xPat1a(P100) antibody or rabbit IgG from oocyte lysates was used as templates for RT-PCR. C) Oocytes were injected either with 45 ng of xPat1a(P100)-FLAG-C mRNA (closed circles) or water (open squares), or not injected (closed squares), incubated for 12–14h, then stimulated with progesterone (PG). Oocytes were scored as a fraction of time for GVBD (top) and collected and analysed for MAPK, c-Mos, Cyclin B1 and xRAP55A by immunoblotting (bottom) every 30 min after progesterone addition. The higher band is the phosphorylated form of MAPK. (The sample at 0.5 h of water-injected oocytes is missing in immunoblots for c-Mos, cyclin B1 and RAP55A). *Source: Nakamura et al, 2010* [184]

As well as CPEB1, xPat1a has been found (through mass spectrometry analysis and co-immunoprecipitation) to interact with Xp54(DDX6), xRAP55A, xRAP55B, 4E-T and Lsm1 in an at least partially RNA-independent manner, and FRGY2/MSY2 in an RNA-dependent manner (Figure 30A) [125,136,184]. Other co-immunoprecipitated proteins included EPABP, eIF4E1b and the mRNA-binding proteins Vera, Elavl2 (ELAV Like RNA Binding Protein 2, Binds poly(U) elements and AU-AREs in the 3'-UTR) and Zar1 (Zygotic arrest 1) [160,183]. mRNAs that co-precipitate with the xPat1a complex included Cyclin B1, c-Mos and RINGO (Figure 30B).

When xPat1a was overexpressed in stage VI *Xenopus* oocytes by microinjection of xPat1a mRNA (followed by 16-18 hours incubation), there was no effect on the global rate of translation as measured by [^{35}S] methionine and cysteine incorporation. However, xPat1a overexpression repressed translation of luciferase reporter mRNA (as measured by luciferase activity) to around 35%, whereas virtually no repression was observed for reporter chloramphenicol acetyltransferase (CAT) mRNA. This reinforces the idea of xPat1a controlling a subset of mRNAs. Tethering xPat1a to luciferase mRNA further decreased luciferase activity to 20% [183].

Ectopic expression of xPat1a significantly impaired the ability of oocytes to mature upon progesterone stimulation. Whereas endogenous (as well as exogenous) xPat1a protein is rapidly broken down after GVBD (Figure 30C), microinjection of xPat1a mRNA leads to its continued synthesis despite progesterone treatment. This continued expression of xPat1a protein resulted in around 20% of oocytes undergoing GVBD 12 hours after progesterone treatment compared to around 85% in water-injected oocytes, reduced accumulation of c-Mos and cyclin B1 protein, which became detectable later and at lower levels than in water-injected oocytes, and delayed the phosphorylation of MAPK by several hours (Figure 30C). These latter effects are likely linked to blocked meiotic maturation in the presence of xPat1a, as indicated by the absence of GVBD in a large proportion of oocytes (the distinction between GV and GVBD oocytes is not made in the subsequent analysis) [183].

Studies on mammalian PATL2, which is almost 200 amino acids shorter in length than amphibian Pat1a (543 aa in *homo sapiens* and 733 aa in *Xenopus,* sequence identity 34%) and lacking large sections of the N-terminal domain including the DDX6 interaction region, had until now been restricted to mammalian cell lines in which it is not naturally expressed.

Chapter 2: Male gametogenesis and protease inhibitors

1. The male reproductive system

The purpose of the male reproductive system is to produce and deliver mature spermatozoa into the female reproductive tract. Sperm cells are produced in the testes within the seminiferous tubules in a process known as spermatogenesis. Spermatozoa ripen and are stored in the epididymides until ejaculation, upon which they pass through the vas deferens to the seminal vesicle and prostate where seminal fluid is added. Transport to the penis for delivery along with other seminal components are facilitated by accessory ducts and glands. Semen is pushed out of the penis through the urethra.

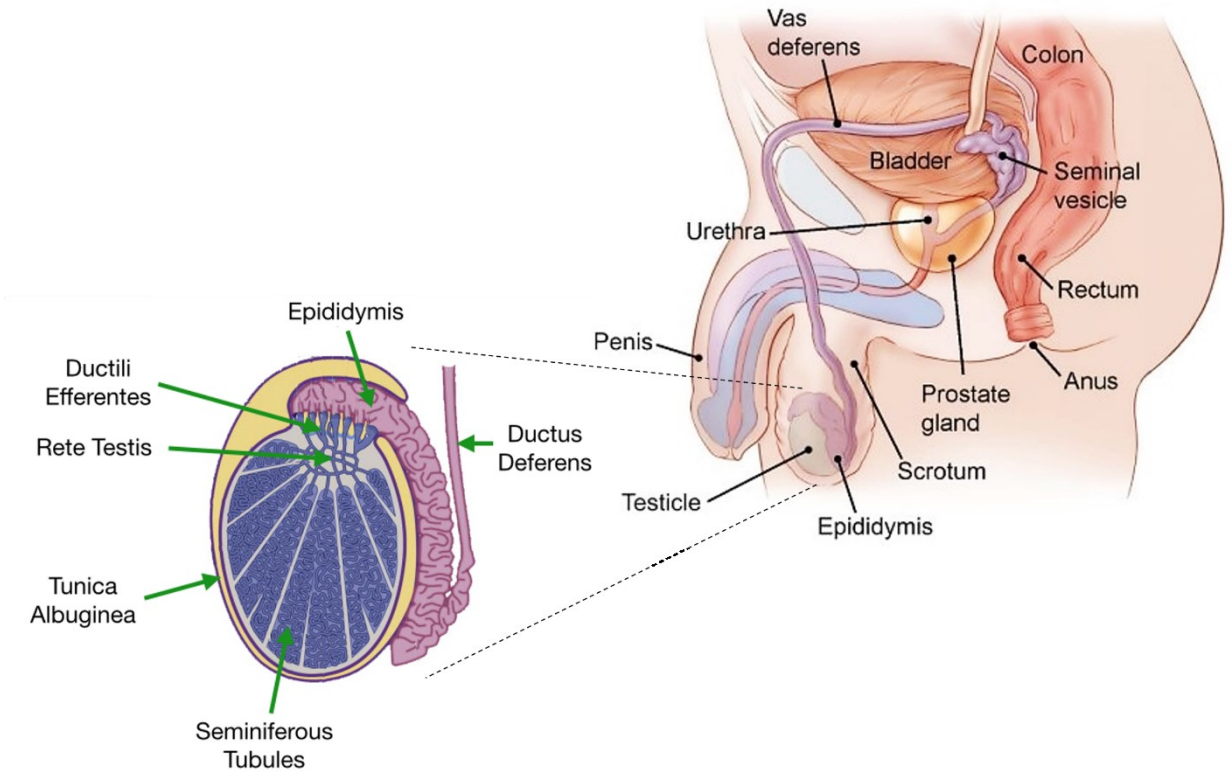

Figure 31. Anatomy of the male reproductive system and vertical cross-section of the testis.
Source: Adapted from American Cancer Society (https://www.cancer.org/content/dam/cancer-org/cancer-control/en/cancer-types/testicular-cancer-complete.pdf) and Yale School of Medicine (http://medcell.med.yale.edu/histology/testis_sperm_development.php)

The coiled seminiferous tubules are the major component of the testes. Undifferentiated germs cells (spermatogonia) embedded in the walls of the tubules in a base of Sertoli cells are renewed via mitosis and undergo spermatogenesis to form spermatozoa. Spermatozoa develop and migrate towards the hollow centre of the tubules, known as the lumen, as they progress through the stages of spermatogenesis and spermiogenesis. Spermatozoa pass through the lumen along the testis duct system, through the rete testis and are transferred to the epididymis where they complete their maturation.

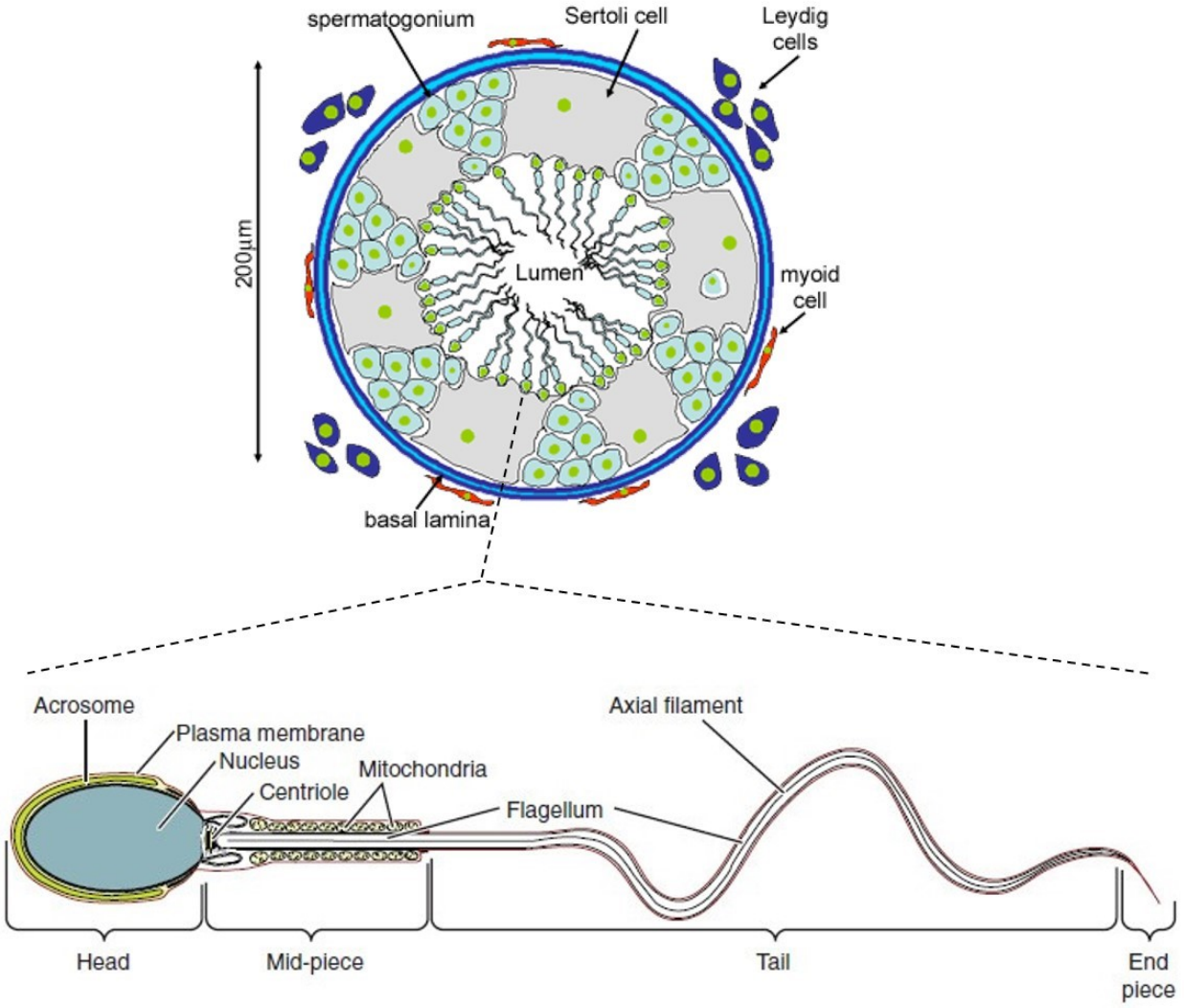

Figure 32. Anatomy of the seminiferous tubule (longitudinal cross section) and spermatozoa.
Source: Adapted from Open Educational Resources (https://courses.lumenlearning.com/suny-ap2/chapter/anatomy-and-physiology-of-the-male-reproductive-system/) and University of Leeds histology guide (https://www.histology.leeds.ac.uk/male/sertoli_cells.php)

1.1. The hypothalamic-pituitary-gonadal axis

As in females, the hypothalamus secretes GnRH (gonadotropin-stimulating hormone) which stimulates the pituitary to produce FSH (Follicle stimulating hormone) and LH ((Luteinising hormone). These hormones then act through receptors on testicular cells, which in return secrete testosterone as a feedback signal. In secreting testosterone, the testes also play an important endocrine function for male reproductive physiology. Testosterone is produced and secreted by the Leydig or interstitial cells in response to LH signalling. FSH stimulates the Sertoli cells to produce androgen binding protein (ADP) which increases the testicular testosterone to a level high enough to promote and maintain spermatogenesis. High circulating testosterone has a negative feedback effect on the hypothalamus and inhibits GnRH and LH production. Inhibin, secreted by the Sertoli cells in response to testosterone, inhibits FSH production as an auto-regulatory mechanism for sperm production [185].

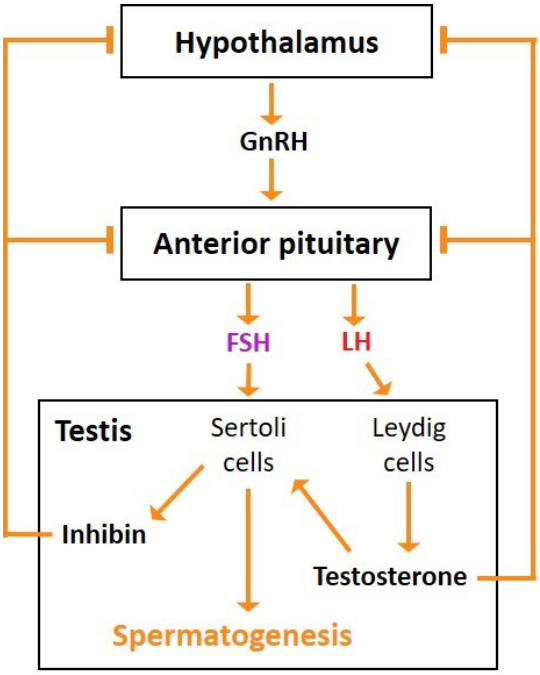

Figure 33. Hormonal control of the male reproductive cycle.
The hypothalamic-pituitary-gonadal axis and spermatogenesis. Arrows indicate positive feedback and bars indicate negative feedback. *Source: Adapted from Open Educational Resources (https://courses.lumenlearning.com/boundless-ap/chapter/physiology-of-the-male-reproductive-system/)*

2. Spermatogenesis

Spermatogenesis is the process of sperm production from primordial germ cells (PGCs) that occurs within the seminiferous tubules from puberty onwards. Around 100 million sperm cells are produced in each testis per day. Several key differences that exist between male and female gametogenesis are given in Table 3. Spermatogenesis can be divided into two main stages: spermatocytogenesis and spermiogenesis, which occur in continuous succession in a cycle that takes approximately 64 days in humans (Figure 34A). Spermatocytogenesis involves a mitotic amplification step which ensures the proliferation and maintenance of spermatogonia and a meiotic reductive step whereby spermatogonia evolve into spermatocytes and then haploid spermatids. Spermiogenesis is the post-meiotic differentiation step during which spermatids differentiate into mature spermatozoa.

Female oogenesis	**Male spermatogenesis**
Meiosis initiated once in a finite population of cells	Meiosis initiated continuously in a mitotically dividing stem cell population
One gamete produced per meiosis	Four gametes produced per meiosis
Completion of meiosis delayed for months or years	Meiosis completed in days or weeks
Meiosis arrested at first meiotic prophase and reinitiated in a smaller population of cells	Meiosis and differentiation proceed continuously without cell cycle arrest
Differentiation of gamete occurs while diploid, in first meiotic prophase	Differentiation of gamete occurs while haploid, after meiosis ends
All chromosomes exhibit equivalent transcription and recombination during meiotic prophase	Sex chromosomes excluded from recombination and transcription during first meiotic prophase

Table 3. Comparison of meiotic process in male and female gametogenesis.
Source: Handel and Eppig, 1997 [186]

The spermatogonial stem cell population (Type A spermatogonia) is rooted in the basal lamina of the seminiferous tubules (Figure 34B). The testes contain over a billion spermatogonia, which divide by mitosis, simultaneously renewing their own population and giving rise to type B spermatogonia. The latter are committed to differentiated into spermatozoa and they continue to divide by mitosis, with their daughter cells migrating towards the lumen. A final mitotic division gives rise to primary spermatocytes which immediately enter the S phase of meiosis I, replicating their DNA, followed by prophase. Prophase lasts around 24 days and is divided into leptotene, zygotene, pachytene, diplotene and diakinesis stages. During this time, chromosomal cross-over occurs between homologous chromosomes. The final stages of meiosis I are shorter

and give rise to secondary spermatocytes, which immediately begin the second meiosis. The second meiosis takes around 5 hours and produces haploid spermatids. During these processes, the spermatogenic cells are structurally and metabolically supported by the Sertoli cells, which also form the blood-testis barrier.

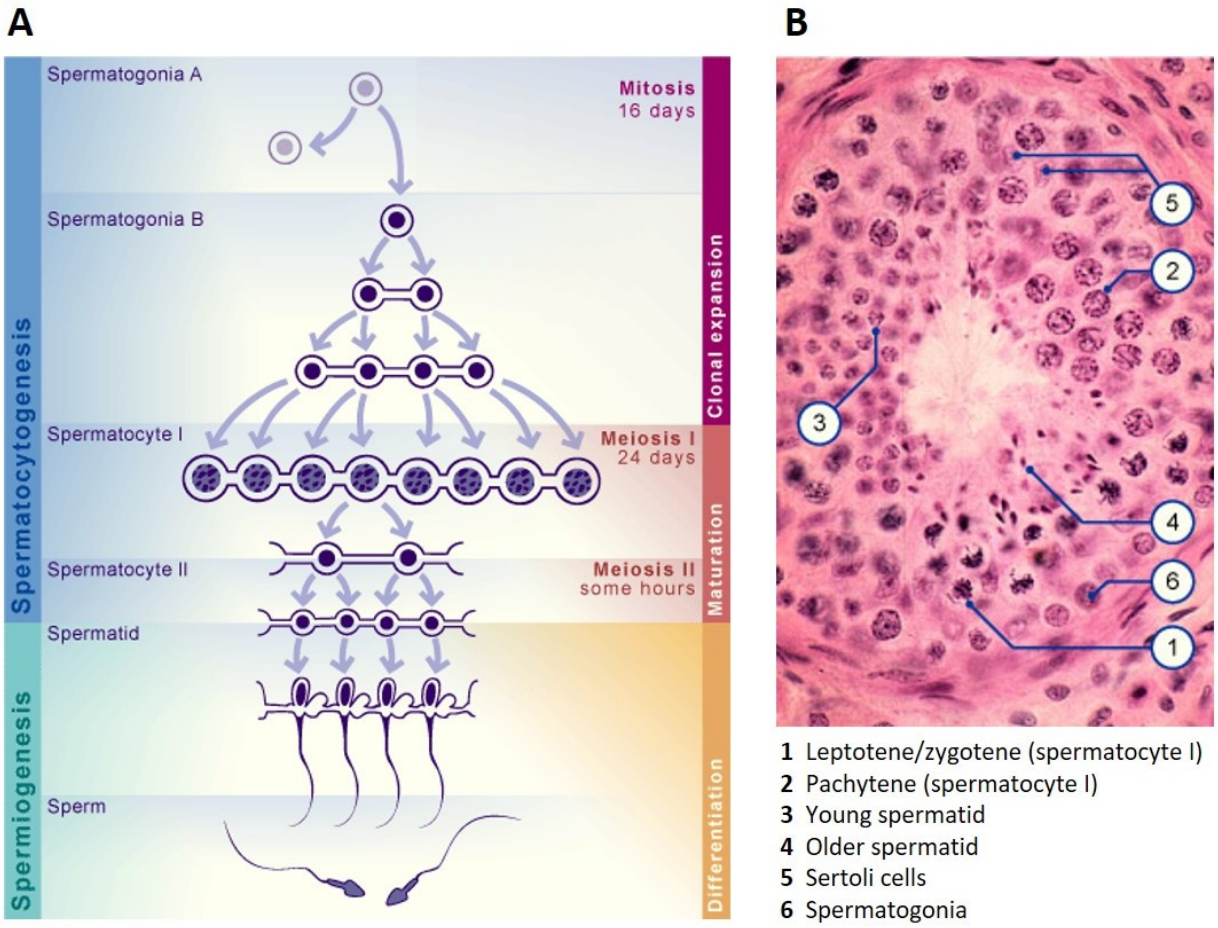

Figure 34. Stages of spermatogenesis.
A) Generations of spermatogenesis divided into spermatocytogenesis and spermiogenesis with time scale indicated. B) Stained seminiferous tubule cross-section (mouse, light microscope) with examples of developmental stages. *Source: embryology.ch (Universities of Fribourg, Lausanne and Bern)*

3. Spermiogenesis

Several events must occur during spermiogenesis, namely compaction of the nucleus, cytoplasm reduction and acrosome and flagellum formation. Distinct phases can be observed: 'young' spermatids with a round central nucleus and the beginnings of an acrosome and axoneme, older spermatids with an elongated nucleus polarised to one side of the cell and mature spermatozoa with a fully condensed nucleus. Acrosome biogenesis begins at the pachytene stage with the fusion of pro-acrosomal vesicles from the Golgi apparatus, which begin to attach to the nuclear envelope during the round spermatid stage to form the acrosomal cap [187]. Once the acrosome cap has formed, the nucleus rotates such that the cap is facing the outer surface of the seminiferous tubule. The flagellum forms from the centriole on the opposite side which extends inwards into the lumen. The flagellum assembles around a central microtubule-based structure known as the axoneme consisting of a central pair and 9 peripheral doublets. Accessory structures: a mitochondrial sheath, fibrous sheath and outer dense fibres form around the axoneme as the spermatid elongates (Figure 35) [188].

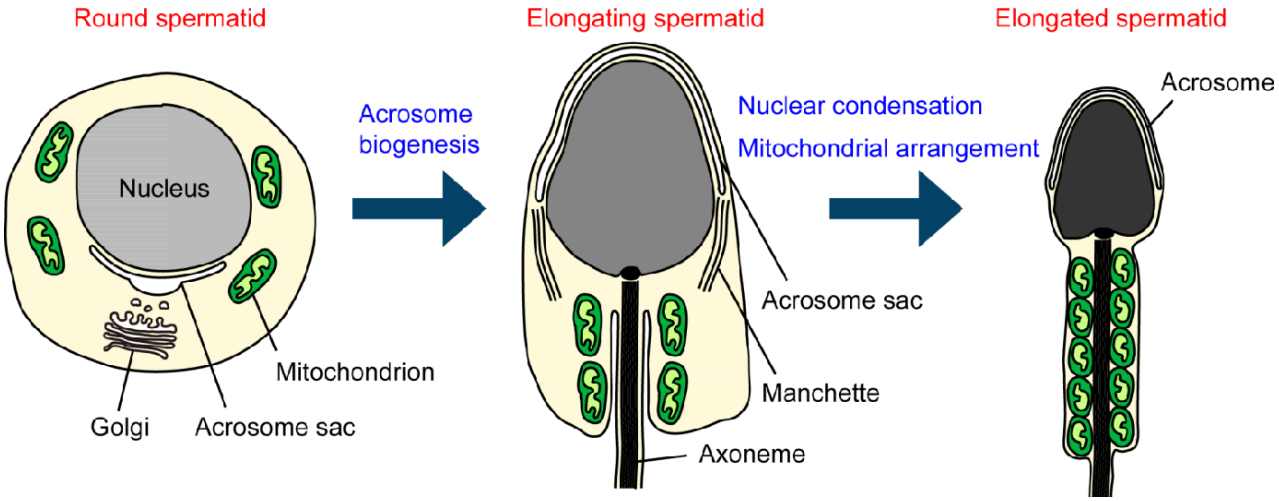

Figure 35. Differentiation events during spermiogenesis.
In round spermatids, the acrosome sac, formed and enlarged by continuous fusion of Golgi-derived vesicles, flattens to cover the anterior half of the nucleus in elongating spermatids. Histone-to-protamine replacement allows the nucleus to become condensed. Mitochondria align along the midpiece and tightly pack to form the helically arranged mitochondrial sheath. *Source: Nakamura, 2013* [189]

Nuclear compaction involves the removal of somatic-like nuclear histones, replacement with testis-specific intermediary histone variants and then replacement of most histones with transition nuclear proteins followed by protamines [190]. Protamines are relatively small proteins composed of over 60% arginine. Transcription ceases with compaction and the disappearance of nucleosomes. This process is crucial in protecting the paternal genome against modification (physical and chemical) on its journey and in creating a compact and streamlined sperm head for optimal mobility [188]. The latter is also the reason for the shedding of residual cytoplasm.

3.1. Acrosome biogenesis and the acrosin protease

During spermiogenesis, pro-acrosomal vesicles synthesised in the trans-Golgi network are transported to the anterior part of the nucleus (Figure 36) defined by the presence of a nuclear dense lamina. These vesicles fuse to form a large acrosomal granule anchored to the nuclear envelope via the acroplaxome, a cytoskeletal scaffold containing F-actin and Sak57 (a keratin orthologue) [191]. The granule enlarges with Golgi-derived glycoprotein-rich contents and gradually flattens and spreads over the nucleus to form a cap structure, while the Golgi apparatus migrates toward the posterior pole of the nucleus. As the spermatid elongates, the acrosome contents condense and the cap continues to spread over the nucleus [192].

The acrosome is an acidic lysosome-like vesicle that contains hydrolytic enzymes required to penetrate the oocyte zona pellucida, including acrosin, hyaluronidase and other trypsin-like enzymes. These enzymes are released during sperm capacitation in response to Ca^{2+} signals in an event known as the acrosome reaction (AR). The digestive enzymes facilitate penetration of the cumulus extra-cellular matrix (containing hyaluronan) and zona pellucida. The acrosome also appears to play a role in oocyte activation at fertilisation, since acrosomal abnormalities led to failed oocyte activation in ICSI (intracytoplasmic sperm injection) [193]. The acrosome thus plays an indispensable role in fertilisation.

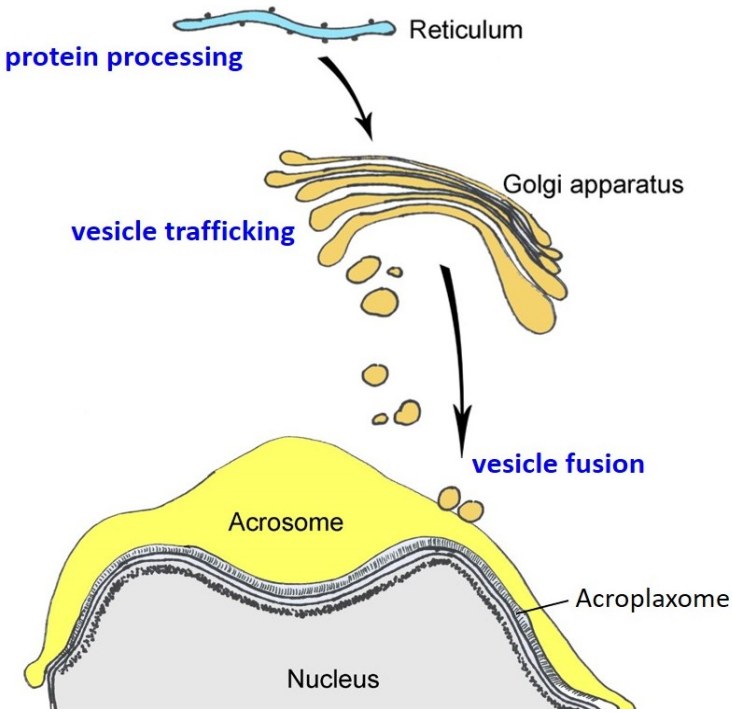

Figure 36. Acrosome biogenesis and proteins involved.
The processes of vesicle formation, trafficking and fusion are portrayed. *Source: Adapted from Coutton et al, 2015* [194]

Acrosin (ACR) is a member of the serine-protease superfamily that is unique to spermatogenic cells. It is a trypsin-like endoprotease that is present in the acrosome of all mammalian spermatozoa studied to date [195]. It participates in the proteolysis of the zona pellucida (ZP) by recognising ZP glycoproteins and regulating the exocytosis of acrosomal components during the acrosome reaction. ACR-deficient male mice are fertile [196], indicating functional redundancy with other serine proteases, although fertilisation times were reportedly slower than for WT sperm. It is synthesised as an inactive precursor known as proacrosin in the endoplasmic reticulum primarily during the round spermatid stage and localises to the inner acrosomal membrane in spermatozoa. Proacrosin, which exists as a doublet of 53 and 55 kDa, is activated with a rising pH during the acrosome reaction (more than 90% of the total acrosin in ejaculated human sperm is in the inactive proacrosin form [197]). Proacrosin is auto-activated at pH 8 into a 49 kDa intermediary form (alpha-acrosin) which is then converted to 30-40 kDa beta-acrosin [195]. The processes controlling the activation of proacrosin remain to be fully characterised, although a number of sperm-associated acrosin-binding proteins and protease inhibitors have been found present in the acrosome such as calcium trypsin inhibitor (caltrin) and ACR binding protein sp32 [198].

4. The SPINK family of protease inhibitors

SPINK (Serine Peptidase Inhibitor, Kazal Type) proteins of the serine protease inhibitor family are expressed in a diverse range of tissues. SPINK proteins contain at least one conserved Kazal domain consisting of 6 cysteine residues that form 3 disulphide bonds, and these domains interact with the catalytic domains of proteases [199]. SPINK proteins have been implicated in the inhibition and regulation of proteases that function in a wide range of physiological reactions [200]. Imbalance between proteases and SPINK proteins have been connected to diseases including pancreatitis, skin barrier defects, celiac disease, and cancer [201]. For example, SPINK1 inhibits trypsin in the pancreas [202] and SPINK5 inhibits the proteolytic activity of kallikrein 5 in the skin [203]. In the pancreas, trypsin is produced in an inactive zymogen (proenzyme) form. SPINK1 blocks trypsin activity in the case of autoactivation thus preventing cell damage.

Several SPINK proteins have been identified in the male reproductive tract in rodent models. SPINKL and SPINK3, for example, are expressed in the seminal vesicles in mice. SPINKL has been shown to inhibit premature sperm capacitation and SPINK3 modulates sperm physiology by reducing nitric oxide levels [204,205]. Five SPINK genes have been found to be epididymis-specific: SPINK8,10,11,12 and 13 [201,206]. SPINK13 was shown to bind the sperm acrosome region and inhibit a premature acrosome reaction and SPINK3 knockdown led to subfertility in male rats [201]. SPINK8 and SPINK12 were found to be secreted and associate with sperm, although knockout of SPINK12 did not impact sperm maturation or fertility in male mice [207]. SPINK2 is specific to male germ cells and reduced expression resulted in impaired male fertility in mice [208].

4.1. SPINK2: testis-expressed trypsin inhibitor

SPINK2 has been shown to have trypsin inhibitory activity [208]. Its sequence identity with other SPINK proteins is less than 50%. Its 3D structure was determined in 2011 by NMR spectroscopy (Figure 37). SPINK2's reactive site was found to be located in the flexible N-terminal region and it was demonstrated that Arg24 in crucial for SPINK2 target enzyme specificity [209]. SPINK2 expression has been linked to cancers such as lymphomas and acute myeloid leukaemia with contrasting effect: high SPINK2 expression levels were associated with lower mortality in primary cutaneous large B-cell lymphoma [210] and higher mortality in acute myeloid leukaemia [211]. SPINK2 is highly expressed in lymphoma cell-lines and in stem cells, however its role and participation in these states remains unclear. Mouse studies indicate that SPINK2 is primarily involved in sperm cell maturation, however it had not yet been associated with a human pathology.

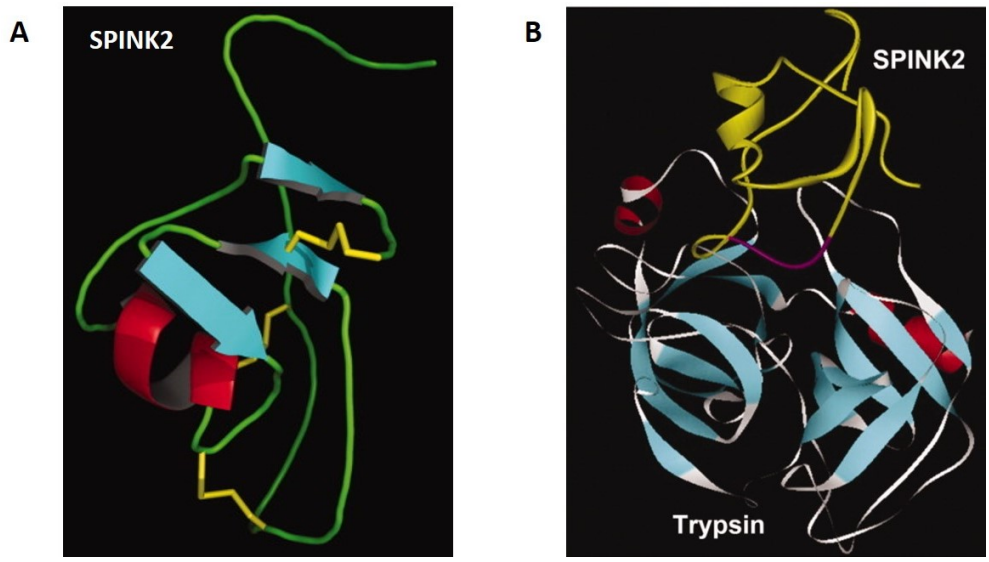

Figure 37. 3D SPINK2 solution structure and predicted trypsin binding.
A) SPINK2 protein structure. The three disulphide bonds are shown in yellow. Three-stranded antiparallel β-sheets are coloured in cyan. An α-helix is coloured red. The loop regions are shown in green. The representative protein structure was generated by using PyMOL. B) The docking complex model of SPINK2 with trypsin. The active region is coloured purple. *Source: Chen et al, 2009* [209]

Chapter 3: Defective gametogenesis and human infertility

1. Infertility: definition and prevalence

Infertility is a disease of the reproductive system defined by the World Health Organisation as the failure to achieve a clinical pregnancy after 12 months or more of regular unprotected sexual intercourse (WHO-ICMART glossary, [212]). The WHO recognises infertility as a global public health issue. A study of the burden of infertility in women from 190 countries based on demographic and reproductive health surveys estimated that 48.5 million couples were affected worldwide in 2010. This rate corresponds to a high global burden of infertility that has remained more or less consistent since 1990 [213].

Infertility can manifest either as the inability to become pregnant or inability to maintain a pregnancy to term. Infertility can also be primary or secondary, where primary infertility refers to couples who have never been able to conceive, and secondary infertility to those who have already carried a pregnancy to term (WHO). A systematic analysis of 277 health surveys conducted in 2010 showed that among women aged 20-44 years deemed susceptible to becoming pregnant, 1.9% suffered primary infertility and 10.5% suffered secondary infertility [213]. In France, according to surveys carried out in 2003 (ENP) and 2008 (Obseff), 18-24% of couples were unable to conceive after 12 months, falling to 8-11% after 24 months. In the year 2015 in France, 3.1% of children were born thanks to Assisted Reproductive Technologies (ART) and the achievement of pregnancy varied from 10 to 22% depending on the technique used (INSERM, 2018).

2. Causes of infertility

The causes of infertility are numerous and can be due to male factors, female factors or a combination. The distribution of causes is difficult to accurately determine due to differences in definitions and criteria and the lack of large-scale comprehensive studies, however an approximate distribution of causes is shown in Figure 38, adapted from Brugo-Olmedo *et al*, 2001 [214]. The ovulatory factor, representing approximately 20% of cases, entails problems relating to the growth, maturation and ovulation of the oocyte. The utero-tubal-peritoneal factor, present in ~30% of couples, concerns the integrity of the fallopian tubes and uterine cavity and the presence of pelvic adhesions which may obstruct the female genital tract. Male factor summarises semen parameters and factors influencing the quality and quantity of spermatozoa in the semen, affecting ~30% of couples. The sperm migration factor comprises a combination of male and female factors influencing the interplay between the spermatozoa and the cervical environment and thus impacting the number and motility of spermatozoa reaching the oocyte. This factor applies to ~10% of couples in which semen parameters are deemed normal. The 'unexplained' category refers to couples for whom no definitive cause is apparent at the time of testing.

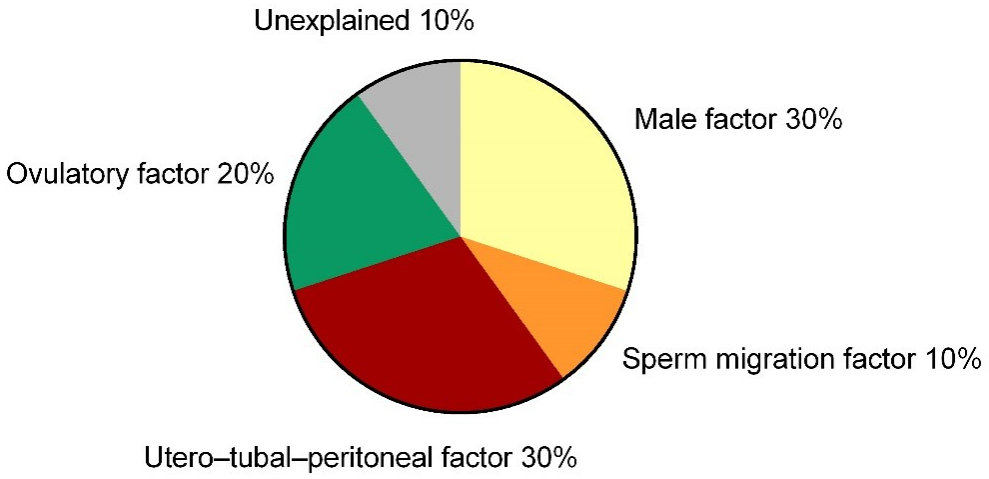

Figure 38. Approximative distribution of the causes of infertility.
Source: Adapted from Brugo-Olmedo et al, 2001 [214]

3. Gonadotropic origin

The balance of reproductive hormones is crucial for normal fertility. In women, endocrine dysfunction leading to lowered levels of the gonadotropins FSH and LH results in insufficient stimulation of ovarian hormone synthesis, or hypogonadism. This condition, known as hypogonadotropic hypogonadism, where low gonadal function results from low gonadotropin secretion can cause anovulation, amenorrhea and can delay or prevent sexual development. It can be acquired through damage to the pituitary gland or hypothalamus through injury, surgery, radiation, infection or tumour. Other causes include genetic abnormalities (e.g Kallmann syndrome), hypothyroidism, hyperprolactinaemia and a number of external factors including certain medication/drug use, stress and nutritional problems. Hyperprolactinaemia, often caused by a prolactinoma (a common type of pituitary tumour that hypersecretes prolactin) impairs gonadotropin secretion since prolactin inhibits GnRH secretion [215].

A considerable proportion of cases of hypogonadotropic hypogonadism in women are due to genetic mutations and inactivating variants of more than 50 genes have been reported to date, thought to account for up to 50% of all apparently hereditary cases [216]. These genes are involved in the synthesis, secretion or detection of GnRH. The predominant cause is inactivating mutation of the pituitary GnRH receptor (*GNRHR*), other causes include deficient hypothalamic *GPR54*/*KISS1*, *TACR3*/*TAC3*, and leptinR/leptin signalling or mutations within the *GNRH1* gene itself [217].

A similar set of endocrine disorders are associated with cases of male infertility, namely hypo/hyper-gonadotropic hypogonadism, hyperprolactinaemia, and adrenal or thyroid dysfunction. In hypogonadotropic hypogonadism in men, insufficient gonadotropin levels due to hypothalamic-pituitary dysfunction lead to inadequate stimulation of the testes to produce testosterone and thus interfere with normal sexual development during puberty. As for women, this condition can be congenital or acquired, with Kallmann syndrome (isolated GnRH deficiency) accounting for the majority of congenital cases and pituitary tumours (particularly prolactinomas) for the majority of acquired cases [218]. Hypergonadotropic hypogonadism describes testicular gonadotropin resistance and can be linked to chromosomal abnormalities (e.g. Klinefelter's syndrome), Leydig cell hyperplasia or *GNAS* inactivation [219,220].

4. Oocyte factor

The most common types of female infertility are linked to complex and multi-factorial syndromes which we have yet to fully understand, such as polycystic ovary syndrome (PCOS), primary ovarian insufficiency (POI), endometriosis and autoimmune diseases. In these syndromes, the reproductive cycle and ovulation are often impaired through a mix of endocrine dysfunction and autoimmune factors [221]. Due to the complex and heterogenous nature of these syndromes arising from an interaction of numerous genetic and external influences, their exact pathogenesis is difficult to determine, and the molecular aetiology remains unresolved in most cases. External factors can include exposure to endocrine disruptors, chemo/radiotherapy, extreme body weight/exercise and stress. Ovulatory disorders account for more than half of female infertility cases [222] and oligo-amenorrhea (infrequent or lack of menstruation) is a common symptom.

4.1. Primary Ovarian Insufficiency (POI)

Primary ovarian insufficiency (POI) previously known as Primary ovarian failure (POF) or premature menopause refers to a loss of ovarian function before the age of 40. The condition is defined by amenorrhea over a period exceeding 4 months, low estradiol serum concentrations and high serum levels of FSH (>40 IU/L in samples taken more than a month apart). In the large majority of cases, POI is associated with premature depletion of the reserve of primordial follicles by an unknown mechanism. Destruction of primary follicles can be caused by accelerated follicular recruitment, activation of proapoptotic pathways or autoimmune response [223]. In rare cases, the ovarian reserve is preserved, and problems arise in the later stages of follicular recruitment, maturation and ovulation. Elevated gonadotropin levels are a compensation mechanism for inadequate response from the ovaries (Figure 39); the condition can thus also be described as hypergonadotropic hypogonadism.

A large proportion of the identified causes is genetic; however, POI can also be acquired through chemotherapy or radiotherapy, ovarian surgery, exposure to viral or environmental toxins or certain drugs (e.g. for various autoimmune diseases). Whereas the condition can resemble a premature menopause, this term is an inaccurate description since varying levels of ovarian

function are retained in around 50% of cases, and 5-10% of women conceive naturally after receiving the diagnosis [224]. Primary ovarian insufficiency is the preferred term, since it best describes the observed spectrum of impaired ovarian function.

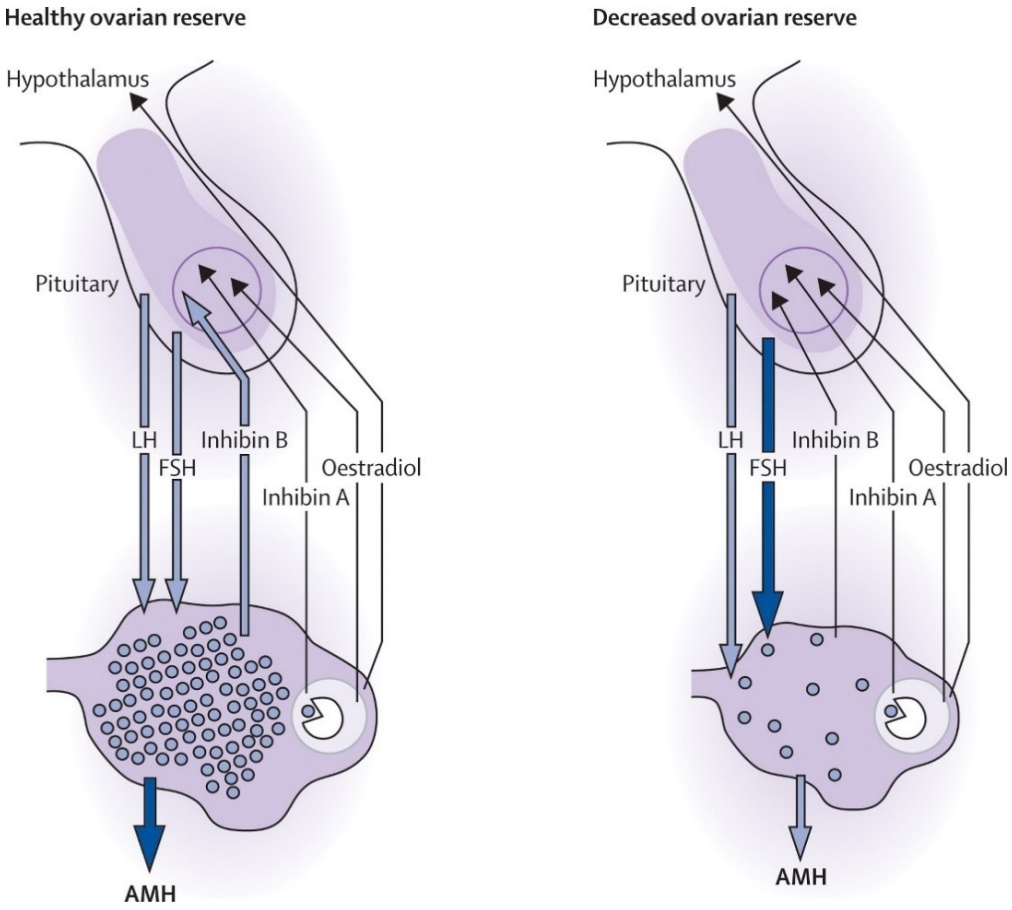

Figure 39. Hormonal alterations in POI/decreased ovarian reserve.
Thickness of arrows shows concentration of hormone secretion. AMH=anti-Mullerian hormone. FSH=follicle-stimulating hormone. LH=luteinising hormone. *Source: De Vos et al, 2010* [223]

4.2. Polycystic Ovary Syndrome (PCOS)

Polycystic ovary syndrome (PCOS) is the most common endocrine pathology in women, affecting around 5-10% of women of reproductive age. It is also the most common cause of anovulatory infertility accounting for around 70% of cases. The majority of PCOS sufferers have ovarian dysfunction, however 60% of patients are fertile by definition despite longer conception times. The syndrome, which typically appears during adolescence, is complex and multifactorial and patients present a wide spectrum of clinical and biochemical features. Diagnosis is based on the

ESHRE/ASRM Rotterdam (2003) consensus of the presence of two of the following: hyperandrogenism, ovulatory dysfunction (oligo-anovulation), and/or polycystic ovarian morphology (PCOM) [225,226].

Due to its heterogeneity, the exact pathogenesis and the direction of causality underlying PCOS is unclear. The most widely supported hypothesis is that PCOS is rooted in a dysregulation of androgen secretion in the ovaries (found in the majority of cases) and/or adrenal glands. This is thought to be due to a steroidogenic dysregulation of the theca cells in PCOS patients which overexpress most steroidogenic enzymes [227]. Androgen hypersecretion is correlated with elevated LH and insulin levels, which in turn is correlated with insulin resistance and lowered SHBG levels (sex hormone-binding globulin: binds and inhibits circulating testosterone and estradiol), increasing the level of free circulating testosterone and thus aggravating the hyperandrogenism. Around 50% of PCOS patients also present a metabolic syndrome of intrinsic and/or obesity-related insulin resistance thus contributing to the imbalance. These deregulations synergistically inhibit ovarian follicle development and ovulation, leading to accumulation of arrested follicles which become the ovarian 'cysts' associated with PCOM [226,228].

4.3. Endometriosis

Endometriosis is one of the most common gynaecological disorders, thought to affect 6-10% of women of reproductive age and accounting for over 20-50% of cases of female infertility [229,230]. It is defined by the presence of endometrial tissue outside of the uterine cavity, most commonly within the fallopian tubes, ovaries and peritoneal cavity. The sites of ectopic endometrial tissue induce a chronic inflammatory reaction, adhesions and scar tissue and may distort the pelvic anatomy. The condition is oestrogen-dependant, thus manifesting after puberty. The three main sub-types of endometriosis are: superficial peritoneal, cystic ovarian (cysts also known as endometriomas) and deeply infiltrating (>5 mm under the peritoneum). Patients often present with chronic pelvic pain, short menstrual cycles, long duration of menstrual flow, early onset of menstruation and infertility relating to tubal obstruction [231]. Aside from these problems, endometriosis can affect oocyte quality for several reasons: 1) it is associated with an enhanced inflammatory state that can impair ovarian function, and 2) the

presence of endometriomas (ovarian cysts) can alter the follicular environment and affect the ovarian reserve [232]. It can also interfere with ovulation through alterations in oestrogen-signalling [233].

Although the pathogenesis of the disease remains unclear, the leading hypothesis (known as the retrograde menstruation or implantation theory) postulates that endometriotic lesions are caused by endometrial fragments that pass through the fallopian tubes during menstruation and proliferate, invade and vascularise surrounding tissue. A competing theory postulates that embryonic cells from the Müllerian ducts (progenitors of the upper female genital tract) persist in ectopic locations and are stimulated to grow by oestrogens at puberty. It is debated whether the different forms of the disease have a single common aetiology or if each subtype has its own separate aetiology [229,234]. The risk of endometriosis is greatly influenced by genetic factors and heritability is estimated at around 50%. The genetic aetiology is complex and requires the interaction of numerous genetic variants and environmental factors.

4.4. Oocyte Maturation Deficiency (OMD)

The syndrome of oocyte maturation failure or oocyte maturation deficiency (OMD) describes a form of primary infertility characterised by the repetitive production and ovulation of primarily immature oocytes which do not mature when cultured *in vitro* (Figure 40) [52,235]. The definition is sometimes extended cases in which oocytes are able to mature to the MII stage but do not complete meiosis upon fertilisation. This syndrome differs from POI in that menstruation is typically undisturbed. According to a study of 487 women having undergone a total of 703 IVF cycles, 8.6% of women produced at least one GV-arrested oocyte in at least one round of hormonal stimulation (Bar-Ami et al, 1994 [236]). In cycles where 25% or more oocytes were GV-arrested, 0 clinical pregnancies were achieved for oocytes having undergone GVBD and rates of pronuclei formation, embryo cleavage and blastocyst development were significantly reduced, indicating impaired developmental competence.

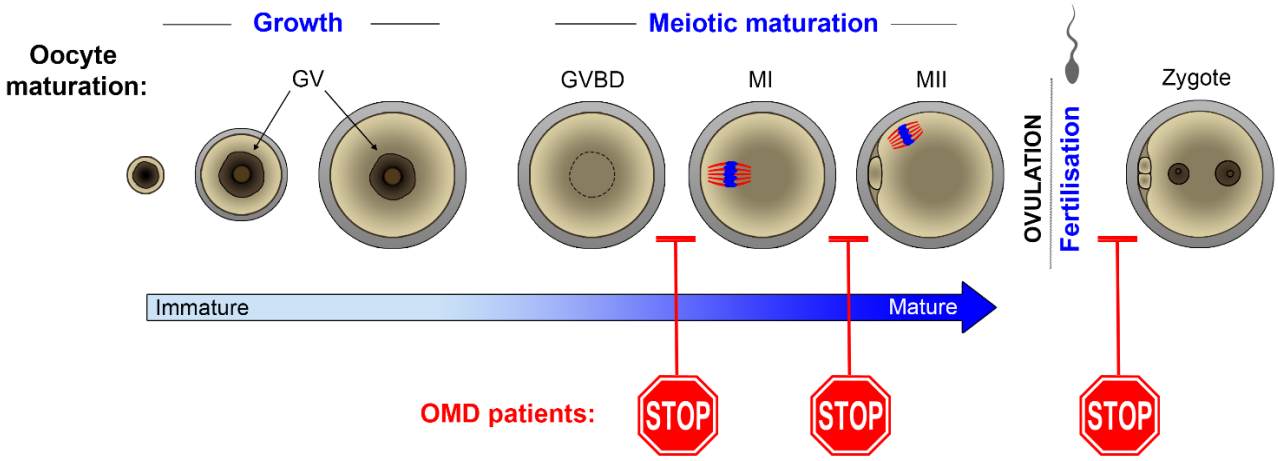

Figure 40. Oocyte maturation and arrest in OMD patients
The stages of oocyte maturation and the different stages of oocyte arrest found in OMD patients. *Source: Own work (adapted from Christou-Kent et al, 2018* [237]*)*

Although rare, reports have described cases for which the syndrome is absolute, i.e. all ovulated oocytes are immature (arrested at GV or MI stages) or do not respond to fertilisation [238–241]. In all of these cases for which the information is available, patients' menstrual cycles were maintained and hormone levels and other fertility parameters found to be normal, resulting in a diagnosis of unexplained primary infertility. These features, along with the rarity and severity of the condition suggest a primarily genetic pathology.

Studies using transgenic animal models have revealed a number of gene candidates linked to various phenotypes of oocyte meiotic arrest. Genes that have been linked to maturation arrest in mouse knockouts include *Cdc25b* and *Pde3a* linked to GV arrest, *Mei1* (meiosis defective 1), *Cks2* (CDC28 Protein Kinase Regulatory Subunit 2), *Mlh1* (MutL Homolog 1) and *Lfng* (Lunatic fringe) linked to meiosis I arrest and *Smc1b* (structural maintenance of chromosomes 1B) linked to meiosis II arrest [242–248]. While these studies have great value in providing insight into the mechanisms of meiosis, their relevance to the human infertility phenotype remains to be confirmed. Only one very recent study has so far identified a genetic variant linked to human OMD: a primate-specific isoform of β-tubulin named *TUBB8* (Tubulin Beta 8 Class VIII), expressed uniquely in developing oocytes (Feng et al, 2016 [249]).

5. Sperm factor

Male infertility can be divided into two broad categories according to semen parameters: oligo-azoospermia referring to inadequate sperm concentration/number and astheno/teratozoospermia referring to low sperm motility and/or abnormal sperm morphology. These phenotypes occur in varying degrees of severity and are often combined, giving rise to the common OATS (oligoasthenoteratozoospermia) phenotype. Sperm factor infertility describes infertility related to testicular causes as opposed to pre-testicular factors (e.g. gonadotropic or external) or post-testicular factors (e.g. physical obstruction), with the key difference being the absence of functional spermatogenesis.

5.1. Oligo-azoospermia

A requirement for normal male fertility is a sufficient sperm concentration in the ejaculate. The WHO considers a healthy sperm concentration at or above 15 million sperm per millilitre (mL) with a total sperm count ≥39 million sperm/ejaculate (Table 4) [250]. Sperm concentrations below this threshold are classified as varying degrees of oligozoospermia, with 10-15 million sperm/mL considered mild, 5-10 million sperm/mL as moderate and less than 5 million sperm/mL as severe. Azoospermia is the term given to the most extreme form: total absence of sperm in the semen. 30% of male infertility cases with oligo or azoospermia are estimated to have a genetic origin [251,252], and non-obstructive azoospermia (NOA) and severe oligozoospermia are deemed the most likely to have a genetic origin. For the severe cases, successful fertilisation is rare in the absence of clinical intervention.

Semen parameter	Lower reference limit (5th centile)
Volume, mL	1.5
Sperm concentration, 10^6/mL	39
Total sperm number, 10^6	15
Total motility (PR + NP), %	40
Progressive motility (PR), %	32
Vitality (live spermatozoa), %	58
Sperm morphology (normal forms), %	4
pH	≥7.2
Seminal fructose, µmol/ejaculate	≥13

Table 4. Semen analyses lower reference limits according to the WHO laboratory manual for the examination of human semen, 2010.
Lower reference limits based on distribution of values from fertile men whose partners had a time-to-pregnancy of 12 months or less. PR: progressive motility, NP: non-progressive motility. *Source: Patel et al, 2018, Cooper et al, 2010* [250,253]

5.2. Astheno/teratozoospermia

As well as sufficient sperm concentration, sperm motility is also an important requisite for male fertility as this factor determines the capacity of sperm to reach and fertilise the egg cell once released into the female tract. Low sperm motility or asthenozoospermia is a common cause or contributing factor of male infertility. According to the WHO, the threshold for asthenozoospermia is less than 32% of sperm in the ejaculate of progressive motility, or less than 40% total motile sperm. Amongst other causes, asthenozoospermia can often be linked to abnormal sperm morphology, particularly flagella and mid-piece abnormalities. Teratozoospermia is the term defined by WHO as less <4% morphologically normal sperm. Various subtypes of astheno and teratozoospermia have been defined with genetic causes attributing to structural or functional sperm defects. Asthenozoospermia is a common symptom associated with the wider syndrome of primary ciliary dyskinesia (PCD), an autosomal recessive disorder or motile cilia which also affects the cilia lining the respiratory tract [252].

6. Diagnosis and treatment

Fertility evaluation should be offered to couples who have been unable to conceive after 1 year of regular unprotected intercourse. For men, a semen analysis is performed with a sample collected after a period of abstinence of 48-72 hours. Semen parameters are checked and further evaluation undertaken depending on the outcome. If of endocrine or pre-testicular origin (which can be indicated through testosterone and FSH testing), the underlying cause may be treatable [254]. Women with regular menstrual cycles are progesterone tested at day 21 of the cycle to confirm ovulation. For anovulatory women, further hormone tests (FSH and estradiol) can distinguish between a hypothalamic-pituitary cause or an ovarian cause. Other hormonal tests also exist (antimüllerian hormone level, clomiphene citrate response test, antral follicle count) to give an indication of the ovarian reserve and predict the response to ovarian stimulation [254].

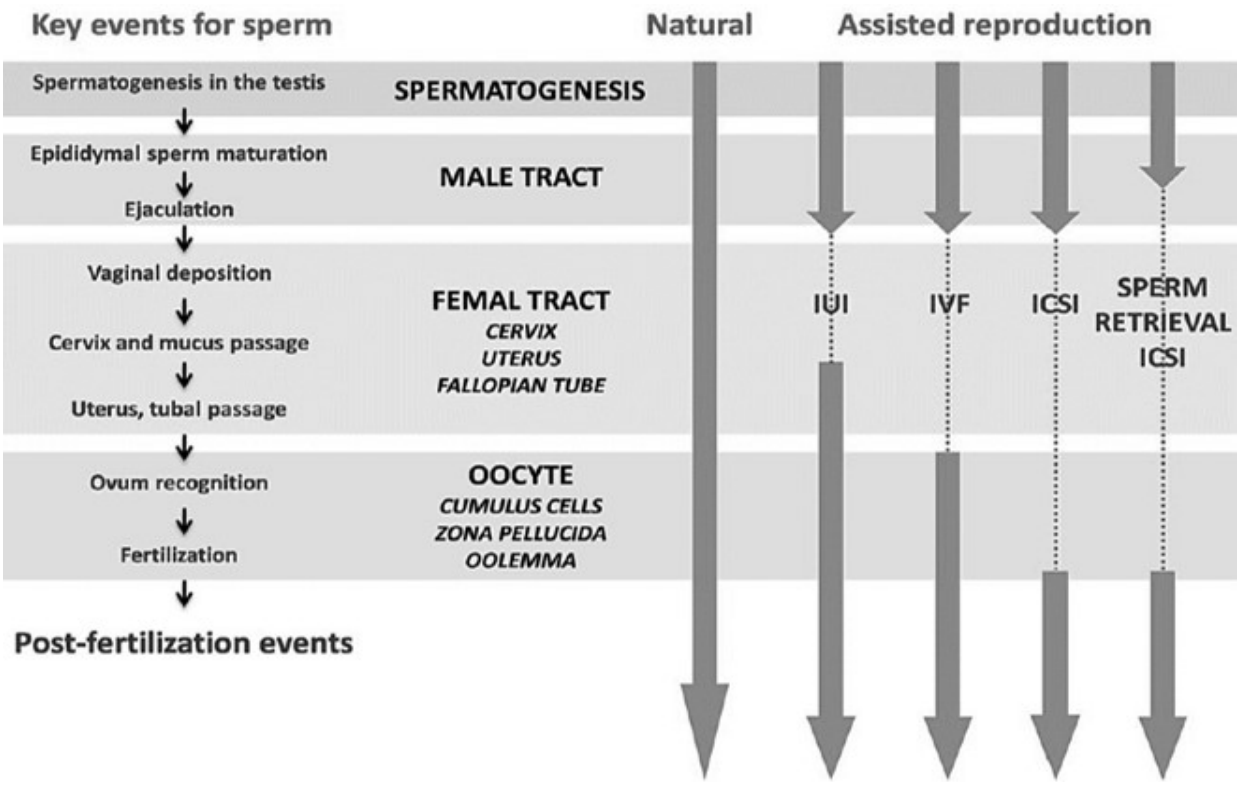

Figure 41. Natural fertilisation events that are bypassed by various ART techniques.
Dashed lines represent the omitted steps when comparing the different *in vitro* assisted reproduction processes with the steps encountered by sperm during natural conception. IUI: intrauterine insemination, IVF: *in vitro* fertilisation, ICSI: intracytoplasmic sperm injection. *Source: Adapted from Sakkas et al, 2015* [255]

If test results fall within normal parameters (i.e. unexplained infertility), couples can be advised to wait a further year before resorting to ART, since 50% of couples conceive within the second year [256]. If results indicate a compatible phenotype, *in vitro* fertilisation (IVF) will likely be attempted. IVF involves the collection and mixing of mature male and female gametes and embryo culture before introducing healthy blastocysts into the uterus, which is possible if sperm motility and number are adequate. If sperm parameters are low, ICSI (intracytoplasmic sperm injection) may be attempted as it can overcome low sperm motility or number (Figure 41). ICSI is a modern technique involving the injection of a sperm cells directly into oocytes. The technique can also overcome certain oocyte factors such as zona pellucida irregularities [257]. A recently developed technique known as round spermatid injection (ROSI) involves surgical retrieval of spermatogenic cells from testes and injection of selected round spermatids into oocytes [258,259]. Despite low efficiency, this technique represents a possibility for men with NOA to father biological children.

For *in vitro* reproductive techniques, women undergo ovarian stimulation by administration of gonadotropins. Repeated FSH injections are administered to promote growth of a large number of follicles which is monitored via transvaginal ultrasound and hormonal testing. hCG (Human chorionic gonadotropin) is administered in the final stages to trigger meiotic maturation, and approximately 35 hours later, large antral follicles are ruptured and oocytes aspirated via a transvaginal needle guided by ultrasound. 10-15 retrieved oocytes is considered a good yield for ART, and larger yields are correlated with higher success rates [260]. Oocyte maturity is judged by the presence of the first polar body as a visual indication of the MII stage. Immature oocytes can be cultured *in vitro* in an attempt to induce maturation to the appropriate stage for fertilisation. This strategy, known as *in vitro* maturation (IVM), is particularly used for patients with PCOS, low ovarian reserve or repeated IVF failure [261].

ICSI, developed in 1992, is now used in 63% of all ART cycles due to its success in overcoming a number of fertility barriers (2010 ICMART survey [262]). Despite such advancements, ART remains ineffective for around 50% of couples [263]. This is partly because all current forms of ART require a developmentally competent MII-stage oocyte as well as having minimal sperm requirements for fertilisation to be possible. For those with severe gametogenesis defects, such treatments are ineffective since the gametes are incompatible with fertilisation and/or subsequent embryo development.

7. Determining aetiologies for human infertility

Genetic diseases can autosomal or sex-linked, and dominant or recessive according to whether or not the gene is haplosufficient. Recessive diseases are associated with haplosufficient genes, in which a single functional copy of the gene is sufficient to maintain normal function. The vast majority of protein-coding genes are haplosufficient [264]. Genetic diseases can also be linked to chromosomal anomalies (structural and numeric) or single nucleotide variation. In theory, alteration of any of the genes controlling key processes in gametogenesis could give rise to infertility. While transgenic animal models and functional studies have allowed the identification of many genes necessary for oogenesis and spermatogenesis, the list of genes that have officially been associated with human infertility is comparably short (Figure 42).

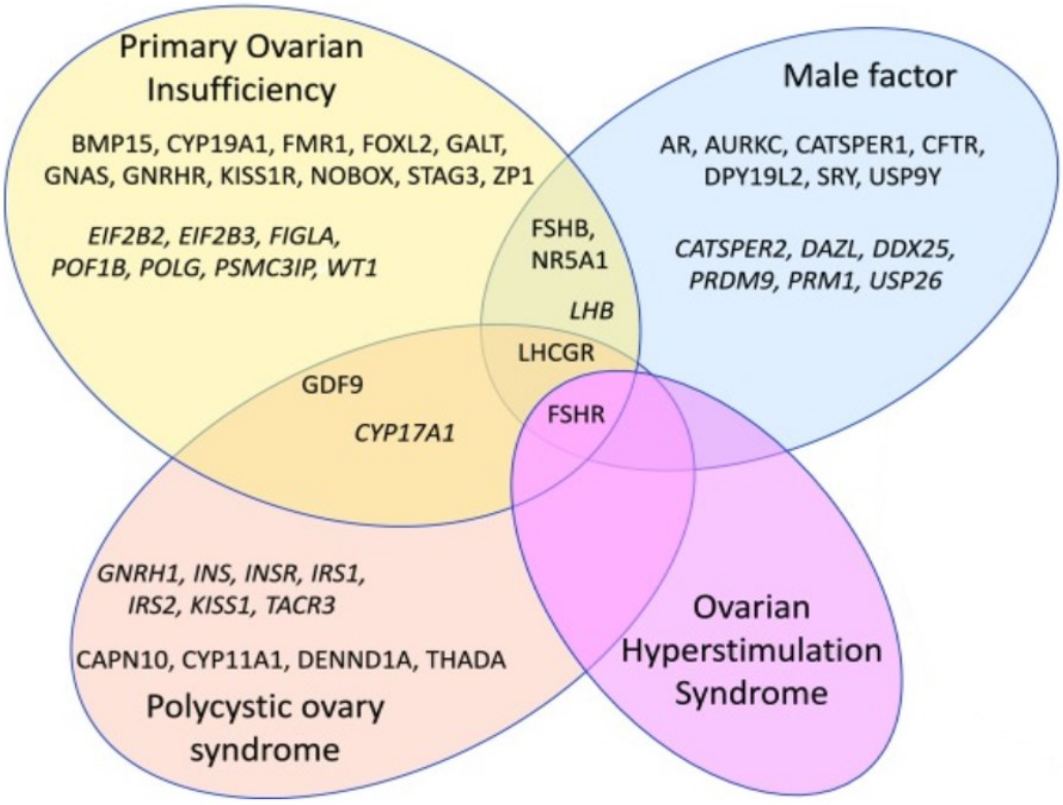

Figure 42. Genes associated with human infertility phenotypes through next generation sequencing.
Source: Patel et al, 2018 [265]

7.1. Genes and genetic disorders associated with POI

a) X-chromosome abnormalities

Amongst the cases for which the cause of POI is determined, the largest subgroup are women with numerical or structural X chromosome abnormalities, representing around 13% of cases. This is because human oocytes, unlike somatic cells, maintain both X chromosomes in the active state during development [266]. Partial or complete loss of the X-chromosome such as in Turner's syndrome (45,X) leads to oocyte loss in the early stages of meiotic prophase due to haploinsufficiency of X-linked genes. The syndrome Trisomy X (47,XXX) has also been linked to POI, however a large proportion of reported cases are due to associated autoimmune disease [267].

b) FMR1 premutation

The second largest subgroup of POI sufferers are those with a 'premutation' allele of X-linked *FMR1* (Fragile X mental retardation syndrome), accounting for around 6% cases and 21% of familial cases. In the *FMR1* premutation allele, expansion of CGG repeats in the 5' UTR (untranslated region) to 55-200 compared to 6-55 in normal alleles (the full mutation allele with >200 repeats leads to fragile X syndrome), is hypothesised to lead to production of a toxic mRNA that causes follicle atresia [268].

c) Single gene variants

As shown in Figure 42, X-linked *BMP15* [269] as well as autosomal *GDF9* [270] whose functions are numerous in all stages of follicle formation, maturation and ovulation have indeed been associated with premature ovarian sufficiency in humans. Several transcription factor variants linked to POI include oocyte factors *NOBOX* [271] and *FIGLA* [272] and the granulosa cell factor *FOXL2* [273]. Other variants associated with POI that are not shown in Figure 42 are RBP-coding *CPEB1* [274], *DAZL* [275] and *EIF2B* [276], gonadotropin receptors *FSHR* [277] and *LHR* [278] and *INHA* (encoding Inhibin A) [279] [223,280].

7.2. *TUBB8*: A genetic cause identified for OMD

A variant of the *TUBB8* gene was identified in a 4-generation familial case of OMD due to MI arrest and different *TUBB8* variants were found to be linked to the same phenotype in 6 other familial cases. This represents the first genetic cause to be associated with human OMD. The authors determined that the *TUBB8* mutation interfered with assembly of the α/β-tubulin heterodimer and thus interfered with meiotic spindle assembly in both human and mouse oocytes (Figure 43). The men were of normal fertility in all of the tested families. This case highlights the importance of correct microtubule polymerisation in spindle formation and chromosome segregation.

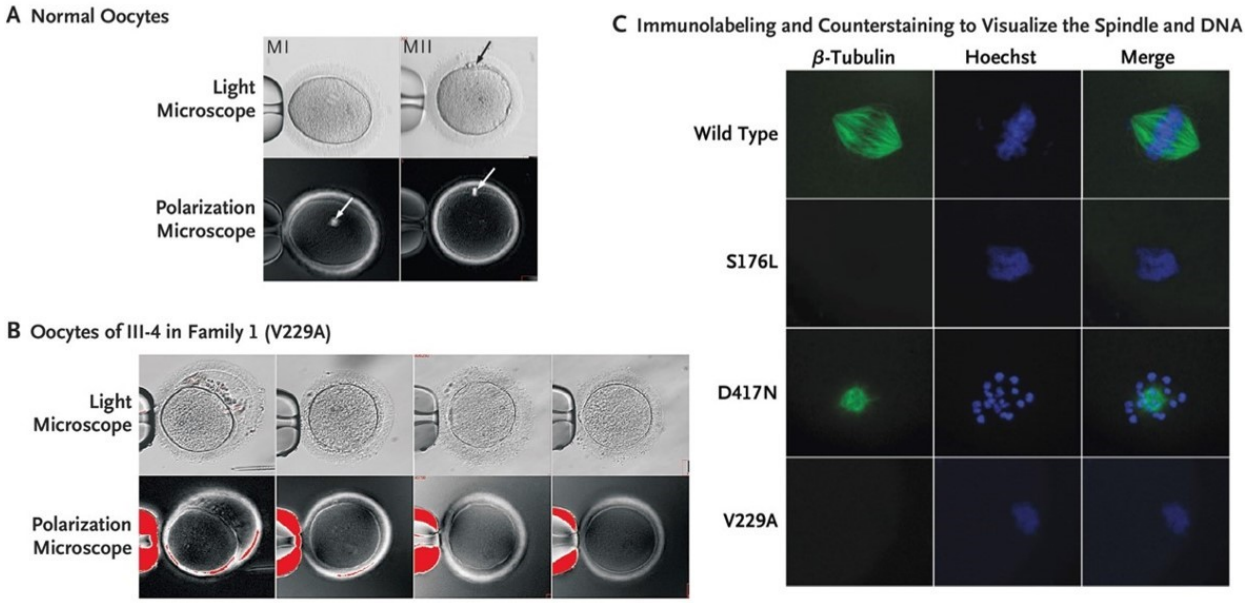

Figure 43. Oocytes from patients with a *TUBB8* variant vs. control oocytes.
V229A, D417N and S176L represent patients for which a deleterious *TUBB8* variant was identified. A) Example MI and MII stage control oocytes. B) Hormonal stimulation for attempted IVF yielded MI oocytes as evidenced by lack of the polar body. C) β-tubulin immunostaining of retrieved oocytes revealed a disorganised meiotic spindle from patient D417N while oocytes from other TUBB8 patients show no visible spindle. *Source: Feng et al, 2016 [42]*

7.3. Genes and genetic disorders associated with NOA

The most common genetic cause of non-obstructive azoospermia (NOA) is Klinefelter syndrome (47,XXY) linked to atrophied testes, diminished spermatogonia and severely disturbed spermatogenesis [281,282]. This syndrome accounts for 11% of NOA patients. Another common cause is microdeletions of the Y chromosome, since the Y chromosome houses several genes necessary for male gonad differentiation and spermatogenesis. Deletions in the AZF (azoospermia factor) region of the long arm of the Y chromosome (Yq) have been shown to lead to Sertoli-cell-only syndrome (Figure 44) and azoospermia due to spermatogenesis failure at varying stages [283,284]. Yq contains three AZF regions: AZFa, AZFb and AZFc, with AZFc regions being the most commonly detected in association with NOA [285]. AZF-associated genes include *DAZ1* (Deleted in Azoospermia) [286], *RBYM1A1* (RNA binding motif protein, Y-linked, family 1), *DBX3Y* (DEAD box helicase 3, Y-linked), *BPY2* (basic charge, Y-linked 2), *USP9Y* (ubiquitin specific peptidase 9, Y-linked), *TSPY1* (testis specific protein, Y-linked 1) and *HSFY1* (heat shock transcription factor Y-linked 1) [285,287].

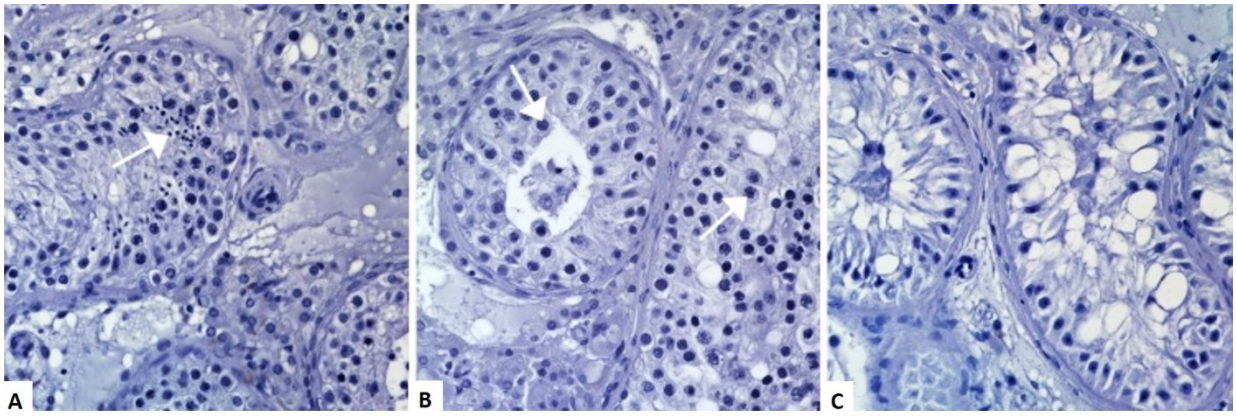

Figure 44. Histological images of human testicular tissue sections from patients with a) normal spermatogenesis, b) meiotic arrest, and c) Sertoli cell-only syndrome.
Most advanced germ cell types (A: elongated spermatids, B: spermatocytes) are indicated by white arrows (Centre of Reproductive Medicine and Andrology, Münster). *Source: Tüttelmann et al, 2018* [252]

7.4. Genes associated with astheno-teratozoospermia

Several sub-categories of astheno/teratospermia have been defined, including MMAF (multiple morphological anomalies of the flagella), which describes short, coiled, or irregular flagella. Whole exomes sequencing (WES) of MMAF patient cohorts has led to the identification of a number of associated gene invalidations including *DNAH1* (Dynein Axonemal Heavy Chain 1), *CFAP43, 44* and *69* (Cilia and Flagella Associated Protein), *WDR66* (WD Repeat Domain 66), *SPEF2* (Sperm Flagella 2), *ARMC2* (Armadillo Repeat Containing 2) and *FSIP2* (Fibrous Sheath Interacting Protein 2) [288–294].

Other subcategories include globozoospermia (Figure 45A), in which the sperm acrosome is unable to form or fuse. A number of genes have been identified in the context of human globozoospermia [194] including mutation of *SPATA16* (Spermatogenesis Associated 16) or *DPY19L2* (Dpy-19 Like 2) (Figure 45B), which leads to a round-headed sperm cell unable to fuse to the zona pellucida [295,296]. Macrozoospermia is a phenotype characterised by large sperm heads, variable number of flagella and increased chromosomal content linked to a variant of the gene *AURKC* (Aurora Kinase C) [297].

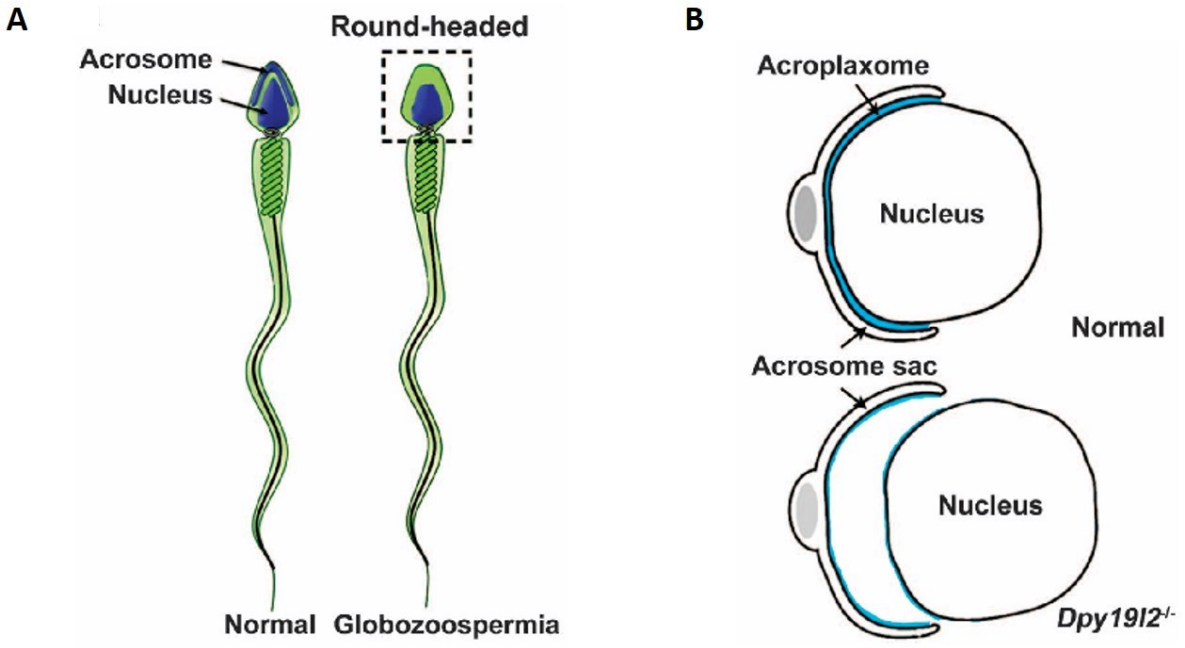

Figure 45. The phenotype of globozoospermia and *DPY19L2* invalidation.
A) The round-headed spermatozoa that is characteristic of globozoospermia. B) The phenotype of Dpy19l2 invalidation: destabilisation of the junction between the acroplaxome and the nuclear envelope. *Source: Chen et al, 2016* [298]

8. Whole Exome Sequencing (WES) and the candidate gene approach

High throughput sequencing technologies such as NGS (Next Generation Sequencing) have revolutionised science and medicine since their commercialisation in 2005. Although high-throughput sequencing is increasingly affordable, the cost remains a deterring factor for routine whole genome sequencing of patients in a clinical context. Whole exome sequencing (WES) is an approach that involves sequencing of only the protein-coding component of the genome, where most disease-causing mutations are known to occur [299]. Since exons represent approximately 1% of the whole genome, this dramatically reduces the cost, time and quantity of data to be analysed and stored. WES sequencing omits information of potentially important non-coding regions, such as regulatory elements and non-coding RNAs, however the technique can be coupled with full Sanger sequencing of genes of interest once identified. Because of its advantages, WES is increasingly applied in clinical settings, allowing the generation of large cohorts for various phenotypes that are of great value for medical research [300]. Like all sequencing technologies, WES must be followed by robust bioinformatics analysis in order to produce meaningful results. Numerous filters and thresholds must be defined to select for variants as promising gene candidates. Optimisation of this pipeline is a crucial part of the procedure. A typical WES/bioinformatics pipeline is illustrated in Figure 46.

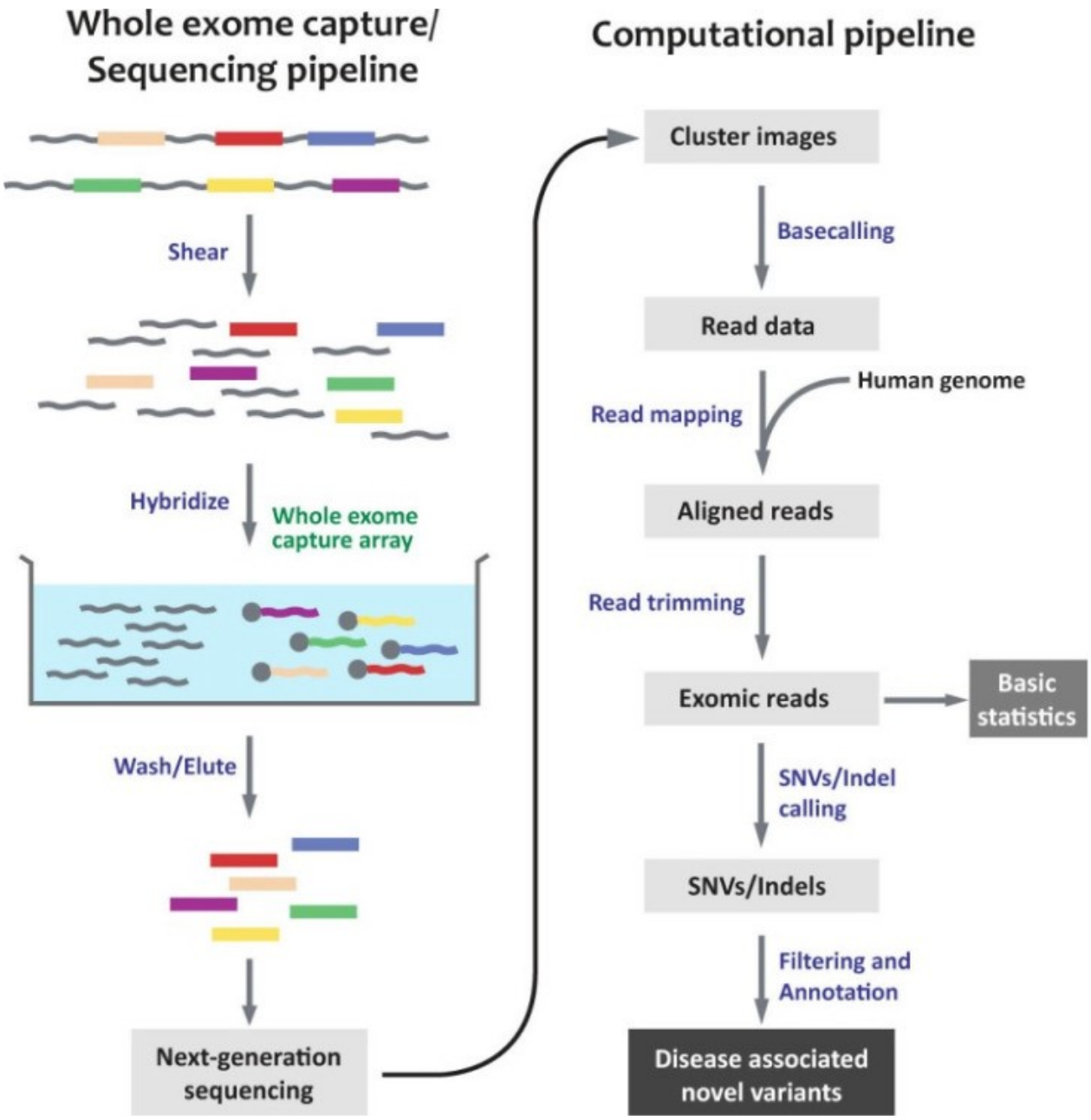

Figure 46. Overview of whole exome sequencing pipeline.
SNV: single nucleotide variant. *Source: Goh and Choi, 2012* [300]

The identification of genetic anomalies within the sequencing data and their association with human pathologies is however a difficult task. Strategies can be described as targeted or candidate-driven and non-candidate-driven depending on whether the method uses pre-specified target regions. Genome-Wide Association Studies (GWAS), for example, are often performed in a non-candidate-driven manner on entire genomes of patients of a specific phenotype who are sequenced alongside healthy controls. Genetic variants are detected

through the presence of single-nucleotide polymorphisms (SNPs) and associated with a disease or control state. According to the EMBL GWAS catalogue (2017), over 3000 GWAS analyses have been performed for over 1800 human diseases and traits, and thousands of SNP associations have been made to date. The weakness of such methods is that, due to the enormous inherent variation present in the human genome, associations are often very weak, and causality is uncertain (this is particularly true for complex/polygenic diseases). By comparison, the 'candidate gene', or targeted genetic association approach looks at genetic variation within a pre-specified region based on prior knowledge of the gene's function or suspected association with a disease phenotype. This approach has proven to be a powerful tool for studying complex diseases, but prone to generating false-positive or negative results [301]. It is also limited by our capacity to define relevant gene candidates.

The genetic analysis of familial cases or consanguineous populations for a particular pathology is a powerful method for identifying robust candidate genes, particularly in association with recessive single-gene disorders. Single-gene disorders occur at a higher frequency in such cohorts than in the general population due to recessive inheritance, and single-gene variants can be distinguished from the noise of background mutation by the frequency at which they are detected. Although rarer than polygenic diseases, single gene disorders provide an invaluable opportunity to decipher gene function and thus better enable us to understand all forms of genetic disease.

8.1. CRISPR/Cas9: a valuable tool for characterising human infertility

Whichever method is used to identify a candidate gene in the context of a human pathology, the association is greatly reinforced by validation through generation of transgenic cell or animal models. For studying infertility phenotypes, the mouse model is the golden standard for a number of reasons 1) high genetic homology to the human, 2) similarities in the reproductive system, 3) short generational turnover and 4) the tools that exist for genetic modification. The invention and commercialisation of the CRISPR/Cas9 genome editing technique in 2012 revolutionised this process, bringing the time to generate a transgenic mouse lineage from over 2 years down to around 6 months. This technology exploits the CRISPR (clustered regularly interspaced short palindromic repeats)/Cas9 bacterial immune system to create a programmable RNA-guided gene editing tool (Figure 47).

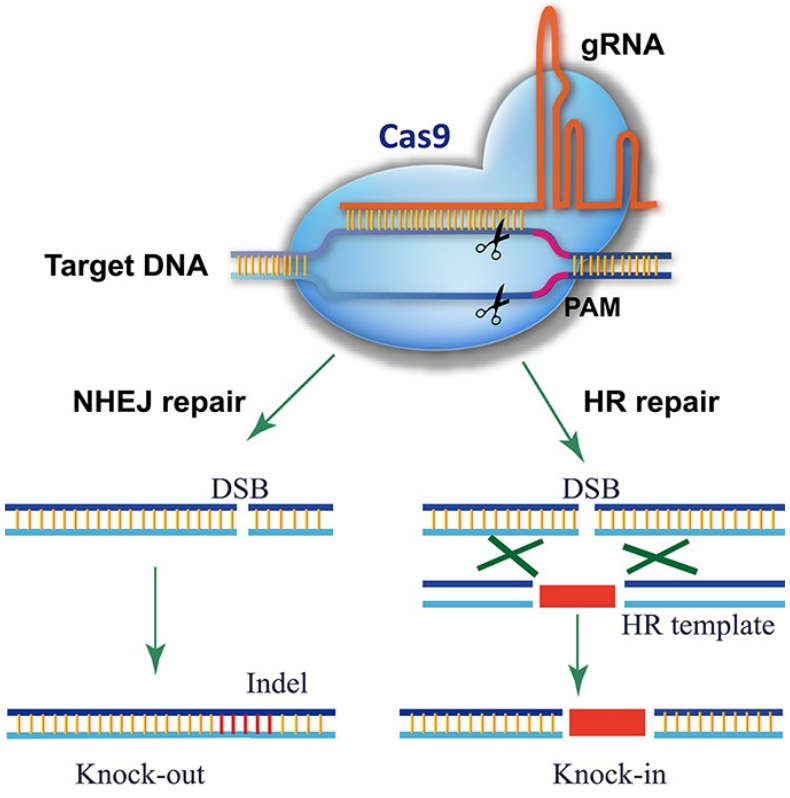

Figure 47. CRISPR/Cas9 genome editing and gene disruption/edition possibilities.
Cas9 nuclease cleaves double-stranded DNA in a site-specific manner activating double-strand break repair machinery. In the absence of a homologous repair template, non-homologous end joining can result in indels disrupting the target sequence. Alternatively, precise mutations and knock-ins can be made by providing a homologous repair template and exploiting the homology directed repair pathway. gRNA: guide RNA, PAM: protospacer adjacent motif, NHEJ: non-homologous end joining, HR: homology-direct repair. *Source: Ding et al, 2016* [302]

Thesis objectives and methodology

The GETI Lab has developed an efficient pipeline for identifying candidate genes in association with human infertility phenotypes through exome sequencing of patients attending Fertility Centres based in North Africa. The rate of consanguineous marriage in this population is around 1/3 [303]. This collaboration has, over a number of years, made it possible to amass sequencing data from patients with severe infertility phenotypes that are most likely caused by rare, recessive single-gene mutations.

Genetic variants appearing in several patients of a common phenotype (confirmed and sequenced in full by Sanger sequencing) satisfying a number of criteria regarding predicted impact on gene function, prior knowledge of gene function and expression, and absence in a control population, are selected for further study through the generation of transgenic mouse models. This allows for the function of the gene to be characterised at the molecular level in a mammalian system. This methodology has proven highly successful in identifying a great number of genes in the context of human infertility as well as in discovering new actors of mammalian gametogenesis [291,294,304–306].

The bases for this thesis are the identification of two gene variants, one of the gene PATL2 in the context of oocyte maturation deficiency (OMD), and the other of SPINK2 in the context of non-obstructive azoospermia (NOA). Both phenotypes are severe forms of primary infertility due to arrested gametogenesis. The body of literature that existed as of the start of these projects (which I have summarised) made both of these genes highly interesting candidates for having important roles in mammalian gametogenesis, and neither gene had been previously been associated with human infertility. Through the study of knockout (KO) and knock-in (KI) mouse lineages (the KI lineage created through CRISPR/Cas9), my objectives where to characterise the murine phenotype associated with the absence of these genes, and to explore their functions at the protein level.

My main objectives were to investigate the spatial and temporal expression profiles of each protein and elucidate their mode of action as best as possible. This was undertaken through a combination of reproductive biology techniques including IVF and fertility analysis, histology and imaging techniques, particularly whole-mount gamete fluorescence imaging, and molecular biology techniques from western blotting to transcriptomic analysis.

Results

A: The role of PATL2 in mammalian oocyte maturation and developmental competence

1. Article: PATL2 is a key actor of oocyte maturation whose invalidation causes infertility in women and mice

Christou-Kent M, Kherraf ZE, Amiri-Yekta A, Le Blévec E, Karaouzène T, Conne B, Escoffier J, Assou S, Guttin A, Lambert E, Martinez G, Boguenet M, Fourati Ben Mustapha S, Cedrin Durnerin I, Halouani L, Marrakchi O, Makni M, Latrous H, Kharouf M, Coutton C, Thierry-Mieg N, Nef S, Bottari SP, Zouari R, Issartel JP, Ray PF, Arnoult C. **EMBO Molecular Medicine, April 2018.**

1.1. Context

This project, which was the primary focus of my PhD, was based on the discovery of a pathogenic variant of the gene PATL2 present in 6 patients of a cohort of 23 patients with Oocyte Maturation Deficiency (OMD) characterised by GV-arrested oocytes. PATL2 belongs to the PAT1 family of RNA-regulatory proteins and is orthologous to xPat1a, whose oocyte-specific role I have described. We obtained PATL2 KO mice and I performed fertility analysis through natural mating and IVF, immunofluorescence analysis of ovulated and fertilised oocytes, histological analysis of the ovaries and transcriptome analysis of GV and MII stage oocytes in comparison to WT mice. I showed that PATL2 KO females were subfertile (KO males were of normal fertility) despite the ovarian reserve being unaffected. As reported in the following article, absence of PATL2 led to a large proportion of ovulated oocytes lacking a polar body and/or displaying spindle assembly defects and a high rate of oocytes with an aberrant response to fertilisation. Oocytes from PATL2 KO mice revealed a dysregulation of numerous transcripts necessary for oocyte growth, meiotic maturation and preimplantation embryo development.

Being unable to produce a specific PATL2 antibody, we generated a PATL2-HA lineage through CRISPR/Cas9, in which a HA tag was inserted at the C-terminal. This lineage allowed for the expression profile of PATL2 to be elucidated through immunostaining of ovary sections and whole-mount oocytes as well as co-staining with potential protein partners. I showed that Patl2 is strongly expressed in growing mouse oocytes, but showed no colocalisation with CPEB1, Msy2 or DDX6.

Through these experiments we were able to conclude that PATL2 indeed plays an important role in oocyte maturation in mice and in humans and that (in mice) it functions at the level of transcript regulation. Much is still to be learned about this exact role in mammals which appears to differ in several key ways from that described for xPat1a in *Xenopus* oocytes.

Research Article

TRANSPARENT PROCESS OPEN ACCESS

EMBO Molecular Medicine

PATL2 is a key actor of oocyte maturation whose invalidation causes infertility in women and mice

Marie Christou-Kent[1], Zine-Eddine Kherraf[1], Amir Amiri-Yekta[1,2,3], Emilie Le Blévec[1], Thomas Karaouzène[1], Béatrice Conne[4], Jessica Escoffier[1], Said Assou[5], Audrey Guttin[6], Emeline Lambert[1], Guillaume Martinez[1,2,7], Magalie Boguenet[1], Selima Fourati Ben Mustapha[8], Isabelle Cedrin Durnerin[9], Lazhar Halouani[8], Ouafi Marrakchi[8], Mounir Makni[8], Habib Latrous[8], Mahmoud Kharouf[8], Charles Coutton[1,2,7], Nicolas Thierry-Mieg[10], Serge Nef[4], Serge P Bottari[1], Raoudha Zouari[8], Jean Paul Issartel[6], Pierre F Ray[1,2,†] & Christophe Arnoult[1,*,†]

Abstract

The genetic causes of oocyte meiotic deficiency (OMD), a form of primary infertility characterised by the production of immature oocytes, remain largely unexplored. Using whole exome sequencing, we found that 26% of a cohort of 23 subjects with OMD harboured the same homozygous nonsense pathogenic mutation in *PATL2*, a gene encoding a putative RNA-binding protein. Using *Patl2* knockout mice, we confirmed that PATL2 deficiency disturbs oocyte maturation, since oocytes and zygotes exhibit morphological and developmental defects, respectively. PATL2's amphibian orthologue is involved in the regulation of oocyte mRNA as a partner of CPEB. However, Patl2's expression profile throughout oocyte development in mice, alongside colocalisation experiments with Cpeb1, Msy2 and Ddx6 (three oocyte RNA regulators) suggest an original role for Patl2 in mammals. Accordingly, transcriptomic analysis of oocytes from WT and *Patl2*$^{-/-}$ animals demonstrated that in the absence of Patl2, expression levels of a select number of highly relevant genes involved in oocyte maturation and early embryonic development are deregulated. In conclusion, PATL2 is a novel actor of mammalian oocyte maturation whose invalidation causes OMD in humans.

Keywords female sterility; oocyte developmental competence; oocyte maturation arrest; oocyte maturation failure; Patl2

Subject Categories Genetics, Gene Therapy & Genetic Disease; Urogenital System

DOI 10.15252/emmm.201708515 | Received 21 September 2017 | Revised 12 March 2018 | Accepted 19 March 2018 | Published online 16 April 2018

EMBO Mol Med (2018) 10: e8515

Introduction

In humans, oocyte production is a lengthy process that begins during embryonic development and is characterised by a long diapause lasting over a decade until resumption of maturation at puberty. The quiescent oocytes, contained within primordial follicles, are arrested in the prophase of meiosis I. Periodically, a group of primordial follicles are recruited to the pool of growing follicles. The germinal vesicle (GV) oocyte and surrounding follicular cells develop in tight coordination to produce a fully grown GV oocyte within an antral follicle. This process takes around 290 days Williams & Erickson, 2012; Li & Albertini, 2013). At this stage, the oocyte is sensitive to hormonal stimulation, which causes meiosis to resume, as revealed by GV breakdown (GVBD), and extrusion of the first polar body before arresting again at the metaphase 2 (MII) stage of meiosis II. The second meiosis is completed, with exclusion of the second polar body, upon fertilisation.

Several reports have been published describing cases of infertile women whose ovaries repeatedly produce mostly/only immature oocytes. This poorly defined syndrome is known as "oocyte factor infertility" or "bad eggs syndrome" (Hartshorne *et al*, 1999; Levran

1 Genetics, Epigenetics and Therapies of Infertility, Institute for Advanced Biosciences, Inserm U1209, CNRS UMR 5309, Université Grenoble Alpes, Grenoble, France
2 UM GI-DPI, CHU de Grenoble, Grenoble, France
3 Department of Genetics, Reproductive Biomedicine Research Center, Royan Institute for Reproductive Biomedicine, ACECR, Tehran, Iran
4 Department of Genetic Medicine and Development, University of Geneva Medical School, Geneva, Switzerland
5 IRMB, INSERM U1183, CHRU Montpellier, Université Montpellier, Montpellier, France
6 Grenoble Neuroscience Institute, INSERM 1216, Université Grenoble Alpes, Grenoble, France
7 UM de Génétique Chromosomique, CHU de Grenoble, Grenoble, France
8 Polyclinique les Jasmins, Centre d'Aide Médicale à la Procréation, Centre Urbain Nord, Tunis, Tunisia
9 Service de Médecine de la Reproduction, Centre Hospitalier Universitaire Jean Verdier, Assistance Publique - Hôpitaux de Paris, Bondy, France
10 Univ. Grenoble Alpes/CNRS, TIMC-IMAG, CNRS UMR 5525, Grenoble, France
*Corresponding author. Tel: +33 476 637 408; E-mail: christophe.arnoult@univ-grenoble-alpes.fr
†These authors contributed equally to this work as senior authors

et al, 2002; Beall *et al*, 2010; Hourvitz *et al*, 2010). We studied a cohort of patients who had all had at least one *in vitro* fertilisation (IVF) cycle yielding only GV, MI or atretic oocytes, and named this phenotype oocyte meiotic deficiency (OMD).

Generation of knockout mouse models has allowed the identification of several genetic variants linked to oocyte meiotic arrest at various stages. For instance, mice deficient in Cdc25b, a gene involved in cyclic AMP control, show GV arrest (Lincoln *et al*, 2002; Vaccari *et al*, 2008). Similarly, deletion of H1foo, a transcription factor for Mei1 (required for normal meiotic chromosome synapsis) and Ubb (a ubiquitin controlling the destruction of key cell cycle regulators), resulted in MI arrest (Libby *et al*, 2002; Furuya *et al*, 2007; Ryu *et al*, 2008). Finally, invalidation of Smc1b, a meiosis-specific component of the cohesin complex, causes MII arrest (Takabayashi *et al*, 2009) while deletion of Mlh3, which maintains homologous chromosome pairing at meiosis, induces mixed arrests (Lipkin *et al*, 2002). While it is tempting to suggest that mutation of any of the above-mentioned genes could cause OMD in women, none has so far been associated with this disease. Recently, heterozygous mis-sense mutations in *TUBB8*, an oocyte-specific tubulin required to form the meiotic spindle, were identified in a cohort of Chinese patients with OMD (Feng *et al*, 2016). Thus, *TUBB8* was established as the first human gene linked to OMD.

Here, we analysed 23 unrelated OMD patients from North Africa and found that six (26%) had the same homozygous truncating mutation in the *PATL2* gene, encoding a putative oocyte-specific RNA-binding protein. The role of this protein has yet to be characterised in mammals. A *TUBB8* variant was only found in a single patient in our cohort, indicating that absence of PATL2 is the main cause of OMD in this region.

Results

A homozygous truncating mutation in *PATL2* identified by whole exome and Sanger sequencing in 26% of tested subjects

We analysed a cohort of 23 infertile women presenting with OMD (Table 1). These patients responded normally to ovarian stimulation, and the number of follicles and oocytes harvested was similar to numbers for control patients. However, examination of the oocytes revealed only either GV or MI-arrested or atretic cells (identified by an irregular shape with a dark ooplasm), and a complete absence of MII oocytes.

Given that most of the patients were Tunisian and that 20–30% of marriages are consanguineous in this country, we hypothesised that infertility could be transmitted through recessive inheritance and we therefore focused on homozygous mutations. Exome analysis was performed first on samples from 15 patients. After exclusion of common variants and application of technical and biological filters (Coutton *et al*, 2018), three genes were found to be homozygously mutated in at least two subjects. Only one gene carried a homozygous variant scored as "high" and was predicted to induce loss of function by the "Variant Effect Predictor" tool (Ensembl). Interestingly, the same variant, p.Arg160Ter, c.478C>T in *PATL2* transcript ENST00000434130, was detected in five different patients. Since the orthologue of PATL2 in *Xenopus* is described as an important factor in *Xenopus* oocyte maturation (Nakamura *et al*, 2010), it was possible that this variant could be the cause of these subjects' infertility. The variant identified is expected to lead to either the production of a truncated protein (Fig 1A) or a complete absence of expression due to possible nonsense-mediated mRNA decay. The truncated protein would contain less than one-third of the complete amino acid sequence, in particular lacking the topoisomerase II-associated protein PAT1 domain. This domain, common to all Pat1 proteins, has been shown to be necessary for its paralogue, PATL1, to function through interaction with its partners (Braun *et al*, 2010) (Fig 1A). Because we did not have access to the relevant biological material (patients' ovaries), it was impossible to assess RNA decay in the presence of this mutation.

The presence of the genetic variant was confirmed by Sanger sequencing for the five mutated patients (Fig 1B). This variant was also identified in a heterozygous state in five out of 148,732 alleles (rs548527219) in the Genome Aggregation Database (gnomAD). This rate corresponds to a very low frequency of 0.003362%, compatible with recessive transmission of a genetic disease. Sanger sequencing of *PATL2* coding sequences was then performed on another eight OMD subjects. An additional patient was identified with the same homozygous mutation, increasing the final number to six out of 23 subjects analysed (26%) carrying the *PATL2* p.Arg160Ter variant.

To complete the analysis of the cohort, WES was performed on the newly recruited patients (n = 8) except for the subject harbouring the PATL2 mutation. WES analysis was therefore performed on a total of 22 subjects. From these data, we also sought *TUBB8* heterozygous mutations, which have also been described to induce OMD (Feng *et al*, 2016). One deleterious heterozygous variant (ENST00000309812.4:c.363_366del, ENSP00000311042.4:p.Lys122ArgfsTer13) was identified in patient P16 (Table 1), which could be the reason for this patient's infertility.

Overall, in this cohort, six out of 23 subjects analysed (26%) were observed to carry the *PATL2* p.Arg160Ter mutation, and one patient presented a new *TUBB8* variant (4.5%, 1/22), the pathogenicity of which remains to be confirmed. In our cohort, we compared patient characteristics between subjects with a *PATL2* mutation or presenting no *PATL2* mutation (Fig EV1). Although both groups were of similar ages at the time of analysis, and the numbers of oocytes retrieved were comparable, the two groups were clearly distinct in terms of the type of oocyte arrest. Oocytes from *PATL2* patients were mainly arrested at the GV stage, whereas oocytes from non-*PATL2* patients were generally arrested at the MI stage (Fig EV1).

During evaluation of our data, PATL2 gene mutations were also reported to be associated with OMD in two Asian studies based on cohorts from China and Saudi Arabia (Chen *et al*, 2017; Maddirevula *et al*, 2017). These findings support the causality of our *PATL2* variant and indicate a wide global spread for *PATL2*-dependent OMD.

Patl2 is not expressed in the hypothalamic–pituitary–gonadal axis in mice

x-pat1a, the *Xenopus* orthologue of *PATL2*, has been reported to be specifically expressed in growing oocytes (Marnef *et al*, 2010;

Table 1. Medical history, laboratory investigations and oocyte collection outcomes for patients presenting with OMD.

	Origin	Age (years)	Number of oocytes collected					FSH U/L	LH U/L	TSH U/L	Prolactin µg/L	Menst.	Comments
			GV	MI	MII	At.	Tot.						
Patients with *PATL2* mutation													
P1	Tunisia	35	4	0	0	1	5			1.36			
		34					2						Medical records not available
		34					8						Medical records not available
P2	Tunisia	28	9	0	0	11	20					YES	
		28.9	15	0	0	4	19						
P3	Tunisia	24	11	0	0	5	16	10.31	3.54		22.28		1 GV maturated to M1 *in vitro*
P4	Tunisia	34.28	8	0	0	2	10			1.07	23	YES	
P5	Arab	41	2	0	0	2	4	9.39	6.1	2.3	12.9	YES	
		42	3	1	0	1	5						
P6	Mauritania	36	2	10	0	4	16	3.01	3.38	2.88	25	YES	Cytoplasmic vacuoles in MI oocyte
		36.8	0	0	0	5	5						
Patients without *PATL2* mutation													
P7	Algeria	37	2	0	0	2	4	10.1	9.15	2.3		YES	
P8	Algeria	32	0	4	0	0	4						
		32	0	2	0	0	2						
P9	Tunisia	32	0	0	0	8	8			3.73			First cousin couple
P10	Tunisia	37	0	2	0	3	5						
		37	2	3	0	3	8						
P11	Tunisia	38.9	0	3	2	2	7	8.49	3.42	1.17	17.05		
P12	Libya	28	2	15	0	0	17	1.8			9.6		
P13	Arab	33	0	3	2	7	12						
		37	3	1	0	11	15						
P14	Tunisia	26	0	0	0	7	7					YES	
P15	Arab	38	0	0	0	4	4						
		39	0	0	0	5	5						
P16	Arab	33	0	5	2	2	9	4.65	2.71		14.25		Heterozygous mutation in *TUBB8*
P17	Arab	34	0	0	0	0	0					YES	
P18	Arab-FR	27	0	8	0	4	12						
P19	Arab-FR	24	0	3	0	0	3						
P20		29	0	0	0	7	7						
P21	Tunisia	29	0	0	0	13	13					YES	
P22	Tunisia	39	0	10	0	0	10						
P23	Tunisia-FR	No data available											No fertilisation
	Mean P1-P23	33.42	2.17	2.50	0.21	3.90	8.45						
	Mean P1-P6	34.00	6.00	1.38	0	3.89	10.00						

Table 1 (continued)

	Origin	Age (years)	Number of oocytes collected					FSH U/L	LH U/L	TSH U/L	Prolactin μg/L	Menst.	Comments
			GV	MI	MII	At.	Tot.						
	Mean P7-P23	33.1	0.45	2.95	0.3	3.9	7.6						
	Control cohort values (n = 238)	34.4	2.2	1.8	6	2.3	9.1	< 10.2	< 16.9	0.5–5	2–20		

Normal values correspond to couples where the male suffers from azoospermia or teratozoospermia (n = 234). Arab-FR = French of Arab origin, At. = atretic, Tot. = total, Menst. = menstruation.

Nakamura *et al*, 2010), and analysis of publicly accessible data banks shows that *PATL2* is also expressed at high levels in both human and mouse oocytes (Appendix Fig S1), indicating an important role for PATL2 in female gametogenesis. It should be noted that PATL2 expression is very low in human follicular cells (Appendix Fig S1), suggesting that the maturation defect is of oocyte rather than follicular origin. It also appears that PATL2 is expressed at low levels in a number of other tissues (Appendix Fig S1). We therefore wondered whether an element of the infertility phenotype could be caused by alteration of the hypothalamic–pituitary–gonadal axis. To address this question, we performed comparative Western blots on extracts from GV oocytes, hypothalamus and pituitary glands from Patl2-HA-tagged mice created using CrispR-cas9 technology. Whereas a clear and specific signal is observed for oocyte extracts from PATL2-HA females, no signal was observed in extracts from the hypothalamus or pituitary gland indicating that the direct control of the hypothalamus/pituitary gland on oocyte maturation is not altered in mice (Appendix Fig S2). Since our *PATL2* patients exhibited normal hormone levels (when data were available, Table 1) and reported regular menstrual cycles, these results taken together suggest that the human infertility phenotype is purely due to an oocyte defect.

Absence of Patl2 modifies the number of the primordial follicles at 26 dpp but not at 12 dpp

To decipher the molecular pathogenesis of the phenotype observed in our *PATL2* patients, we assessed the reproductive phenotype of Patl2-deficient mice ($Patl2^{-/-}$). The gene was invalidated by insertion of a LacZ cassette and deletion of exon 7, inducing a downstream translational frameshift (Appendix Fig S3). The putative transcript produced from this construct would consist of the first 102 amino acids (out of 529) tethered to β-galactosidase. Even if a protein product was generated from the modified Patl2 gene, it would not contain the topoisomerase II-associated protein (PAT1) domain and would therefore not be functional.

Initially, we performed a comparative histological study of control and $Patl2^{-/-}$ ovaries at 12 and 26 days postpartum (dpp). At 12 dpp, ovary sections from control and $Patl2^{-/-}$ females revealed no differences in the mean number of primordial, primary and secondary follicles (Appendix Fig S4). These data indicate that Patl2 plays a marginal role during the development of embryonic ovaries. At 26 dpp, a similar number of primary and secondary follicles were also observed in ovary sections (Fig EV2A and B). However, there was an unexpected increase in the number of primordial oocytes per section in $Patl2^{-/-}$ ovaries (Fig EV2B). To take the range of secondary follicle sizes into account and to assess follicle growth, we compared histograms plotting the amplitude of follicle diameter for secondary follicles between $Patl2^{-/-}$ and control animals and found no difference (Fig EV2C).

Patl2 may play a major role in oocyte growth: it is expressed in oocytes from the primary follicle stage and is less abundant from the late GV stage

We used PATL2-HA mice to characterise the function of Patl2 in mouse oocytes. The HA tag was selected for its small size (nine amino acids) making it is less likely to induce tag-dependent relocalisation. Homozygous Patl2-HA females' fertility parameters are well within the normal range for this strain in natural mating (first litters 24 days after crossing with males and litter sizes of 7 and 8, n = 2), implying that the HA tag does not impair the function of Patl2. We performed IF and confocal microscopy to quantify the expression of Patl2-HA in the different stages of GV oocytes, in MII oocytes and in ovary sections from tagged mice. The specificity of the fluorescence signal was first validated by immunostaining WT ovary sections alongside Patl2-HA sections using the same anti-HA antibody. No signal was observed in any oocyte in control sections (Appendix Fig S5). In Patl2-HA ovary sections, primordial follicle oocytes produced no detectable fluorescence signal (Fig 2). Signal intensity increased, interpreted as an increase in protein concentration, in oocytes from primary to pre-antral secondary follicles, becoming weaker in oocytes contained in tertiary/antral follicles. It should be noted that fluorescence intensity is not a direct measure of total protein quantity, since oocyte volume increases as follicular stages progress. Because the volume of antral follicle oocytes is larger than that of pre-antral follicle oocytes (approx. 70 versus 50 μm), the total quantity of Patl2 in antral follicle oocytes remains greater, indicating that production of Patl2 is continuous during oocyte growth (Fig 2A–C).

We next compared Patl2-HA immunostained GV oocytes at various stages, and MII oocytes obtained after hormonal stimulation. GV oocytes from pre-antral and antral follicles were obtained by collagenase treatment and ovarian puncture, respectively. In agreement with our results on ovarian sections, the strongest fluorescence signal was observed in pre-antral (secondary) follicle oocytes. GV oocytes from antral follicles can be divided into two categories

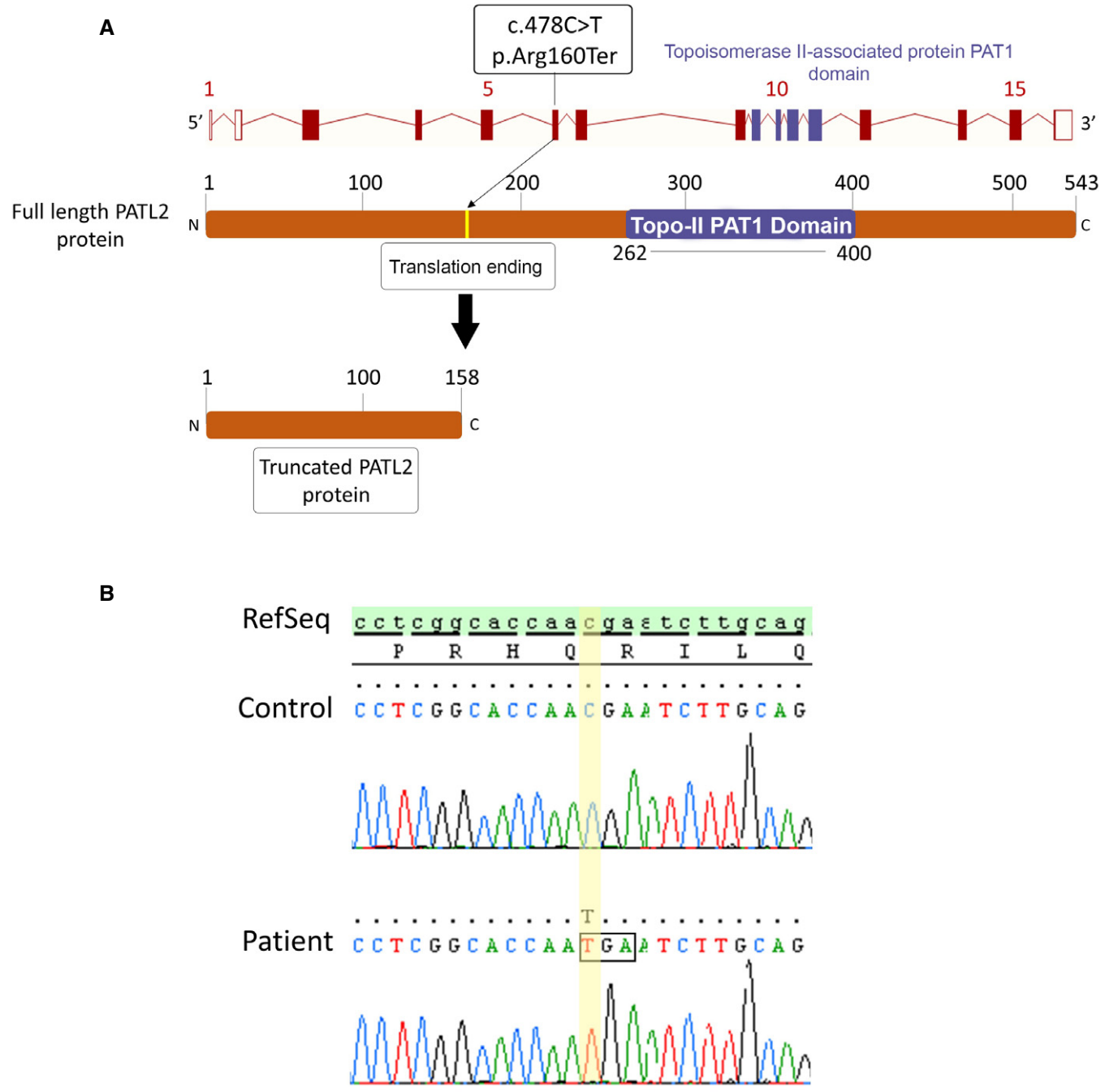

Figure 1. Identification of a truncating mutation in *PATL2*.

A Location of the *PATL2* mutation in the intron–exon structure and in a representation of the corresponding amino acid sequence. The variant identified, homozygous in the six patients, is located in exon 6 and creates a STOP codon, ending translation and producing a truncated 158-amino acid (aa) protein instead of the full-length 543 aa, and lacking the essential PAT1 (topoisomerase II-associated protein PAT1) domain.

B Electropherograms of Sanger sequencing for patients harbouring *PATL2* mutations compared to reference sequence.

based on the nuclear distribution of their chromatin: the non-surrounded nucleolus (NSN) to surrounded nucleolus (SN) conformational change occurs in the final stages of GV oocyte development and correlates with transcriptional arrest (De La Fuente, 2006). Stronger Patl2-HA fluorescence was observed in NSN than in SN GV oocytes (Fig 2D). PATL2-HA was also detected in MII oocytes at a level comparable to that in SN GV oocytes (Fig 2D).

During oocyte growth, a large quantity of stable mRNA necessary for growth and maturation accumulates within the oocyte. Up to 30% of this mRNA is translationally repressed until meiotic

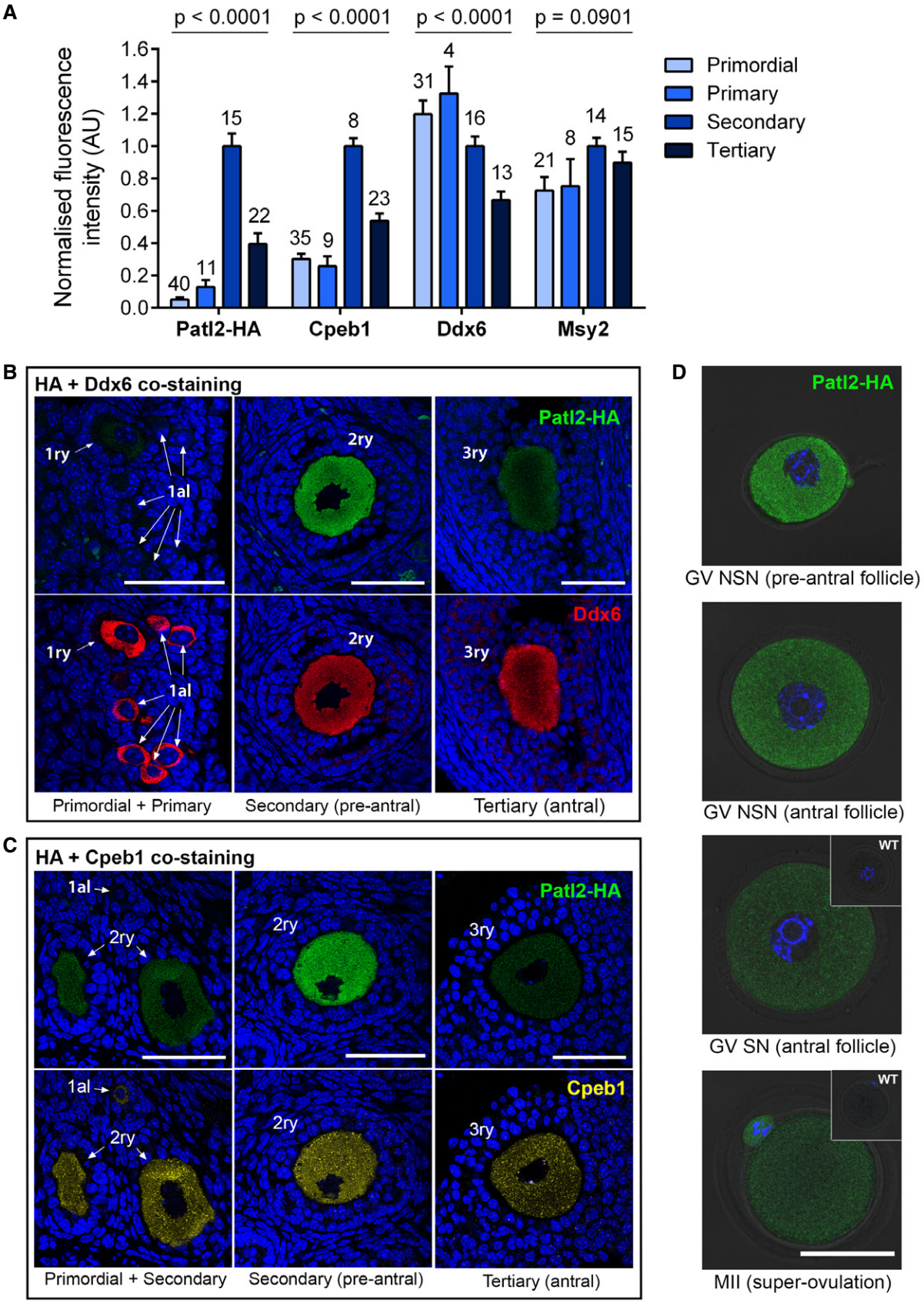

Figure 2.

Figure 2. Patl2, Cpeb1, Ddx6 and Msy2 expression profiles during oocyte growth and meiotic maturation.

A Ovary sections (3 μm thick) from Patl2-HA homozygous mice were co-stained with antibodies against the HA tag and either Cpeb1, Ddx6 or Msy2. Normalised mean fluorescence intensity at different follicle stages (as indicated) was measured using confocal microscopy. The mean fluorescence intensity of secondary follicle oocytes was used to normalise intensities for each protein to take into account variations in overall staining intensity between slides and obtain comparable values. Numbers above bars correspond to the size of the sample. Data are presented as mean ± SEM. Statistical differences were determined based on ANOVA test, *P*-value as indicated.

B Variation in fluorescence intensity for Patl2 and Ddx6 during oocyte growth. Confocal images obtained from the same section of an ovary from a Patl2-HA female, co-stained with antibodies against HA tag and Ddx6. Patl2 staining is not detectable in primordial oocytes, barely detectable in primary oocytes, and has a maximum intensity in secondary oocytes. Note that Ddx6 staining is strong in primordial oocytes. Primordial (1al), primary (1ry), secondary (2ry) follicles are indicated. Sections were counterstained with Hoechst to reveal the nucleus. Scale bar = 50 μm.

C Variation in fluorescence intensity for Patl2 and Ddx6 during oocyte growth. Confocal images obtained from the same section of an ovary from a Patl2-HA female, co-stained with antibodies against HA tag and Cpeb1. Note that Cpeb1 is detectable in primordial oocytes and that its staining is more punctiform than Patl2 staining, with numerous foci observable at all stages. Primordial (1al), primary (1ry), secondary (2ry) follicles are indicated. Sections were counterstained with Hoechst to reveal the nucleus. Scale bar = 50 μm.

D Comparative Patl2 staining of GV oocytes from pre-antral, antral with NSN (non-surrounded nucleolus) chromatin, antral with SN (surrounded nucleolus) chromatin and MII oocytes from Patl2-HA-tagged mice. GV oocytes were isolated by ovarian puncture, and MII oocytes were collected in the oviduct from stimulated Patl2-HA females. After fixation, oocytes were stained with anti-HA antibody and observed by confocal microscopy. In GV SN and MII oocytes, insets correspond to WT oocytes at the same developmental stage, showing no fluorescent staining. Scale bar = 50 μm.

maturation or after fertilisation. RNA processing involves very large complexes of ribonucleoproteins (RNPs), which are involved in the storage, processing, regulation and/or degradation of mRNA, and whose function often depends on the protein's phosphorylation status and the protein composition of the RNP. Clusters of RNP complexes are known as P-bodies. In *Xenopus* oocytes, x-Pat1a binds to the cytoplasmic polyadenylation element binding complex (CPEB), a central RNP involved in RNA translation/storage (Marnef *et al*, 2010; Nakamura *et al*, 2010). We therefore wondered whether other proteins known to be RNP components expressed in mouse oocytes, such as Cpeb1, Msy2 (thought to be x-Pat1a partners) and Ddx6 (a crucial P-body component) presented similar patterns of expression/abundance to Patl2 during oocyte growth (Flemr *et al*, 2010; Medvedev *et al*, 2011). To answer this question, we quantified these proteins in oocytes at the different follicular stages by IF and confocal microscopy (Fig 2A). Cpeb1 showed a similar, but not identical, pattern of intensities to that observed for Patl2. The main difference was that Cpeb1 is expressed in primordial follicle oocytes (in which Patl2 is undetectable). As for Patl2, the intensity was highest in secondary follicle oocytes and weakened in tertiary follicle oocytes (Fig 2B). Unlike Patl2, Msy2 and Ddx6 were abundantly expressed in primordial follicle oocytes, and their fluorescence intensity varied little throughout oocyte growth (Fig 2C and also Fig EV2 for Msy2).

We next assessed possible colocalisation between Patl2 and Cpeb1, Msy2 and Ddx6 (Fig 3). These experiments were performed on ovarian sections of secondary/pre-antral follicles, where the strongest Patl2 signal was recorded. Cpeb1 and ddx6 present a clear punctiform signal (Fig 3: A4, B4), unlike Msy2, for which the signal is more homogenous (Fig 3: C4). The Patl2-HA signal can be described as a homogenous scattering of small dots (Fig 3: A3, B3, C3). The dots are clearly smaller in size than those corresponding to Cpeb1 and Ddx6 staining, and no obvious colocalisation between Patl2 and any of the three proteins was observed (Fig 3: A2, B2, C2).

Subfertility in *Patl2*$^{-/-}$ female mice is due to compromised oocyte maturation and poor developmental competence of oocytes and embryos

We next assessed fertility in *Patl2*$^{-/-}$ animals by crossing them with WT animals and counting the number of live pups per litter, the total number of live pups born and the number of litters per month over a 6-month period. *Patl2*$^{-/-}$ females exhibited severe subfertility: the number of pups per litter dropped from 7.3 ± 0.8 (n = 14 litters for three females) for WT to 2.3 ± 0.4 (n = 7 litters for three females) for *Patl2*$^{-/-}$ mice (Fig 4A and B), and both the total number of pups and of litters per month per female were reduced (Fig 4C and D). Conversely, *Patl2*$^{-/-}$ males showed normal fertility: no difference in litter size was observed compared to WT (7.6 ± 0.7, n = 17 litters for five WT males and 7.6 ± 0.5, n = 28 litters for five *Patl2*$^{-/-}$ males) (Fig 4E).

Next, ovarian stimulation was performed and oocytes were collected for morphological and IVF studies. Stimulation with pregnant mare serum gonadotropin (PMSG) was used to obtain GV oocytes with well-defined nucleoli from both WT and *Patl2*$^{-/-}$ females. However, GV oocytes from *Patl2*$^{-/-}$ mice were smaller in diameter than those from WT mice, suggesting that the absence of Patl2 affected oocyte growth (Fig EV3A and B). Full stimulation (PMSG + hCG) produced a comparable number of oocytes in *Patl2*$^{-/-}$ and WT mice (Fig EV3C). This result concurs with observations that patients harbouring *PATL2* mutations produce a comparable number of oocytes to control patients (Table 1). *Patl2*$^{-/-}$ mice produced MII stage oocytes (Fig EV3D), identified by the presence of the first polar body (PB1), indicating that the phenotype is not as severe in mice as in humans, where no MII oocytes were produced (Table 1). As for GV oocytes, MII *Patl2*$^{-/-}$ oocytes were smaller in diameter than control MII oocytes (Fig EV3E), indicating that oocyte meiotic maturation as well as oocyte growth was impaired in the absence of Patl2. This finding was corroborated by the increased percentage of oocytes released at stages before MII: 26% for WT and 45% for *Patl2*$^{-/-}$ (Fig 5A). These oocytes were probably blocked in metaphase I (MI), as indicated by the absence of PB1 (Fig 5B). Notably, many apparent MI-arrested oocytes presented misaligned chromosomes and abundant cytoplasmic asters (Fig 5B). A significant increase in morphological defects such as abnormal spindle morphology, misalignment of chromosomes on the spindle and numerous cytoplasmic asters was also observed in *Patl2*$^{-/-}$ MII oocytes (Fig 5C and D). Thus, both women carrying a *PATL2* mutation and *Patl2*$^{-/-}$ mice exhibit oocyte maturation defects.

Next, the developmental competence of the oocytes collected was challenged in IVF experiments. We chose not to denude oocytes for these experiments since removal of cumulus cells has a negative impact on fertilisation. For WT females, the percentage of eggs

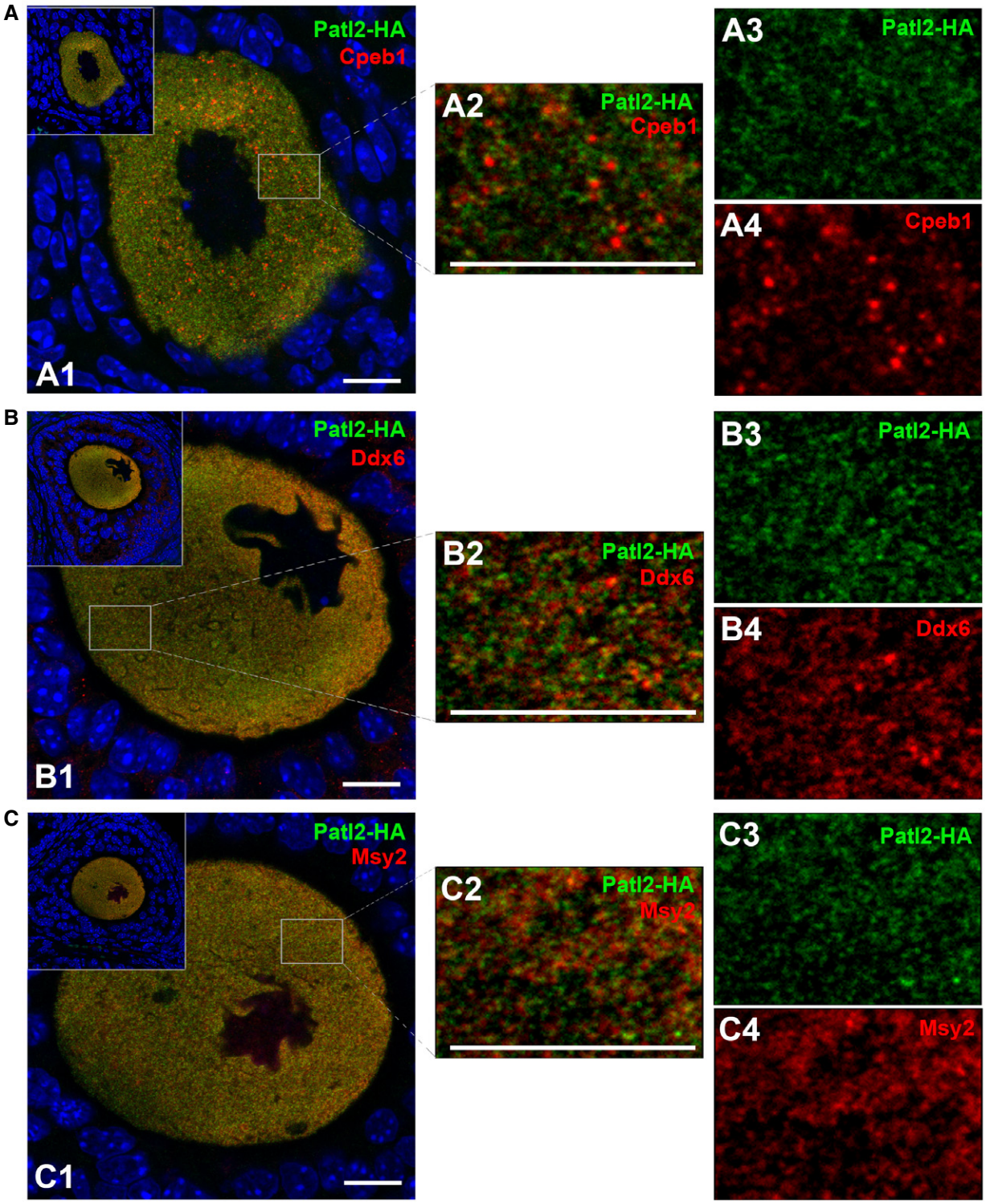

Figure 3. Analysis of possible colocalisation of Patl2 with Cpeb1, Ddx6 and Msy2.

A Confocal image of secondary follicle oocytes from Patl2-HA homozygous females co-stained with antibodies against HA tag (green) and Cpeb1 (red) and counterstained with Hoechst to reveal the nucleus (A1). Insets show the follicular environment of the oocyte studied. White rectangles indicate the zones of enlargement, shown on the right (A2). This image corresponds to a merge of Patl2 (A3) and Cpeb1 (A4) signals. Scale bars = 10 μm.

B Similar experiments performed with secondary follicle oocytes from Patl2-HA homozygous females co-stained with antibodies against HA tag (green) and Ddx6 (red). Scale bars = 10 μm.

C Similar experiments performed with secondary follicle oocytes from Patl2-HA homozygous females co-stained with antibodies against HA tag (green) and Msy2 (red). Scale bars = 10 μm.

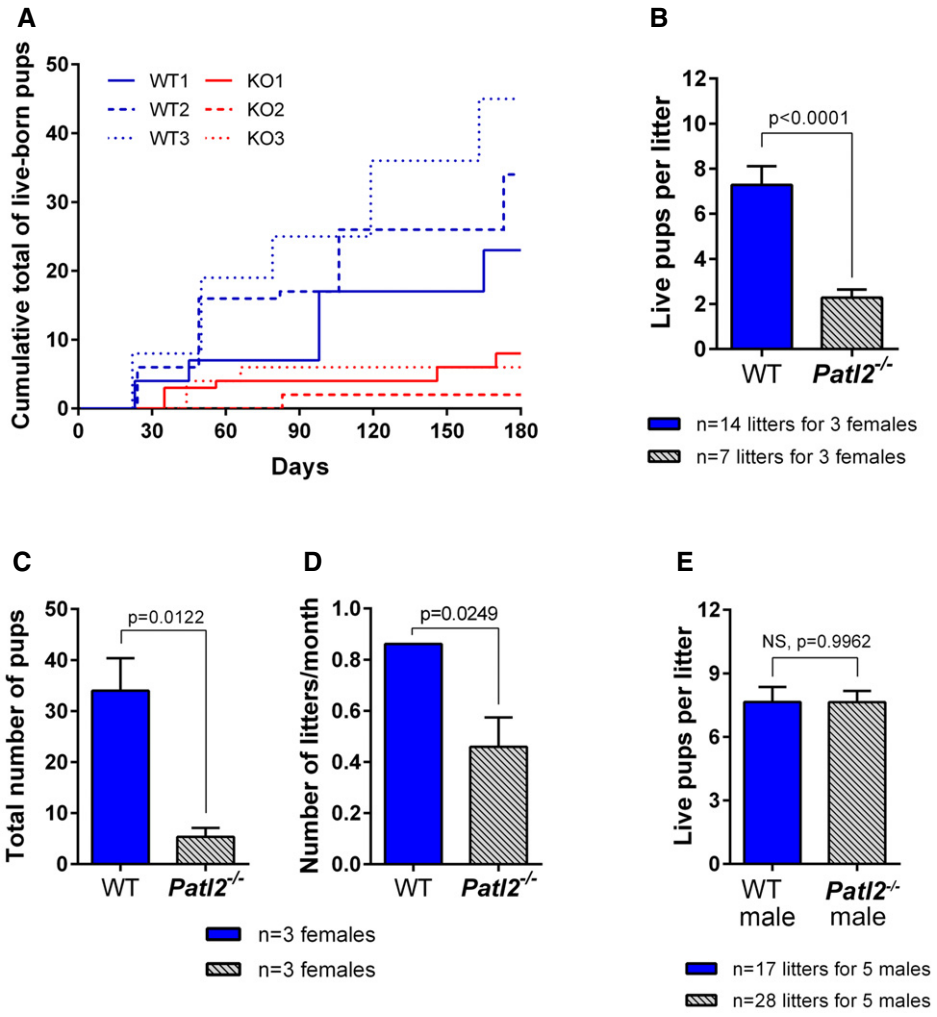

Figure 4. *Patl2* knockout (*Patl2*$^{-/-}$) females exhibit a severe subfertility phenotype when mated with WT males, whereas *Patl2*$^{-/-}$ males are fertile.

A Comparative accumulation of live pups over a period of 6 months from three WT and three *Patl2*$^{-/-}$ females crossed with WT males shows severe hypofertility of *Patl2*$^{-/-}$ females.

B Histograms showing the number of pups per litter (mean ± SEM) obtained by crossing three WT (n = 14 total litters) and three *Patl2*$^{-/-}$ females (n = 7 total litters) with WT males. Statistical test: two-tailed unpaired t-test with Welch's correction.

C Total number (mean ± SEM) of pups produced by a WT or *Patl2*$^{-/-}$ female over a 6-month period (n = 3 per genotype). Statistical test used: two-tailed unpaired t-test.

D The number of litters per month (mean ± SEM) is significantly decreased for *Patl2*$^{-/-}$ versus WT females. Statistical test: two-tailed unpaired t-test.

E *Patl2*$^{-/-}$ males produce comparable litter sizes to WT males when mated with WT females (mean ± SEM). Statistical test: two-tailed unpaired t-test.

reaching the two-cell stage was 67.7% ± 8.1 (n = 5 experiments, 10 females) (Fig 6A). Given that only 74% of ovulated oocytes can be assumed to be at the MII stage (Fig 5A), this proportion translates to 90% of WT MII oocytes reaching the two-cell stage. In contrast, for *Patl2*$^{-/-}$ females the percentage of eggs reaching the two-cell stage dropped to 36.4% ± 6.4, which translates to 65% success if we consider that only 55% of ovulated oocytes from *Patl2*$^{-/-}$ females are MII oocytes (Fig 5A). The IVF outcomes were therefore significantly altered in *Patl2*$^{-/-}$ females, indicating compromised developmental competence for *Patl2*$^{-/-}$ oocytes. This decrease in numbers of two-cell *Patl2*$^{-/-}$ embryos correlates with the abnormal development of *Patl2*$^{-/-}$ zygotes, which exhibited numerous defects, including delayed pronucleus formation, absence of sperm DNA decondensation and/or polyspermy. In contrast, almost all fertilised WT zygotes contained two pronuclei (2PN) (Fig 6B–D). Finally, the reduced developmental competence of *Patl2*$^{-/-}$ eggs and their altered fertilisation also severely affected pre-implantation development since only 27.2% ± 5.1 (n = 4 experiment, eight females) of two-cell embryos generated with *Patl2*$^{-/-}$ eggs reached the blastocyst stage in contrast to 87.1% ± 5.6 with WT eggs (Fig 6A).

Absence of Patl2 significantly alters the transcriptome of GV and MII oocytes

Since x-Pat1a, the *Xenopus* orthologue of *PATL2,* is a RNA-binding protein (Marnef *et al*, 2010; Nakamura *et al*, 2010), we next

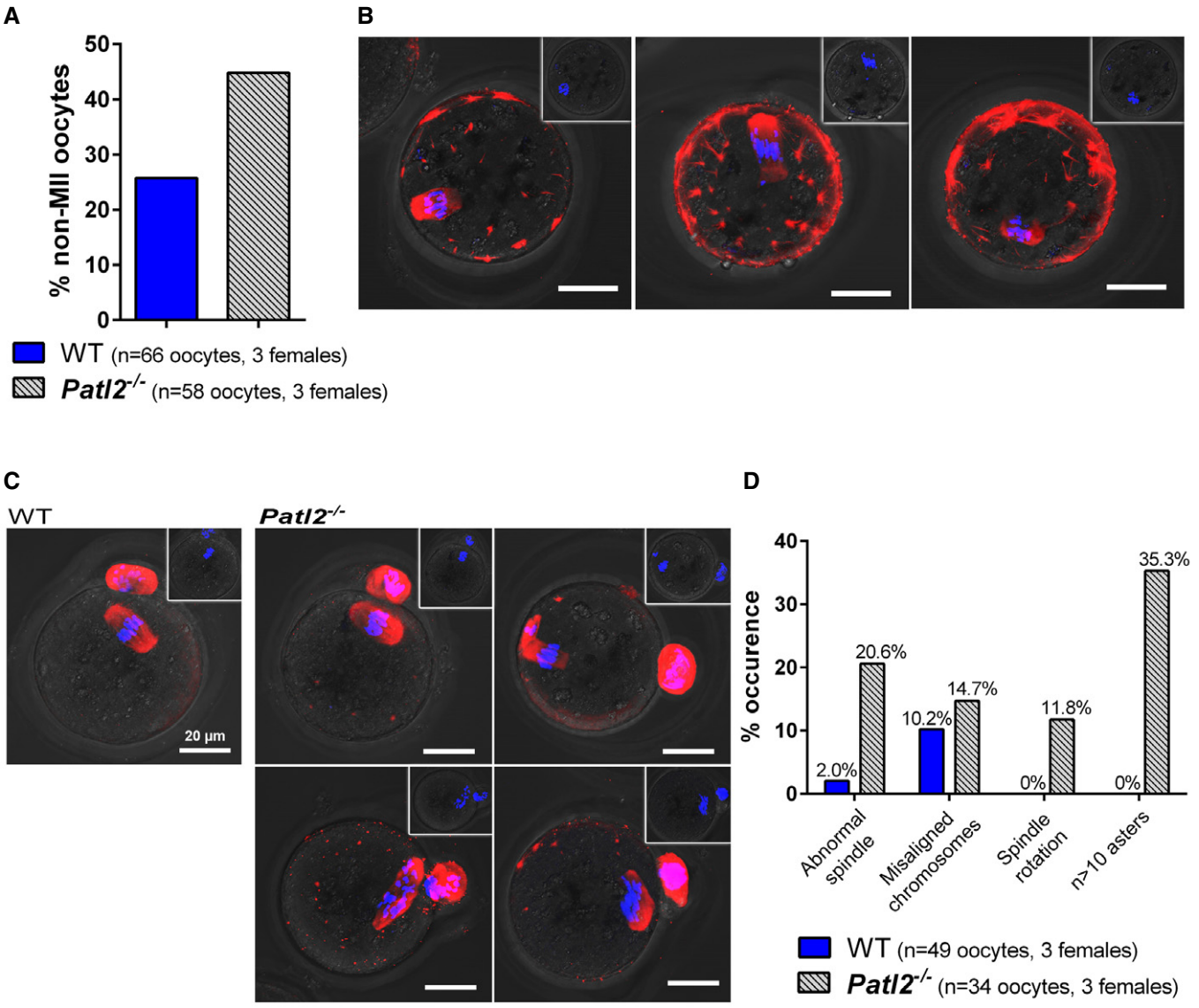

Figure 5. Infertility of *Patl2*-deficient female mice is due to oocyte maturation defects.

A Oocytes collected after ovarian stimulation were labelled with a tubulin antibody (red) and counterstained with DAPI to reveal DNA (blue). An increase in non-MII oocytes (MI arrest, absence of PB) after full ovarian stimulation was observed in *Patl2*$^{-/-}$ mice (n = 3 females per genotype).

B IF images of tubulin-stained *Patl2*$^{-/-}$ oocytes arrested at MI stage showing various defects such as irregular spindle shape and abnormal chromosome distribution. Scale bar = 20 µm. Inset in each panel shows overlay of phase contrast image and Hoechst staining of the corresponding oocyte. No polar bodies were observed for MI oocytes.

C IF images of tubulin-stained WT and *Patl2*$^{-/-}$ MII oocytes, as evidenced by PB1. In control MII oocytes, stack projections of confocal images show that the spindle was symmetric and the chromosomes distributed in the middle of the spindle. In contrast, in *Patl2*$^{-/-}$ MII oocytes various defects were observed such as irregular spindle shape, spindle rotation and numerous cytoplasmic asters. Slightly greater numbers of oocytes with abnormal chromosome distribution were also observed. Scale bar = 20 µm. Inset in each panel shows overlay of phase contrast image and Hoechst staining of the corresponding oocyte. One polar bodies was observed for MII oocytes.

D Histograms quantifying the % defects observed in *Patl2*$^{-/-}$ MII oocytes.

assessed how the absence of Patl2 affected the oocyte transcriptome during oocyte maturation in mice. To do so, global gene expression analysis was performed on oocytes collected at GV and MII stages from WT and *Patl2*$^{-/-}$ females.

Expression levels for nearly 66,000 transcripts were measured across the different oocyte groups using Affymetrix microarrays. First, we verified that oocyte RNA purification was not contaminated by RNA from follicular cells, by comparing expression levels of genes specific to follicular cells and oocytes, respectively (Appendix Fig S6A). The absence of exon 7 transcription in *Patl2*$^{-/-}$ oocyte extracts was also verified in the microarray data (Appendix Fig S6B). The results of this analysis revealed no

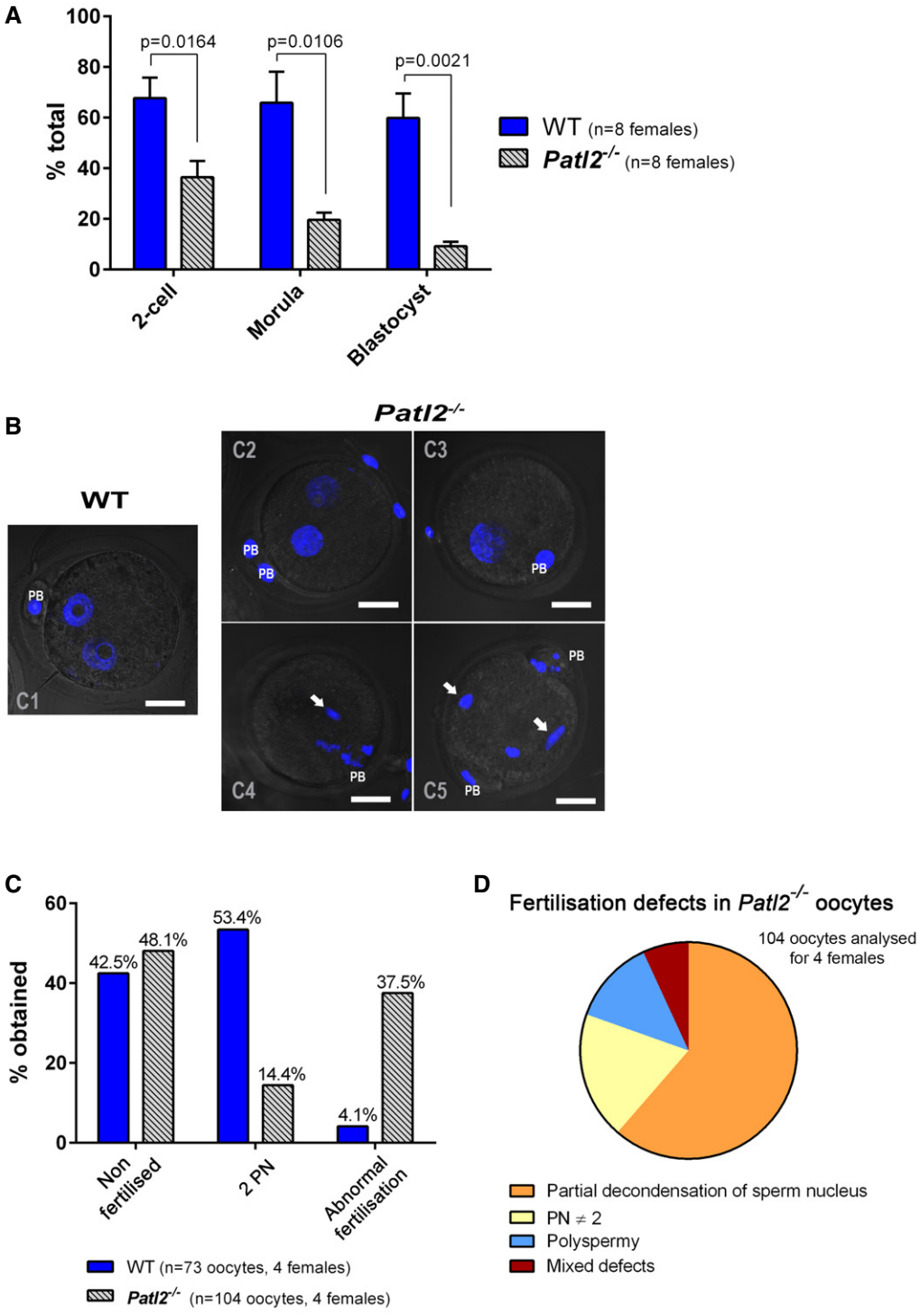

Figure 6. MII oocytes from *Patl2*$^{-/-}$ female mice exhibit abnormal fertilisation preventing normal embryo development.

A IVF outcomes (mean ± SEM) measured at the two-cell, morula and blastocyst stages show that the developmental competence of *Patl2*$^{-/-}$ oocytes is compromised. Oocytes were collected from stimulated WT and *Patl2*$^{-/-}$ females and sperm from WT males. For each IVF replicate (different WT males), IVF outcomes at different stages were compared for WT and *Patl2*$^{-/-}$ oocytes. Statistical differences were assessed using unpaired two-tailed *t*-tests.

B *Z*-stack projections of confocal images of 2PN zygotes obtained from WT and *Patl2*$^{-/-}$ oocytes 6-8 h after sperm–egg mixing. Fertilised WT oocytes exhibit normal 2PN stage (C1) whereas the number of fertilised *Patl2*$^{-/-}$ oocytes exhibiting normal 2PN stage is strongly reduced (C2) and most of them show defects such as absence of a male pronucleus (C3), partial decondensation of male PN (C4, C5, white arrows) or polyspermy (C5 white arrows). Scale bar = 20 μm, PB = polar body, PN = pronucleus.

C, D The percentage of 2PN obtained 6–8 h after fertilisation drops from 53.4% for WT to 14.4% for *Patl2*$^{-/-}$ oocytes, which exhibit various fertilisation abnormalities including partial decondensation of sperm DNA, polyspermy, abnormal number of PN or mixed defects (D).

difference in overall purified RNA concentration between WT and *Patl2*$^{-/-}$ oocytes, for both GV and MII stages, indicating that unlike Msy2, Patl2 is not a global regulator of mRNA stability and translation (Yu *et al*, 2001) (Appendix Fig S6C).

However, significant changes were observed for specific transcripts, both at GV and MII stages (Fig 7A). At the GV stage, lack of Patl2 induced a > twofold decrease for 95 transcripts ($P < 0.05$) and > twofold increase for 39 transcripts (Dataset EV1). At the MII stage, a > twofold decrease in 124 transcripts and > twofold increase in 122 transcripts were observed (Dataset EV2). Approximately one-third of the genes down-regulated at the GV stage (32) were also down-regulated at the MII stage, and half of the genes up-regulated at the GV stage (19) were also up-regulated at the MII stage (Dataset EV3 and Fig 7B). The impact of Patl2 deletion on gene expression at the GV and MII stages was then visualised using hierarchical clustering of genes with an absolute fold-change ((aFC))> 2, $P < 0.05$ (Fig 7C).

Phosphorylation, oxidation and other pathways are down-regulated in the absence of Patl2

Literature mining to determine the functions of the genes down-regulated in *Patl2*$^{-/-}$ oocytes identified several groups of genes reported to be involved in oocyte maturation. The proteins encoded are involved in several signalling pathways implicated in oocyte differentiation, oxidative stress, transcription and translation, exocrine modulation, meiosis and spindle formation (Table 2). We therefore suspect that the decreased expression of these genes interferes with normal oocyte differentiation. Regarding signalling pathways that are activated during oocyte maturation, significant down-regulation of transcripts for proteins involved in mTORC1, Wnt, NF-kB, MAP kinase and phosphatase signalling pathways was observed. It is worth noting that we also detected a more than twofold decrease in Pgrmc1, a receptor required to slow down oocyte meiotic progression (Guo *et al*, 2016; Table 2). This decrease in Pgrmc1 in GV oocytes was confirmed by RT–qPCR experiments (Appendix Fig S7).

Oocyte maturation is controlled by bidirectional crosstalk between the follicular cells and the oocyte: the secretion of oocyte-produced factors is necessary for follicle cell differentiation; follicle cells in turn secrete factors activating different signalling pathways within the oocyte (Li & Albertini, 2013). Interestingly, two factors, Cxcl14 and Adm2, known to play a crucial role in cumulus cell maturation (Bobe *et al*, 2006; Chang *et al*, 2011), were down-regulated in *Patl2*$^{-/-}$ oocytes (Table 2). We also observed a strong deregulation of several other interesting transcription factors, such as Sohlh2, which was down-regulated 2.2-fold and 5.3-fold at the GV and MII stages, respectively, and Eef1e1 (Table 2). We also noticed that two glutathione-S-transferases were repressed in *Patl2*$^{-/-}$ GV oocytes (Table 2). This down-regulation may increase oxidative stress within the oocyte. Spindle defects may also be aggravated by repression of Pak4 and Ccdc69 (Table 2), two proteins known to affect spindle assembly (Pal *et al*, 2010; Bompard *et al*, 2013). RT–qPCR experiments confirmed the down-regulation of Ccdc69 and Eef1e1 in GV oocytes (Appendix Fig S7).

Some transcripts, such as *Fgf9* and *Cdc25a* which control meiosis II (Assou *et al*, 2006), are known to be strongly up-regulated in oocytes after GVBD. Interestingly, both these transcripts were significantly down-regulated in *Patl2*$^{-/-}$ MII oocytes (Table 2). This decreased expression probably hampers final oocyte maturation. Among the list of genes up-regulated at both GV and MII (Dataset EV3), two particular genes, *Prr11* and *Ska2* (spindle and kinetochore associated complex subunit 2), are known to be required for spindle stability (Zhang *et al*, 2012). Ska2 up-regulation was confirmed by RT–qPCR for GV oocytes (Appendix Fig S7).

Finally, the lists of all down- and up-regulated proteins in *Patl2*$^{-/-}$ oocytes at the GV and MII stages were uploaded directly into Ingenuity Pathway Analysis (IPA) software, to explore their molecular and biological functions. At the GV stage, the most significantly down-regulated pathways were the ephrin receptor pathway and ephrin A signalling, which control embryo/trophoblast development (Fig EV4A and Table 2). Interestingly, at the MII stage, the cell cycle G1/S checkpoint was also significantly down-regulated (Fig EV4B), in accordance with the cell cycle defects visible in Fig 5.

The transcripts differentially expressed between MII and GV in WT and *Patl2*$^{-/-}$ samples affect a similar set of biological pathways and functions

To assess a possible role for Patl2 in the GV-MII transition, we identified the up- or down-regulated differential expression transcripts (DET) ($P < 0.05$, absolute fold-change > 2) between the GV and MII transcript lists for WT and *Patl2*$^{-/-}$ samples (Datasets EV4 and EV5). The lists of corresponding proteins were directly uploaded into IPA software to explore their molecular and biological functions. The functional pathways or networks with the highest confidence scores were then determined by right-tailed Fisher's exact tests. This analysis showed that a large portion of DET in WT samples were involved in energy production (oxidative phosphorylation and mitochondrial (dys)function, Appendix Fig S8) protein synthesis (EIF2 signalling, regulation of eIF4 and p7056K signalling) and DNA replication, recombination and repair (Fig EV5A). It is worth noting that the up- and down-regulated transcripts included in the DET lists were documented to functionally interact with each other, forming tightly connected networks. This observation strengthens the relevance of the data (Appendix Fig S9A). A similar analyse of DET from *Patl2*$^{-/-}$ samples indicated that the eight pathways with highest confidence scores were identical to those recorded for WT samples (Fig EV5B), suggesting that Patl2 only plays a minor role (or no role) in the

Figure 7. Transcriptional analysis of GV and MII oocytes from WT and Patl2$^{-/-}$ mice.

A Comparison of the transcriptional profiles in *Patl2*$^{-/-}$ oocytes versus WT oocytes at the GV or MII stages. GV oocytes were collected 44 h after PMSG injection and MII 13 h after hCG injections. For both MII and GV, two replicates for WT and three replicates for *Patl2*$^{-/-}$ oocytes were analysed.

B Venn diagrams representing down- or up-regulated genes in *Patl2*$^{-/-}$ oocytes (absolute fold-change ((aFC))> 2, $P < 0.05$) with respect to WT oocytes at the GV and MII stages.

C Hierarchical clustering of gene expression data for the down- and up-regulated genes (aFC> 2, $P < 0.05$) of *Patl2*$^{-/-}$ and WT oocytes at GV (left) and MII (right) stages, demonstrating the clustering of replicates to their respective groups.

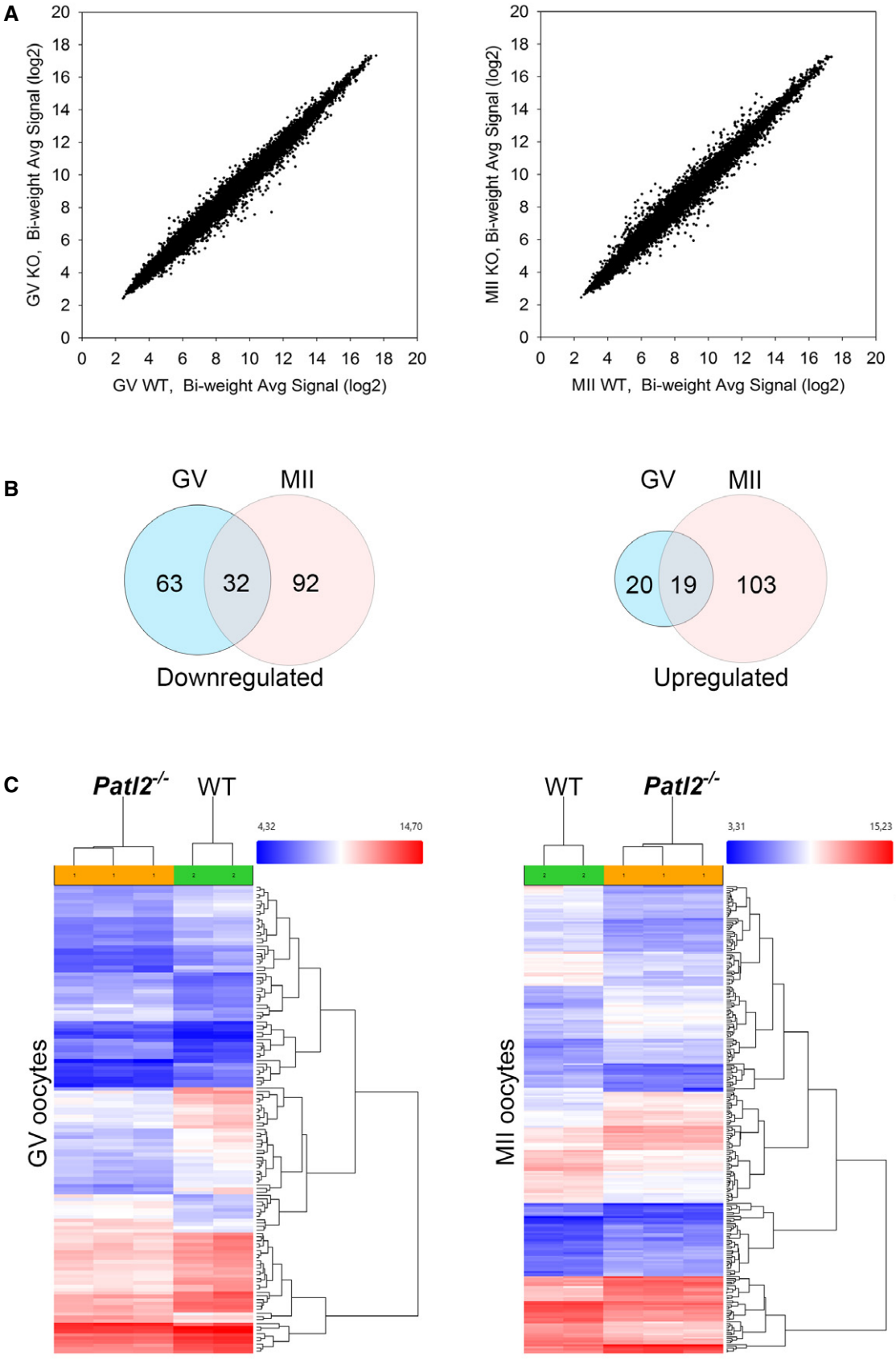
A
GV KO, Bi-weight Avg Signal (log2)
GV WT, Bi-weight Avg Signal (log2)
MII KO, Bi-weight Avg Signal (log2)
MII WT, Bi-weight Avg Signal (log2)
B
GV
MII
63
32
92
Downregulated
20
19
103
Upregulated
C
Patl2-/-
WT
4,32
14,70
GV oocytes
WT
Patl2-/-
3,31
15,23
MII oocytes

Figure 7.

Table 2. Gene ontology analysis of microarray data.

Gene symbol	Gene name	WT GV	KO GV	Fold-change	WT MII	KO MII	Fold-change	(Possible) role in oocyte maturation and early embryo development	References
Elements of signalling pathways activated during oocyte maturation									
Gatsl3	GATS protein-like 3	9.64	8.12	−2.88	9.26	8.99	−1.21	CASTOR (gatsl3) is an arginine sensor for the mTORC1 pathway. Arginine breaks the CASTOR/GATOR2 complex. GATOR2 activates mTORC1. Activated mTORC1 will phosphorylate translation inhibitor 4E-BP1, releasing it from eukaryotic translation initiation factor 4E (eIF4E) which is then free to join the translation initiation complex. When the mTORC pathway is inhibited, bovine oocytes are blocked at the M1 stage	Chantranupong *et al* (2016), Mayer *et al* (2014)
Pygo1	Pygopus 1	8.68	6.9	−3.43	8.25	6.73	−2.87	Pygopus is a Wnt transcriptional component. Knockdown of Axin-1, a negative regulator of Wnt signalling leads to defective spindles, misaligned chromosomes, PB1 extrusion failure and impaired PN formation. Embryo development is also impacted since maternal Wnt/STOP signalling promotes cell division during early *Xenopus* embryogenesis. WNT signalling pathway is important for proper oocyte maturation	He *et al* (2016), Huang *et al* (2015), Spate *et al* (2014)
Ppp1r14b	Protein phosphatase 1, regulatory (inhibitor) subunit 14B	12.62	11.11	−2.84	12.65	11.34	−2.49	PP1 is an important protein involved in the cell cycle and controls dephosphorylation of numerous proteins such as proteins phosphorylated by Cdc2 and downstream mitotic kinases. Likely impacts meiotic control	
Ppp1r15a	Protein phosphatase 1, regulatory (inhibitor) subunit 15A	8.26	7.29	−1.96	9.12	8.17	−1.92		
Dusp1	Dual specificity phosphatase 1	11.94	10.49	−2.72	12.78	11.78	−2.01	Dusp1 is able to dephosphorylate MAP kinase, known to be very important in oocyte maturation and meiosis	Liang *et al* (2007)
Nfkbia	Nuclear factor of kappa light polypeptide gene enhancer in B cells inhibitor, alpha	9.78	8.33	−2.73	9.43	7.7	−3.31	NFKBIA is a gene involved in maintaining meiotic transcriptional arrest. Inhibits the NF-κB transcription factor. Change during GV-MII transition. Highly expressed at embryonic genome activation	Paciolla *et al* (2011)
Pgrmc1	Progesterone receptor membrane component 1	9.16	7.97	−2.27	9.53	8.01	−2.86	P4–PGRMC1 interaction attenuated oocyte meiotic progression and primordial follicle formation by decreasing intra-oocyte cAMP levels. When PGRMC1 is low, oocytes are not blocked by P4 and mature too fast	Guo *et al* (2016)
Secreted factors									
Cxcl14	Chemokine (C-X-C motif) ligand 14	8.08	6.99	−2.13	8.59	7.5	−2.13	Important factor for oocyte maturation in fish	Bobe *et al* (2006)

Table 2 (continued)

Gene symbol	Gene name	WT GV	KO GV	Fold-change	WT MII	KO MII	Fold-change	(Possible) role in oocyte maturation and early embryo development	References
Adm2	Adrenomedullin 2	11.75	10.64	−2.16	12.4	11.91	−1.4	ADM2 is a novel oocyte-derived ligand important for the regulation of cell interactions in COCs that functions, in part, by suppressing cumulus cell apoptosis	Chang *et al* (2011)
Transcription translation factors									
Med11	Mediator complex subunit 11;	9.84	8.28	−2.94	9.78	8.39	−2.62	Mediator of RNA polymerase II transcription, subunit 11 homologue (*S. cerevisiae*)	
Med29	Mediator complex subunit 29	11.01	9.33	−3.2	7.97	7.32	−1.57	Mediator complex subunit 29 (MED29) is part of a large multiprotein coactivator complex that mediates regulatory signals from gene-specific activators to general transcription machinery in RNA polymerase II mediated transcription	
Sohlh2	Spermatogenesis and oogenesis specific basic helix-loop-helix 2	7.18	6.06	−2.18	8	5.58	−5.33	SOHLH2 is a transcription factor that coordinates oocyte differentiation without affecting meiosis I and drives oocyte growth and survival but not meiosis I	Choi *et al* (2008), Shin *et al* (2017)
Slx2	Sycp3 like X-linked	8.04	6.81	−2.36	5.97	5.77	−1.15	SLX2 might be involved in DNA recombination, synaptonemal complex formation as well as sex body maintenance during meiosis	Shi *et al* (2013)
Prmt5	Protein arginine N-methyltransferase 5	9.05	7.88	−2.25	8.72	8.16	−1.47	PRMT5 negatively affects cyclin E1 promoter activity. Cyclin E1 is activated during meiosis in *Xenopus*. Prmt5 is critical in biological function in a wide range of cellular processes including development and methylates histones H2A and H4 in oocytes	Stopa *et al* (2015), Wilczek *et al* (2011)
Eef1e1	Eukaryotic translation elongation factor 1 epsilon 1	13.39	12.26	−2.19	13.24	11.78	−2.76	DNA damage response. Regulator of translation	Uniprot
E2f4	E2F transcription factor 4	13.61	12.5	−2.17	14.02	13.18	−1.8	Regulator of translation	
Oxidative stress									
Gstp2	Glutathione S-transferase, pi 2	12.04	10.41	−3.11	10.28	9.51	−1.71	Important in oxidative stress. A high level of gluthatione transferase is associated with higher oocyte developmental quality. Glutathione S-transferase is a marker of oocyte maturity in pigs	Paczkowski and Krisher (2010), Rausell *et al* (2007)
Gstp1	Glutathione S-transferase, pi 1	11.43	9.91	−2.86	9.74	9.14	−1.51		
Spindle assembly									
Pak4	p21 protein (Cdc42/Rac)-activated kinase 4	11.32	10.32	−2.01	12.02	11.41	−1.52	Ran is a substrate for p21-activated kinase 4 (PAK4). RanGTP is an important actor of spindle formation and asymmetric division during meiosis	Bompard *et al* (2013)

Table 2 (continued)

Gene symbol	Gene name	WT GV	KO GV	Fold-change	WT MII	KO MII	Fold-change	(Possible) role in oocyte maturation and early embryo development	References
Ccdc69	Coiled-coil domain containing 69	14.63	13.54	−2.13	14.8	13.87	−1.91	CCDC69 regulates central spindle assembly	Pal *et al* (2010)
Embryo/trophoblast factors									
Phlda2	Pleckstrin homology-like domain, family A, member 2	10.3	7.56	−6.7	7.7	7.05	−1.57	PHLDA2 is an imprinted gene, and only the maternal copy is expressed. This gene is associated with placental dysfunction. KO mice exhibit foetal growth deficiency	Frank *et al* (2002), Jensen *et al* (2014)
Efna1	Ephrin A1	9.73	7.34	−5.24	9.05	8.02	−2.04	Ephrins A1-4 were expressed in blastocysts. The ephrin A system is involved in regulating contact between blastocysts and endometrium during embryo implantation	Fu *et al* (2012), Fujii *et al* (2006)
Efna4	Ephrin A4	8.7	7.08	−3.07	8.55	7.21	−2.54		
Efna2	Ephrin A2	8.9	7.49	−2.66	8.81	7.86	−1.93		
Cstb	Cystatin B	11.81	9.44	−5.17	10.85	9.5	−2.55	The cathepsin–cystatin system plays an important role in trophoblast cell invasion and normal embryonic growth	Nakanishi *et al* (2005)
Prl8a2	Prolactin family 8, subfamily a, member 2	9.51	7.17	−5.05	9.12	5.93	−9.16	In Prl8a2 null tissues, genes expressed in the trophoblast are down-regulated	Alam *et al* (2015)
Crabp2	Cellular retinoic acid binding protein II	12.73	10.5	−4.69	12.34	10.73	−3.06	Altered expression level of endometrial CRABP2 is involved in abnormal endometrium-trophoblast interaction, which leads to implantation failure	Lee *et al* (2011)
Tlr8	Toll-like receptor 8	7.34	5.49	−3.61	7.15	5	−4.46	TLR8 is expressed in the trophoblast. Its inhibition suggests that it is necessary for successful establishment of early gestation in ewes	Kaya *et al* (2017), Ruiz-Gonzalez *et al* (2015)
Specific MII regulation									
Fgf9	Fibroblast growth factor 9	6.64	6.1	−1.45	7.21	5.88	−2.51	FGF9 counteracts retinoic acid, which promotes entry into meiosis. Its expression increases at MI stage and reaches highest level at the MII stage	Feng *et al* (2014)
Cdc25a	Cell division cycle 25A	11.59	11.55	−1.03	12.31	11.18	−2.19	Its expression increases significantly at the MII stage. Cdc25a is crucial in the MI-MII transition and its down-regulation results in fewer oocytes resuming meiosis and reaching MII	Solc *et al* (2008)

GV-MII transition. Similarly, in *Patl2*$^{-/-}$ samples, DET formed tightly connected networks (Appendix Fig S9B).

Discussion

Genetic basis of OMD

The genetic basis of OMD was unexplored until 2016 when heterozygous mutations of *TUBB8* were reported to account for approximately 30% (7/23) of OMD Han Chinese familial cases (Feng *et al*, 2016). In our 22-subject cohort, only one *TUBB8* deletion variant was identified by WES analysis, suggesting that *TUBB8* mutations may not be a common cause of OMD in North African women. No down-regulation of the expression of tubulin genes was observed in GV or MII oocytes from *Patl2*$^{-/-}$ mice, indicating that *PATL2*-dependent OMD does not involve tubulin deregulation. These results suggest geographical heterogeneity of the genetic causes of OMD. Indeed, 26% of our patients were found to present the same homozygous truncation of *PATL2*, demonstrating that *PATL2* mutation is a major cause of OMD

in North Africa. Interestingly, the same mutation was detected in all our patients, suggesting a founder effect. This hypothesis was reinforced by the analysis of the variants from WES data in the regions surrounding *PATL2*, which revealed a common homozygous haplotype (Dataset EV6). During the assessment of our data, two other studies were published associating *PATL2* with human OMD. The first was carried out on a cohort of 180 Han Chinese patients: it identified 5 *PATL2* nonsense variants and four mis-sense variants in five unrelated subjects. If the mis-sense variants are proven to be deleterious, this corresponds to a frequency of ~3% in the subjects tested (5/180) (Chen *et al*, 2017). In the second study, two homozygous *PATL2* variants were identified in two OMD subjects each from two different Saudi Arabian families. One of these variants is the same p.Arg160Ter variant presented here, whereas the other is a new mis-sense variant (Maddirevula *et al*, 2017). With cases across two continents, these studies, in combination with the present study, provide strong evidence that *PATL2* mutation is a major cause of human OMD whose phenotype is characterised by arrested development at the germinal vesicle stage.

Comparison of expression profiles and distribution for Patl2 and other RNA-binding proteins suggest a niche role for Patl2

By IF, we showed that (i) Patl2 is undetectable in primordial follicle oocytes; (ii) significant Patl2 translation begins at the primary follicle stage; (iii) Patl2 concentration peaks in secondary follicle oocytes; (iv) Patl2 is expressed only in the cytoplasm; (v) staining is relatively homogenous; and (vi) taking oocyte volume into account, the total amount of Patl2 increases as oocytes grow. These results clearly indicate that Patl2 plays a key role during oocyte growth and that it does not contribute to the maintenance of the primordial follicle pool in mouse ovaries. This conclusion is corroborated by our data showing comparable numbers of primordial follicles in control and Patl2$^{-/-}$ ovaries at 12 dpp. Nevertheless, the number of primordial follicles was found to be significantly higher at 26 dpp in Patl2$^{-/-}$ ovaries. This puzzling result deserves further investigation; it may indicate that expression of Patl2 is required for the primordial/primary follicle transition. The importance of Patl2 in oocyte growth is reinforced by our data showing that GV and MII oocytes are smaller in diameter in the absence of Patl2. Interestingly, although signal intensity for Patl2 declined during the GV NSN to SN transition, the protein remained clearly detectable in MII oocytes. This observation contrasts with data from *Xenopus* oocytes, where x-Pat1a was shown to completely disappear upon progesterone-induced meiotic maturation (Marnef *et al*, 2010; Nakamura *et al*, 2010). This discrepancy suggests that the function of Patl2 may have evolved in mammals to include a role during fertilisation and/or early development. A similar evolution has been reported for the germ-cell-specific translational repressor Msy2, which is detectable until the late two-cell embryo stage, undergoing changes in its phosphorylation state which presumably influence its interaction with mRNA (Yu *et al*, 2001).

Oocyte growth is characterised by extensive mRNA synthesis and accumulation within the cytoplasm. Although most of the mRNA synthesised during oocyte growth is immediately translated to support the growing oocyte, up to 30% of mRNAs are stored for subsequent translation and are required at meiotic resumption or for early zygote development (Pique *et al*, 2008). Several molecular mechanisms controlling mRNA stability have been described and involve a number of RNA-binding proteins (Clarke, 2012), although their relative contributions remain poorly understood. The best-described translational repression mechanism in oocytes involves a specific mRNA sequence, the cytoplasmic polyadenylation element (CPE), which is present in the 3′ UTR of the affected mRNAs. It associates with its binding factor, CPEB, as well as the cytoplasmic polyadenylation machinery (Racki & Richter, 2006; Sousa Martins *et al*, 2016). The role of CPEB in mediating translational repression is well documented, but its precise mechanism of action—in particular the roles of its molecular partners—remains to be fully elucidated. x-Pat1a, for example, was described to be an RNA-binding protein and a partner of CPEB in *Xenopus* oocytes, but its precise role in translational repression remains unknown (Nakamura *et al*, 2010). Apart from CPEB, the RNA-binding protein Msy2 also plays a key role in RNA stability. The *Xenopus* orthologue of Msy2 (Ybx2) has been reported to participate in the same complex as x-Pat1a and CPEB in *Xenopus* oocytes (Medvedev *et al*, 2011). Absence of Msy2 in mice leads to infertility and modulates the expression of around 7,000 transcripts (> twofold absolute change), that is approximately 30% of all transcripts. This broad effect could be explained if it acts as a sequence-independent RNA-binding protein or global regulator of mRNA stability. Finally, P-bodies, central to RNA processing in somatic cells, have been described in mammalian oocytes. The RNA helicase and translational repressor Ddx6 is a key component of all known types of P-body. Several studies have reported the existence of P-bodies containing Ddx6 in immature mouse oocytes, which disappear during oocyte growth, dispersing Ddx6 as well as Msy2 and Cpeb within the cytoplasm (Swetloff *et al*, 2009; Flemr *et al*, 2010). We therefore endeavoured to find out whether Patl2 may be part of a similar, temporary, structure.

To assess the possibility that Patl2 works in synergy with these proteins which are important for mRNA stability, we compared their expression profiles and abundance and performed colocalisation experiments. Patl2 localisation was determined using Patl2-HA mice. Msy2 and Ddx6 proteins were found to be expressed at significant levels in primordial follicle oocytes, whereas Patl2 was undetectable at this stage. The Msy2 concentration appeared constant throughout oocyte growth, and its abundance in antral follicle oocytes is in line with its role in the oocyte-embryo transition (Yu *et al*, 2001). Ddx6 is strongly expressed in primordial and primary follicle oocytes, with signal intensity gradually decreasing in secondary and tertiary follicle oocytes. As Ddx6 is a P-body component, this result is compatible with the disappearance of P-bodies in fully grown oocytes (Flemr *et al*, 2010). Unlike Patl2, Cpeb1 was detectable in primordial follicle oocytes, but its signal intensity pattern was otherwise similar to that of Patl2, peaking in secondary follicle oocytes and weakening in tertiary follicle oocytes. However, Cpeb1 appears to be localised in small RNPs, as evidenced by its clear punctiform staining (Fig 3). In colocalisation experiments performed on secondary follicle stage oocytes, Patl2 failed to clearly colocalise with any of the three mRNA regulatory proteins. Taken together, these results suggest that Patl2 may be involved in a new pathway controlling the stability of specific mRNA. This new pathway merits further study.

Impact of *Patl2* invalidation on the oocyte transcriptome

In this study, we assessed the impact of the absence of Patl2 on the transcriptomic profiles of GV and MII oocytes and on the

transcriptomic variation observed at the GV-MII transition. The GV-MII transition had previously been reported to be associated with specific degradation of a large number of transcripts associated with protein synthesis, DNA replication and energy production (Su *et al*, 2007). Our results confirm these previous findings, as the pathways that underwent the most significant changes during the GV-MII transition in WT oocytes were associated with oxidative phosphorylation and mitochondrial (dys)function (energy production), EIF2 and regulation of eIF4 and p7056K signalling (protein synthesis) and DNA repair (Su *et al*, 2007). Su *et al* (2007) also showed that 62 out of 88 transcripts in the oxidative phosphorylation pathways were down-regulated at the GV-MII transition. Here, we report down-regulation of 45 out of 88 transcripts, of which 32 are included in the set reported by Su *et al* (2007). Interestingly, our IPA analysis revealed other pathways that are modulated during the GV-MII transition, such as sirtuin signalling and mTOR signalling. The similarity of our results to previous reports, together with RT–qPCR analysis of selected genes, reinforces the conclusions drawn from the transcriptomic analyses. Importantly, we observed effects on the same major pathways in the GV-MII transition in *Patl2*$^{-/-}$ oocytes and in WT oocytes, suggesting that Patl2 is not involved in this transitional phase.

Our data show that the absence of Patl2 induces transcriptomic deregulation, affecting 135 genes at the GV stage and 248 genes at the MII stage with an absolute fold-change > 2, ($P < 0.05$). This relatively small list includes genes of highly relevant function (Table 2). Indeed, several of the corresponding proteins, such as Prgmc1 and Slohlh2, are reported to be involved in oocyte maturation. Sohlh2 is of particular interest as it has been described to be required for oocyte growth, and Sohlh2$^{-/-}$ females were found to be infertile (Choi *et al*, 2008). Interestingly, this factor does not affect meiosis I (Shin *et al*, 2017), which is line with the observation that *Patl2*$^{-/-}$ females are able to generate MII oocytes. The factors Cxcl14 and Adm2, known to be necessary for cumulus cell maturation, were also found to be down-regulated. However, no decrease in follicle size or any other visible defects were observed in ovarian sections at 26 dpp, suggesting that any follicular defects are subtle. Importantly, several key proteins protecting cells against oxidative stress were down-regulated (GST forms). Oocytes are very sensitive to oxidative stress, which causes spindle abnormalities (Choi *et al*, 2007) and affects developmental competence (Rausell *et al*, 2007); in addition, glutathione S-transferase has been reported to be a marker of oocyte maturity in pigs (Paczkowski & Krisher, 2010).

Some of the up-regulated transcripts could also interfere with normal oocyte maturation. The most extensively up-regulated gene at the MII stage was *Prr11*. In WT MII oocytes, its expression was low, suggesting that its role in normal oogenesis is minimal or null. *Prr11* deregulation has however been shown to dramatically modify the cell cycle, although how it does so remains unclear (Li *et al*, 2017). Its strong up-regulation may therefore interfere with meiosis or early development. Another remarkable gene up-regulated at both GV and MII is *Ska2* (spindle and kinetochore associated complex subunit 2), which is known to control spindle stability during meiosis (Zhang *et al*, 2012). This up-regulation could explain the numerous defects observed in MI and MII meiotic spindles. Up-regulation of these genes could be a cellular response attempting to address the transcript deregulation induced by Patl2-deficiency. Taken together, these results underline the importance of PATL2 in the regulation of a specific subset of mRNAs required for the generation of mature oocytes.

Moreover, a considerable number of genes known to be involved in pre-implantation embryonic development were also found to be down-regulated in both GV and MII oocytes from *Patl2*$^{-/-}$ mice. This down-regulation may contribute to the poor pre-implantation developmental competence observed for *Patl2*$^{-/-}$ embryos (Fig 6). These results suggest that Patl2 plays an essential role in maintaining the integrity of a small pool of mRNAs synthesised during oocyte growth and necessary after fertilisation and during early embryo development. This role is compatible with the presence of Patl2 in MII oocytes and its function as a translation repressor, as described for its *Xenopus* homologue (Marnef *et al*, 2010).

In conclusion, we report that PATL2 is a vital player in oocyte growth and maturation, where it regulates the expression of mRNAs encoding proteins crucial for oocyte meiotic progression and early embryonic development, and that its invalidation causes OMD in humans. Unravelling the molecular basis of OMD will help patients by improving diagnosis and our understanding of their disease. This work will also be of tremendous interest to the fast-growing field of clinical *in vitro* oocyte maturation, necessary for the development of a number of applications, such as fertility preservation for cancer patients (in particular for young prepubertal girls; Kim *et al*, 2016) before commencing reprotoxic chemotherapy, or *in vitro* maturation of primary/secondary follicles for patients with premature ovarian failure (Kim, 2012; Yin *et al*, 2016).

Materials and Methods

Ethics

After sperm analysis and IVF treatment, performed independently of the research presented in this paper, couples presenting an interesting phenotype (male and/or female infertility) were selected and referred by their physician. The physician explained the study and its objectives before subjects signed an informed consent form in line with the local IRB protocols and the principles of the Declaration of Helsinki. DNA samples from couples of interest were collected and the identity of patients coded in such a manner that subjects could not be identified. All medical records were saved. No specific treatment was given to any female patient for research purposes, and all oocytes collected were used for IVF/ICSI treatment only.

Patients and biological samples

A total of 23 patients were recruited. All subjects were of North African descent, mainly Tunisia and Algeria, with one patient from Mauritania. All had undergone one or two cycles of ovarian stimulation to allow egg collection for use in IVF. Human DNA samples were obtained from patients consulting for diagnosis and assisted reproductive techniques at the PolyClinique des Jasmins (Tunis, Tunisia) ($n = 21$) or at the reproductive unit located in Bondy, France ($n = 2$).

Patients underwent standard controlled ovarian stimulation by the administration of gonadotropins using either the long agonist or the antagonist protocol. Women were given between 150 and 225 IU recombinant follicle-stimulating hormone (Gonal-F; Merck-Serono). Subsequently, ultrasound was performed and follicular response

recorded from day 5 of gonadotropin stimulation. When at least two follicles were ≥ 18 mm in diameter, 6,500 IU or 10,000 IU human chorionic gonadotropin was administered. Oocytes were retrieved 34–36 h later by vaginal ultrasound-guided follicular puncture.

Control cohort: Since 2007, and in parallel to this study on OMD, we also performed a large study on male infertility, involving several hundred couples. Most of these couples had IVF/ICSI treatments, and female partners of infertile men with normal fertility levels were considered as fertile controls. Their characteristics were recorded and used anonymously. These cohorts have already been described in our previous works concerning male infertility (Dieterich *et al*, 2007; Harbuz *et al*, 2011; Ben Khelifa *et al*, 2014; Coutton *et al*, 2018; Kherraf *et al*, 2018).

Exome sequencing and bioinformatics analysis

Genomic DNA was isolated from saliva using Oragene saliva DNA collection kit (DNAgenotek Inc., Ottawa, Canada). Exome capture was performed using NimblGen SeqCap EZ Kit version 2 (Roche). Sequencing was conducted on Illumina HiSeq2000 instruments with paired-end 76-nt reads. Sequence reads were aligned against the reference genome (hg19) using MAGIC (SEQC/MAQC-III Consortium, 2014). Duplicate reads and reads mapping to multiple locations in the genome were excluded from further analysis. Positions with a sequence coverage of < 10 on either the forward or reverse strand were excluded. Single nucleotide variations (SNV) and small insertions/deletions (indels) were identified and quality-filtered using in-house scripts. The most promising candidate variants were identified using an in-house bioinformatics pipeline which is described in (Coutton *et al*, 2018). Variants with a minor allele frequency > 5% in the NHLBI ESP6500 or in 1,000 Genomes Project phase 1 data sets, or > 1% in ExAC, were discarded. These variants were also compared to an in-house database of 56 control exomes. All variants present in a homozygous state in this database were excluded. Variant Effect Predictor (Ensembl) was used to predict the impact of the selected variants. Only variants affecting splice donor/acceptor sites or causing frameshift, inframe insertions/deletions, stop gain, stop loss or mis-sense variants were retained, except for those scored as "tolerated" by SIFT (sift.jcvi.org) and as "benign" by Polyphen-2 (genetics.bwh.harvard.edu/pph2). All steps from sequence mapping to variant selection were performed using the ExSQLibur pipeline (https://github.com/tkaraouzene/ExSQLibur).

SANGER sequencing

Sanger sequencing was carried out using the primers listed in Appendix Table S1A. PCR amplification (35 cycles) was performed with a melting temperature of 60°C. Sequencing reactions were performed using BigDye Terminator v3.1 (Applied Biosystems). Sequence analyses were carried out on ABI 3130XL (Applied Biosystems). Sequences were analysed using seqscape software (Applied Biosystems). The primers used for Sanger verification of *PATL2* mutations in patients are listed in Appendix Table S1A.

Mice

All animal procedures were performed according to the French and Swiss guidelines on the use of animals in scientific investigations after approval of the study protocol by the local Ethics Committee (ComEth Grenoble No. 318, ministry agreement number #7128 UHTA-U1209-CA) and the Direction Générale de la Santé (DGS) for the State of Geneva. *Patl2*$^{FL/FL}$ mice (C57BL/6NTac-Patl2 < tm1a) were generated by the EUCOMM Consortium (http://www.mousephenotype.org/about-ikmc/eucomm). They were obtained from the Mouse Clinical Institute—MCI, Strasbourg, France. Deletion of exon 7 was obtained by crossing them with adult heterozygous EIIaCre transgenic mice (Lakso *et al*, 1996), obtained from Institut Cochin—Inserm 1016—CNRS 8104—Paris. The ellaCre carries a Cre transgene under the control of the adenovirus EIIa promoter. This construction targets expression of Cre recombinase to early mouse embryos. Cre expression is thought to occur prior to implantation in the uterine wall. Cre-mediated recombination thus affects a wide range of tissues, including the germ cells that transmit the genetic alteration to progeny.

Patl2-HA knock-in mice were generated by CRISPR/Cas9 technology (Kherraf *et al*, 2018). Twenty-seven nucleotides encoding the HA tag were inserted in the c-terminal of the *Patl2* gene, immediately before the TAG stop codon (TAC CCA TAC GAT GTT CCA GAT TAC GCT TAG) in C57BL/6 mice. One plasmid containing one sgRNA and Cas9 was injected (5 ng/μL) with the single-stranded DNA (50 ng/μl) for homology-directed repair. The single-stranded DNA was 187 nt long and contained two 80 nt long arms homologous to the nucleotides located before and after the *Patl2* stop codon, surrounding the 27 nucleotides encoding the HA tag, and ending with a TAG stop codon. The sgRNA sequence overlapped the native Patl2 stop codon which, eight nucleotides later, was followed by a TGG representing a suitable protospacer adjacent motif (PAM) sequence. The synthetic ssDNA was purchased from IDT (Leuven, Belgium). After injection, zygotes were left for 4–6 h before introducing them into pseudopregnant host females where they were carried to term. Edited founders were identified by Sanger sequencing from digit biopsies. Mice carrying the desired modification were crossed with C57BL6/J to verify germline transmission and eliminate any possible mosaicism. Heterozygous animals with the same modification were then mated to produce homozygous offspring.

Mice were housed with unlimited access to food and water in a facility with 12-h light per day. Animals were sacrificed by cervical dislocation at the ages indicated.

Genotyping

DNA for genotyping was isolated from tail biopsies. Tail biopsies (2 mm long) were digested in 200 μl lysis buffer (Direct PCR Lysis Reagent (Tail); Viagen Biotech inc, CA, USA) and 0.2 mg proteinase K for 12–15 h at 55°C, followed by 1 h at 85°C to inactivate proteinase K. The DNA was directly used to perform PCRs. Multiplex PCR was done for 35 cycles, with an annealing temperature of 62°C and an elongation time of 45 s at 72°C. PCR products were separated by 2% agarose gel electrophoresis. Genotypes were determined depending on the migration pattern. Primers for Patl2-KO and Patl2-HA-tagged mice are listed in Appendix Table S1B,C.

RT–qPCR

To verify the microarray results, RT–qPCR was performed on GV-stage oocytes from wild-type and knockout mice using the TaqMan® Gene Expression Cells-to-CT™ Kit (Ambion). Ten cells were washed

twice in PBS before lysis in 50 μl lysis/DNase buffer, giving a final lysate concentration of 0.2 cells/μl. 10 μl of cell lysate was added to 1× RT buffer for a final volume of 50 μl, resulting in a final concentration of 0.04 cell/μl. Gene expression was quantified using 4 μl of the resulting cDNA. Reactions were performed in 96-well plates on a StepOnePlus instrument (Applied Biosystems). Primers and probes (TaqMan Gene Expression assays) were ordered form Applied Biosystems and consist of a pair of unlabelled PCR primers and a TaqMan probe with a dye label (FAM) on the 5′ end, and a minor groove binder (MGB) and non-fluorescent quencher (NFQ) on the 3′ end. Normalisation was performed relative to *Gapdh* (fold-change found equal to 1 by microarray analysis). The ΔCt, which is determined by subtracting the Ct number for the reference gene from that of the target gene was statistically analysed. Relative quantification (RQ) was calculated ($2^{-\Delta\Delta Ct}$) and used to graphically present the results. Primers are listed in Appendix Table S1B.

Phenotypic analysis of mutant mice

Collection of GV and MII oocytes

GV oocytes were collected from 3- to 8-week-old females by puncturing ovaries with a 26-gauge needle in M2 medium (Sigma-Aldrich, Lyon, France) containing 150 μM dibutyryl cyclic AMP to prevent GV oocyte maturation and GVBD. Follicular cells surrounding GV oocytes were enzymatically (hyaluronidase 0.1%) and mechanically removed using a pipette with an inner diameter of around 100 μm. To extract GV oocytes from pre-antral follicles, follicles were treated with 2 mg/ml collagenase IV and 1 mg/ml hyaluronidase and ruptured with a fine pipette. For MII oocytes, 48 h after PMSG injection, 5 UI of human chorionic gonadotropin (hCG) was injected (Chorulon, Intervet), and cumulus-oocytes complexes (COCs) released from the ampullae were collected in M2 medium after 13 h. COCs were incubated in hyaluronidase enzyme (0.1 mg/ml, Sigma-Aldrich) for 5 min, and follicle-cell-free MII oocytes were obtained by pipetting.

In vitro fertilisation (IVF)

Eggs were collected from 4- to 8-week-old females, synchronised by exposing to 5 units of PMSG (Synchropart, Intervet, Beaucouze, France) and 5 units of hCG. Sperm from healthy males (B6D2 F1) capacitated for 80 min in M16 + 2% BSA (A3803 Sigma-Aldrich) were simultaneously added to the COCs and incubated in M16 medium for 4 h at 37°C under 5% CO_2. Unbound sperm were washed away after 4-h incubation. 24 h after fertilisation, the different stages, that is unfertilised oocytes and two-cell embryos (as an indication of successful fertilisation), were scored. Embryos were cultured in potassium simplex optimised medium (KSOM) (1×, Life technologies) supplemented with essential and non-essential amino acids (KSOM/EAA): two-cell embryos were incubated in KSOM/EAA medium at 37°C under 5% CO_2 and cultured up to the blastocyst stage.

Analysis of fertilised oocytes

After fertilisation, zygotes were transferred to a clean well containing M16 media and left for a further 2 h before being fixed in PFA 4% for 10 min and stained with Hoechst 33342 (2 μg/ml in PBS-PVP 0.5%). Oocytes were observed under confocal microscopy in drops of PBS-PVP covered with mineral oil on LabTeK chambered coverglass plates (Thermo Fisher Scientific, Villebon sur Yvette, France).

Immunostaining of GV and MII oocytes

Cumulus-free MII or GV oocytes prepared as described above were fixed in 4% PFA for 15 min, washed twice in PBS-PVP (0.5%) and permeabilised in PBS-Triton 0.25% for 20 min. Oocytes were then blocked in blocking solution (2% NGS, 0.1% Triton) for 90 min at room temperature and stained overnight at 4°C with primary antibodies (Appendix Table S2). All antibodies were diluted in blocking solution. Following staining, oocytes were washed twice with PBS-PVP 0.5% and incubated for 1 h at 37°C in secondary antibody and Hoechst 33342 at 2 μl/ml in blocking solution. Oocytes were finally washed twice and observed by confocal microscopy (Zeiss LSM 710) in drops of PBS-PVP covered with mineral oil on LabTeK coverglass plates. Images were processed using Zen 2.1 software.

Immunostaining of ovarian sections for oocyte counting

Mice were sacrificed by cervical dislocation, and ovaries were collected and fixed for 4 h in paraformaldehyde (4%). Ovaries were dehydrated embedded in paraffin, and 3-μm sections were cut. For histological analysis, after deparaffinisation, HIER and blocking slides were incubated with anti-Msy2 antibody (Appendix Table S2) for 1 h followed by a fluorophore-conjugated secondary antibody and Hoechst 33342 counterstaining. Stained sections were digitised at ×40 magnification using an Axioscope microscope (Zeiss, Germany) equipped with a motorised X–Y-sensitive stage. For each ovary, three sampling zones separated by 100–200 μm were studied. For each sampling zone, six to seven consecutive sections were stained and follicles counted, and the mean number of each class of follicle was calculated per sampling zone for WT and *Patl2*$^{-/-}$ mice.

Protein extraction and Western Blot

WT and PATL2-HA-tagged mice were sacrificed by cervical dislocation, and the hypothalamus, pituitary glands and livers were collected, snap-frozen in liquid nitrogen and stored at −80°C. The day of the experiment, organs were thawed in RIPA lysis buffer (50 mM Tris–HCl pH 7.5, 150 mM NaCl, 1% NP-40, 0.5% sodium deoxycholate, Complete EDTA-free protease inhibitor cocktail tablet (Roche)) and homogenised using a Dounce tissue grinder before mixing the supernatant with loading buffer in equal volumes (4% SDS, 62.5 mM Tris pH 6.8, 0.1% bromophenol blue, 15% glycerol, 5% bromophenol blue). The cytoplasmic fraction was isolated by centrifugation at 3,000 × *g* for 10 min. GV oocytes were collected in M2 medium supplemented with 150 mg/ml dbcAMP and prepared as described above. Oocytes were washed three times in PBS-PVP 0.5% to remove proteins from the M2 medium and added to an equal volume of loading buffer for a final volume of 20 μL. All protein samples were heated to 65°C for 15 min before loading onto a 4–20% TGX Mini-PROTEAN stain-free precast gel (Bio-Rad). Proteins were transferred onto a PVDF membrane, blocked in 5% milk and incubated overnight at 4°C in anti-HA antibody (Appendix Table S2) in blocking solution.

Oocyte RNA profiling

Total RNAs were purified from wild-type or *Patl2*$^{-/-}$ mouse oocytes using Norgen Biotek's Single cell Purification kit (Cat. 51800; Thorold, ON, Canada) according to the manufacturer's protocol. The GV oocyte samples (two WT and three *Patl2*$^{-/-}$ samples)

The paper explained

Problem

Infertility is considered a global public health issue since it affects more than 70 million couples worldwide. The common treatment for infertile couples is IVF (*in vitro* fertilisation) or ICSI (intracytoplasmic sperm injection); however, both of these techniques require mature egg cells having correctly completed both meiotic divisions. In rare cases, women who undergo hormonal stimulation for IVF or ICSI produce only immature eggs which cannot be fertilised or made to mature *in vitro*. We named this condition "oocyte meiotic deficiency". This condition is very poorly understood.

Results

We analysed a group of 23 women with oocyte meiotic deficiency by whole exome sequencing and identified a genetic mutation in the gene *PATL2* in 26% of patients. *PATL2* encodes an RNA-binding protein that has been shown to play an important role in egg cell maturation in frogs, but its function in mammals has not been studied until now. Using a knockout mouse model, we showed that Patl2 deficiency leads to defective oocyte maturation due to the deregulation of important genes involved in egg cell growth, meiosis and early embryo development. We also showed that Patl2 has a unique expression profile in comparison with other known oocyte RNA-binding proteins. These results indicate a specific, niche function for Patl2 in mRNA regulation during egg cell maturation in mammals.

Impact

We have identified *PATL2* mutation as a major cause of oocyte meiotic deficiency. This finding can benefit patients through an improved understanding of their condition and allowing for better informed decisions regarding treatment options. We have also demonstrated that mouse Patl2 plays an important role in mRNA regulation, furthering our understanding of the process of mammalian oocyte maturation. This finding is highly relevant to the fast-growing field of clinical *in vitro* oocyte maturation, with wide-ranging applications including fertility treatment for patients with premature ovarian failure and fertility preservation for cancer patients facing reprotoxic chemotherapy.

contained a total number of cells ranging between 20–32 oocytes/sample; the MII oocyte samples (2 WT and 3 $Patl2^{-/-}$ samples) contained between 32 and 46 oocytes. Purified RNA concentrations were assessed by RT–qPCR using the Affymetrix RNA quantification kit. Sample RNAs (250 pg) were converted to biotin-labelled single-strand cDNAs using the Affymetrix Genechip WT pico kit. Labelled and fragmented ss-cDNA (5.5 μg) were hybridised to Affymetrix arrays (Genechip Clariom D mouse). The array complexity allowed analysis of the expression of more than 66,000 different transcripts (including transcript variants and non-coding-cRNA) by measuring the expression level of their individual exons.

The data obtained for the whole set of samples were normalised by applying the RMA process (Affymetrix Expression Consol). Raw and normalised data were uploaded to the GEO database (Accession number GSE100117). Probe-set annotation, quantitative expressions of all the transcripts and comparisons between the different groups of samples (GV-KO versus GV-WT; MII-KO versus MII-WT) were analysed using TAC.v3 software (Affymetrix). Expression levels are reported as log2 conversions of the intensities measured for the ss-cDNA hybridised to the arrays. Differential expression of transcripts between two groups of samples was considered significant when the expression ratios of the transcripts between the two groups were at least twofold higher or lower (in linear scale) with a P-value < 0.05 (ANOVA test).

Transcriptomic analysis by IGA

IPA software (https://www.qiagenbioinformatics.com/products/ingenuity-pathway-analysis/) was used for the functional assessment of DET that were deregulated in $Patl2^{-/-}$ versus WT samples and to construct molecular interaction networks. IPA is software application that helps classify the molecular networks and functions most relevant to transcripts of interest. DET were imported to IPA for analysis. IPA generates pathways based on the transcripts contained in a data set and the information stored in the Ingenuity Pathways Knowledge Base. The significance of the transcripts' annotation is indicated by a P-value of < 0.05, as determined by a right-tailed Fisher's exact test.

RT–qPCR validation experiments

Quantification of gene expression levels by RT–qPCR was performed on GV-stage oocytes from WT and $Patl2^{-/-}$ mice. cDNAs were produced from oocyte lysates using the TaqMan® Gene Expression Cells-to-CT™ Kit. Oocytes were isolated from the ovaries of 4-week-old mice (average of 50 GV per mouse) and washed twice in PBS-PVP 0.5% before lysis. Each lysis reaction was performed with 10 oocytes in a total volume of 50 μl of lysis buffer supplemented with DNase at a ratio of 1:100. RT reactions were performed using 10 μl of the lysate in a total volume of 50 μl using the same kit. Real-time PCR was performed in 96-well plates on the StepOnePlus system (Applied Biosystems). Reactions were performed in a total volume of 20 μl, comprising 4 μl of cDNA, 1 μl of TaqMan Assays and 10 μl of Master Mix. Data were normalised relative to expression levels measured for the *Gapdh* reference gene. ΔCt, which is determined by subtracting the Ct of the reference gene from that of the target gene, was the subject of statistical analysis.

Statistical analyses

Statistical analyses were performed using SigmaPlot or GraphPad prism 6. Unpaired t-tests were used to compare WT and $Patl2^{-/-}$ samples. Data are represented as mean ± SEM. Statistical tests for which the two-tailed P-value ≤ 0.05 were considered significant.

Data availability

Transcriptomic data are available in the GEO database: accession number GSE100117 (https://www.ncbi.nlm.nih.gov/geo/query/acc.cgi). Clinical exomic data are available in the EGA data base: EGAS00001002903 (https://www.ebi.ac.uk/ega/home).

Expanded View for this article is available online.

Acknowledgements

We thank the IAB microscopy platform and Mylene PEZET, Alexei GRICHINE, Jacques MAZZEGA for their technical help. We thank Emeline FONTAINE PELLETIER (INSERM 1209, CNRS UMR 5309) for her generous donation of antibodies. We thank Marie-Christine BIRLING for helping with mouse genotyping. We thank Marcio CRUZEIRO (Institut Cochin, Paris, France) for providing the EIIaCre transgenic mice and Julien Fauré for access to molecular biology facility. Lastly, we thank all patients and control subjects for their participation.

We are also grateful to Jacques Brocard from the Photonic Imaging Centre at Grenoble Institute Neuroscience (Univ Grenoble Alpes—Inserm U1216—ISdV core facility and certified by the IBiSA label). This work was supported by the following grants: "Investigation of the genetic aetiology of oocyte meiotic failure (OMF) by exome sequencing" (awarded by the Fondation Maladies Rares (FMR) for the "High throughput sequencing and rare diseases 2012" programme), funding for the "MAS-Flagella" project (French National agency for research (ANR)) and the "Whole genome sequencing of patients with Flagellar Growth Defects (FGD)" (DGOS for the PRTS 2014 programme).

Author contributions

CA and PFR analysed the data and wrote the manuscript; Z-EK, AA-Y, CC and MB performed molecular work; TK and NT-M analysed genetic data; MC-K performed IF and histological experiments; MC-K, JE, ELB and GM performed IVF experiments; JPI, AG and SA performed transcriptome analyses; EL and SPB performed biochemistry experiments; MC-K, EL and ELB performed histological study. SN, BC and Z-EK made HA-tagged mice. SFBM, IC-D, LH, OM, MM, HL, MK and RZ provided clinical samples and data; CA and PFR designed the study, supervised all laboratory work, had full access to all the data in the study and took responsibility for the integrity of the data and its accuracy. All authors contributed to the manuscript.

Conflict of interest

The authors declare that they have no conflict of interest.

For more information

OMIM gene number 614661: http://omim.org/entry/614661, phenotype entry 617743: http://omim.org/entry/617743.

References

Alam SM, Konno T, Soares MJ (2015) Identification of target genes for a prolactin family paralog in mouse decidua. *Reproduction* 149: 625 – 632

Assou S, Anahory T, Pantesco V, Le Carrour T, Pellestor F, Klein B, Reyftmann L, Dechaud H, De Vos J, Hamamah S (2006) The human cumulus–oocyte complex gene-expression profile. *Hum Reprod* 21: 1705 – 1719

Beall S, Brenner C, Segars J (2010) Oocyte maturation failure: a syndrome of bad eggs. *Fertil Steril* 94: 2507 – 2513

Ben Khelifa M, Coutton C, Zouari R, Karaouzene T, Rendu J, Bidart M, Yassine S, Pierre V, Delaroche J, Hennebicq S *et al* (2014) Mutations in DNAH1, which encodes an inner arm heavy chain dynein, lead to male infertility from multiple morphological abnormalities of the sperm flagella. *Am J Hum Genet* 94: 95 – 104

Bobe J, Montfort J, Nguyen T, Fostier A (2006) Identification of new participants in the rainbow trout (*Oncorhynchus mykiss*) oocyte maturation and ovulation processes using cDNA microarrays. *Reprod Biol Endocrinol* 4: 39

Bompard G, Rabeharivelo G, Cau J, Abrieu A, Delsert C, Morin N (2013) P21-activated kinase 4 (PAK4) is required for metaphase spindle positioning and anchoring. *Oncogene* 32: 910 – 919

Braun JE, Tritschler F, Haas G, Igreja C, Truffault V, Weichenrieder O, Izaurralde E (2010) The C-terminal alpha-alpha superhelix of Pat is required for mRNA decapping in metazoa. *EMBO J* 29: 2368 – 2380

Chang CL, Wang HS, Soong YK, Huang SY, Pai SY, Hsu SY (2011) Regulation of oocyte and cumulus cell interactions by intermedin/adrenomedullin 2. *J Biol Chem* 286: 43193 – 43203

Chantranupong L, Scaria SM, Saxton RA, Gygi MP, Shen K, Wyant GA, Wang T, Harper JW, Gygi SP, Sabatini DM (2016) The CASTOR proteins are arginine sensors for the mTORC1 pathway. *Cell* 165: 153 – 164

Chen B, Zhang Z, Sun X, Kuang Y, Mao X, Wang X, Yan Z, Li B, Xu Y, Yu M *et al* (2017) Biallelic mutations in PATL2 cause female infertility characterized by oocyte maturation arrest. *Am J Hum Genet* 101: 609 – 615

Choi WJ, Banerjee J, Falcone T, Bena J, Agarwal A, Sharma RK (2007) Oxidative stress and tumor necrosis factor-alpha-induced alterations in metaphase II mouse oocyte spindle structure. *Fertil Steril* 88: 1220 – 1231

Choi Y, Yuan D, Rajkovic A (2008) Germ cell-specific transcriptional regulator sohlh2 is essential for early mouse folliculogenesis and oocyte-specific gene expression. *Biol Reprod* 79: 1176 – 1182

Clarke HJ (2012) Post-transcriptional control of gene expression during mouse oogenesis. *Results Probl Cell Differ* 55: 1 – 21

Coutton C, Vargas AS, Amiri-Yekta A, Kherraf ZE, Ben Mustapha SF, Le Tanno P, Wambergue-Legrand C, Karaouzene T, Martinez G, Crouzy S *et al* (2018) Mutations in CFAP43 and CFAP44 cause male infertility and flagellum defects in trypanosoma and human. *Nat Commun* 9: 686

De La Fuente R (2006) Chromatin modifications in the germinal vesicle (GV) of mammalian oocytes. *Dev Biol* 292: 1 – 12

Dieterich K, Soto RR, Faure AK, Hennebicq S, Ben Amar B, Zahi M, Perrin J, Martinez D, Sele B, Jouk PS *et al* (2007) Homozygous mutation of AURKC yields large-headed polyploid spermatozoa and causes male infertility. *Nat Genet* 39: 661 – 665

Feng CW, Bowles J, Koopman P (2014) Control of mammalian germ cell entry into meiosis. *Mol Cell Endocrinol* 382: 488 – 497

Feng R, Sang Q, Kuang Y, Sun X, Yan Z, Zhang S, Shi J, Tian G, Luchniak A, Fukuda Y *et al* (2016) Mutations in TUBB8 and human oocyte meiotic arrest. *N Engl J Med* 374: 223 – 232

Flemr M, Ma J, Schultz RM, Svoboda P (2010) P-body loss is concomitant with formation of a messenger RNA storage domain in mouse oocytes. *Biol Reprod* 82: 1008 – 1017

Frank D, Fortino W, Clark L, Musalo R, Wang W, Saxena A, Li CM, Reik W, Ludwig T, Tycko B (2002) Placental overgrowth in mice lacking the imprinted gene Ipl. *Proc Natl Acad Sci USA* 99: 7490 – 7495

Fu Y, Fu J, Ren Q, Chen X, Wang A (2012) Expression of Eph A molecules during swine embryo implantation. *Mol Biol Rep* 39: 2179 – 2185

Fujii H, Tatsumi K, Kosaka K, Yoshioka S, Fujiwara H, Fujii S (2006) Eph-ephrin A system regulates murine blastocyst attachment and spreading. *Dev Dyn* 235: 3250 – 3258

Furuya M, Tanaka M, Teranishi T, Matsumoto K, Hosoi Y, Saeki K, Ishimoto H, Minegishi K, Iritani A, Yoshimura Y (2007) H1foo is indispensable for meiotic maturation of the mouse oocyte. *J Reprod Dev* 53: 895 – 902

Guo M, Zhang C, Wang Y, Feng L, Wang Z, Niu W, Du X, Tang W, Li Y, Wang C *et al* (2016) Progesterone receptor membrane component 1 mediates progesterone-induced suppression of oocyte meiotic prophase i and primordial folliculogenesis. *Sci Rep* 6: 36869

Harbuz R, Zouari R, Pierre V, Ben Khelifa M, Kharouf M, Coutton C, Merdassi G, Abada F, Escoffier J, Nikas Y *et al* (2011) A recurrent deletion of DPY19L2 causes infertility in man by blocking sperm head elongation and acrosome formation. *Am J Hum Genet* 88: 351 – 361

Hartshorne G, Montgomery S, Klentzeris L (1999) A case of failed oocyte maturation *in vivo* and *in vitro*. *Fertil Steril* 71: 567 – 570

He XQ, Song YQ, Liu R, Liu Y, Zhang F, Zhang Z, Shen YT, Xu L, Chen MH, Wang YL *et al* (2016) Axin-1 regulates meiotic spindle organization in mouse oocytes. *PLoS ONE* 11: e0157197

Hourvitz A, Maman E, Brengauz M, Machtinger R, Dor J (2010) *In vitro* maturation for patients with repeated *in vitro* fertilization failure due to "oocyte maturation abnormalities". *Fertil Steril* 94: 496 – 501

Huang YL, Anvarian Z, Doderlein G, Acebron SP, Niehrs C (2015) Maternal Wnt/STOP signaling promotes cell division during early *Xenopus* embryogenesis. *Proc Natl Acad Sci USA* 112: 5732 – 5737

Jensen AB, Tunster SJ, John RM (2014) The significance of elevated placental PHLDA2 in human growth restricted pregnancies. *Placenta* 35: 528 – 532

Kaya MS, Kose M, Guzeloglu A, Kiyma Z, Atli MO (2017) Early pregnancy-related changes in toll-like receptors expression in ovine trophoblasts and peripheral blood leukocytes. *Theriogenology* 93: 40 – 45

Kherraf ZE, Conne B, Amiri-Yekta A, Christou-Kent M, Coutton C, Escoffier J, Nef S, Arnoult C, Ray PF (2018) Combining whole exome sequencing and CRISPR-Ca9 technology to study male infertility and spermatogenesis defects. *Mol Cell Endocrinol* https://doi.org/10.1016/j.mce.2018.03.002

Kim JY (2012) Control of ovarian primordial follicle activation. *Clin Exp Reprod Med* 39: 10 – 14

Kim SY, Kim SK, Lee JR, Woodruff TK (2016) Toward precision medicine for preserving fertility in cancer patients: existing and emerging fertility preservation options for women. *J Gynecol Oncol* 27: e22

Lakso M, Pichel JG, Gorman JR, Sauer B, Okamoto Y, Lee E, Alt FW, Westphal H (1996) Efficient *in vivo* manipulation of mouse genomic sequences at the zygote stage. *Proc Natl Acad Sci USA* 96: 5860 – 5865

Lee J, Oh JS, Cho C (2011) Impaired expansion of trophoblast spheroids cocultured with endometrial cells overexpressing cellular retinoic acid-binding protein 2. *Fertil Steril* 95: 2599 – 2601

Levran D, Farhi J, Nahum H, Glezerman M, Weissman A (2002) Maturation arrest of human oocytes as a cause of infertility: case report. *Hum Reprod* 17: 1604 – 1609

Li R, Albertini DF (2013) The road to maturation: somatic cell interaction and self-organization of the mammalian oocyte. *Nat Rev Mol Cell Biol* 14: 141 – 152

Li J, Sun P, Yue Z, Zhang D, You K, Wang J (2017) miR-144-3p induces cell cycle arrest and apoptosis in pancreatic cancer cells by targeting proline-rich protein 11 expression via the mitogen-activated protein kinase signaling pathway. *DNA Cell Biol* 36: 619 – 626

Liang CG, Su YQ, Fan HY, Schatten H, Sun QY (2007) Mechanisms regulating oocyte meiotic resumption: roles of mitogen-activated protein kinase. *Mol Endocrinol* 21: 2037 – 2055

Libby BJ, De La Fuente R, O'Brien MJ, Wigglesworth K, Cobb J, Inselman A, Eaker S, Handel MA, Eppig JJ, Schimenti JC (2002) The mouse meiotic mutation mei1 disrupts chromosome synapsis with sexually dimorphic consequences for meiotic progression. *Dev Biol* 242: 174 – 187

Lincoln AJ, Wickramasinghe D, Stein P, Schultz RM, Palko ME, De Miguel MP, Tessarollo L, Donovan PJ (2002) Cdc25b phosphatase is required for resumption of meiosis during oocyte maturation. *Nat Genet* 30: 446 – 449

Lipkin SM, Moens PB, Wang V, Lenzi M, Shanmugarajah D, Gilgeous A, Thomas J, Cheng J, Touchman JW, Green ED *et al* (2002) Meiotic arrest and aneuploidy in MLH3-deficient mice. *Nat Genet* 31: 385 – 390

Maddirevula S, Coskun S, Alhassan S, Elnour A, Alsaif HS, Ibrahim N, Abdulwahab F, Arold ST, Alkuraya FS (2017) Female infertility caused by mutations in the oocyte-specific translational repressor PATL2. *Am J Hum Genet* 101: 603 – 608

Marnef A, Maldonado M, Bugaut A, Balasubramanian S, Kress M, Weil D, Standart N (2010) Distinct functions of maternal and somatic Pat1 protein paralogs. *RNA* 16: 2094 – 2107

Mayer S, Wrenzycki C, Tomek W (2014) Inactivation of mTor arrests bovine oocytes in the metaphase-I stage, despite reversible inhibition of 4E-BP1 phosphorylation. *Mol Reprod Dev* 81: 363 – 375

Medvedev S, Pan H, Schultz RM (2011) Absence of MSY2 in mouse oocytes perturbs oocyte growth and maturation, RNA stability, and the transcriptome. *Biol Reprod* 85: 575 – 583

Nakamura Y, Tanaka KJ, Miyauchi M, Huang L, Tsujimoto M, Matsumoto K (2010) Translational repression by the oocyte-specific protein P100 in *Xenopus*. *Dev Biol* 344: 272 – 283

Nakanishi T, Ozaki Y, Blomgren K, Tateyama H, Sugiura-Ogasawara M, Suzumori K (2005) Role of cathepsins and cystatins in patients with recurrent miscarriage. *Mol Hum Reprod* 11: 351 – 355

Paciolla M, Boni R, Fusco F, Pescatore A, Poeta L, Ursini MV, Lioi MB, Miano MG (2011) Nuclear factor-kappa-B-inhibitor alpha (NFKBIA) is a developmental marker of NF-kappaB/p65 activation during *in vitro* oocyte maturation and early embryogenesis. *Hum Reprod* 26: 1191 – 1201

Paczkowski M, Krisher R (2010) Aberrant protein expression is associated with decreased developmental potential in porcine cumulus-oocyte complexes. *Mol Reprod Dev* 77: 51 – 58

Pal D, Wu D, Haruta A, Matsumura F, Wei Q (2010) Role of a novel coiled-coil domain-containing protein CCDC69 in regulating central spindle assembly. *Cell Cycle* 9: 4117 – 4129

Pique M, Lopez JM, Foissac S, Guigo R, Mendez R (2008) A combinatorial code for CPE-mediated translational control. *Cell* 132: 434 – 448

Racki WJ, Richter JD (2006) CPEB controls oocyte growth and follicle development in the mouse. *Development* 133: 4527 – 4537

Rausell F, Pertusa JF, Gomez-Piquer V, Hermenegildo C, Garcia-Perez MA, Cano A, Tarin JJ (2007) Beneficial effects of dithiothreitol on relative levels of glutathione S-transferase activity and thiols in oocytes, and cell number, DNA fragmentation and allocation at the blastocyst stage in the mouse. *Mol Reprod Dev* 74: 860 – 869

Ruiz-Gonzalez I, Minten M, Wang X, Dunlap KA, Bazer FW (2015) Involvement of TLR7 and TLR8 in conceptus development and establishment of pregnancy in sheep. *Reproduction* 149: 305 – 316

Ryu KY, Sinnar SA, Reinholdt LG, Vaccari S, Hall S, Garcia MA, Zaitseva TS, Bouley DM, Boekelheide K, Handel MA *et al* (2008) The mouse polyubiquitin gene Ubb is essential for meiotic progression. *Mol Cell Biol* 28: 1136 – 1146

SEQC/MAQC-III Consortium (2014) A comprehensive assessment of RNA-seq accuracy, reproducibility and information content by the Sequencing Quality Control Consortium. *NatBiotechnol* 32: 903 – 914

Shi YQ, Zhuang XJ, Xu B, Hua J, Liao SY, Shi Q, Cooke HJ, Han C (2013) SYCP3-like X-linked 2 is expressed in meiotic germ cells and interacts with synaptonemal complex central element protein 2 and histone acetyltransferase TIP60. *Gene* 527: 352 – 359

Shin YH, Ren Y, Suzuki H, Golnoski KJ, Ahn HW, Mico V, Rajkovic A (2017) Transcription factors SOHLH1 and SOHLH2 coordinate oocyte differentiation without affecting meiosis I. *J Clin Invest* 127: 2106 – 2117

Solc P, Saskova A, Baran V, Kubelka M, Schultz RM, Motlik J (2008) CDC25A phosphatase controls meiosis I progression in mouse oocytes. *Dev Biol* 317: 260 – 269

Sousa Martins JP, Liu X, Oke A, Arora R, Franciosi F, Viville S, Laird DJ, Fung JC, Conti M (2016) DAZL and CPEB1 regulate mRNA translation synergistically during oocyte maturation. *J Cell Sci* 129: 1271 – 1282

Spate LD, Brown AN, Redel BK, Whitworth KM, Murphy CN, Prather RS (2014) Dickkopf-related protein 1 inhibits the WNT signaling pathway and improves pig oocyte maturation. *PLoS ONE* 9: e95114

Stopa N, Krebs JE, Shechter D (2015) The PRMT5 arginine methyltransferase: many roles in development, cancer and beyond. *Cell Mol Life Sci* 72: 2041 – 2059

Su YQ, Sugiura K, Woo Y, Wigglesworth K, Kamdar S, Affourtit J, Eppig JJ (2007) Selective degradation of transcripts during meiotic maturation of mouse oocytes. *Dev Biol* 302: 104 – 117

Swetloff A, Conne B, Huarte J, Pitetti JL, Nef S, Vassalli JD (2009) Dcp1-bodies in mouse oocytes. *Mol Biol Cell* 20: 4951 – 4961

Takabayashi S, Yamauchi Y, Tsume M, Noguchi M, Katoh H (2009) A spontaneous smc1b mutation causes cohesin protein dysfunction and sterility in mice. *Exp Biol Med* 234: 994 – 1001

Vaccari S, Horner K, Mehlmann LM, Conti M (2008) Generation of mouse oocytes defective in cAMP synthesis and degradation: endogenous cyclic AMP is essential for meiotic arrest. *Dev Biol* 316: 124 – 134

Wilczek C, Chitta R, Woo E, Shabanowitz J, Chait BT, Hunt DF, Shechter D (2011) Protein arginine methyltransferase Prmt5-Mep50 methylates histones H2A and H4 and the histone chaperone nucleoplasmin in *Xenopus laevis* eggs. *J Biol Chem* 286: 42221 – 42231

Williams CJ, Erickson GF (2012) *Morphology and physiology of the ovary*. South Dartmouth, MA: MDText.com, Inc.; 2000

Yin O, Cayton K, Segars JH (2016) *In vitro* activation: a dip into the primordial follicle pool? *J Clin Endocrinol Metab* 101: 3568 – 3570

Yu J, Hecht NB, Schultz RM (2001) Expression of MSY2 in mouse oocytes and preimplantation embryos. *Biol Reprod* 65: 1260 – 1270

Zhang QH, Qi ST, Wang ZB, Yang CR, Wei YC, Chen L, Ouyang YC, Hou Y, Schatten H, Sun QY (2012) Localization and function of the Ska complex during mouse oocyte meiotic maturation. *Cell Cycle* 11: 909 – 916

Expanded View Figures

Figure EV1. Quality of oocytes collected from patients harbouring *PATL2* mutation and control patients after ovarian stimulation.

A The mean age of the six patients harbouring a *PATL2* mutation at the time of 11 hormonal stimulations was compared to the non-*PATL2* patients within the cohort and also to a control cohort corresponding to women from infertile couples of similar geographical origin where the male was diagnosed with a male infertility (mean ± SEM, n = 234). There was no significant (NS) age difference between the *PATL2* patients, the non-*PATL2* patients and the control cohort.

B Numbers of oocytes retrieved after hormonal stimulation (mean ± SEM) were similar in *PATL2* patients, non-*PATL2* patients and the control cohort.

C Collected oocytes were sorted according to their maturation stage. For patients harbouring *PATL2* mutation, the mean numbers of GV and atretic oocytes were significantly increased and no MII oocytes were collected. Non-*PATL2* patients from the same cohort showed a comparably larger proportion of MI-arrested oocytes.

Data information: Statistical differences were assessed using unpaired two-tailed t-tests.

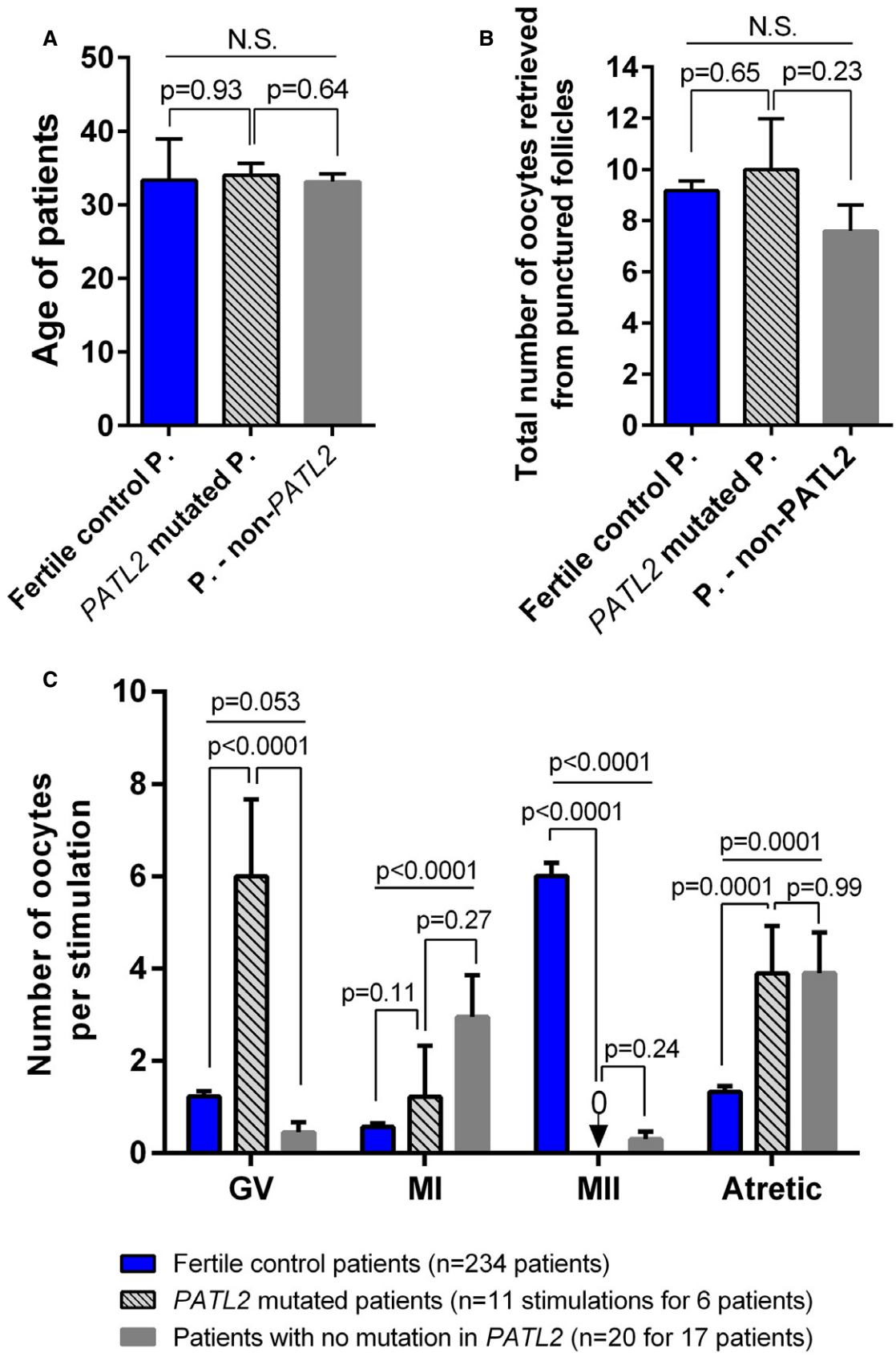

Figure EV1.

Figure EV2. Histological analysis of ovaries from control and *Patl2*$^{-/-}$ females at 26 days postpartum (dpp).

A Whole section (3 μm thick) of an ovary from a control female at 26 ddp. Section was stained with an antibody against Msy2 (orange staining) to make oocytes clearly visible. Sections were counterstained with Hoechst to reveal the nucleus (blue staining). Right image, corresponding to the enlargement of the red square on the left image, shows the different classes of follicle: primordial (1al), primary (1ry) and secondary (2ry).

B Similar images for an ovary from a *Patl2*$^{-/-}$ female at 26 ddp.

C Comparative numbers of primordial and primary follicle oocytes per section in *Patl2*$^{-/-}$ and control ovaries. Nine different 3-μm sections from three different mice (for each section, four-seven technical replicates corresponding to successive sections were counted). Data are presented on box and whisker plots indicating min. and max. values. Statistical differences were assessed using *t*-test, *P*-value as indicated.

D Comparative number of follicles per section from control and *Patl2*$^{-/-}$ ovaries. Only follicles where oocytes were visible were counted (n = 9 sections per genotype, between four to seven technical replicates). Data are presented on box and whisker plots indicating min. and max. values. Statistical differences were assessed using *t*-test, *P*-value as indicated.

E Comparative amplitude histograms of follicle size per section from control and *Patl2*$^{-/-}$ ovaries (n = 9 sections per genotype with four to seven technical replicates). Statistical differences were assessed using Kolmogorov-Smirnov test.

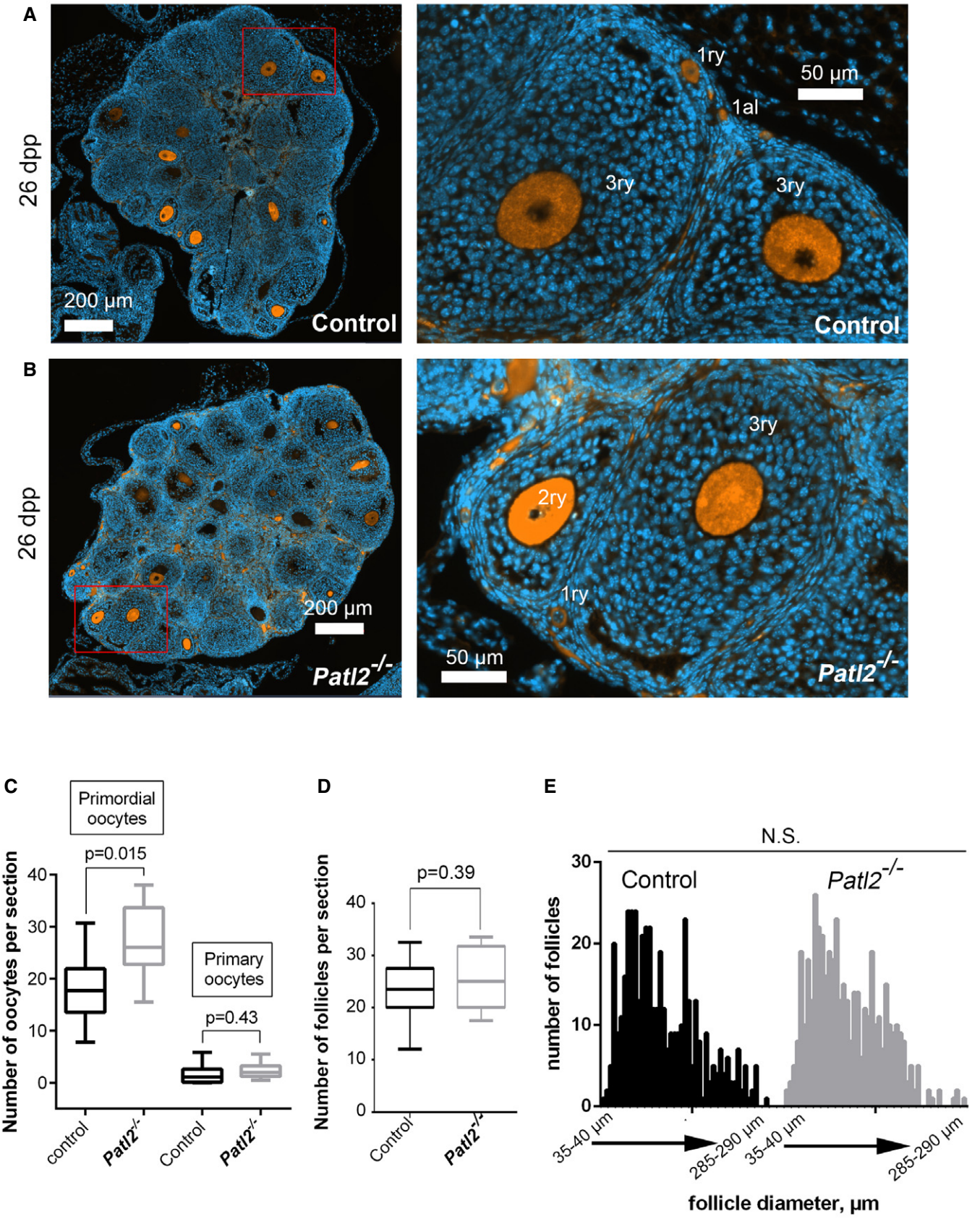

Figure EV2.

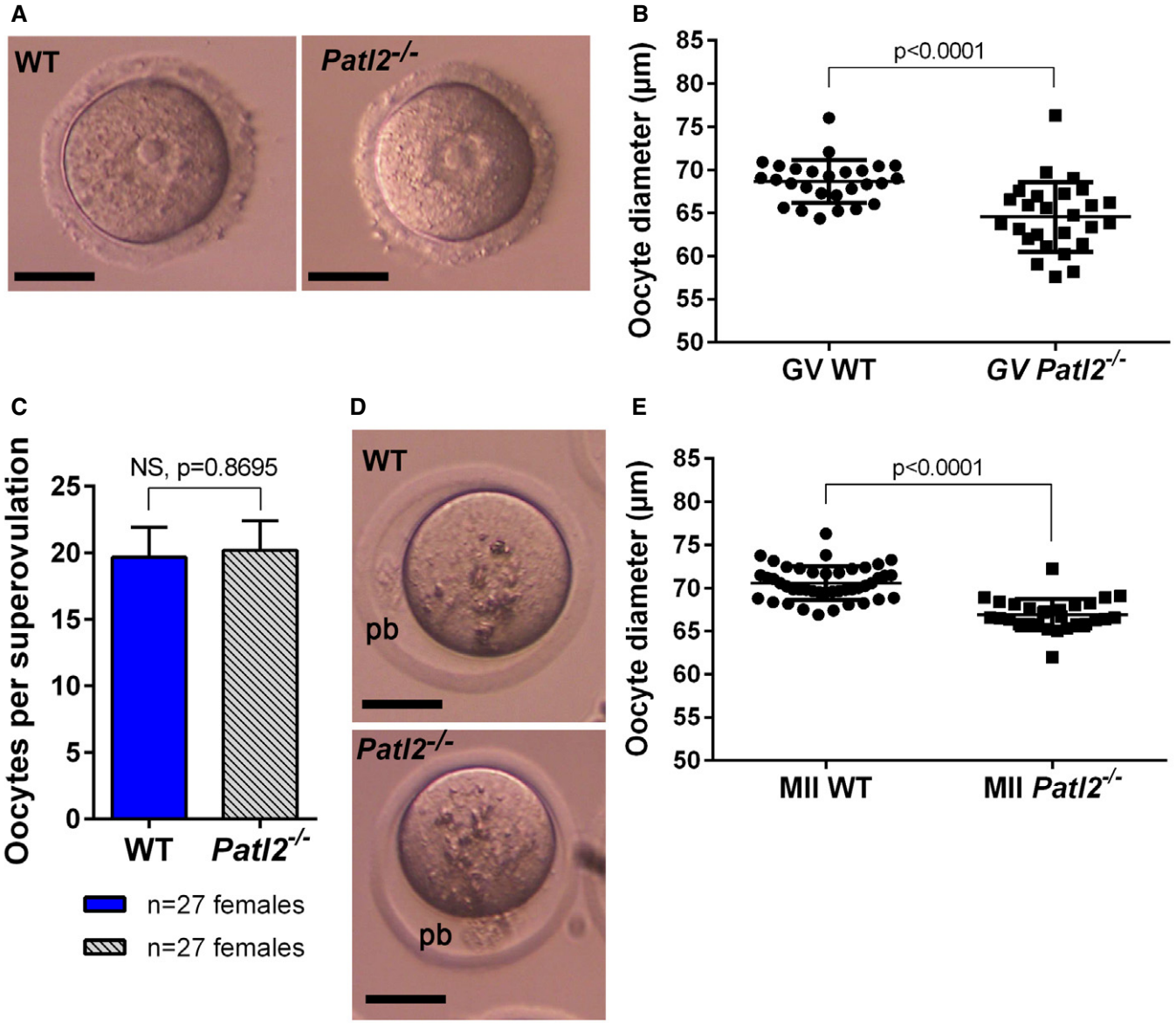

Figure EV3. Lack of Patl2 does not affect number of oocytes produced, but impairs oocyte growth.

A Representative images for a GV oocyte from WT and *Patl2*$^{-/-}$ females stimulated with 5 UI PSMG. Scale bars = 35 µm.

B Comparison of WT and *Patl2*$^{-/-}$ GV oocyte diameter. In the absence of Patl2, the diameter (mean ± SEM) dropped from 68.6 ± 0.5 to 64.5 ± 0.8 µm ($P < 0.0001$). Statistical difference was assessed using unpaired two-tailed *t*-test with Welch's correction.

C The number of oocytes (mean ± SEM) harvested 13 h after full hormonal stimulation (PMSG followed 48 h later by 5 UI HCG) was similar in WT and Patl2-deficient females. Statistical difference was assessed using unpaired two-tailed *t*-test.

D Images of a MII oocytes from WT and *Patl2*$^{-/-}$ females after stimulation (pb = 1st polar body). Scale bars = 35 µm.

E Diameter of WT and *Patl2*$^{-/-}$ MII oocytes (mean ± SEM), the mean drops from 70.6 ± 0.3, $n = 44$ in the WT to 66.9 ± 0.3, $n = 28$ in *Patl2*$^{-/-}$ ($P < 0.0001$), oocytes were collected from three females in each case. Statistical difference was assessed using unpaired two-tailed *t*-test.

Figure EV4. Biological functions and pathways associated with up- or down-regulated differential expression transcripts in *Patl2*$^{-/-}$ versus WT samples at the GV and MII stages.

To investigate possible interactions of up and down-regulated transcripts ($P < 0.05$, absolute fold-change > 2), genes with altered expression profile identified by the Affymetrix microarray were imported into the Ingenuity Pathway Analysis software (IPA) for analysis.

A Canonical pathways identified by IPA that were significantly enriched among transcripts deregulated in *Patl2*$^{-/-}$ GV oocytes with respect to GV-WT oocytes.
B Canonical pathways identified by IPA that were significantly enriched among transcripts deregulated in *Patl2*$^{-/-}$ MII oocytes with respect to MII-WT oocytes.

Data information: *Y*-axis indicates the significance (−log *P*-value) of the functional pathway association, which depends on the number of genes in a class as well as biological relevance. The threshold line represents a *P*-value of 0.05 and was calculated by applying Fischer's test.

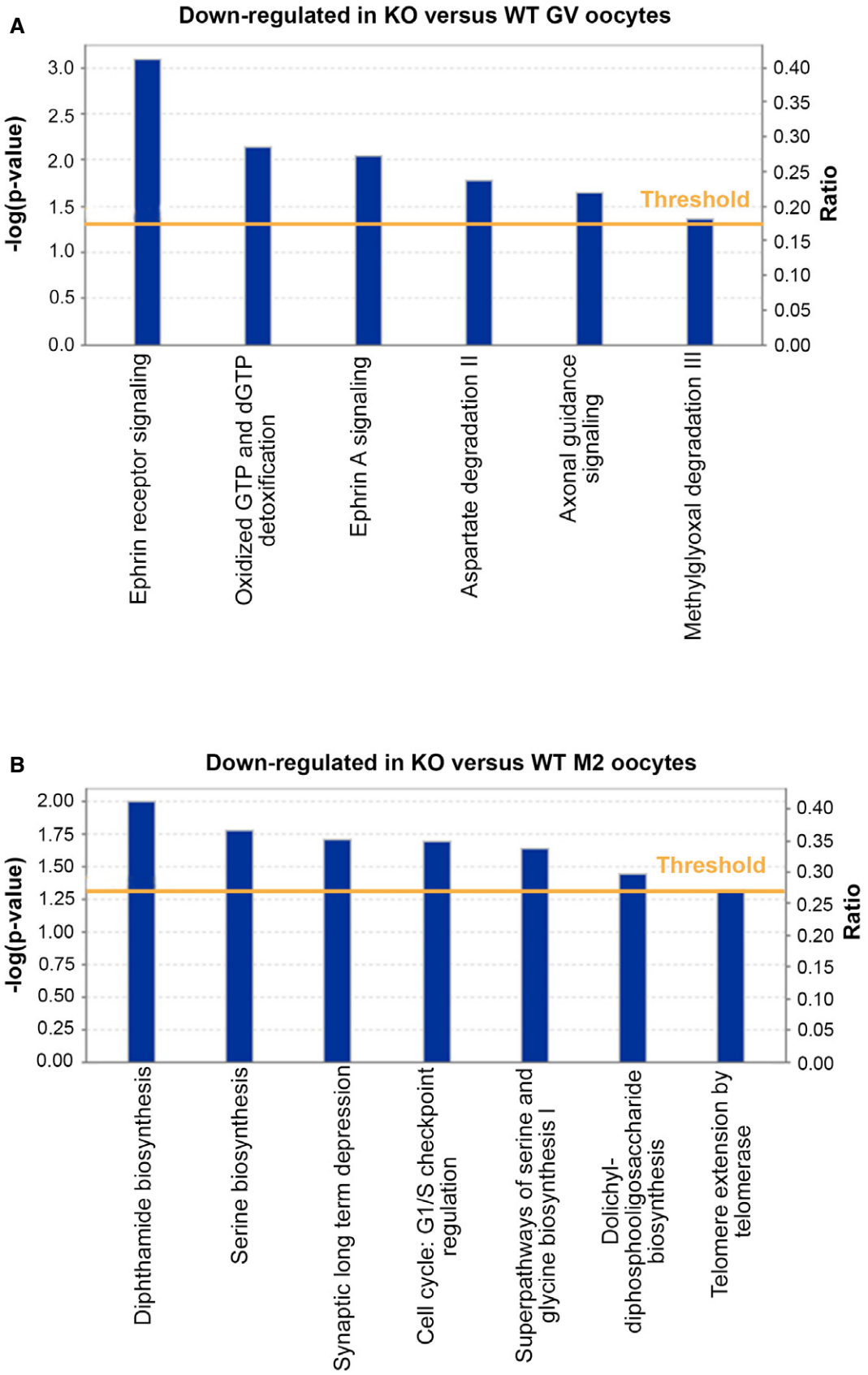
A
Down-regulated in KO versus WT GV oocytes
-log(p-value)
Ratio
Threshold
Ephrin receptor signaling
Oxidized GTP and dGTP detoxification
Ephrin A signaling
Aspartate degradation II
Axonal guidance signaling
Methylglyoxal degradation III
B
Down-regulated in KO versus WT M2 oocytes
-log(p-value)
Ratio
Threshold
Diphthamide biosynthesis
Serine biosynthesis
Synaptic long term depression
Cell cycle: G1/S checkpoint regulation
Superpathways of serine and glycine biosynthesis I
Dolichyl-diphosphooligosaccharide biosynthesis
Telomere extension by telomerase

Figure EV4.

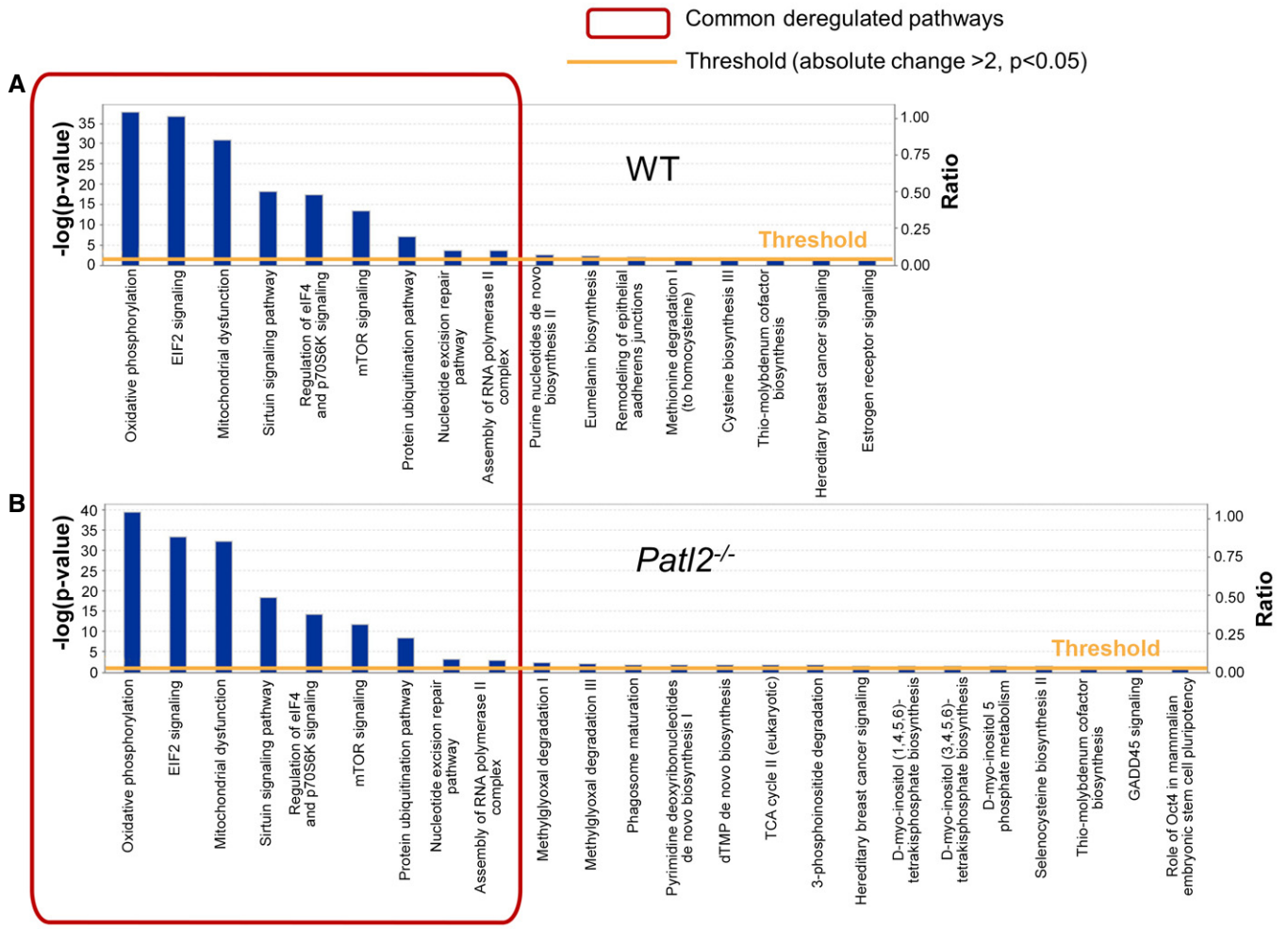

Figure EV5. Transcriptomic analysis of the GV-MII transition. Biological functions and pathways associated with up- or down-regulated differential expression in MII versus GV oocytes from WT and *Patl2*$^{-/-}$ samples.

To investigate possible interactions of up- and down-regulated transcripts ($P < 0.05$, absolute fold-change > 2) between GV and MII stages, genes with an altered expression profile identified by the Affymetrix microarray were imported into the Ingenuity Pathway Analysis software (IPA) for analysis.

A Canonical pathways identified by IPA that were significantly enriched among changed transcripts identified in WT samples at the GV-MII transition.

B Canonical pathways identified by IPA that were significantly enriched among changed transcripts identified in *Patl2*$^{-/-}$ samples at the GV-MII transition.

Data information: *Y*-axis indicates the significance (−log *P*-value) of the functional pathway association, which depends on the number of genes in a class as well as biological relevance. The threshold line represents a *P*-value of 0.05 and was calculated by applying Fischer's test.

APPENDIX

PATL2 is a key actor of oocyte maturation whose invalidation causes infertility in women and mice

Table of contents

SUPPLEMENTARY FIGURES

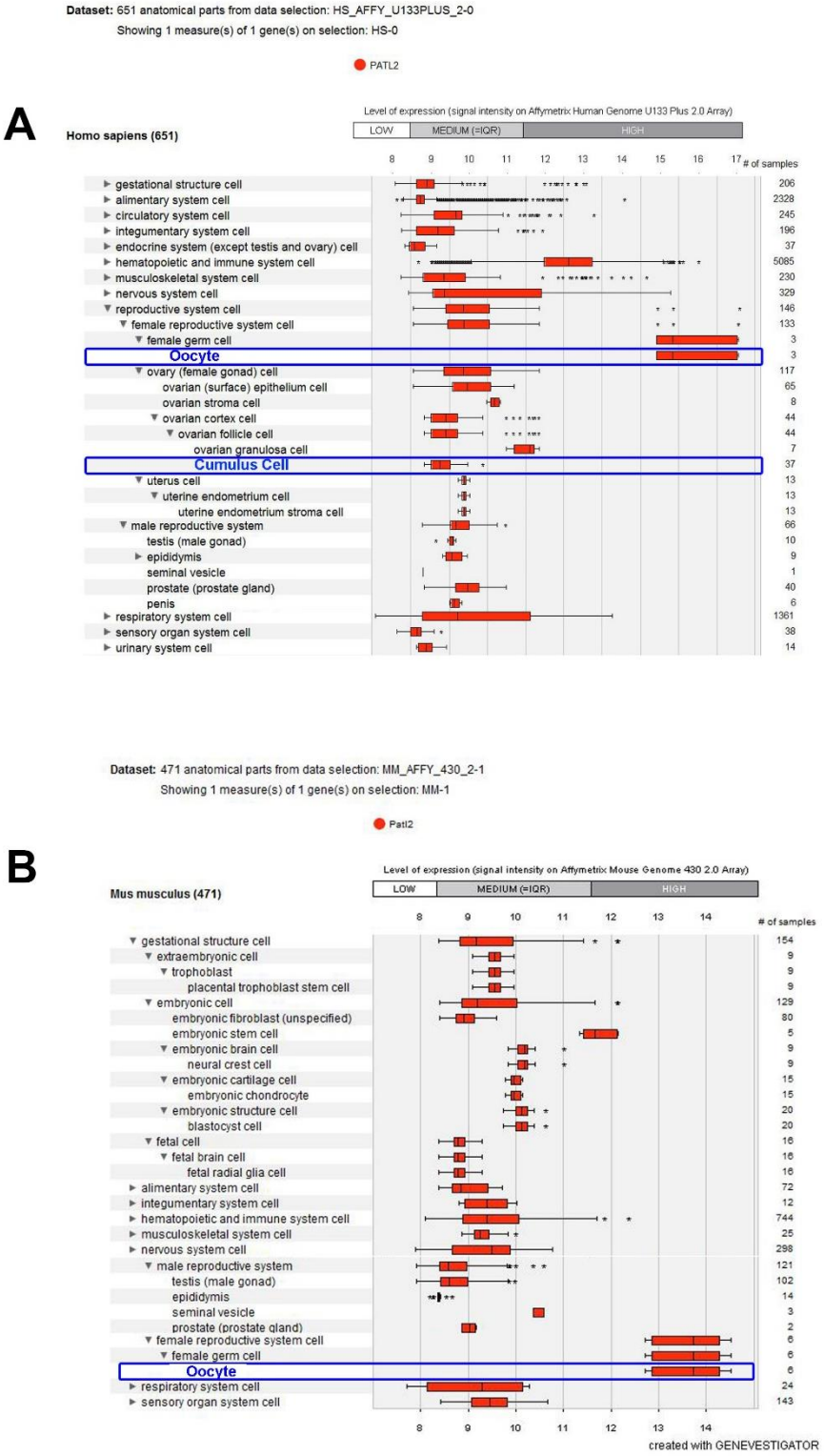

Figure S1. **Relative mRNA expression levels for human and mouse *PATL2* transcripts.**

(A) *PATL2* mRNA levels were measured in different tissues/cells in Humans using Affymetrix microarrays (data available from the Genevestigator database, https://genevestigator.com). Blue rectangles highlight the expression level in oocytes and follicular cells. Oocytes exhibit the highest level of *PATL2* expression, whereas its level is very low in follicular cells. **(B)** Similar data for mice. Data were generated with Genevestigator (Hruz T, Laule O, Szabo G, Wessendorp F, Bleuler S, Oertle L, Widmayer P, Gruissem W and P Zimmermann (2008) Genevestigator V3: a reference expression database for the meta-analysis of transcriptomes. Advances in Bioinformatics 2008, 420747)

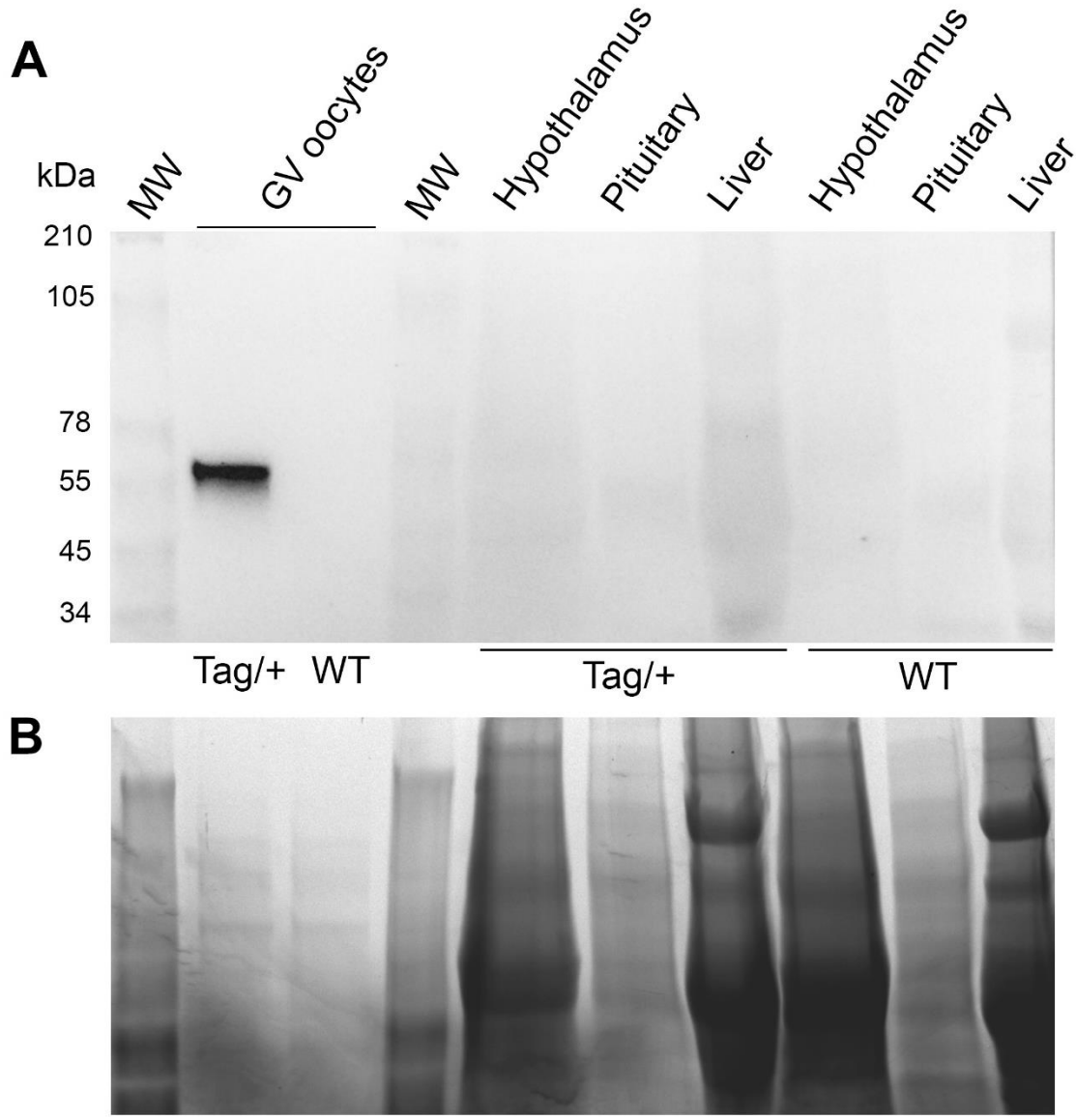

Figure S2. **Western blot comparison of expression of Patl2-HA in oocyte, hypothalamus and pituitary gland extracts.**

(**A**) Western blot of protein extracts from different tissues as indicated and revealed with anti-HA antibodies. Tissues were collected from WT or from Patl2-HA tagged females (tag/+) and 130-140 GV oocytes were loaded per well. Protein extracts were obtained by pooling the organs of 3 different WT or Patl2-HA tagged animals. In the lane loaded with GV oocyte extract from Patl2-HA tag mice, a band at around 60 kDa was observed (expected MW for mouse Patl2-HA = 60.74 KDa), whereas no bands were observed in the other extracts. MW = Molecular Weight (**B**) Protein loads of the Western blot presented in (A) were controlled with TGX stain free™ precast gels.

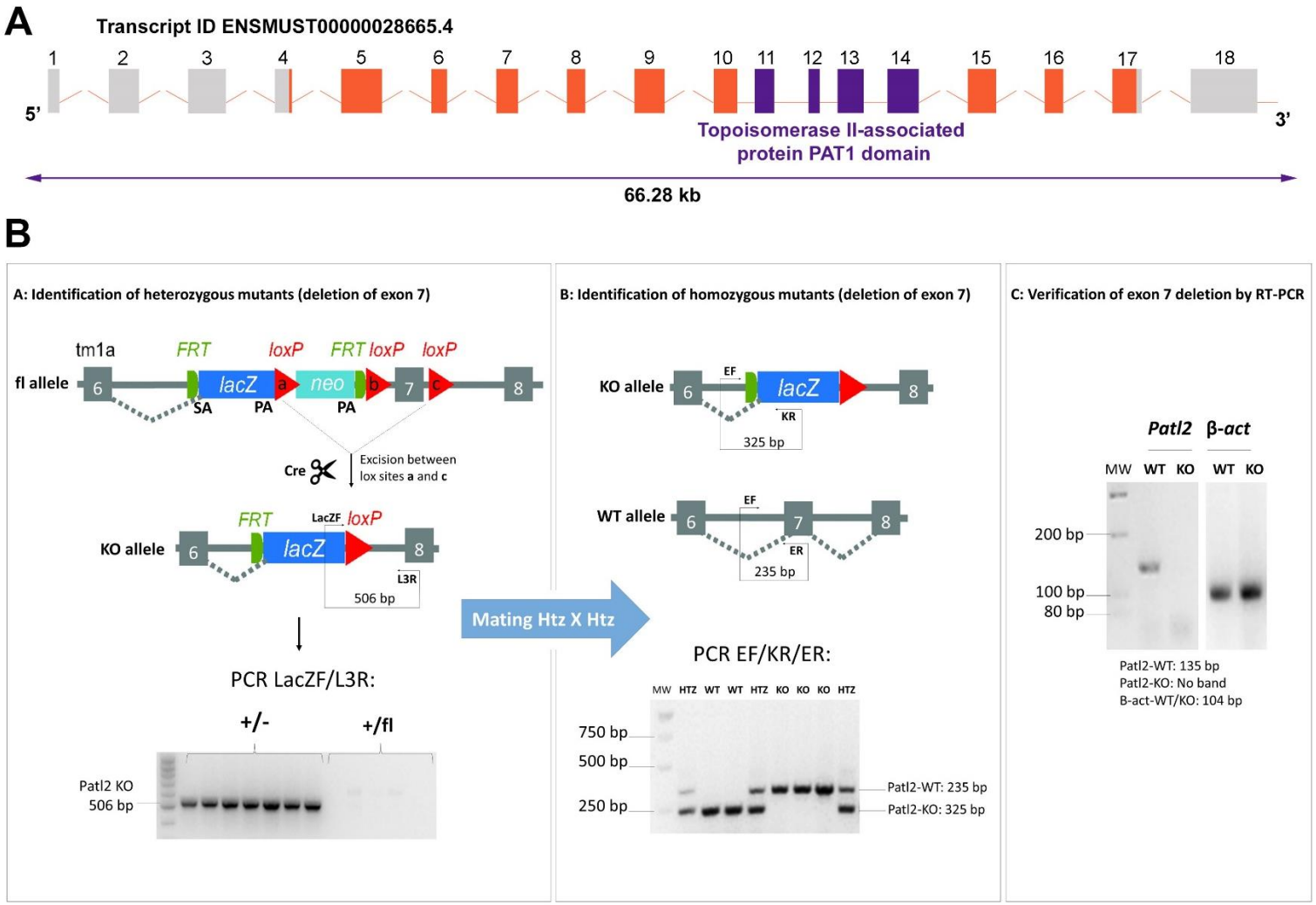

Figure S3. **Genetic modification of *Patl2*-deficient mice and genotyping strategy**

(A) Exon map showing the localization of the topoisomerase II associated Pat1 domain, downstream of exon 7 **(B1)** *Patl2*$^{-/-}$ mice (C57BL/6NTac-Patl2<tm1a) were generated by the EUCOMM Consortium (http://www.mousephenotype.org/about-ikmc/eucomm). The allele map shows the insertion of a LacZ and a neomycin cassette between exons 6 and 7. The critical exon 7 is surrounded by two LoxP sequences. *Patl2*$^{-/-}$ mice were crossed with adult heterozygous EIIaCre transgenic mice which express the CRE-recombinase enzyme ubiquitously from an early stage. Offspring were screened by PCR using LacZF/L3R primers to detect exon 7 deletion. **(B2)** Heterozygous mutant mice showing deletion of exon 7 were mated together and homozygous exon-7-deleted animals were identified by multiplex PCR using EF/KR/ER primers. **(B3)** RT-PCR was carried out on selected F2 animals to verify deletion of exon 7 in *Patl2*$^{-/-}$ animals using primers within exon 7. The band at 135 bp was sequenced and corresponded to *Patl2*. Sequences of all primers are indicated in Table S6.

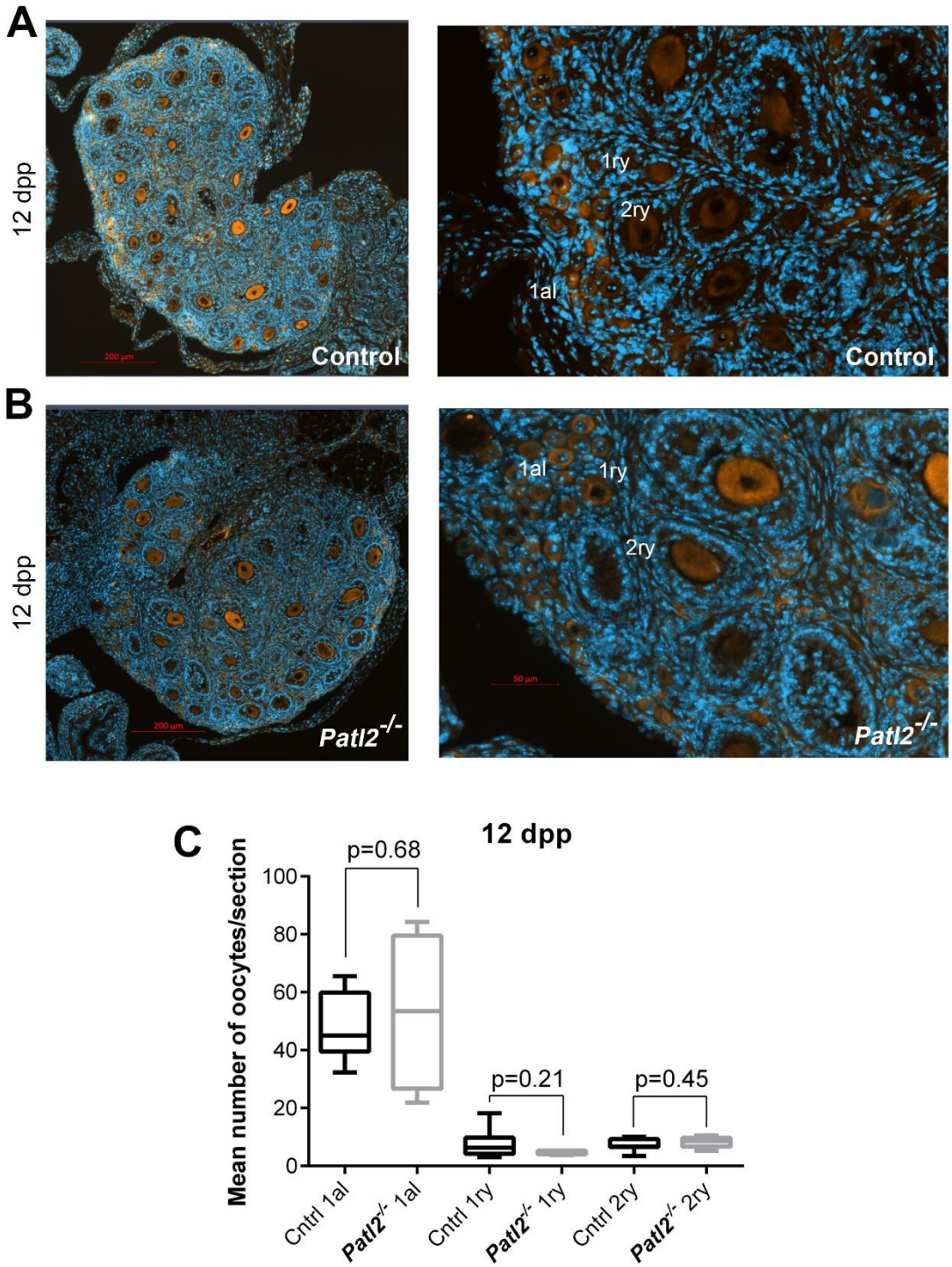

Figure S4 **Ovaries from WT and *Patl2* deficient females have a similar anatomical structure and cellular composition at 12 dpp.**

12-day-old females were euthanised and ovaries were collected and subjected to histological studies by IF. Sections (3 µm thick) were stained with Hoechst to reveal nuclei (blue staining) and an anti-Msy2 antibody (orange staining) to identify oocytes. All oocyte stages were stained by anti-Msy2 **(A)** WT ovaries and **(B)** *Patl2*$^{-/-}$ ovaries. No obvious morphological differences were observed between WT and *Patl2*$^{-/-}$ ovaries. (**C**) The different classes of oocytes (primordial, primary and secondary) were counted in 9 different 3-µm sections from 3 different mice (for each section, 4-7 technical replicates, corresponding to successive sections were counted). n=9, Statistical differences were measured with t-test. P value as indicated.

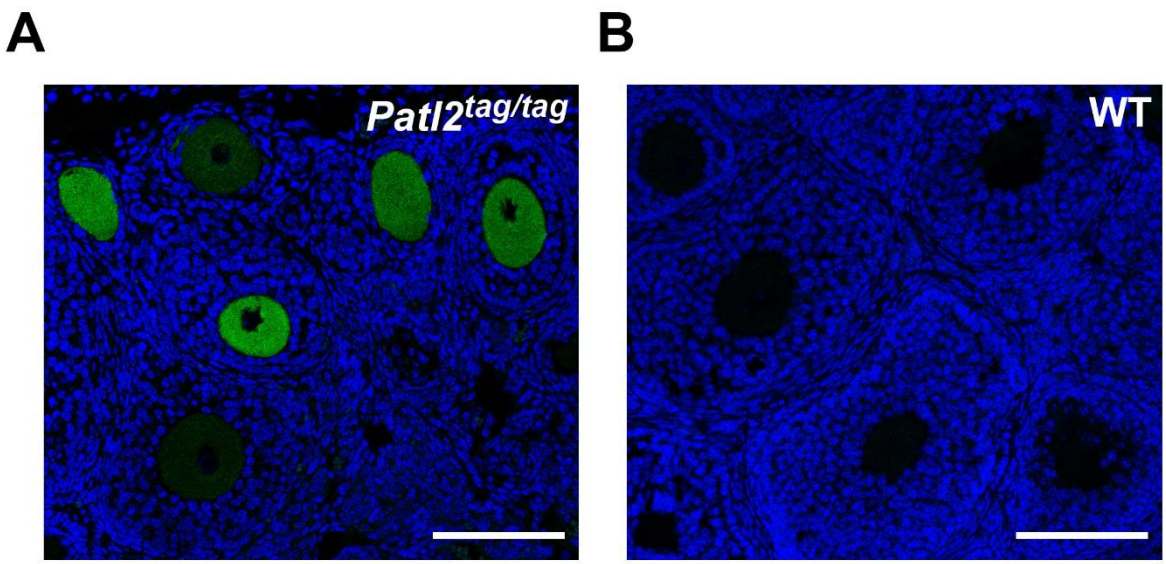

Figure S5. **Validation of the specificity of the HA-antibody in IF experiments**

Comparative fluorescent signals of sections of ovaries from HA-tagged Patl2 (A) and WT (B) mice. Ovaries were stained with Hoechst and an anti-HA tag antibody and observed under confocal microscopy.

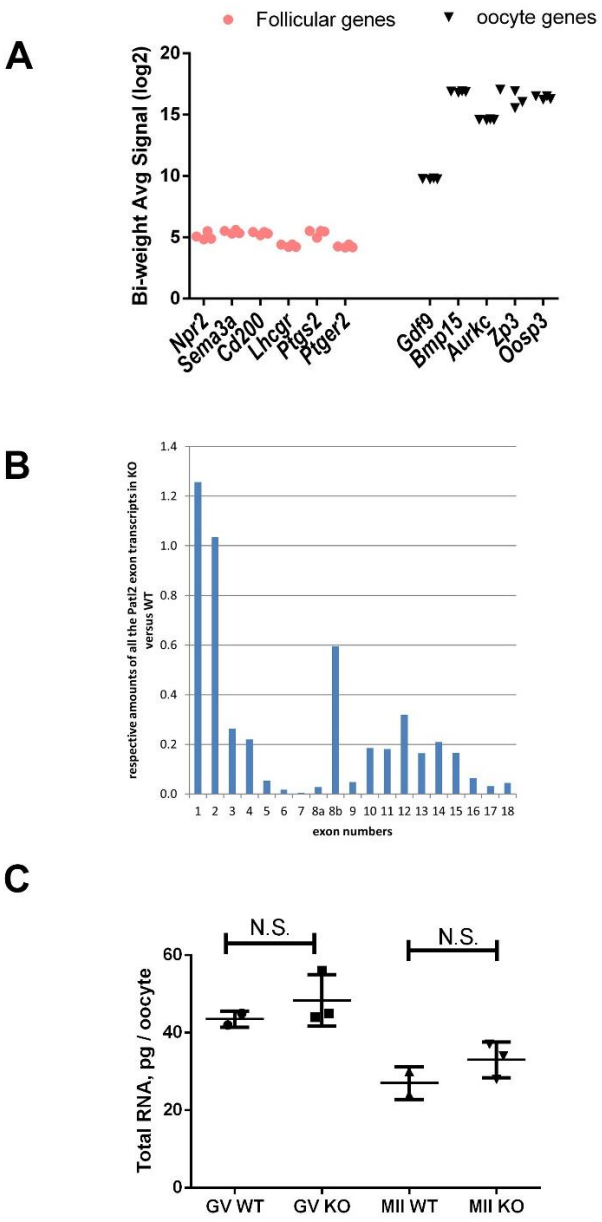

Figure S6. **Characterisation of the RNA sample used in transcriptomic approach.**

(A) Expression levels for specific follicular and oocyte genes. The expression levels for follicle-specific genes were around 5, which is considered a very low level. In contrast, the expression levels for oocyte genes were above 9 and reached the highest values (17). The follicular genes analysed were: Natriuretic peptide receptor 2 (*Npr2*), semaphorin 3A (*Sema3a*), CD200 antigen (C*d200*), luteinizing hormone/choriogonadotropin receptor (*Lhcgr*), prostaglandin G/H synthase 2 (*Ptgs2*) and prostaglandin E receptor 2 (*Ptger*2). The oocyte-specific genes were: growth differentiation factor 9 (*Gdf9*), bone morphogenetic protein 15 (*Bmp15*), aurora kinase C (*Aurkc*), zona pellucida glycoprotein 3 (*Zp3*), oocyte secreted protein 3 (*Oosp3*). **(B)** Comparative expression levels for the different *Patl2* exons. As expected, the level of exon 7 is close to 0, confirming deletion of exon 7 in knock-out females. The expression levels for all 19 Patl2 exons (according to the exon map nomenclature from Affymetrix) were expressed as the ratio (y axis and in linear scale) between exon transcript levels in Patl2$^{-/-}$ oocytes compared to wild type oocytes. In *Patl2*$^{-/-}$ oocytes, *Patl2* exons 1 and 2 were expressed in nearly identical amounts relative to levels measured for wild type oocytes. All the other exons were more or less severely underexpressed or absent. **(C)** Total RNA was extracted from WT and *Patl2*$^{-/-}$ oocytes (both at GV and MII stages) as described in materials and methods. After RT-qPCR assays, the RNA amounts recovered from the purification columns were expressed in pg purified RNA per lysed oocyte. Assuming a consistent RNA recovery yield from the columns, we can conclude that there are non-significant differences in RNA concentrations per oocyte between WT and *Patl2*$^{-/-}$ GV oocytes, as well as between WT and *Patl2*$^{-/-}$ MII oocytes. However, there is a nearly 30 to 40% decrease in the RNA level between MII stage oocytes and GV stage oocytes, as already reported (Su YQ, Sugiura K, Woo Y, et al. Selective degradation of transcripts during meiotic maturation of mouse oocytes. Developmental biology 2007;302:104-17).

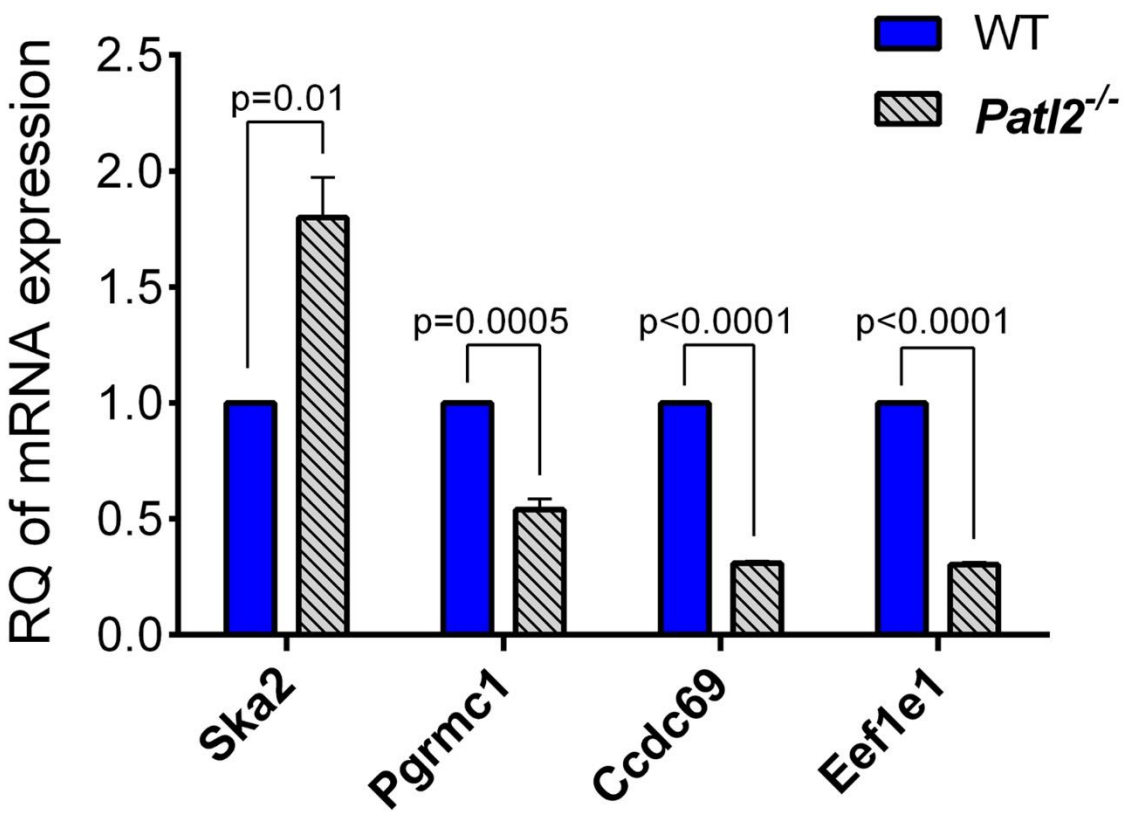

Figure S7. **RT-qPCR experiments validating Affymetrix measures**

Relative quantification (RQ) of 4 genes (*Ska2*, *Pgrmc1*, *Ccdc69* and *Eef1e1*) in germinal vesicle (GV) oocytes from both wild-type (blue) and *Patl2*$^{-/-}$ (grey) mice. n = 8.

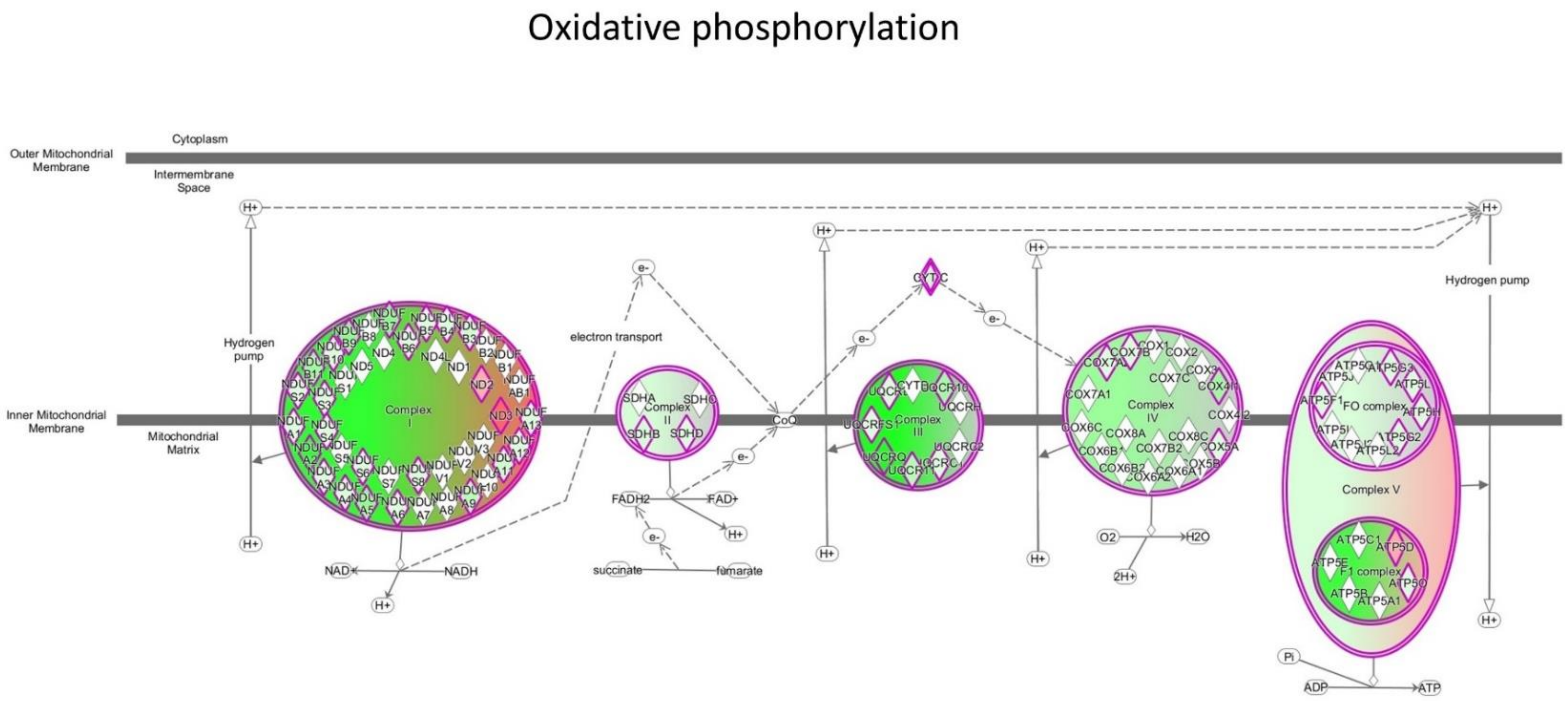

Figure S8. **Deregulated transcripts related to the oxidative phosphorylation pathway**. The interaction network was generated using Ingenuity software and shows that many genes from the oxidative phosphorylation pathway (the major pathway for conversion of energy from NADH oxidation into ATP) are deregulated in both WT and KO samples. Up-regulated transcripts are shown in pink and down-regulated transcripts are indicated in green.

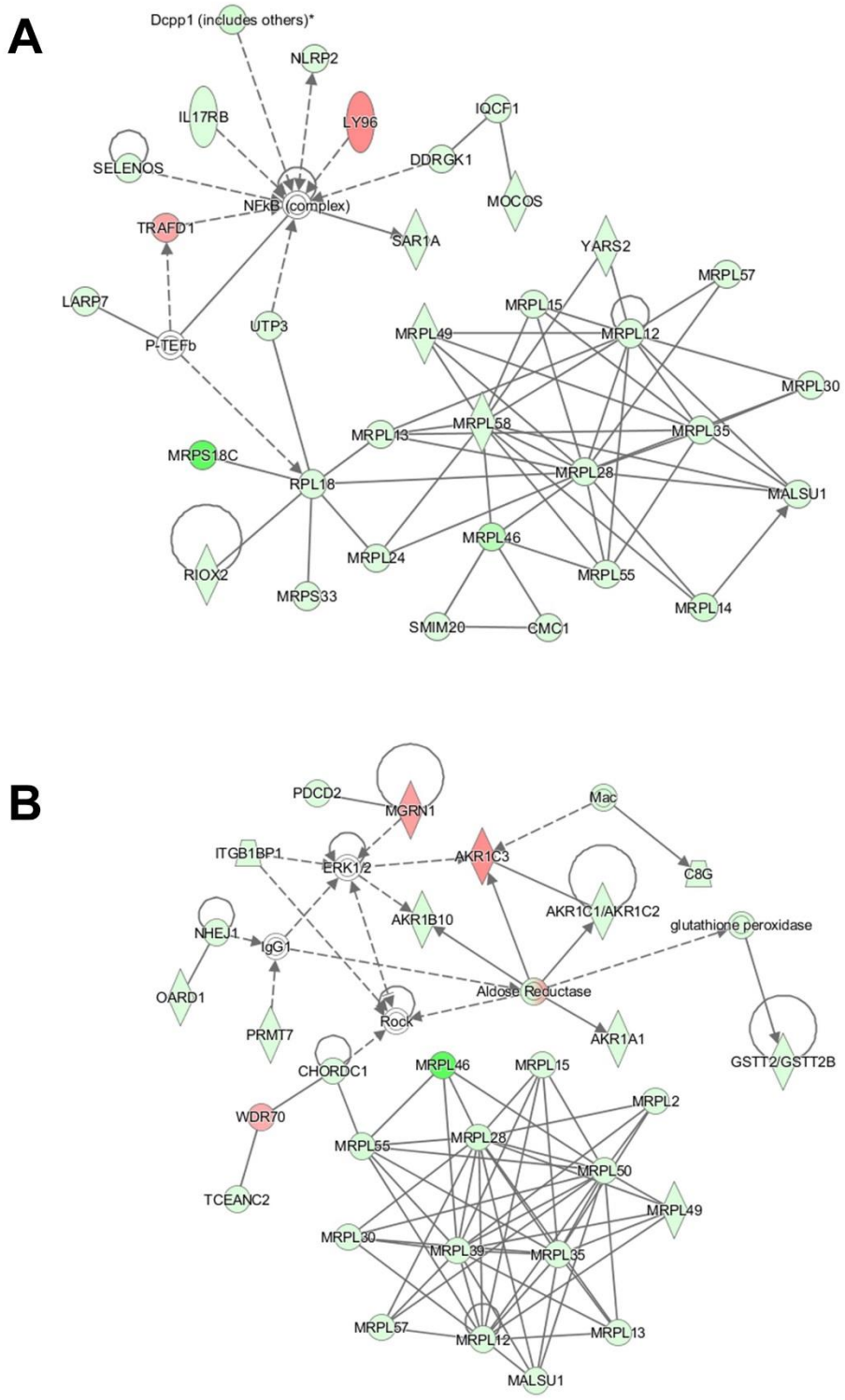

Figure S9. **Functional Network analyses by Ingenuity pathway analysis.** (A) The most significant networks identified in WT included transcripts related to gene expression, protein synthesis, cellular assembly and organisation, and maintenance. (B) The most significant networks in *Patl2*$^{-/-}$ mice assembled transcripts related to gene expression, protein synthesis and lipid metabolism. Up-regulated transcripts are shown in pink and down-regulated transcripts are indicated in green. Continuous lines between nodes indicate direct molecular interactions between connected transcripts; dotted lines indicate indirect functional interactions between transcripts.

SUPPLEMENTARY TABLES

Table S1A. Primer list for Sanger sequencing verification of PATL2 mutation

Oligo name	Sequence	Product size (bp)
PATL2H-Ex6F2	ATGTGCCATGTGGCTGACTT	286
PATL2H-Ex6R2	CAACTGGTCACAAGGGGAGA	

Table S1B. List of primers used to genotype *Patl2 KO* mice and for RT-PCR

	Oligo name	Sequence	Product size (bp)
Genotyping	Patl2-Ef	AAGCTCTGTTGGGTTTGAGGAGAAAA	WT allele: 235 KO allele: 325
	Patl2-Er	CAGCCTCTTTCCCCTGAATAATTTCA	
	Patl2-Kr	GGGCAAGAACATAAAGTGACCCTCC	
	C-LacZ-F	CCCGTCAGTATCGGCGGAAT	KO allele: 506
	L3R	TGTAATCTGGCTGCAGACAATCTAGGC	
RT-PCR	Patl2-RTseq-Ex7F	TCTGTGTTTCCAAGAGCCAGTTC	WT: 135 KO: no band
	Patl2-RTseq-Ex8R	GAGCTGGGTCAGATGACTGG	
	βact-F	ACCAGAGGCATACAGGGACA	104
	βact-R	CTAAGGCCAACCGTGAAAAG	

Table S1C. List of primers used to genotype *Patl2-HA tagged* mice and for RT-PCR

Oligo name	sequence	Product size (bp)
gRNA	5'-CAAGCAATTAGTTCAGCAGC-3'	
Patl2_HA-F primer	5'-CAGACTTTGCCTGGACATCA-3'	351 (WT) 378 (KI)
Patl2_HA-R primer	5'-GACCATGCTTGGCTCATAG-3'	

Table S1**. List of primers used for mouse genotyping**

Target /Antigen	Species	Supplier	REF	DILUTION
Tubulin	Mouse	Sigma Aldrich	T4026	1/800
MSY2	Mouse	Santa cruz Technology	SC393840	1/200 for IF
HA High Affinity	Rat	Roche/Sigma	11815016001	1/800 for IF, 1/1000 for WB
DDX6	Rabbit	Biotechne	NB200-191	1/500 for IF
CPEB1	Rabbit	Abcam	ab3465	1/200 for IF
Secondary antibody DyLight549 Goat anti mouse	Goat	Jackson Immuno Research	115-505-062	1/800
Secondary antibody AlexaFluor488 Goat anti rabbit	Goat	Jackson Immuno Research	115-545-144	1/800
Secondary antibody AlexaFluor488 Goat anti rat	Goat	Life Technologies	A-11006	1/800
Secondary antibody cy3 (?) Goat anti rabbit	Goat	Jackson Immuno Research	111-165-144	1/400
Secondary antibody HRP conjugate goat anti-rat	Goat	Millipore	AP136P	1/5000

Table S2. **List of antibodies**

2. « Nouvelle » : Échec de maturation ovocytaire Un rôle essentiel pour la protéine PATL2 dans l'ovogenèse

Christou-Kent M, Ray PF, Arnoult C. **Médecine/Sciences (Paris), December 2018**

Échec de maturation ovocytaire

Un rôle essentiel pour la protéine PATL2 dans l'ovogenèse

Marie Christou-Kent[1], Pierre F. Ray[1,2], Christophe Arnoult[1]

[1]Génétique, épigénétique et thérapies de l'Infertilité, Institut pour l'avancée des biosciences, Inserm U1209, CNRS UMR 5309, université Grenoble Alpes, 38000 Grenoble, France.
[2]Unité de génétique de l'infertilité et diagnostic pré-implantatoire, CHU de Grenoble, 38000 Grenoble, France.
christophe.arnoult@univ-grenoble-alpes.fr

› L'infertilité qui représente un enjeu majeur de santé, touche un couple sur sept et un facteur féminin est retrouvé dans plus de 70 % des infertilités de couple. Parmi les différentes causes connues d'infertilité féminine, les anomalies génétiques jouent un rôle prépondérant et sont impliquées dans les infertilités les plus sévères, comme l'insuffisance ovarienne [1] (➜).

(➜) Voir la Nouvelle de S. Caburet et E. Vilain, *m/s*, n° 2, février 2015, page 129

Il est donc important d'identifier ces causes génétiques afin de proposer un meilleur diagnostic et d'envisager, par la compréhension moléculaire des physiopathologies de l'ovogenèse, des alternatives thérapeutiques.

L'ovogenèse et la déficience méiotique ovocytaire (DMO)

Chez la femme, la production d'ovocytes matures est un processus long et complexe qui débute lors du développement embryonnaire et s'arrête pendant une douzaine d'années pour reprendre à la puberté. Les ovocytes quiescents sont bloqués en prophase de méiose I. Ils sont entourés de quelques cellules folliculaires, l'ensemble formant les follicules primordiaux. Des follicules primordiaux sont recrutés de manière périodique. Ils commencent une croissance au cours de laquelle la taille des ovocytes va être multipliée par 10 et le nombre de cellules folliculaires par plus de 1 000, *via* une stimulation croisée entre cellules folliculaires et ovocyte. Le follicule mature, ou follicule antral, contient un ovocyte qui est au stade de vésicule germinale ou germinative (VG), encore bloqué au stade de prophase I. Le terme VG se réfère au noyau de l'ovocyte qui présente alors une membrane nucléaire qui peut être observée à l'aide d'une loupe binoculaire. Dans l'espèce humaine, ce processus se réalise en 290 jours [2, 3]. À ce stade, l'ovocyte est en attente d'une stimulation hormonale qui provoquera la reprise de la méiose, la rupture de la vésicule germinale (GVBD : *germinal vesicle breakdown*) et l'extrusion du premier globule polaire. Les ovocytes arrêtent de nouveau leur maturation au stade métaphase de méiose II (MII). Ils attendent un signal provenant du spermatozoïde pour poursuivre la méiose.

Un type d'infertilité féminine, que nous avons appelé « déficience méiotique ovocytaire (DMO) », se caractérise par un échec de maturation de l'ovocyte [4,5]. Les femmes atteintes de ce syndrome, produisent, malgré un cycle menstruel d'apparence normal, des ovocytes immatures qui ne sont pas aptes à la fécondation. Dans le cas d'une procréation médicalement assistée, ces ovocytes, récoltés après stimulations ovariennes, ne pourront donner des embryons. Le couple est alors stérile. Jusqu'à récemment, seul le gène *TUBB8* (*tubulin beta 8 class VIII*), codant une isoforme de la tubuline, avait été identifié comme étant impliqué dans ce contexte d'infertilité [6].

Séquençage exomique d'une cohorte de patientes atteintes de la DMO

Afin d'identifier des variants génétiques pouvant expliquer la déficience méiotique ovocytaire (DMO), nous avons analysé, par séquençage total de l'exome (ADN codant), une cohorte de 23 patientes atteintes de ce syndrome, présentant des blocages de maturation à divers stades (stade VG, stade M1) ou des ovocytes atrétiques[1]. L'analyse génétique a permis d'identifier une mutation délétère dans le gène *PATL2* (*protein-associated with topoisomerase II homolog 2*) dans 26 % des ADN de patientes analysés ; ces patientes présentant un phénotype en commun : un blocage des ovocytes au stade immature VG *(Figure 1)*.

Transcription et contrôle des ARN messagers au cours d'ovogenèse - La protéine PATL2

Lors de la reprise de la méiose, la transcription est arrêtée jusqu'à l'activation du génome embryonnaire (EGA). C'est pourquoi, au cours de la croissance de l'ovocyte, on assiste à une synthèse massive d'ARN messagers (ARNm) nécessaires à la synthèse des protéines de l'ovocyte, mais également de protéines qui seront utilisées dans l'embryon avant l'EGA. Chez l'homme, l'EGA est assez tardif et est observé au stade 4-8 cellules. La gestion des ARNm au cours de l'ovogenèse est très spécifique et les voies de dégradation des transcrits sont en grande partie réprimées jusqu'à la fécondation [7]. Pour cela, des protéines régulatrices associées dans des complexes macromoléculaires avec les ARNm sont indispensables pour le développement ovocytaire. Parmi

[1] Ovocytes de mauvaise qualité qui se détruisent spontanément.

https://doi.org/10.1051/medsci/2018287

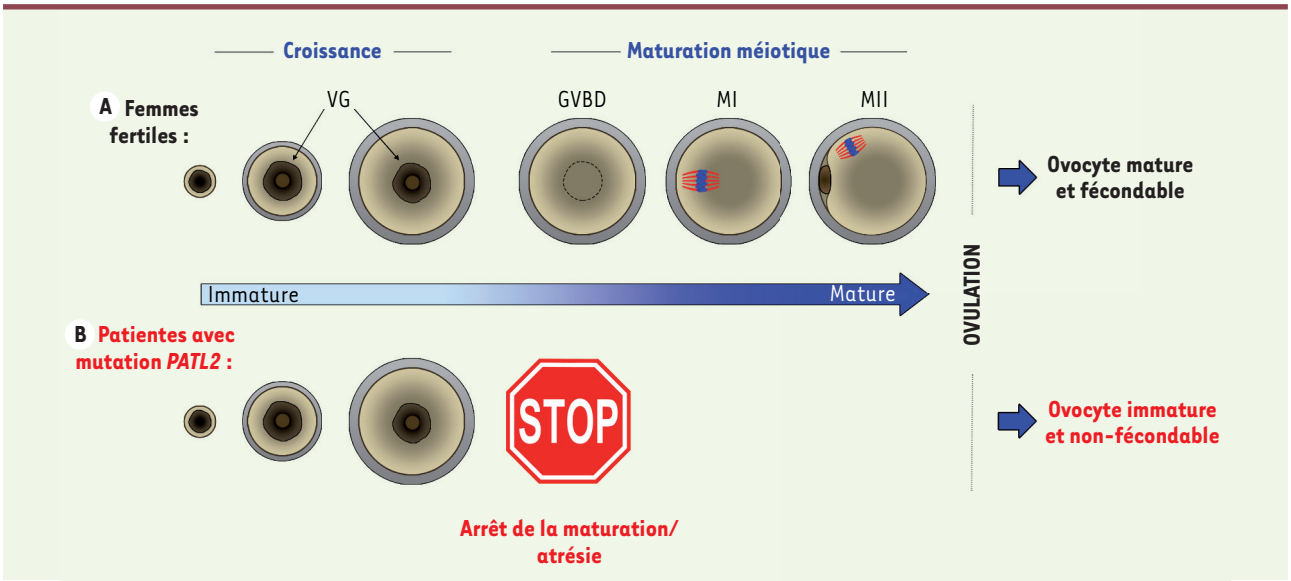

Figure 1. ***Le phénotype de « déficience méiotique ovocytaire (DMO) » chez des patientes avec un variant homozygote pathogène de PATL2. A.*** L'ovogenèse à partir d'ovocytes quiescents de follicules primordiaux et jusqu'à l'ovulation chez les femmes fertiles. VG : Vésicule germinale, GVBD : rupture de la vésicule germinale *(Germinal vesicle breakdown)*, MI : métaphase I, MII : métaphase II. ***B.*** Le phénotype de blocage de maturation ovocytaire chez les patientes atteintes d'une mutation de *PATL2*.

les différents acteurs, PATL2 pourrait jouer un rôle spécifique : son orthologue, chez le batracien *Xenopus laevis* (x-patl1a), est en effet essentiel dans la régulation des ARNm maternels et son expression est spécifique de l'ovocyte [8,9]. Afin de mieux explorer la fonction de la protéine humaine PATL2, nous avons généré une lignée de souris déficiente pour le gène *PATL2*.

Phénotype des souris déficientes en *PATL2*

Nous avons dans un premier temps étudié le phénotype reproductif des souris déficientes en *PATL2* (*PATL2*$^{-/-}$). Pour évaluer leur fertilité, les femelles *PATL2*$^{-/-}$ ont été mises en accouplement avec des mâles sauvages pendant une période de 6 mois. La taille moyenne des portées obtenues était plus de trois fois inférieure à la taille moyenne de celles des femelles contrôles pour la même période, et leur fréquence deux fois plus faible. Dans les expériences de fécondation *in vitro* (FIV), le taux de développement des embryons au stade « 2 cellules » des femelles *PATL2*$^{-/-}$ était diminué de moitié en comparaison des taux des embryons sauvages et le taux de développement jusqu'au stade blastocyste était plus de 6 fois inférieur à celui des contrôles *(Figure 2)*.

L'observation par immunofluorescence des ovocytes ovulés des femelles *PATL2*$^{-/-}$ révèle : (1) un plus grand pourcentage d'ovocytes ovulés sans globule polaire (signe d'immaturité méiotique et absence du stade attendu MII), et (2) parmi les ovocytes avec globule polaire, un pourcentage élevé d'ovocytes qui présentent les signes de défauts méiotiques : fuseau malformé ou mal positionné, chromosomes mal alignés et augmentation du nombre d'« asters » (étoiles de tubuline) dans le cytoplasme *(Figure 2)*.

En analysant les zygotes de femelles *PATL2*$^{-/-}$ après fécondation, nous avons observé une réduction du pourcentage de zygotes au stade attendu de 2 pro-noyaux (14,4 % *versus* 53,4 %) et un nombre élevé de zygotes atypiques. Parmi ces zygotes anormaux, nous avons identifié soit un nombre atypique de pro-noyaux, soit une non-décondensation des chromosomes paternels et maternels souvent accompagnée d'une polyspermie[2], indication d'une absence de réponse de l'ovocyte à la fécondation.

Ce travail sur les souris déficiente *PATL2*$^{-/-}$ a donc permis de confirmer que la déficience de PATL2 entraînait un phénotype de DMO. Cependant, de manière surprenante, chez la souris, l'absence de *PATL2* entraîne un phénotype moins sévère que chez l'homme.

Analyse du transcriptome des ovocytes VG de souris *PATL2*$^{-/-}$

Étant donné le rôle de PATL2 chez les amphibiens, nous avons voulu explorer les conséquences de l'absence du gène au niveau des transcrits. Les ovocytes de femelles *PATL2*$^{-/-}$ isolés en stade VG sont légèrement plus petits que ceux des femelles sauvages au même stade, mais ils ne présentent pas d'autres défauts visuels. Les coupes d'ovaires des femelles *PATL2*$^{-/-}$, à 12 jours et à 26 jours, ne montrent pas non plus d'anomalies morphologiques du développement des follicules. Pourtant, l'analyse transcriptomique met en évidence le

[2] Fécondation d'un ovule par plusieurs spermatozoïdes.

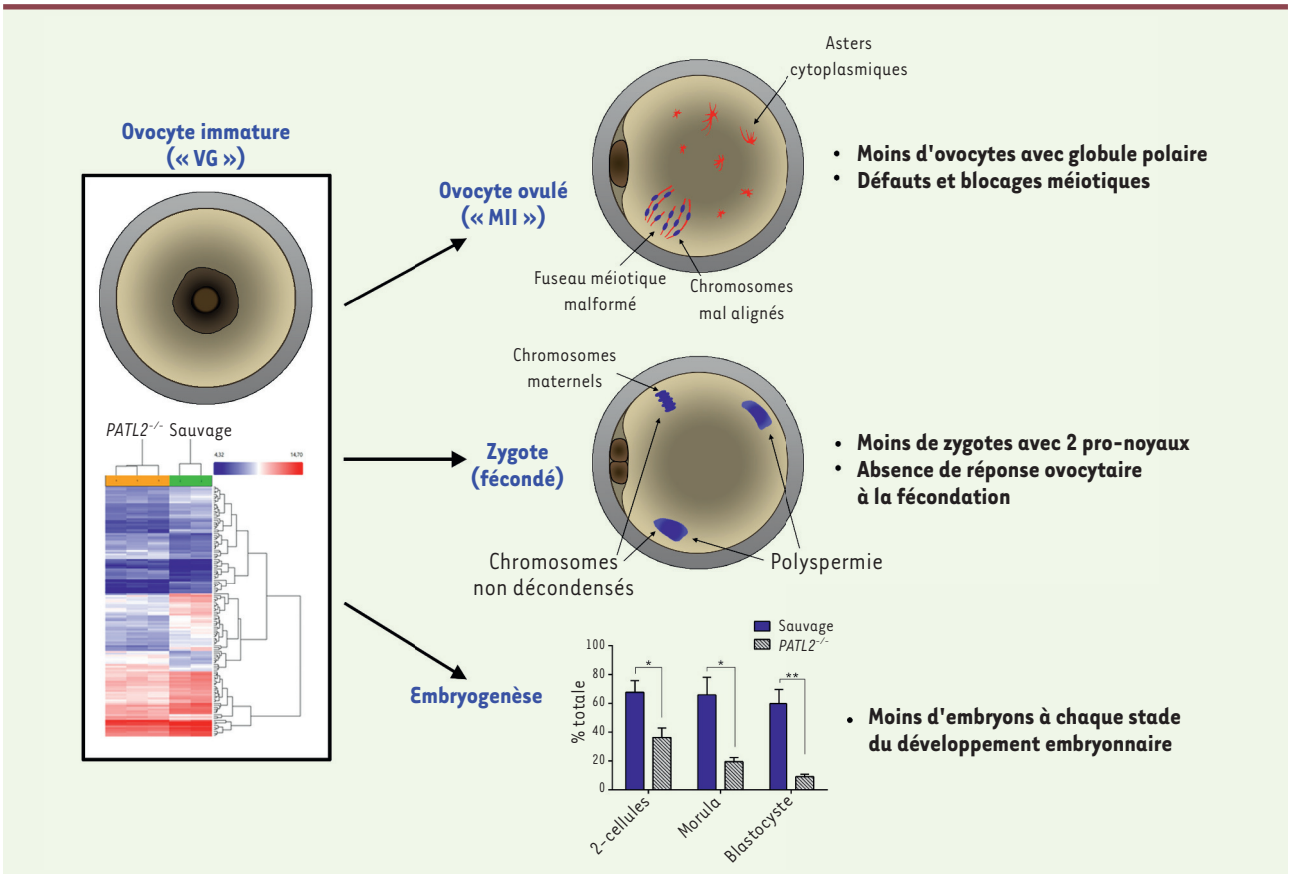

Figure 2. ***La dérégulation du transcriptome des ovocytes VG de souris PATL2$^{-/-}$ et ses conséquences morphologiques et développementales.*** Comparaison des ovocytes de souris *PATL2*$^{-/-}$ et sauvages : (1) diminution de l'abondance des ARN messagers (ARNm) mesurée par analyse transcriptomique (micropuce), (2) différence de morphologie analysée par immunofluorescence (marquage de la β-tubuline et de l'ADN, en rouge et bleu respectivement) et (3) détermination des taux de développement obtenus par fécondation *in vitro*. (VG : vésicule germinale, MII : métaphase II). Ovocyte : en beige ; zone pellucide : en gris ; vésicule germinale/globules polaires : en marron ; fuseau méiotique/microtubules : en rouge ; et chromosomes : en bleu (figure adaptée de [10]).

fait que les ovocytes VG *PATL2*$^{-/-}$ issus de follicules antraux présentent une dérégulation, d'un facteur supérieur à 2, de l'expression de 134 gènes dont 95 sont sous-exprimés et 39 sur-exprimés. Ce nombre limité de gènes indique que PATL2 intervient de manière spécifique et ciblée dans la régulation des ARNm.

Parmi les gènes dont l'expression est modulée, on retrouve des gènes codant des protéines ayant différentes fonctions : des facteurs de croissance et de différenciation de l'ovocyte, de l'assemblage et de la stabilité du fuseau méiotique, du contrôle de la méiose II et de la gestion du stress oxydatif, ainsi que des facteurs secrétés qui participent à l'interaction avec le cumulus (les cellules folliculaires). Étonnamment, une partie de ces transcrits correspondent à des protéines nécessaires à l'implantation de l'embryon. Ces dérégulations expliquent les défauts ovocytaires et embryonnaires observés, ainsi que les taux de développement diminués en l'absence de PATL2. Elles correspondent également au rôle de PATL2 comme régulateur de l'expression des ARNm. Restait donc à caractériser le rôle précis de PATL2 dans la gestion de ces ARNm.

Une nouvelle fonction de PATL2 chez les mammifères ?

Chez *Xenopus laevis*, la protéine codée par l'orthologue de *PATL2*, *x-Patl1a*, est associée, au sein d'un complexe macromoléculaire, à plusieurs autres protéines, comme Cpeb1 (*cytoplasmic polyadenymation element-binding protein 1*) et Frgy2 (*frog Y-box protein 2*), et est impliquée dans la régulation spécifique de certains ARNm. Nous n'avons pas trouvé que ces ARNm soient dérégulés dans le transcriptome des ovocytes VG des souris *PATL2*$^{-/-}$. Dans la lignée de souris « PATL2-étiquettée » (chez lesquelles une étiquette HA [*human influenza hemagglutinin*] est insérée à l'extrémité C-terminale de la protéine par la technique fondée sur CRISPR/Cas9), la réalisation d'un co-marquage sur des coupes d'ovaires n'a pas mis en évidence une co-localisation de PATL2 avec Cpeb1 et Ybx2

(*Y box protein 2*, alias Msy 2), la protéine murine équivalente à Frgy2. Chez la souris, le profil d'expression de la protéine codée par *PATL2* semble différent de ceux de ces deux protéines. Une autre différence entre x-Patl*a* (chez le xénope) et PATL2 (chez la souris) apparaît : chez le xénope, x-Patl*a* est en effet fortement dégradée après la rupture de la vésicule germinale (GVBD, *germinal vesicle breakdown*) alors que PATL2 reste présente jusqu'au stade zygote chez la souris. Il est donc possible que la fonction de PATL2 ait évoluée entre ces deux vertébrés. Il serait donc très intéressant d'identifier les protéines partenaires et les ARNm cibles de PATL2 chez les mammifères afin de mieux comprendre son rôle dans l'ovogenèse.

La pertinence médicale

La mutation du gène *PATL2* est donc une cause importante de la déficience méiotique ovocytaire chez la femme. Ces résultats devraient permettre aux patientes de bénéficier d'un meilleur diagnostic et d'une meilleure compréhension de leur pathologie. À plus long terme, des stratégies thérapeutiques pourront ainsi être envisagées. Nous avons également révélé le rôle important que PATL2 joue dans la régulation des ARNm maternels chez la souris. Ces découvertes améliorent notre compréhension des mécanismes de stockage et de contrôle des ARNm dans l'ovocyte de mammifères pendant sa maturation. Nos résultats pourraient être très pertinents dans le domaine novateur de la maturation *in vitro* des ovocytes. Cette technique a des applications potentielles multiples, comme le traitement de patientes atteintes d'insuffisance ovarienne précoce, mais également la préservation de la fertilité en vue d'une future reproduction pour les personnes atteintes de cancer et traitées par chimiothérapie. ◊

Oocyte maturation failure: an essential role for the protein PATL2 in human oogenesis

LIENS D'INTÉRÊT

Les auteurs déclarent n'avoir aucun lien d'intérêt concernant les données publiées dans cet article.

RÉFÉRENCES

1. Caburet S, Vilain E. Mutation de STAG3 Une nouvelle cause d'insuffisance ovarienne prématurée. *Med Sci (Paris)* 2015 ; 31 : 129-31.
2. Li R, Albertini DF. The road to maturation: somatic cell interaction and self-organization of the mammalian oocyte. *Nat Rev Mol Cell Biol* 2013 ; 14 : 141-52.
3. Williams CJ, Erickson GF. Morphology and physiology of the ovary. In : De Groot LJ, *et al.* eds. South Dartmouth (MA) : MDText.com, Inc ; 2012.
4. Beall S, Brenner C, Segars J. Oocyte maturation failure: a syndrome of bad eggs. *Fertil Steril* 2010 ; 94 : 2507-13.
5. Levran D, Farhi J, Nahum H, *et al.* Maturation arrest of human oocytes as a cause of infertility: case report. *Hum Reprod* 2002 ; 17 : 1604-9.
6. Feng R, Sang Q, Kuang Y, *et al.* Mutations in TUBB8 and human oocyte meiotic arrest. *N Engl J Med* 2016 ; 374 : 223-32.
7. Svoboda P, Franke V, Schultz RM. *Sculpting the transcriptome during the oocyte-to embryo transition in mouse*, 1st ed. New York : Elsevier Inc., 2015 : 306 p.
8. Nakamura Y, Tanaka KJ, Miyauchi M, *et al.* Translational repression by the oocyte-specific protein P100 in Xenopus. *Dev Biol* 2010 ; 344 : 272-83.
9. Marnef A, Maldonado M, Bugaut A, *et al.* Distinct functions of maternal and somatic Pat1 protein paralogs. *RNA* 2010 ; 16 : 2094-107.
10. Christou-Kent M, Kherraf Z-E, Amiri-Yekta A, *et al.* PATL2 is a key actor of oocyte maturation whose invalidation causes infertility in women and mice. *EMBO Mol Med* 2018 ; 10 : e8515.

B: The role of SPINK2 in spermiogenesis

1. Article: SPINK2 deficiency causes infertility by inducing sperm defects in heterozygotes and azoospermia in homozygotes

Kherraf ZE, **Christou-Kent M**, Karaouzène T, Amiri-Yekta A, Martinez G, Vargas AS, Lambert E, orel C, Dorphin B, Aknin-Seifer I, Mitchell MJ, Metzler-Guillemain C, Escoffier J, Nef S, Grepillat M, Thierry-Mieg N, Satre V, Bailly M, Boitrelle F, Pernet-Gallay K, Hennebicq S, Fauré J, Bottari SP, Coutton C, Ray PF & Arnoult C. **EMBO Molecular Medicine, May 2017.**

1.1. Context

A splicing variant of the gene *SPINK2* was identified in two brothers with non-obstructive azoospermia (NOA). For one of the two brothers, a testis biopsy had been performed and sections were obtained for RT-PCR, revealing the presence of truncated SPINK2 transcripts. A *Spink2* KO mouse lineage was obtained and the phenotype characterised through histological analysis of the testes and epididymis, immunofluorescent staining of spermatogenic cells and electron microscopy of round spermatids with wild type controls. We demonstrated in the following article that absence of the SPINK2 protein, which is located in the acrosome of maturing and mature spermatozoa in mice and in men, leads to post-meiotic arrest and azoospermia due to autophagy at the round-spermatid stage. This is plausibly due to aberrant acrosin activity in the absence of its inhibitor, corroborated by absence of the acrosome, fragmentation of the Golgi apparatus, and presence of vesicles indicative of microautophagy in round spermatids. Absence of SPINK2 also prevented the fusion of proacrosomal vesicles and their aggregation at the nuclear envelope.

In addition, we were able to show that SPINK2 neutralises acrosin activity in HEK293 cells transfected with proacrosin, SPINK2 or both in real-time cell analysis. The morphology and motility of mature sperm from heterozygous mice was also analysed and a phenotype of asthenoteratospermia was found, indicating the existence of a dose-dependent pathological continuum. My major contribution to this project was the histological analysis and fluorescent staining of human and mouse testis sections and immunofluorescent staining of human and mouse mature spermatozoa and mouse immature spermatogenic cells.

Research Article

TRANSPARENT PROCESS OPEN ACCESS

EMBO Molecular Medicine

SPINK2 deficiency causes infertility by inducing sperm defects in heterozygotes and azoospermia in homozygotes

Zine-Eddine Kherraf[1,†], Marie Christou-Kent[1,†], Thomas Karaouzene[1], Amir Amiri-Yekta[1,2,3], Guillaume Martinez[1], Alexandra S Vargas[1], Emeline Lambert[1], Christelle Borel[4], Béatrice Dorphin[5], Isabelle Aknin-Seifer[6], Michael J Mitchell[7], Catherine Metzler-Guillemain[7], Jessica Escoffier[1], Serge Nef[4], Mariane Grepillat[1], Nicolas Thierry-Mieg[8], Véronique Satre[1,9], Marc Bailly[10,11], Florence Boitrelle[10,11], Karin Pernet-Gallay[12], Sylviane Hennebicq[1,13], Julien Fauré[2,12], Serge P Bottari[1,14], Charles Coutton[1,9], Pierre F Ray[1,2,‡,*] & Christophe Arnoult[1,‡]

Abstract

Azoospermia, characterized by the absence of spermatozoa in the ejaculate, is a common cause of male infertility with a poorly characterized etiology. Exome sequencing analysis of two azoospermic brothers allowed the identification of a homozygous splice mutation in *SPINK2*, encoding a serine protease inhibitor believed to target acrosin, the main sperm acrosomal protease. In accord with these findings, we observed that homozygous *Spink2* KO male mice had azoospermia. Moreover, despite normal fertility, heterozygous male mice had a high rate of morphologically abnormal spermatozoa and a reduced sperm motility. Further analysis demonstrated that in the absence of Spink2, protease-induced stress initiates Golgi fragmentation and prevents acrosome biogenesis leading to spermatid differentiation arrest. We also observed a deleterious effect of acrosin overexpression in HEK cells, effect that was alleviated by SPINK2 coexpression confirming its role as acrosin inhibitor. These results demonstrate that SPINK2 is necessary to neutralize proteases during their cellular transit toward the acrosome and that its deficiency induces a pathological continuum ranging from oligoasthenoteratozoospermia in heterozygotes to azoospermia in homozygotes.

Keywords azoospermia; exome sequencing; genetics; infertility; spermatogenesis

Subject Categories Genetics, Gene Therapy & Genetic Disease; Urogenital System

DOI 10.15252/emmm.201607461 | Received 13 December 2016 | Revised 14 April 2017 | Accepted 26 April 2017 | Published online 29 May 2017

EMBO Mol Med (2017) 9: 1132–1149

Introduction

The World Health Organization estimates that 50 million couples worldwide are confronted with infertility. Assisted reproduction technologies (ART) initiated 35 years ago by Nobel Prize Winner Robert Edwards have revolutionized the practice of reproductive medicine, and it is now estimated that approximately 15% of couples in Western countries seek assistance from reproductive clinics for infertility or subfertility. Despite technological breakthroughs and advances, approximately half of the couples concerned still fail to achieve a successful pregnancy even after repeated treatment cycles. Alternative treatment strategies should therefore be

1 Genetic Epigenetic and Therapies of Infertility, Institute for Advanced Biosciences, Inserm U1209, CNRS UMR 5309, Université Grenoble Alpes, Grenoble, France
2 CHU de Grenoble, UF de Biochimie Génétique et Moléculaire, Grenoble, France
3 Department of Genetics, Reproductive Biomedicine Research Center, Royan Institute for Reproductive Biomedicine, ACECR, Tehran, Iran
4 Department of Genetic Medicine and Development, University of Geneva Medical School, Geneva 4, Switzerland
5 Laboratoire d'Aide Médicale à la Procréation, Centre AMP 74, Contamine-sur-Arve, France
6 Laboratoire de Biologie de la Reproduction, Hôpital Nord, Saint Etienne, France
7 Aix Marseille Univ, INSERM, GMGF, Marseille, France
8 Univ. Grenoble Alpes / CNRS, TIMC-IMAG, Grenoble, France
9 CHU de Grenoble, UF de Génétique Chromosomique, Grenoble, France
10 Department of Reproductive Biology and Gynaecology, Poissy General Hospital, Poissy, France
11 EA 7404 GIG, Université de Versailles Saint Quentin, Montigny le Bretonneux, France
12 Grenoble Neuroscience Institute, INSERM 1216, Grenoble, France
13 CHU de Grenoble, UF de Biologie de la procréation, Grenoble, France
14 CHU de Grenoble, UF de Radioanalyses, Grenoble, France
*Corresponding author. Tel: +33 4 76 76 55 73; E-mail: pray@chu-grenoble.fr
†These authors contributed equally to this work
‡These authors contributed equally to this work as senior authors

envisaged to improve ART success rate, especially for patients impervious to usual assisted reproductive technologies. Improvement in treatment efficiency essentially depends upon an accurate diagnosis and the characterization of the molecular etiology of the defect. These efforts to better characterize infertility subtypes should first be concentrated on the most severe defects since they generally have a poor prognosis and affected patients would benefit the most from new treatments. Moreover, the most severe phenotypes are more likely to be caused by monogenic defects which are easier to identify. As such, the genetic exploration of non-obstructive azoospermia (NOA), the absence of spermatozoa in the ejaculate due to a defect in spermatogenesis, should be considered a priority. NOA is a common cause of infertility found in approximately 10% of the couples assessed for infertility. Although a genetic etiology is likely to be present in most cases of azoospermia, only a few defective genes have so far been associated with this pathology accounting for a minority of cases. At present, only chromosomal abnormalities (mainly 47XXY, Klinefelter syndrome identified in 14% of cases) and microdeletions of the Y chromosome are routinely diagnosed, resulting in a positive genetic diagnosis in < 20% of azoospermia cases (Tuttelmann *et al*, 2011). The evolution of sequencing technologies and the use of whole-exome or whole-genome sequence (WES/WGS) analysis paves the way to a great improvement in our ability to characterize the causes of genetically heterogeneous pathologies such as NOA.

Spermatogenesis can be subdivided into three main steps: (i) multiplication of diploid germ cells; (ii) meiosis, with the shuffling of parental genes and production of haploid cells; and (iii) spermiogenesis, the conversion of round spermatids into one of the smallest and most specialized cells in the body, the spermatozoa. NOA is expected to be mainly caused by failures in steps 1 and 2, and it is indeed what has been observed in a majority of cases so far. Very recently, defects in six genes were linked to azoospermia in man. Most of these genes code for meiosis-controlling proteins such as TEX11, TEX15, SYCE1, or MCM8, and the absence of the functional proteins induces a blockage of meiosis (Tuttelmann *et al*, 2011; Maor-Sagie *et al*, 2015; Okutman *et al*, 2015; Yang *et al*, 2015; Yatsenko *et al*, 2015). Another WES analysis of two consanguineous families identified likely causal mutations in *TAF4B* and *ZMYND15* (Ayhan *et al*, 2014). Study of *Taf4b* KO mice showed that homozygous mutant males are subfertile with extensive pre-meiotic germ cell loss due to altered differentiation and self-renewal of the spermatogonial stem cell pool, thus illustrating that pre-meiotic block induces NOA. More surprisingly, *ZMYND15* codes for a spermatid-specific histone deacetylase-dependent transcriptional repressor and its absence in mice induced a significant depletion of late-stage spermatids (Yan *et al*, 2010) suggesting that NOA can also be induced by post-meiotic defects.

Here, WES analysis of two brothers with NOA led to the identification of a homozygous truncating mutation in the *SPINK2* gene coding for a Kazal family serine protease inhibitor. Studying KO mice, we observed that homozygous KO animals also suffered from azoospermia thus confirming the implication of SPINK2 in NOA. Furthermore, we observed that SPINK2 is expressed from the round-spermatid stage onwards thus confirming that post-meiotic anomalies can result in NOA. We suggest that SPINK2 is necessary to neutralize the action of acrosomal proteases shortly after their synthesis and before they can be safely stored in the acrosome where they normally remain dormant until their release during the acrosome reaction. We also show that in the absence of SPINK2, protease-induced stress initiates Golgi fragmentation contributing to the arrest of spermatid differentiation and their shedding from the seminiferous epithelium. The characterization of the molecular pathophysiology of this defect opens several novel therapeutic perspectives which may allow the restoration of a functional spermatogenesis.

Results

Medical assessment of two brothers with defective sperm production

Two French brothers (Br1 and Br2), born from second cousin parents (Fig 1A), and their respective wives sought medical advice from infertility clinics in France (Chatellerault, Tours, Poissy, and Grenoble) between 2005 and 2014 after 2 years of unsuccessful attempts to spontaneously conceive. Analyses of their ejaculates (Fig 1B; $n = 5$) evidenced the absence of spermatozoa for the first brother (Br1) and a very low concentration (0–200,000/ml, mean 126,000/ml $n = 5$) for the second (Br2). Moreover, all spermatozoa were immotile and presented an abnormal morphology (pin-shaped head devoid of acrosome; detached flagella) and were not suitable for *in vitro* fertilization (IVF) with intracytoplasmic sperm injection (ICSI). Interestingly, ejaculates of both brothers presented a significant concentration of germ cells ($8.6 \times 10^6 \pm 6.2 \times 10^6$/ml and $9.0 \times 10^6 \pm 7.0 \times 10^6$/ml for Br-1 and Br-2, respectively) likely corresponding to spermatids. As Br1 and Br2 both present a severe default of sperm production with a high number of spermatids in the ejaculate, we believe that they present the same phenotype, likely caused by the same genetic defect. A normal karyotype was observed for both brothers (46,XY), and no deletions of the Y

Figure 1. Azoospermia in two consanguineous brothers.

A Genetic tree of the studied family showing affected brothers Br1 and Br2 illustrating the consanguinity of the parents (P1 and P2).

B Comparisons of ejaculate volume ($n = 5$) and spermograms ($n = 5$) of brothers Br1 and Br2 with those of fertile controls ($n = 35$) evidence the absence of mature sperm and the presence of round cells in the ejaculates. Data represent mean ± SEM. *P*-values are $P = 4 \times 10^{-4}$ (a), $P = 0.6$ (b, non-significant), and $P = 4 \times 10^{-5}$ (c); statistical differences were assessed using *t*-test.

C, D Testis sections from a fertile control and (D) patient Br1 stained with periodic acid–Schiff (PAS). The lumen of tubules from the control is large and mature sperm are present (C), whereas the lumen of most of seminiferous tubules from patient Br1 is filled with non-condensed and early condensed round spermatids and no mature sperm are observed. Scales bars, 100 μm.

E, F In the fertile control (E) seminiferous tubule cross sections, spermatogonia (Sg), spermatocytes (Sc) and spermatids (RS) are regularly layered, whereas the different types of spermatogenic cells are disorganized in patient Br1 (F). Scales bars, 100 μm.

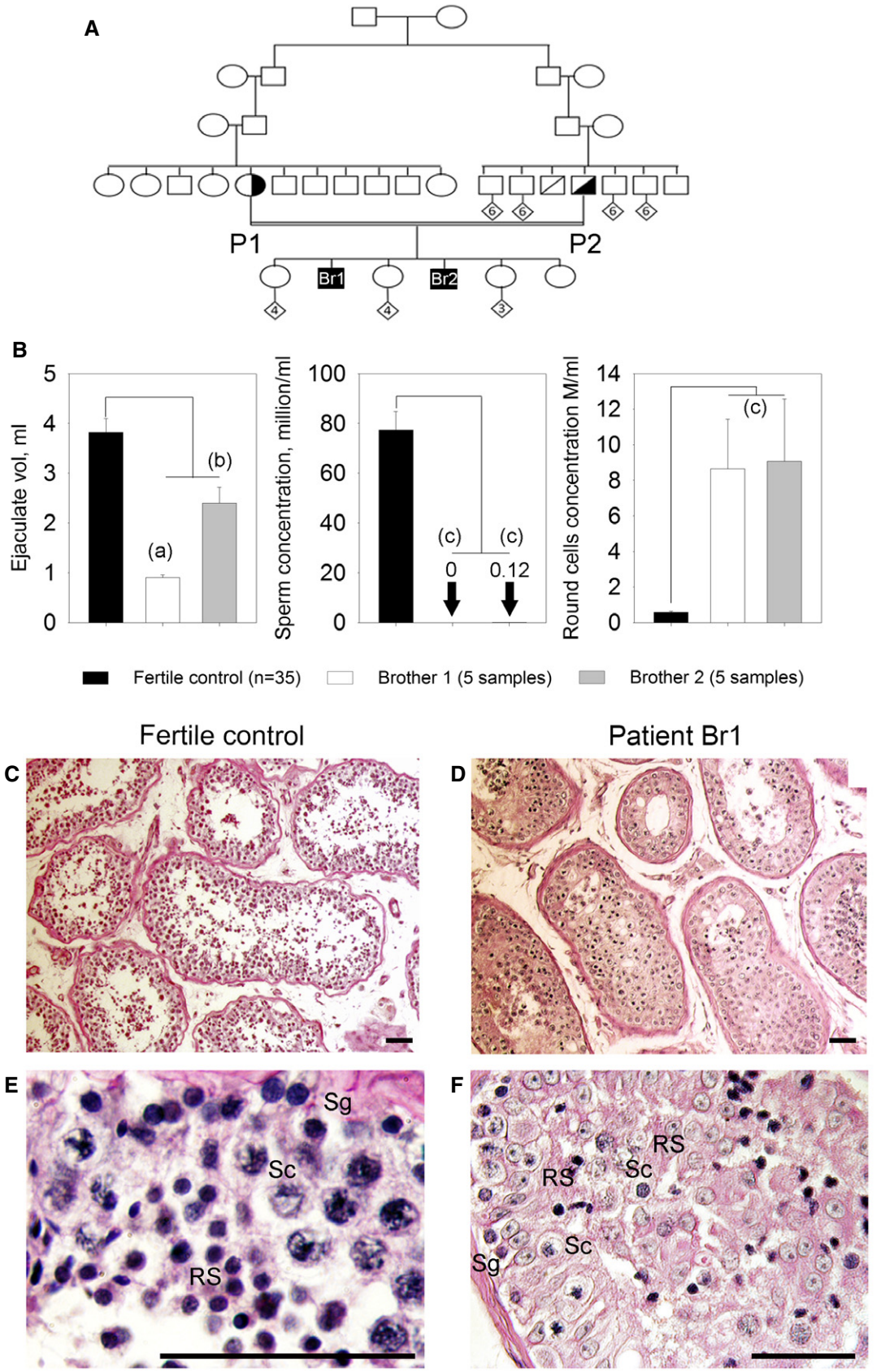

Figure 1.

chromosome were observed at the AZF loci. Testis sperm extraction was carried out twice for Br1 in 2008 and 2014. Each time the recovery was unsuccessful (although a few spermatozoa were observed in fixed dilacerated testicular tissues) suggesting a diagnosis of post-meiotic NOA. Histological analysis of seminiferous tubules obtained from Br1 biopsies showed: (i) a disorganization of the structure of the tubules; (ii) that the lumen of the seminiferous tubules were filled with immature germ cells, an indication of intense desquamation of the germinal epithelium; and (iii) a reduced number of round spermatids, with an overrepresentation of early round spermatids (Fig 1C–F). Brother Br2 has only had spermograms for diagnostic purposes which did not show any ICSI-compatible spermatozoa and has not been able to attempt ART.

Whole-exome sequencing identifies a homozygous truncating mutation in *SPINK2*

Since the brothers were married to unrelated women, we excluded the possibility of a contributing female factor and focused our research on the brothers. Given the familial history of consanguinity, we postulated that their infertility was likely caused by a common homozygous mutation. We proceeded with WES to identify a possible genetic defect(s) which could explain the observed azoospermia. After exclusion of common variants, both bothers carried a total of 121 identical missense heterozygous variants (none appearing as obvious candidate) and only five identical homozygous variants common to both brothers (Appendix Table S1). Among these different genes, only the Chr4:57686748G>C *SPINK2* variant was described to be predominantly expressed in human testis (Appendix Fig S1A) as well as in mouse testis (Appendix Fig S1B). The mutation was validated by Sanger sequencing in both brothers (homozygous) and their parents (heterozygous) (Fig 2A). *SPINK2* thus appeared as the best candidate to explain the human condition. The variant Chr4:57686748G>C was not present in > 121,000 alleles analyzed in the ExAC database (http://exac.broadinstitute.org) and could have an effect on RNA splicing. *SPINK2* is located on chromosome 4 and contains four exons (Fig 2B). The gene codes for a Kazal type 2 serine protease inhibitor also known as an acrosin–trypsin inhibitor. The Ensembl expression database (www.ensembl.org) predicts the presence of four transcripts. We studied the expression of the different transcripts in human testis by RT–PCR, and only one band was present corresponding to NM_021114, ENST00000248701, which codes for a protein of 9.291 kDa consisting of 84 amino acids (Fig 2C). All nucleotide sequences herein refer to this transcript. The identified mutation, c.56-3C>G, is located three nucleotides before exon 2 and may create a new splice acceptor site, leading to a frameshift and premature stop codon in exon 2 and the generation of an abnormal transcript (T1) and/or to the skipping of exon 2 (44 nt) giving rise to an early stop codon at the beginning of exon 3 and the generation of another abnormal transcript (T2) (Fig 2B). To validate these hypotheses, RT–PCR was performed on testicular extract from Br1. Two bands were observed (Fig 2C) and sequenced after isolation of each band following gel electrophoresis. Sequence analysis demonstrated that the bands corresponded to T1 and T2, demonstrating that both abnormal transcripts were present in the patient's testis (Fig 2D). Since the protease inhibitor and binding sites of the protein are coded mostly by exon 3, it is expected that the truncated proteins corresponding to T1 and T2 transcripts are not functional (Appendix Fig S2). Sequencing of Br1's transcripts therefore confirms that the identified splice variant abrogates the production of a full-length protein thereby confirming its role as a deleterious mutation.

Importance of *SPINK2* variants as a cause for human infertility: sequence analysis of a cohort of infertile men with an altered spermatogenesis

We sequenced *SPINK2* whole coding sequences of 611 patients affected by azoo- or oligozoospermia (210 patients with azoospermia, 393 subjects with oligozoospermia and 8 with unspecified cause). Only one variant, identified in patient 105 (P105), was not described in ExAC and was likely deleterious (Appendix Table S2). This variant, c.1A>T (Fig EV1A), abrogates the *SPINK2* start codon and was present heterozygously in P105, a man with oligozoospermia. An alternate start site could potentially be used in the middle of exon 3 allowing the synthesis of a truncated protein of 2 kDa lacking the reactive site and disulfide bonds, both known to be crucial for SPINK2 function (Fig EV1B). However, overexpression of the mutated gene in HEK cells did not produce any portion of the SPINK2 protein indicating that the putative alternative start site is not functional and that the alteration of the initial start site does not permit the synthesis of any part of the SPINK2 protein. This was evidenced by transfecting HEK293 cells with a plasmid containing the full human *SPINK2* ORF sequence with the c.1A>T mutation and a C-terminus DDK-tagged. Extracted proteins were loaded onto a 20% acrylamide gel and detected with anti-DDK or anti-SPINK2 antibodies (Fig EV1C). P105 and his wife, born from non-consanguineous parents, experienced a 5-year period of infertility before giving birth to a healthy boy conceived spontaneously. They sought medical advice 2 years after their son's birth to initiate a second pregnancy. Sperm analysis resulted in the diagnosis of oligozoospermia associated with a reduced percentage of progressive motile spermatozoa (Table EV1). The patient's sperm morphology was assessed with Harris–Shorr staining using the modified David's classification and showed that 34–39% of sperm had a normal morphology ($n = 2$). The main defects observed were abnormal acrosome (34–39%) and defective neck–head junction (40–46%), defects that are similar to those observed in patient Br2.

This analysis indicates that *SPINK2* defects are extremely rare with an allelic frequency of approximately 1/1,200 in the cohort of infertile men analyzed. The rarity of *SPINK2* variants and the fact that P2, the father of Br1 and Br2, also harboring a heterozygous mutation, presents in a milder phenotype than P105 could indicate that *SPINK2* haploinsufficiency induces a milder phenotype of oligozoospermia with an incomplete penetrance on infertility.

Homozygous *Spink2* KO mice have azoospermia due to a spermiogenesis blockade at the round-spermatid stage

In order to confirm that the absence of SPINK2 leads to azoospermia, homozygous *Spink2* KO ($^{-/-}$) mice were obtained and their reproductive phenotype was studied. We first performed qRT–PCR on *Spink2*$^{+/+}$ and *Spink2*$^{-/-}$ testis mRNA extracts to validate the absence of *Spink2* mRNA and thus of protein. Contrary to what was observed in WT littermates, we observed no *Spink2* amplification in KO males, confirming Spink2 deficiency (Appendix Fig S3). Males

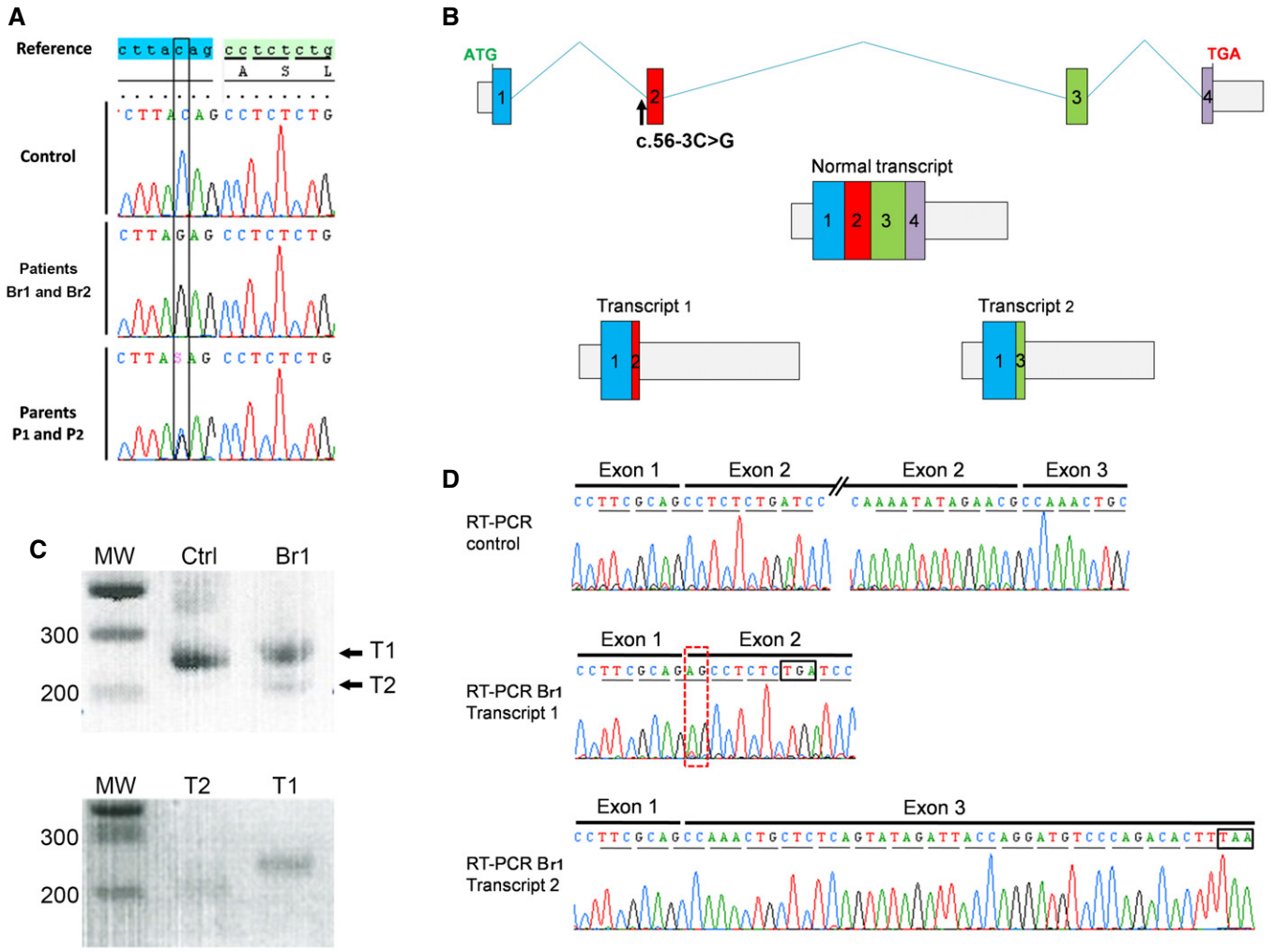

Figure 2. Identification of a *SPINK2* variant (c.56-3C>G) by exome sequencing and its consequences on splicing and translation.

A The identified variant, homozygous in patients 1 and 2 and heterozygous in their parents, is located three nucleotides before exon 2 and creates an AG that immediately precedes the original AG splice acceptor site.

B If recognized during splicing, this new acceptor site is expected to add two nucleotides (AG) at the beginning of exon 2, inducing a frameshift leading to a stop codon 3 amino acids later (transcript 1). The non-recognition of the abnormal acceptor site is expected to induce the skipping of exon 2 (transcript 2). The first stop codon can be observed 15 codons after the mis-inserted exon 3.

C RT–PCR of mRNA extracts from fertile control (Ctrl) and the brother Br1. Results show one band for Ctrl. The sequencing of this band showed that it corresponds to transcript NM_021114. For Br1, two bands were present, named T1 and T2. Bottom gel shows T1 and T2 after gel isolation.

D Transcripts T1 and T2 were collected and sequenced: T1 showed the insertion of an additional AG (red-dashed rectangle) leading to a premature stop codon (black box), whereas transcript T2 showed that exon 2 had been excised; these two transcripts correspond to the expected transcripts 1 and 2 from panel (B). Stop codons are shown in black boxes.

were completely infertile, whereas no reproductive defects were observed in females (Fig 3A1). Homozygous KO mice had comparatively smaller sized testes and a testis/body weight ratio half that of their wild-type (WT) littermates [3.63 ± 0.21 in WT and 1.77 ± 0.03 in KO (Fig 3A2)]. Furthermore, there was a complete absence of spermatozoa in *Spink2*$^{-/-}$ caudal epididymis (Fig 3A3) which only contained round cells likely corresponding to round spermatids and multinucleated cells, known as symblasts. Histological studies of KO seminiferous tubules stained with periodic acid–Schiff (PAS) revealed the presence of germ cells up to the early round-spermatid stage but condensed and elongated spermatids and mature spermatozoa were completely absent, contrary to WT (Fig 3B1 and C1). The lumen of the seminiferous tubules of Spink2$^{-/-}$ males contained round cells and symblasts (Fig EV2A and B), a result in agreement with observations of the cellular content of the cauda epididymis, which showed the presence of round cells only (Fig EV2C). In contrast to what was observed in WT (Fig 3B2), sections of caudal epididymis confirmed the absence of spermatozoa and the presence of symblasts and round cells (Fig 3C2). Comparing PAS staining of *Spink2*$^{+/+}$ and *Spink2*$^{-/-}$ seminiferous tubules, we noticed that contrary to WT, *Spink2*$^{-/-}$ round spermatids did not contain an acrosomal vesicle, suggesting

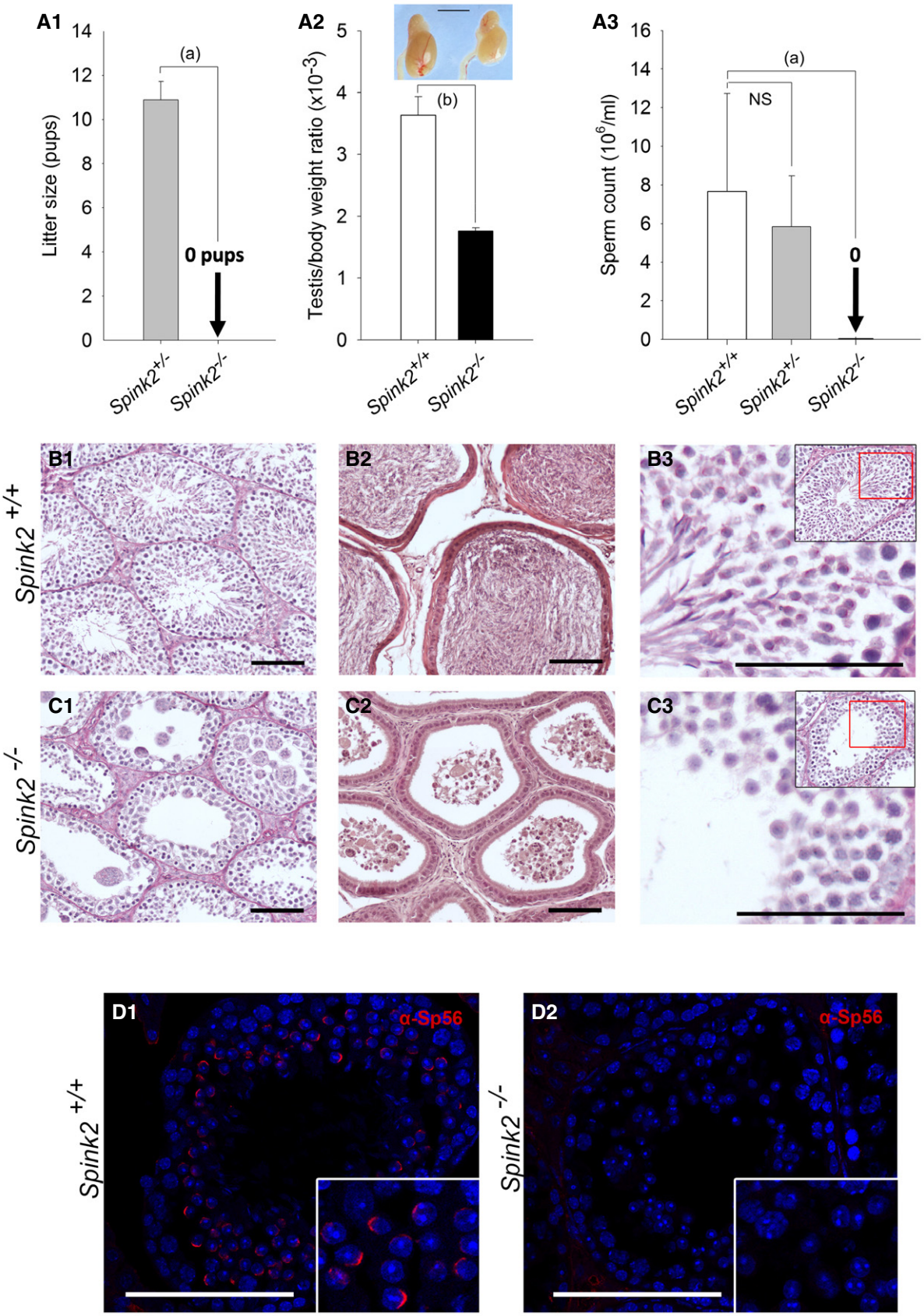

Figure 3.

Figure 3. *Spink2*$^{-/-}$ males are infertile and azoospermic, and spermatogenesis presents a post-meiotic blockade.

A1 Litter size of *Spink2*$^{-/-}$ *and Spink2*$^{+/-}$ males mated with wild-type females (n = 5).

A2 Testis/body weight ratio for WT and *Spink2*$^{-/-}$ mice (n = 6) and morphology and size of wild-type and *Spink2*$^{-/-}$ testes of male siblings. Scale bar, 5 mm.

A3 Sperm concentrations from the cauda epididymis of wild-type, *Spink2*$^{+/-}$, *and Spink2*$^{-/-}$ male testes (n = 10).

B, C Histological comparisons of testis and epididymis from WT and *Spink2*$^{-/-}$ mice. (B1, C1) Periodic acid–Schiff (PAS) staining of seminiferous tubule cross sections shows complete spermatogenesis in WT (B1) contrary to *Spink2*$^{-/-}$ mice (C1), where condensed, elongated spermatids and mature sperm are absent. (B2, C2) Sections of epididymis stained with eosin/hematoxylin. In the lumen of tubules from WT mice, mature sperm are present (B2), whereas only round cells and multinucleated symblasts occupy the lumen of tubules from *Spink2*$^{-/-}$ mice (C2). (B3, C3) Enlargement of seminiferous tubule sections stained with PAS evidences deep pink staining in round spermatids, which corresponds to the acrosome in WT mice (B3), whereas round spermatids from *Spink2*$^{-/-}$ mice present no deep pink staining, indicating that the acrosome is not formed (C3). Scale bars, 100 μm.

D1, D2 Immunofluorescence experiments using an anti-Sp56 antibody (red staining) confirm the presence of the acrosome in seminiferous tubule sections from WT contrary to those from *Spink2*$^{-/-}$ mice, where no staining is observed. Scale bars, 100 μm.

Data information: Data represent mean ± SEM. *P*-values are $P = 1 \times 10^{-5}$ (a) and $P = 1 \times 10^{-4}$ (b); statistical differences were assessed using *t*-test. NS, not statistically significant.

that the absence of Spink2 prevents acrosome biogenesis (Fig 3B3 and C3). This point was confirmed by immunofluorescent staining using the Sp56 antibody, a specific marker of the acrosome (Kim *et al*, 2001) (Fig 3D1 and D2). We then identified the spermatogonia using an anti-PLZF antibody (Zhang *et al*, 2014) (Fig EV3A and B) and observed no significant difference in the median number of spermatogonia per tubule (n = 30) between *Spink2*$^{+/+}$ and *Spink2*$^{-/-}$ mice (Fig EV3C). These results indicate that the absence of Spink2 does not impact spermatogonial survival but leads to an early arrest of round-spermatid differentiation. Overall, the *Spink2*$^{-/-}$ mouse phenotype perfectly mimics the human condition and confirms that SPINK2 deficiency is involved in human azoospermia.

SPINK2 is an acrosomal protein

In order to further investigate the molecular pathogeny of this SPINK2-dependent azoospermia, we determined the localization of SPINK2 in human and mouse testis. We first verified the specificity of a SPINK2 antibody through Western blot (WB) and immunofluorescence (IF) experiments on HEK293 cells overexpressing human SPINK2. In Western blots, the SPINK2 antibody recognized three bands of less than 17 kDa weight, likely corresponding to oligomeric complexes (Appendix Fig S4A). No bands appeared in non-transfected cells. Moreover, the overexpressed SPINK2 featured a DDK-tag which was recognized by an anti-DDK-tag antibody revealing three bands of identical molecular mass (Appendix Fig S4B). No bands were observed when the primary antibody was omitted. SPINK2 expression was also studied by IF and confocal microscopy. Transfected cells displayed a cytoplasmic staining, whereas no staining was observed in non-transfected cells (Appendix Fig S4C). Taken together, these results demonstrate the specificity of this antibody in WB and IF experiments. Next, the localization of SPINK2 was determined by IF in human and mouse seminiferous tubule cross sections and in mature sperm (Fig EV4). In mouse, SPINK2 was present in the acrosomal vesicle from the beginning of the acrosome's biogenesis at the round-spermatid stage as indicated by a colocalization with Sp56, a marker of the acrosome (Fig EV4A and B). In accordance with the results shown in Fig 3D2, no SPINK2 staining was observed in *Spink2*$^{-/-}$ testis cross sections (Fig EV4C). A similar localization was observed for SPINK2 in human seminiferous tubule sections (Fig EV4D). Finally, we observed that SPINK2 remains present in the acrosome of human and mouse mature spermatozoa (Fig EV4E and F).

Ultrastructure of *Spink2*$^{-/-}$ round spermatids shows that fusion of proacrosomal vesicles is hampered and that the Golgi apparatus is fragmented

We showed that SPINK2 is located in the acrosome and that its absence prevents acrosome biogenesis. To understand the reasons for the absence of acrosome biogenesis, we performed transmission electronic microscopy (EM) to study the ultrastructure of round spermatids from *Spink2*$^{-/-}$ males (Fig 4). In wild-type round spermatids, proacrosomal vesicles generated by the Golgi apparatus docked in a specialized area of the nuclear envelope (NE) and fused together to form a giant acrosomal vesicle (Fig 4A). Contrary to WT, in *Spink2*$^{-/-}$, the proacrosomal vesicles generated by the Golgi apparatus of round spermatids were mostly unable to fuse (Fig 4B2, white arrowheads), likely explaining the absence of acrosome biogenesis. Moreover, the Golgi apparatus from *Spink2*$^{-/-}$ animals produced abnormal proacrosomal vesicles of irregular sizes (Fig 4B2) and showed a considerable disorganization with a decreased proportion of flattened membrane stacks (Fig 4B2) displaying shorter lengths (Fig 4C). Acrosome biogenesis is dependent on the simultaneous synthesis of vesicles by the Golgi apparatus and the modification of the nuclear envelope (NE) facing the Golgi apparatus, with tight apposition of both nuclear membranes and aggregation of a nuclear dense lamina (NDL) on the nuclear side of the inner nuclear membrane (Kierszenbaum *et al*, 2003). In *Spink2*$^{-/-}$ round spermatids, the densification of the NE appears to occur normally and the NDL is clearly visible in EM (Fig 4B2). Using IF, the modification of the NE facing the Golgi apparatus was followed with an anti-Dpy19l2 antibody. We indeed had previously shown that Dpy19l2 participates in linking the acrosome to the nucleus and that it is located in the nuclear membrane facing the forming acrosome (Pierre *et al*, 2012) and is thus a component of this specialized area of the nuclear envelope. In costaining experiments using anti-Dpy19l2 and anti-GM130 antibodies to stain the nuclear envelope facing the acrosomal vesicle (evidenced by the NDL in EM) and the Golgi apparatus, respectively, we found that in WT round spermatids, the Golgi apparatus is either located immediately in front of the NDL in the early phase of acrosome biogenesis or, at a slightly later stage, lies adjacent to it (Fig 4D1 and D2). In contrast to WT, the Golgi apparatus of *Spink2*$^{-/-}$ round spermatids was positioned randomly around the nucleus, often found on the opposite side of the NDL (Fig 4D3–D6) indicative of a disruption of the polarity of the NDL and of the Golgi apparatus, which should both be located at the apical face of the round spermatid.

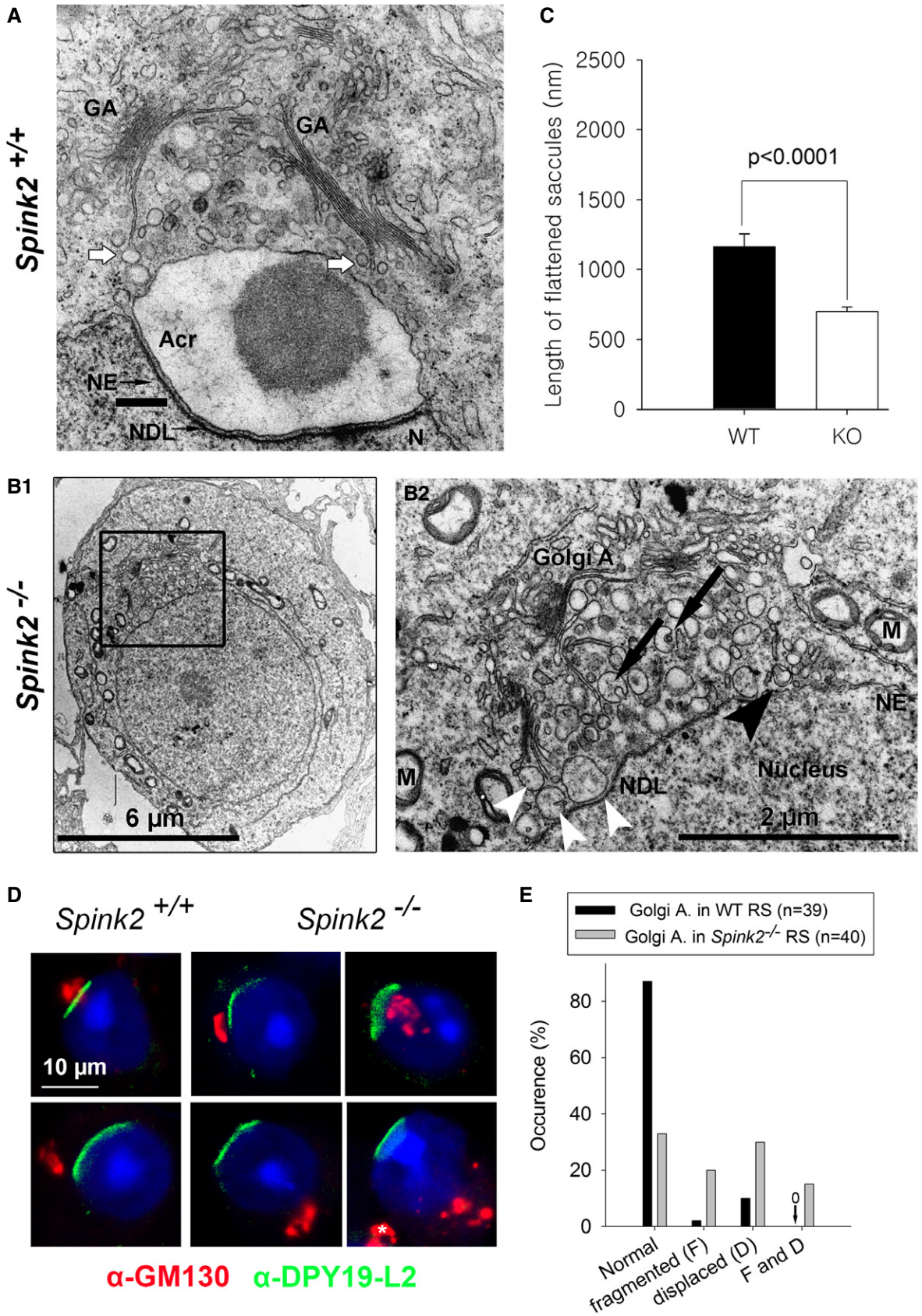

Figure 4.

Figure 4. Lack of Spink2 prevents the fusion of proacrosomal vesicles and induces a disorganization of the Golgi apparatus.

A Partial section of a WT round spermatid observed by EM showing the early biogenesis of the acrosome (Acr) due to the continuous formation and aggregation of small vesicles (white arrows) coming from the Golgi apparatus (GA). The nuclear envelope (NE) facing the acrosome has a specific organization and is associated with the nuclear dense lamina (NDL). N, nucleus. Scale bar, 400 nm.

B Ultrastructure of the Golgi apparatus in *Spink2*$^{-/-}$ round spermatid observed by EM. (B1) Ultrastructure of a *Spink2*$^{-/-}$ round spermatid observed at low magnification. The black box corresponds to the Golgi apparatus and is enlarged in (B2). (B2) In the absence of Spink2, vesicles do not aggregate at the nuclear envelope although modification of the NE and formation of the NDL occur. Unfused vesicles of different sizes accumulate in the cytoplasm with very few docking on the nuclear envelope (white arrowhead). Moreover, the GA shows disorganization with strong decrease or absence of stacks of flattened membranes. Finally, microautophagy-like structures and vesicles with a double membrane (black arrowhead) are observed around the GA (black arrows). M, mitochondria. Scale bars, 6 μm (B1) and 2 μm (B2).

C The length of flattened saccules is statistically reduced in *Spink2*$^{-/-}$ round spermatids (WT saccules, n = 74; and KO saccules, n = 136). Data represent mean ± SEM; the statistical difference was assessed with t-test, P-value as indicated.

D Absence of Spink2 induces Golgi apparatus fragmentation and mislocalization. (D1, D2) IF experiments using an anti-Dpy19l2 antibody marking the specific NE facing the NDL (green staining) and an anti-GM130 antibody marking the cis-Golgi (red staining) show that the Golgi apparatus (GA) is a compact structure and located either in front of the NDL or close to it in WT round spermatids (normal). (D3–D6) In contrast, similar double staining of round spermatids from *Spink2*$^{-/-}$ mice shows that only one-third of GA are compact and normally placed (D3) and the other GA are either displaced (D4), fragmented (D5), or both (D6). In panel (D6), white asterisk corresponds to a GA belonging to a different cell.

E Quantification of the morphology and the relative localization of the GA and Dpy19l2 staining in WT (n = 40) and *Spink2*$^{-/-}$ (n = 39) round spermatids.

Disjunction of the Golgi apparatus and of the NDL was also observed in EM (Fig EV5A). Moreover, anti-GM130 staining in *Spink2*$^{-/-}$ round spermatids appeared disseminated and punctuated, confirming the disorganization of the Golgi apparatus and indicating a fragmentation of the organelle (Fig 4D4–D6).

Interestingly, EM observations of *Spink2*$^{-/-}$ round spermatids showed the presence of multivesicular bodies, a known biomarker of microautophagy (Li *et al*, 2012) (Fig EV5B). These latter structures strongly suggest that the absence of Spink2 activates an uncharacterized self-degradation pathway. Visual signs of the initial events of microautophagy occurring at the Golgi apparatus level are the engulfment of vesicles (Fig 4B2, black arrows) and the presence of already engulfed vesicles (Fig 4B2, black arrowhead). We note that the thorough examination of round spermatids on EM images did not reveal any detectable signs of morphological hallmarks of apoptosis such as chromatin condensation, fragmentation of the plasma membrane, and the presence of apoptotic bodies. Moreover, no differences in DNA damage were observed between WT and *Spink2*$^{-/-}$ round spermatids when assessed by terminal deoxynucleotidyl transferase (TdT)-mediated deoxyuridine triphosphate (dUTP)-nick-end labeling (TUNEL) test (Appendix Fig S5). Altogether, these results suggest that the absence of Spink2 at the round-spermatid stage does not activate the apoptotic pathway.

Rescue of acrosin-induced cell proliferation defects by coexpression with SPINK2

During spermatid differentiation, several enzymes, involved in sperm penetration through the protective layers surrounding the oocytes, accumulate in the acrosomal vesicle. Among these different enzymes, several proteases have been described to play a key role, including acrosin, believed to be the main acrosomal protease (Liu & Baker, 1993). Acrosin, a trypsin-like protease, is synthesized in the reticulum as a zymogen (proacrosin), transits through the Golgi apparatus, and accumulates in the acrosomal vesicle. Autoactivation of acrosin is pH-dependent and occurs at a pH > 6 (Meizel & Deamer, 1978) leading to sequential N-ter and C-ter cleavages of the proacrosin (46 kDa), eventually giving active forms of acrosin with lower weights of 20–34 kDa (Baba *et al*, 1989; Zahn *et al*, 2002). Since the pH of both the endoplasmic reticulum and the Golgi apparatus is greater than 6 (Rivinoja *et al*, 2012), we postulated that Spink2, as a serine peptidase inhibitor, prevents acrosin autoactivation in these cellular compartments, thus preventing cellular stress induced by uncontrolled protease activation. Such stress would cause cellular defects including Golgi apparatus destabilization and defective acrosome biogenesis leading to spermatid differentiation arrest. To test this hypothesis, heterologous expressions of human C-terminus DDK-tagged proacrosin (ACR), SPINK2, or both were carried out in HEK293 cells and the kinetics of cell proliferation were followed using xCELLigence Real-Time Cell Analysis (RTCA) technology for the different conditions. It is worth noting that no members of the SPINK family are reported to be expressed in HEK293 cells. Analyses of kinetics showed that proacrosin expression quickly led to cell proliferation arrest and detachments in contrast to what was observed in the control condition (Fig 5A and B). Interestingly, cells showed a normal proliferation when SPINK2 was coexpressed with proacrosin (Fig 5A and B), therefore demonstrating that cell stress and damages induced by the proacrosin were prevented by SPINK2 coexpression. The presence of the different overexpressed proteins was verified in the different conditions by Western blotting using the SPINK2 antibody (Fig 5C), an anti-acrosin (Fig 5D), and the anti-DDK (Fig 5E) antibodies. In extracts of HEK293 cells transfected with proacrosin only and revealed with an anti-acrosin antibody (Fig 5D), two bands were present at around 46 and 34 kDa. The latter (red arrowhead) likely corresponds to the active form of acrosin resulting from the cleavage of proacrosin upon autoactivation. This band was not present when acrosin was coexpressed with SPINK2 or in non-transfected cells (control). Moreover, a closer inspection of the band around 46 kDa in the extracts of cells transfected with proacrosin only or proacrosin + SPINK2 shows that this band is of lower MW and was less intense in "acrosin" extract compared to "acrosin + SPINK2" cell extract, showing the process of successive cleavages occurring during proacrosin autoactivation (Zahn *et al*, 2002). Similar results were obtained with the anti-DDK antibody (Fig 5E). It is worth noting that anti-DDK antibody immunodecorates the zymogen form only and not the active form of acrosin because the C-terminus containing the DDK-tag is cleaved upon autoactivation. Western blot results thus demonstrate that coexpression of proacrosin with SPINK2 prevented its autoactivation. We can thus conclude that in the absence of a serine peptidase inhibitor, proacrosin can autoactivate and induces a cellular stress leading to

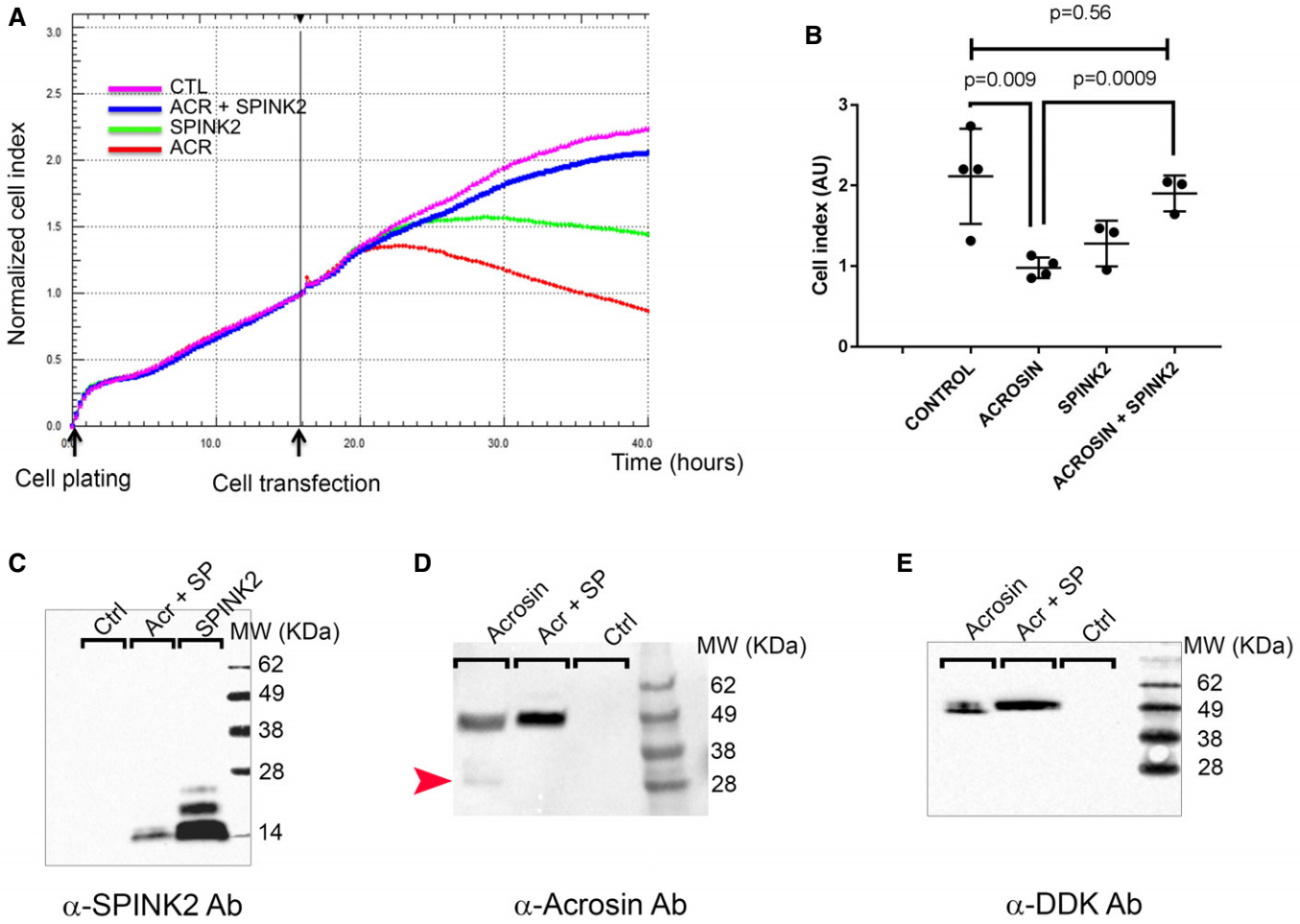

Figure 5. Heterologous expression of proacrosin in HEK293 cells induces acrosin activation and cell proliferation arrest, a phenotype rescued by SPINK2 coexpression.

A Representative kinetics of HEK293 cell proliferation measured with Real-Time Cell Analysis (RTCA) technology in different conditions as indicated. Each point corresponds to the mean of four technical replicates measured simultaneously. Black arrows indicate the time of cell plating (t = 0 h) and introduction of the different plasmids in the cell chambers (t = 16 h).

B Scatter plots showing the mean and SD of the cell index measured at 40 h after plating (corresponding to cell proliferation and detachment) in different transfection conditions and measured for three independent biological replicates. Statistical differences were assessed using t-test, P-values as indicated.

C Western blot using an anti-SPINK2 antibody showing the expression of SPINK2 in cell extracts of HEK293 cells transfected with different plasmids containing SPINK2 (SP) or acrosin and SPINK2.

D Representative Western blot using an anti-acrosin antibody. In extracts of HEK293 cells transfected with proacrosin only (lane "acrosin"), two bands were observed, one at around 34 kDa and corresponding to the active form of acrosin (red arrowhead) and one at 46 kDa and corresponding to the zymogen form, whereas in extracts of HEK293 cells transfected with proacrosin and SPINK2 (lane "Acr + SP"), only the zymogen form was observed. Equal protein loading was verified by stain-free gel technology (Taylor & Posch, 2014) and Western blots against tubulin (Appendix Fig S6). Note that the zymogen form in lane "acrosin" has a slightly lower mass and that the band is less intense than that in lane "Acr + SP".

E Representative Western blot using an anti-DDK antibody showing the expression of the proacrosin zymogen form in HEK293 cells transfected with different plasmids as indicated. Note that once more, the zymogen form in the lane "acrosin" has a slightly lower mass and that the band is less intense than that in lane "Acr + SP". Similarly, equal protein loading was verified by stain-free gel technology (Appendix Fig S6).

cell proliferation arrest and cell detachment, a phenotype similar to that observed in round spermatids from *Spink2*$^{-/-}$ males.

SPINK2 haploinsufficiency induces sperm defects with incomplete penetrance in man

Only one additional subject, P105, was identified with a *SPINK2* heterozygous deleterious variant, and we cannot be sure that this variant is the cause of the patient's oligozoospermia. Two arguments could in fact suggest that *SPINK2* haploinsufficiency is not deleterious: (i) Br1 and Br2's father is SPINK2 heterozygous and has conceived six children spontaneously, and unfortunately, we could not obtain sperm samples to characterize this man's sperm parameters; and (ii) because heterozygous *Spink2*$^{+/-}$ male mice are fertile, they did not produce litters of reduced size (Fig 3A). We however carried out a detailed characterization of *Spink2*$^{+/-}$ and *Spink2*$^{+/+}$

sperm parameters to address the question of the impact of SPINK2 haploinsufficiency on mouse spermatogenesis. Heterozygous males displayed a significant increase in teratozoospermia (Fig 6A). Abnormal spermatozoa showed non-hooked heads, isolated heads, or a malformed base of the head (Fig 6B). Moreover, sperm motility of heterozygous males was impaired with lower total and progressive motility (Fig 6C). We note that the observed defects are very similar to those observed in the heterozygous patient P105 (Table EV1). We can therefore conclude that in mice, *SPINK2* haploinsufficiency induces asthenoteratospermia with no alteration of reproductive fitness, whereas in man it leads to oligoteratozoospermia with variable expressivity and infertility with an incomplete penetrance.

Discussion

SPINK family emerges as an important family for human genetic diseases

SPINK proteins are serine protease inhibitors containing one or several Kazal domains which interact directly with the catalytic domains of proteases blocking their enzymatic activity (Rawlings *et al*, 2004). The Kazal domain structure contains three disulfide bonds which are highly conserved. Different SPINK proteins are specifically expressed in different tissues and inhibit a number of serine proteases, such as secreted trypsin in the pancreas, acrosin in sperm, or kallikrein in the skin. Downregulation of the activity of different SPINK proteins leads to severe pathologies such as chronic pancreatitis and Netherton syndrome. In the pancreas, trypsin is produced as an inactive zymogen to prevent cell damage, yet the trypsinogen is occasionally able to autoactivate. This protease activity is then blocked by SPINK1. Chronic pancreatitis can be triggered by mutations of *SPINK1* that decrease or suppress its trypsin inhibitor function, leading to cell distress (Chen *et al*, 2000; Witt *et al*, 2000). In the skin, kallikrein-related peptidases are controlled by SPINK5 and unopposed kallikrein-peptidase activity due to *SPINK5* deficiency leads to Netherton syndrome, a severe skin disease (Furio & Hovnanian, 2014). SPINK6 and SPINK9 are also expressed in the skin, and altered expression levels are associated with atopic dermatitis or psoriasis (Redelfs *et al*, 2016). The other members of the SPINK family, including SPINK2, have not yet been associated with a human pathology. Here, we have clearly demonstrated that the absence of SPINK2 induces azoospermia, a severe infertility phenotype, emphasizing the importance of this family in human pathologies.

Role of SPINK2 during spermiogenesis

We have shown that SPINK2 is located in the acrosomal vesicle in round spermatids and remains present in mature spermatozoa, suggesting that this protein is necessary for spermiogenesis and sperm survival. SPINK proteins are known to control protease activities in different tissues (Witt *et al*, 2000; Rawlings *et al*, 2004; Ohmuraya *et al*, 2012; Furio & Hovnanian, 2014) and since SPINK2 is located in the acrosome, it very likely neutralize acrosomal proteases before their release prior fertilization. Several proteases have been described to be present in the acrosome (Arboleda & Gerton, 1987; Kohno *et al*, 1998; Cesari *et al*, 2004). Among these, acrosin (Acr) was the first to be described and is the acrosomal protein which has been the most studied. Acrosin is present in the acrosome as a zymogen called proacrosin (Huang-Yang & Meizel, 1975) which is predicted to be activated during the acrosome reaction (Brown & Harrison, 1978) upon a rise in acrosomal pH to 7 which induces pH-dependent proacrosin autoactivation (Baba *et al*, 1989). Before the acrosome reaction, at least two mechanisms prevent autoactivation: The first is the acrosomal acidic pH which is below 5, which blocks autoactivation of proacrosin (Meizel & Deamer, 1978); and the second is the presence in the sperm of a non-fully characterized proacrosin conversion inhibitor of 12 kDa which has been purified from boar acrosome (Kennedy *et al*, 1982). The presented results strongly suggest that this protein is in fact SPINK2. Proacrosin is however produced in the endoplasmic reticulum and transits through the Golgi apparatus, two cellular compartments with a pH of approximately 7 and 6.5, respectively. In these compartments, autoactivation of proacrosin is thus possible and would result in the release of active acrosin within these apparatuses. We therefore believe that SPINK2, which transits through the same cellular compartments, quenches this premature protease activity and prevents the described cascade of events leading to azoospermia. This hypothesis is supported by heterologous expression experiments: We have indeed demonstrated that proacrosin expression in HEK293 cells induces (i) autoactivation of proacrosin and (ii) cellular proliferation arrest and cell detachment. Moreover, cellular toxicity of proacrosin expression is prevented by SPINK2 coexpression, showing the ability of SPINK2 to inhibit acrosin activity.

One of the most striking effects of SPINK2 deficiency is the fragmentation of the Golgi apparatus, a key organelle for protein processing and translocation, in particular for membrane proteins. The notable strong desquamation of the germinal epithelium may be due to severe changes in membrane protein composition resulting from a defective Golgi apparatus function.

Impact of SPINK2 deficiency

We have shown that the absence of SPINK2 in round spermatids leads to several subcellular defects targeting the process of proacrosomal vesicle formation by the Golgi apparatus. The observed abnormalities include the disorganization and delocalization of the Golgi apparatus, the presence of vesicles of various sizes, and the absence of proacrosomal vesicle fusion. The absence of SPINK2 likely allows proacrosin autoactivation within the reticulum and the Golgi apparatus compartments, leading to the above-described subcellular defects. It was previously shown that transgenic expression of porcine proacrosin in mice led to post-meiotic cell death and oligozoospermia, supporting the hypothesis that unbalanced expression of acrosin/Spink2 is deleterious (O'Brien *et al*, 1996). Interestingly, we have demonstrated that the cell responds to this stress by activating a microautophagy-like pathway: First, we showed that larger vacuoles engulfed small vacuoles, likely leading to the observed heterogeneity in vacuole size in the vicinity of the Golgi apparatus; and secondly, multivesicular bodies, a hallmark of microautophagy (Li *et al*, 2012), were clearly observed within Spink2$^{-/-}$ round spermatids, whereas they were never observed in WT. Furthermore, the lack of various SPINK proteins induces autophagy-induced cell death in regenerating Hydra (Chera *et al*, 2009)

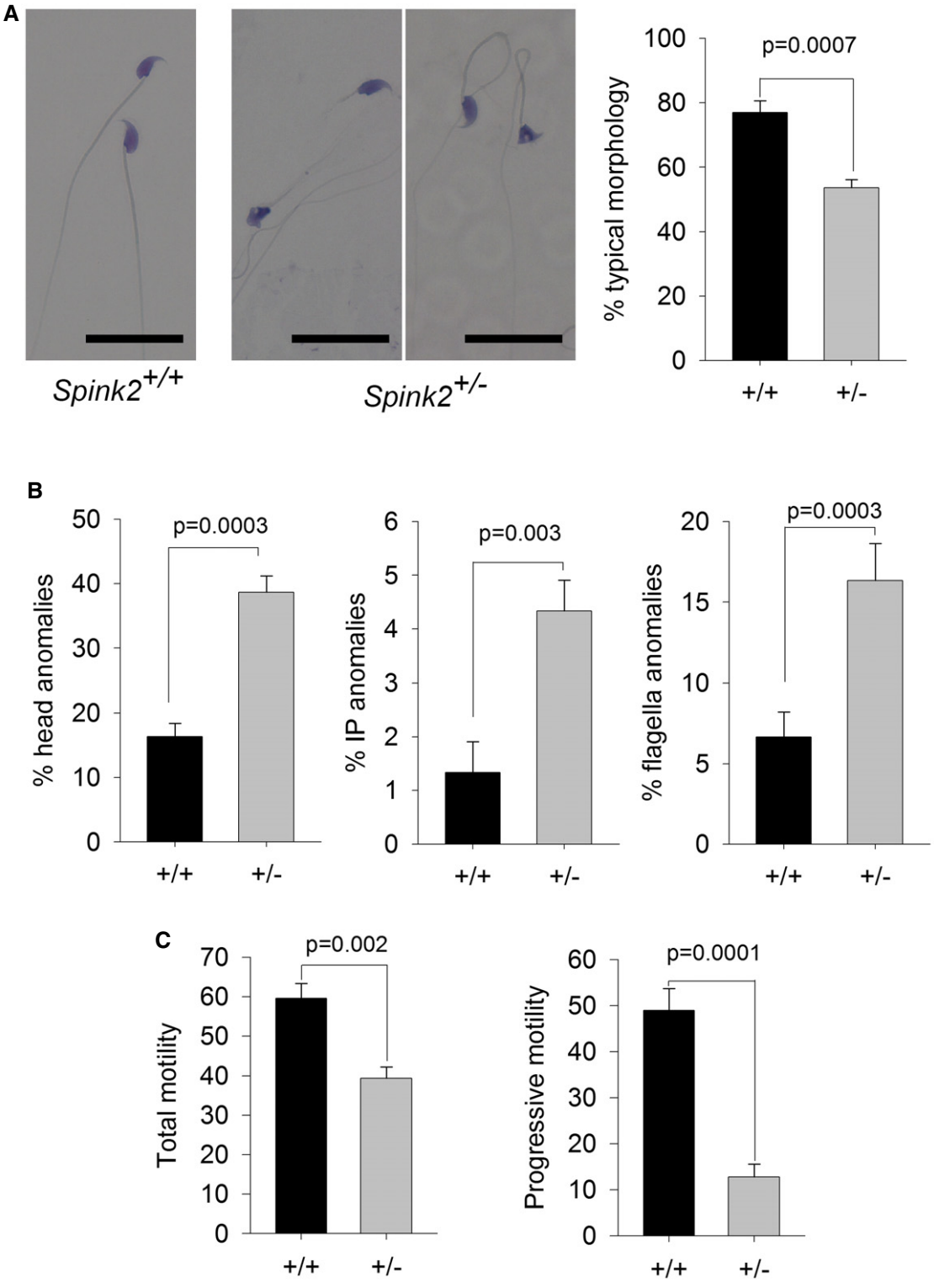

Figure 6. Sperm from *Spink2*$^{+/-}$ heterozygous mice exhibit morphological defects and low motility.

A Light microscopy analysis of sperm from *Spink2*$^{+/-}$ heterozygous mice reveals the presence of numerous non-typical forms of sperm. Scale bars, 25 μm. Graph on the right shows the mean ± SD percentage of defective sperm in WT (n = 3) and *Spink2*$^{+/-}$ mice (n = 3).

B Anomalies were observed in the head and the mid- and principle pieces in WT and *Spink2*$^{+/-}$ mice (n = 3).

C Total and progressive sperm motility were strongly decreased in *Spink2*$^{+/-}$ heterozygous mice (n = 5) in comparison with WT sperm (n = 5).

Data information: n represents the number of biological replicates, and for each replicate, more than 100 sperm were assessed per condition. Data are presented as mean ± SD. Statistical differences were assessed using t-test, P-values as indicated.

and was also described in newborn mice when *Spink3* (orthologue of *Spink1*) is mutated (Ohmuraya *et al*, 2005). Based on these results, it has been postulated that SPINK1/Spink3 could have the dual function of protease inhibitor and negative regulator of autophagy (Ohmuraya *et al*, 2012). Our results show that the absence of SPINK2 induces a microautophagy-like pathway in germ cells thereby further supporting this hypothesis.

Oligozoospermia and azoospermia is a continuum correlated with *SPINK2* haploinsufficiency

We observed that in man, the presence of a homozygous *SPINK2* mutation leads to azoospermia while a heterozygous mutation can induce oligozoospermia suggesting that *SPINK2* haploinsufficiency can result in oligozoospermia. In mice, we showed that the complete absence of the protein leads to azoospermia. We also showed that heterozygous animals have terato-astheno-zoospermia but with no obvious decrease in sperm number and no impact on fertility. A previous study carried out in a different mouse hypomorphic mutant line showed that a significant inactivation of *Spink2* (likely in excess of 90%) led to a reduction by half of sperm number within the epididymis and a five-fold increase in morphologically abnormal spermatozoa. Male mice also exhibited a reduced fertility and produced litters of reduced size with an average of 5.19 pups by litter compared to 8.56 in controls (Lee *et al*, 2011). These results and the results presented therein thus confirm that in mice, the severity of the phenotype is dependent on *Spink2* expression levels and that there is a phenotypic continuum ranging from (i) azoospermia in the complete absence of the protein (ii) to teratozoospermia and oligozoospermia associated with subfertility when only a fraction of the protein is present and finally (iii) to astheno-teratozoospermia with no impact on fertility when half of the protein is present. These observations in mice strongly support the notion that SPINK2 heterozygous mutations in man will impact spermatogenesis with a variable effect on fertility. We identified only one heterozygous mutation out of 611 analyzed patients indicating that *SPINK2* variants are very rare, likely because heterozygous variants underwent a strong negative selection during evolution. This hypothesis is supported by data from the ExAC database which indicate that the *SPINK2* gene has a high probability of loss of function intolerance (pLI = 0.72).

The testis is the organ which expresses the highest number of tissue-specific transcripts ($n > 500$) (Feig *et al*, 2007; Dezso *et al*, 2008) and altered spermatogenesis has been observed in knockout mouse models for more than 388 genes (Massart *et al*, 2012). It is therefore expected that NOA is genetically highly heterogeneous and that few patients carry causal defects on the same gene. Due to the involvement of the corresponding proteins in multiple phases of spermatogenesis, the causes of azoospermia are numerous and involve genes controlling spermatogonial self-renewal, meiosis, and spermiogenesis. Here, we have confirmed that alterations of spermiogenesis do not only lead to teratozoospermia as described several times previously (Dieterich *et al*, 2007; Harbuz *et al*, 2011; Ben Khelifa *et al*, 2014) but also to azoospermia. The vast majority of patients with an altered spermatogenesis can be treated with IVF or by the direct injection of a sperm into the oocyte (ICSI). Most patients with NOA however cannot benefit from ICSI-IVF treatments. Identifying the genetic defects responsible for NOA and characterizing their molecular pathogeny will provide a basis for the development of therapeutic solutions tailored to the patient. In this particular case, we have shown that SPINK2 deficiency can induce azoospermia and demonstrated that unrestricted acrosomal protease activity induces the arrest of spermiogenesis. Moreover, we provided evidence that this process activates a microautophagy-like pathway. As we have shown that the pool of undifferentiated spermatogonia is not affected, we can envisage a method of treatment targeting protease activity using a protease inhibitor, as is done for chronic pancreatitis caused by SPINK1 deficiency (Kambhampati *et al*, 2014).

Materials and Methods

Patients and biological samples

Human sperm were obtained from patients consulting for diagnosis or assisted reproductive techniques at the fertility center of the Grenoble University Hospital. All patients signed an informed consent for use of part of their samples in research programs respecting the WMA declaration of Helsinki. The samples were then stored in the CRB Germetheque (certification under ISO-9001 and NF-S 96-900) following a standardized procedure. Consent for CRB storage was approved by the CPP Sud-Ouest of Toulouse (coordination of the multisite CRB Germetheque). The storage and transfer authorization number for the CRB Germetheque is AC2009-886. The scientific and ethical board of the CRB Germetheque approved the transfer of the semen samples for this study. Additional DNA samples from patients with azoospermia and oligozoospermia were obtained from the CHU of Grenoble, Saint Etienne, and Marseille. All patients gave their informed consent for the anonymous use of their leftover samples. Brothers Br1 and Br2 are French citizens from a traveling group originating from Romania but whose recent ancestors lived in Spain and the south of France. Subject P105 is also a French citizen with eastern ascendants (from Russia).

Exome sequencing and bioinformatic analysis

Genomic DNA was isolated from saliva using Oragene saliva DNA collection kit (DNA Genotek Inc., Ottawa, Canada). Exome capture was performed using NimbleGen SeqCap EZ Kit version 2 (Roche). Sequencing was conducted on an Illumina HiSeq 2000 instrument with paired-end 76-nt reads. Sequence reads were aligned to the reference genome (hg19) using MAGIC (SEQC/MAQC-III Consortium, 2014). Duplicate reads and reads that mapped to multiple locations in the exome were excluded from further analysis. Positions with sequence coverage below 10 on either the forward or reverse strand were excluded. Single nucleotide variations (SNV) and small insertions/deletions (indels) were identified and quality-filtered using in-house scripts. The most promising candidate variants were identified using an in-house bioinformatics pipeline. Variants with a minor allele frequency > 5% in the NHLBI ESP6500 or in 1000 Genomes Project phase 1 datasets, or > 1% in ExAC, were discarded. We also compared these variants to an in-house database of 56 control exomes. All variants present in a homozygous state in this database were excluded. We used Variant Effect Predictor (VEP) to predict the impact of the selected variants. We only retained variants impacting splice donor/acceptor sites or

causing frameshift, in-frame insertions/deletions, stop gain, stop loss, or missense variants except those scored as "tolerated" by SIFT (sift.jcvi.org) and as "benign" by PolyPhen-2 (genetics.bwh.harvard.edu/pph2). All steps from sequence mapping to variant selection were performed using the ExSQLibur pipeline (https://github.com/tkaraouzene/ExSQLibur). Our datasets were obtained from subjects who have consented to the use of their individual genetic data for biomedical research, but not for unlimited public data release. Therefore, we submitted it to the European Genome-phenome Archive, through which researchers can apply for access of the raw data under the accession number EGAD00001003326.

Sanger sequencing

Sanger sequencing of the four *SPINK2* exons and intron borders was carried out using the primers described in Appendix Table S3. Thirty-five cycles of PCR amplification were carried out with a hybridization temperature of 60°C. Sequencing reactions were performed using BigDye Terminator v3.1 (Applied Biosystems). Sequence analyses were carried out on ABI 3130XL (Applied Biosystems). Sequences were analyzed using seqscape software (Applied Biosystems).

RT–PCR and quantitative real-time PCR

Total RNA from various tissues including testes from three WT and homozygous KO mice was extracted using the mirVana™ PARIS™ Kit (Life Technologies®) according to the manufacturer's protocol. Human cDNAs were obtained from Life Technologies® mRNA.

Reverse transcription was carried out with 5 µl of extracted RNA (~500 ng). Hybridization of the oligo dT was performed by incubating for 5 min at 65°C and quenching on ice with the following mix: 5 µl RNA, 3 µl of poly-T-oligo primers (dT) 12–18 (10 mM; Pharmacia), 3 µl of the four dNTPs (0.5 mM, Roche Diagnostics) and 2.2 µl of H_2O. Reverse transcription then was carried out for 30 min at 55°C after the addition of 4 µl of 5× buffer, 0.5 µl RNase inhibitor, and 0.5 µl Transcriptor reverse transcriptase (Roche Diagnostics). One microliter of the obtained cDNA mix was used for the subsequent PCR. Primers are described in Appendix Table S4.

A specific region of the transcript was amplified using a StepOnePlus™ Real-Time PCR System (Life Technologies®) with Power SYBR® Green PCR Master Mix (Life Technologies®) according to the manufacturer's protocol. PCR without template was used as a negative control to verify experimental results. The sequence for oligonucleotide primers used and their product sizes are summarized in Appendix Table S5.

After amplification, the specificity of the PCR was determined by both melt-curve analysis and gel electrophoresis to verify that only a single product of the correct size was present. Quantification of the fold change in gene expression was determined by the relative quantification method ($2^{-\Delta\Delta C_T}$) using the beta-actin gene as a reference. Data are shown as the average fold increase ± standard error of the mean.

Primary antibodies

SPINK2 rabbit polyclonal antibody was from Sigma-Aldrich (HPA026813) and used at 1/1,000 for Western blot analysis. Sperm protein Sp56 and Golgi matrix protein GM130 (610822) mouse monoclonal antibodies were from QED Bioscience Inc. (used at 1/800 and 1/200, respectively). Promyelocytic leukemia zinc finger protein PLZF rabbit polyclonal antibody (Sc-22839) was from Santa Cruz Biotechnology. Dpy19l2 antibodies were produced in rabbit as polyclonal antibodies raised against RSKLREGSSDRPQSSC and CTGQARRRWSAATMEP peptides corresponding to amino acids 6–21 and 21–36 of the N-terminus of mouse Dpy19l2 (Pierre *et al*, 2012). DDK antibody was from OriGene (TA50011) or Sigma-Aldrich (FLAG® M2F1804) and used at 1/10,000 for Western blot analysis. Acrosin antibody was previously described (Gallo *et al*, 1991) and is a gift from Denise Escalier.

Western blot analysis

HEK293 cells were lysed in 25 mM Tris pH 7.4, 5 mM EDTA, 1% Triton X-100, and complete protease inhibitor cocktail (Roche) and were then centrifuged. After centrifugation at 20,000 *g* for 15 min at 4°C, the soluble supernatant was conserved and subjected to SDS–PAGE. The protein concentration from supernatants was quantified by the bicinchoninic acid assay (BCA assay) using bovine serum albumin as a standard. Sample concentrations were adjusted and mixed with 1× high-SDS sample buffer (4% SDS, 62 mM Tris–HCl pH 6.8, 0.1% bromophenol blue, 15% glycerol, 5% ß-mercaptoethanol) and separated using 4–20% SDS mini-PROTEAN® TGX Stain-Free™ Precast Gels (Bio-Rad) or 10 and 20% polyacrylamide–SDS gels and transferred into PVDF membranes (Millipore, 0.2 µm) using Trans-Blot® Turbo™ Blotting System and Midi Transfer Packs (Bio-Rad). The membranes were blocked in 5% non-fat dry milk in PBS/0.1% Tween and incubated for 1 h at room temperature with the primary antibody, followed by 45-min incubation with a species-matched horseradish peroxidase-labeled secondary antibody (1/10,000) (Jackson ImmunoResearch). Immunoreactivity was detected using chemiluminescence detection kit reagents (Luminata; Millipore) and a ChemiDoc Station (Bio-Rad).

Real-time cell analysis

The growth, proliferation, and adhesion kinetics of HEK293 cells were determined using RTCA technology (ACEA Biosciences, San Diego, CA, USA). Fifty microliters of DMEM supplemented with 10% HI-FBS and 50 µg/ml gentamicin (cell culture medium) was loaded in each well of the E-plate 96 (gold-microelectrode array integrated E-plate; ACEA Biosciences). E-plate 96 was then connected to the system to obtain background impedance readings. Around 1.5×10^4 cells in 50 µl were added to the wells containing 50 µl of culture medium. The E-plates were placed on the RTCA SP Station located in a 37°C, 5% CO_2 tissue culture incubator for continuous impedance recording. The cell index values measured by continuous impedance recordings every 5 min are proportional to the number of adherent cells. After 16–17 h, cells were transfected as described below, and for each of the conditions, four replicates were done. The assay was conducted for 40 h.

Mice

All animal procedures were run according to the French guidelines on the use of animals in scientific investigations with the approval of

the local ethical committee (Grenoble-Institut des Neurosciences—ethical committee, study agreement number 004). Mice were euthanized by cervical dislocation.

The Spink2tm1.1 (KOMP)Vlcg mouse strain used for this research project was created from ES cell clone Spink2_AG5_M7, generated by Regeneron Pharmaceuticals, Inc. and made into live mice by the KOMP Repository (www.komp.org) and the Mouse Biology Program (www.mousebiology.org) at the University of California Davis. The methods used to create the VelociGene targeted alleles have been published (Valenzuela *et al*, 2003). They were then reared by the Mouse Clinical Institute—MCI—located in Strasbourg as part of the "knockout mouse project". The colony used in this study was initiated from two couples consisting of heterozygous females and males. Mice were housed with unlimited access to food and water and were sacrificed after 8 weeks of age (the age of sexual maturity).

Genotyping

DNA for genotyping was isolated from tail biopsies. Tail biopsies (2 mm in length) were digested in 200 μl of DirectPCR Lysis Reagent (Tail) (Viagen Biotech Inc, CA, USA) and 0.2 mg of proteinase K for 12–15 h at 55°C followed by 1 h at 85°C for proteinase K inactivation. The DNA was directly used for PCRs. Multiplex PCR was done for 35 cycles, with an annealing temperature of 58°C, and an elongation time of 60 s at 72°C. PCR products were separated by 2% agarose gel electrophoresis. Genotypes were determined according to the migration pattern. Primers are described in Appendix Table S6.

Phenotypic analysis of mutant mice

To test fertility, pubescent *Spink2*$^{-/-}$ males (8-week-old) were mated with WT females.

To determine sperm concentration, sperm samples were collected from the cauda epididymis and vas deferens of 8-week-old males, and sperm number was determined using a hemocytometer under a light microscope.

Sperm motility analysis

Experiments were performed on a CASA CEROS v.12 (Hamilton Thorne Biosciences, Beverly, MA, USA) using Leja double-chamber slides (Leja Products B.V., the Netherlands) for standard count with 100 μm depth. After epididymal extraction, sperm cells were allowed to swim for 10 min at 37°C and then were immediately analyzed. At least 150 cells were analyzed per sample with the following parameters: acquisition rate: 60 Hz; number of frames: 45; minimum contrast: 50; minimum cell size: 5; low static-size gate: 0.3; high static-size gate: 1.95; low static-intensity gate: 0.5; high static-intensity gate: 1.3; minimum elongation gate: 0; maximum elongation gate: 87; and magnification factor: 0.7. The motility parameters measured were curvilinear velocity (VCL), straight-line velocity (VSL), average path velocity (VAP), and amplitude of lateral head displacement (ALH). Motile sperm were defined by VAP > 1 and progressive sperm were defined by VAP > 30 and VSL/VAP > 0.7.

Histological analysis

To analyze testicular integrity, testes from adult *Spink2*$^{+/+}$ and *Spink2*$^{-/-}$ mice were fixed by immersion in 4% paraformaldehyde (PFA) for 14 h, embedded in paraffin, and sectioned (4 μm). For histological analysis, after being deparaffinized slides were stained with hematoxylin and eosin or by the PAS technique. The colored sections were digitized at ×40 magnification through an Axioscope microscope (Zeiss, Germany) equipped with a motorized X–Y-sensitive stage. For sperm morphology analysis, sperm were washed twice in PBS and then displayed over slides, dried at room temperature, and then fixed in 75% ethanol for Harris–Shorr staining. At least 100 sperm cells were analyzed per sample.

Testicular germ cell dissociation

C57BL/6 male or *Spink2* KO mice (8-week-old) were euthanized by cervical dislocation. The testes were surgically removed and placed in PBS (at room temperature). The tunica albuginea was removed from the testes with sterile forceps and discarded. Then, the testes were incubated in 1 mg/ml of collagenase solution in EKRB cell buffer containing (in mM) 2 $CaCl_2$, 12.1 glucose, 10 HEPES, 5 KCl, 1 $MgCl_2$, 6 Na-lactate, 150 NaCl, 1 NaH_2PO_4, and 12 $NaHCO_3$ pH 7, and agitated horizontally at a maximum of 120 rpm for 30 min at 25°C. The dispersed seminiferous tubules were then washed with PBS and cut thinly. Cells were dissociated by gentle pipetting filtered through a 100-μm filter and then pelleted by centrifugation at 500 *g* for 7 min. Cells were resuspended in 1 ml PBS, fixed with 4% PFA solution, washed with PBS, and finally layered onto polylysine-coated slides.

Immunohistochemistry

Mice were anesthetized by intraperitoneal injection of a ketamine/xylazine cocktail (87.5 mg/kg ketamine and 12.5 mg/kg xylazine) and sacrificed through intracardiac perfusion of PFA (4%). The testes and epididymides were removed and fixed for a further 8 h before paraffin embedding and sectioning. Mature sperm cells were obtained for analysis through mechanical dilaceration of the epididymis. Sperm cells were fixed in 4% PFA for 1 min and washed in PBS before being spotted onto poly-L-lysine-pre-coated slides. Spermatogenic cells of the round-spermatid stage were purified by unit gravity sedimentation from a spermatogenic cell suspension obtained from sexually mature males as described in Yassine *et al* (2015).

For immunofluorescence experiments, heat-induced antigen retrieval was performed by boiling slides immersed in either 0.01 M sodium citrate buffer–0.05% Tween-20, pH 6.0, or 10 mM Tris base–1 mM EDTA solution–0.05% Tween-20, pH 9.0, for 15–25 min. Sections were blocked in 2% goat serum–0.1% Triton X-100 for 1 h at RT and incubated with primary antibodies overnight at 4°C. The slides were then washed and incubated with secondary antibody (DyLight 549-conjugated goat anti-mouse IgG or DyLight 488-conjugated goat anti-rabbit IgG, Jackson ImmunoResearch) and Hoechst 33342 for 2 h at RT, rinsed, and mounted with Dako mounting medium (Life Technology). Images were taken by confocal microscopy (Zeiss LSM 710) and processed using Zen 2009 software.

Electron microscopy (EM)

Adult male mice were anesthetized and fixed by intracardiac injection with 2% glutaraldehyde and 2.5% PFA in 0.1 M cacodylate, pH 7.2. For morphological analysis, samples were fixed with 2.5% glutaraldehyde in 0.1 M cacodylate buffer pH 7.4 over 24 h at room temperature. Samples were then washed with buffer and post-fixed with 1% osmium tetroxide and 0.1 M cacodylate pH 7.2 for 1 h at 4°C. After extensive washing with water, cells were further stained with 1% uranyl acetate pH 4 in water for 1 h at 4°C before being dehydrated through graded alcohol (30%–60%–90%–100%–100%–100%) and infiltrate with a mix of 1/1 epon/alcohol 100% for 1 h and several baths of fresh epon (Flukka) during 3 h. Finally, samples were embedded in a capsule full of resin that was left to polymerize over 72 h at 60°C. Ultrathin sections of the samples were cut with an ultramicrotome (Leica), and the sections were post-stained with 5% uranyl acetate and 0.4% lead citrate before being observed with an electron microscope at 80 kV (JEOL 1200EX). Images were acquired with a digital camera (Veleta; SIS, Olympus), and morphometric analysis was performed with iTEM software (Olympus).

Cell culture and transfection

Mycoplasma-free HEK293 cells were a gift from A. Andrieux from Grenoble Neuroscience Institute and grown in Dulbecco's modified Eagle's medium supplemented with 10% FBS (Invitrogen, France) and 50 μg/ml gentamicin (Sigma) in a 37°C, 5% CO_2 cell culture incubator and transiently transfected with Cter-DDK-tagged human acrosin (RC214256; OriGene, Rockville, MD, USA) and/or human *SPINK2* (RC205388; OriGene) and/or human c.1A>T mutated *SPINK2*-containing pCMV6 plasmids, using JetPRIME Transfection Reagent (Polyplus, France) according to the manufacturer's instructions. For immunochemistry experiments, transfected cells were fixed with 4% PFA 2 days after transfection.

DNA strand breaks

Sections were permeabilized using a 0.1% (v/v) Triton X-100 and 0.1% (w/v) sodium citrate in 1× PBS for 2 min and labeled by terminal deoxynucleotidyl transferase-mediated deoxy-UTP nick-end labeling (TUNEL) according to the Roche protocol of the *In Situ* Cell Detection Kit (Roche Diagnostics, Mannheim, Germany). Nuclei were counterstained in a 0.5 μg/ml Hoechst solution for 3 min, washed in PBS for 3 min, and mounted with DAKO mounting medium.

Statistical analyses

n represents the number of biological replicates. For sperm analyses, for each replicate, more than 100 sperm were assessed per condition. Statistical analyses were performed with SigmaPlot 10 and GraphPad Prism 7. *t*-Tests were used to compare WT and KO samples. Data represent mean ± SEM or SD, as indicated. Statistical tests with a two-tailed *P*-value ≤ 0.05 were considered significant.

Expanded View for this article is available online.

The paper explained

Problem
Infertility concerns one in seven couples and is usually addressed by performing *in vitro* fertilization (IVF) often by injecting spermatozoa directly into the oocytes by intracytoplasmic sperm injection (ICSI). Some men have a non-obstructive azoospermia (NOA), caused by a deficient spermatogenesis, and have no spermatozoa in the ejaculate. In some cases, a testicular biopsy can be performed in hope of finding some mature spermatozoa that will be used for ICSI, but most men with NOA will not be able to have biological children. It is believed that most cases of NOA are caused by a genetic factor, but a diagnosis is obtained for only approximately 20% of patients.

Results
We performed exome sequencing on two brothers with NOA and identified a homozygous mutation in the *SPINK2* gene coding for a serine protease inhibitor believed to target the acrosin, the main protease of the acrosome, a large vesicle located to the anterior part of the spermatozoa and containing an enzyme mix necessary to perforate the zona pellucida of the oocyte to achieve fertilization. Mouse study allowed to observe that homozygous KO male also had NOA, confirming the human diagnostic. Germ cells could go through meiosis but were blocked at the round-spermatid stage. We further observed that in the round spermatids, in the absence of SPINK2, the acrosin could autoactivate during its transit through the endoplasmic reticulum and the Golgi apparatus leading to a disorganization of the Golgi and its inability to form the acrosome and a block at the round-spermatid stage. We further demonstrate that the presence of a heterozygous SPINK2 mutation was also deleterious leading to the production of sperm with variable levels of anomalies.

Impact
We identified a new gene leading to male infertility permitting to improve the diagnostic efficiency for NOA patients. We demonstrate that whole-exome sequencing is an efficient technique to identify new infertility genes and to realize a diagnostic for affected men. We showed that the control of proteases by antiproteases, and in particular by SPINK2, is critical during spermiogenesis and demonstrate that the SPINK gene family is involved not only in pancreatitis or skin disease but also in male infertility.

Acknowledgements
We thank the GIN electron microscopy platform and Anne Bertrand, and the IAB microscopy platform and Alexei Grichine and Jacques Mazzega for their technical help. We thank Myriam Dridi for her work on HEK cells and antibody validation, Jean Pascal Hograindleur for his help for CASA experiments and Denise Escalier for her generous gift of human anti-acrosin antibody. This work was mainly supported by the French research agency (ANR) within the 2009 Genopat program for the ICG2I project "Identification and characterization of genetic causes of male infertility" to PR and CA. Support was also obtained from the Fondation Maladies Rares (FMR) for the project R16070CC, "Identification of genetic causes of human NOA".

Author contributions
PFR and CA designed the study, supervised all laboratory work, and wrote the manuscript. They have full access to all of the data in the study and take responsibility for the integrity of the data and its accuracy. All authors read, corrected, and made a significant contribution to the manuscript. Z-EK, TK, AA-Y, CB, MG, NT-M, and CC produced and analyzed the genetic data, and Z-EK, MC-K, AA-Y, and ASV performed immunohistochemistry (IF) experiments. SPB, JE and EL performed Western blot experiments and real-time cell

analyses. Z-EK and GM performed sperm analyses; KP-G and ASV performed the electron microscopy; and BD, IA-S, MM, CM-G, SN, VS, MB, FB, JF, and SH provided clinical samples and data and supplied biological materials.

Conflict of interest

The authors declare that they have no conflict of interest.

References

Arboleda CE, Gerton GL (1987) Studies of three major proteases associated with guinea pig sperm acrosomes. *J Exp Zool* 244: 277 – 287

Ayhan O, Balkan M, Guven A, Hazan R, Atar M, Tok A, Tolun A (2014) Truncating mutations in TAF4B and ZMYND15 causing recessive azoospermia. *J Med Genet* 51: 239 – 244

Baba T, Michikawa Y, Kawakura K, Arai Y (1989) Activation of boar proacrosin is effected by processing at both N- and C-terminal portions of the zymogen molecule. *FEBS Lett* 244: 132 – 136

Ben Khelifa M, Coutton C, Zouari R, Karaouzene T, Rendu J, Bidart M, Yassine S, Pierre V, Delaroche J, Hennebicq S *et al* (2014) Mutations in DNAH1, which encodes an inner arm heavy chain dynein, lead to male infertility from multiple morphological abnormalities of the sperm flagella. *Am J Hum Genet* 94: 95 – 104

Brown CR, Harrison RA (1978) The activation of proacrosin in spermatozoa from ram bull and boar. *Biochim Biophys Acta* 526: 202 – 217

Cesari A, Sanchez JJ, Biancotti JC, Vazquez-Levin MH, Kaiser G, Palma GA, Alberio R, Vincenti AE, Fornes MW (2004) Immunolocalization of bovine sperm protease BSp120 by light and electron microscopy during capacitation and the acrosome reaction: its role in *in vitro* fertilization. *Mol Reprod Dev* 69: 411 – 418

Chen JM, Mercier B, Audrezet MP, Ferec C (2000) Mutational analysis of the human pancreatic secretory trypsin inhibitor (PSTI) gene in hereditary and sporadic chronic pancreatitis. *J Med Genet* 37: 67 – 69

Chera S, Buzgariu W, Ghila L, Galliot B (2009) Autophagy in Hydra: a response to starvation and stress in early animal evolution. *Biochim Biophys Acta* 1793: 1432 – 1443

Dezso Z, Nikolsky Y, Sviridov E, Shi W, Serebriyskaya T, Dosymbekov D, Bugrim A, Rakhmatulin E, Brennan RJ, Guryanov A *et al* (2008) A comprehensive functional analysis of tissue specificity of human gene expression. *BMC Biol* 6: 49

Dieterich K, Soto RR, Faure AK, Hennebicq S, Ben Amar B, Zahi M, Perrin J, Martinez D, Sele B, Jouk PS *et al* (2007) Homozygous mutation of AURKC yields large-headed polyploid spermatozoa and causes male infertility. *Nat Genet* 39: 661 – 665

Feig C, Kirchhoff C, Ivell R, Naether O, Schulze W, Spiess AN (2007) A new paradigm for profiling testicular gene expression during normal and disturbed human spermatogenesis. *Mol Hum Reprod* 13: 33 – 43

Furio L, Hovnanian A (2014) Netherton syndrome: defective kallikrein inhibition in the skin leads to skin inflammation and allergy. *Biol Chem* 395: 945 – 958

Gallo JM, Escalier D, Grellier P, Precigout E, Albert M, David G, Schrevel J (1991) Characterization of a monoclonal antibody to human proacrosin and its use in acrosomal status evaluation. *J Histochem Cytochem* 39: 273 – 282

Harbuz R, Zouari R, Pierre V, Ben Khelifa M, Kharouf M, Coutton C, Merdassi G, Abada F, Escoffier J, Nikas Y *et al* (2011) A recurrent deletion of DPY19L2 causes infertility in man by blocking sperm head elongation and acrosome formation. *Am J Hum Genet* 88: 351 – 361

Huang-Yang YH, Meizel S (1975) Purification of rabbit testis proacrosin and studies of its active form. *Biol Reprod* 12: 232 – 238

Kambhampati S, Park W, Habtezion A (2014) Pharmacologic therapy for acute pancreatitis. *World J Gastroenterol* 20: 16868 – 16880

Kennedy WP, Swift AM, Parrish RF, Polakoski KL (1982) Proacrosin conversion inhibitor. Purification and initial characterization of a boar sperm protein which prevents the conversion of proacrosin into acrosin. *J Biol Chem* 257: 3095 – 3099

Kierszenbaum AL, Rivkin E, Tres LL (2003) Acroplaxome, an F-actin-keratin-containing plate, anchors the acrosome to the nucleus during shaping of the spermatid head. *Mol Biol Cell* 14: 4628 – 4640

Kim KS, Cha MC, Gerton GL (2001) Mouse sperm protein sp56 is a component of the acrosomal matrix. *Biol Reprod* 64: 36 – 43

Kohno N, Yamagata K, Yamada S, Kashiwabara S, Sakai Y, Baba T (1998) Two novel testicular serine proteases, TESP1 and TESP2, are present in the mouse sperm acrosome. *Biochem Biophys Res Commun* 245: 658 – 665

Lee B, Park I, Jin S, Choi H, Kwon JT, Kim J, Jeong J, Cho BN, Eddy EM, Cho C (2011) Impaired spermatogenesis and fertility in mice carrying a mutation in the Spink2 gene expressed predominantly in testes. *J Biol Chem* 286: 29108 – 29117

Li WW, Li J, Bao JK (2012) Microautophagy: lesser-known self-eating. *Cell Mol Life Sci* 69: 1125 – 1136

Liu DY, Baker HW (1993) Inhibition of acrosin activity with a trypsin inhibitor blocks human sperm penetration of the zona pellucida. *Biol Reprod* 48: 340 – 348

Maor-Sagie E, Cinnamon Y, Yaacov B, Shaag A, Goldsmidt H, Zenvirt S, Laufer N, Richler C, Frumkin A (2015) Deleterious mutation in SYCE1 is associated with non-obstructive azoospermia. *J Assist Reprod Genet* 32: 887 – 891

Massart A, Lissens W, Tournaye H, Stouffs K (2012) Genetic causes of spermatogenic failure. *Asian J Androl* 14: 40 – 48

Meizel S, Deamer DW (1978) The pH of the hamster sperm acrosome. *J Histochem Cytochem* 26: 98 – 105

O'Brien DA, Welch JE, Goulding EH, Taylor AA Jr, Baba T, Hecht NB, Eddy EM (1996) Boar proacrosin expressed in spermatids of transgenic mice does not reach the acrosome and disrupts spermatogenesis. *Mol Reprod Dev* 43: 236 – 247

Ohmuraya M, Hirota M, Araki M, Mizushima N, Matsui M, Mizumoto T, Haruna K, Kume S, Takeya M, Ogawa M *et al* (2005) Autophagic cell death of pancreatic acinar cells in serine protease inhibitor Kazal type 3-deficient mice. *Gastroenterology* 129: 696 – 705

Ohmuraya M, Sugano A, Hirota M, Takaoka Y, Yamamura K (2012) Role of intrapancreatic SPINK1/Spink3 expression in the development of pancreatitis. *Front Physiol* 3: 126

Okutman O, Muller J, Baert Y, Serdarogullari M, Gultomruk M, Piton A, Rombaut C, Benkhalifa M, Teletin M, Skory V *et al* (2015) Exome sequencing reveals a nonsense mutation in TEX15 causing spermatogenic failure in a Turkish family. *Hum Mol Genet* 24: 5581 – 5588

Pierre V, Martinez G, Coutton C, Delaroche J, Yassine S, Novella C, Pernet-Gallay K, Hennebicq S, Ray PF, Arnoult C (2012) Absence of Dpy19l2, a new inner nuclear membrane protein, causes globozoospermia in mice by preventing the anchoring of the acrosome to the nucleus. *Development* 139: 2955 – 2965

Rawlings ND, Tolle DP, Barrett AJ (2004) Evolutionary families of peptidase inhibitors. *Biochem J* 378: 705 – 716

Redelfs L, Fischer J, Weber C, Wu Z, Meyer-Hoffert U (2016) The serine protease inhibitor of Kazal-type 9 (SPINK9) is expressed in lichen simplex chronicus, actinic keratosis and squamous cell carcinoma. *Arch Dermatol Res* 308: 133 – 137

Rivinoja A, Pujol FM, Hassinen A, Kellokumpu S (2012) Golgi pH, its regulation and roles in human disease. *Ann Med* 44: 542 – 554

SEQC/MAQC-III Consortium (2014) A comprehensive assessment of RNA-seq accuracy, reproducibility and information content by the Sequencing Quality Control Consortium. *Nat Biotechnol* 32: 903 – 914

Taylor SC, Posch A (2014) The design of a quantitative western blot experiment. *Biomed Res Int* 2014: 361590

Tuttelmann F, Werny F, Cooper TG, Kliesch S, Simoni M, Nieschlag E (2011) Clinical experience with azoospermia: aetiology and chances for spermatozoa detection upon biopsy. *Int J Androl* 34: 291 – 298

Valenzuela DM, Murphy AJ, Frendewey D, Gale NW, Economides AN, Auerbach W, Poueymirou WT, Adams NC, Rojas J, Yasenchak J *et al* (2003) High-throughput engineering of the mouse genome coupled with high-resolution expression analysis. *Nat Biotechnol* 21: 652 – 659

Witt H, Luck W, Hennies HC, Classen M, Kage A, Lass U, Landt O, Becker M (2000) Mutations in the gene encoding the serine protease inhibitor, Kazal type 1 are associated with chronic pancreatitis. *Nat Genet* 25: 213 – 216

Yan W, Si Y, Slaymaker S, Li J, Zheng H, Young DL, Aslanian A, Saunders L, Verdin E, Charo IF (2010) Zmynd15 encodes a histone deacetylase-dependent transcriptional repressor essential for spermiogenesis and male fertility. *J Biol Chem* 285: 31418 – 31426

Yang F, Silber S, Leu NA, Oates RD, Marszalek JD, Skaletsky H, Brown LG, Rozen S, Page DC, Wang PJ (2015) TEX11 is mutated in infertile men with azoospermia and regulates genome-wide recombination rates in mouse. *EMBO Mol Med* 7: 1198 – 1210

Yassine S, Escoffier J, Nahed RA, Pierre V, Karaouzene T, Ray PF, Arnoult C (2015) Dynamics of Sun5 localization during spermatogenesis in wild type and Dpy19l2 knock-out mice indicates that Sun5 is not involved in acrosome attachment to the nuclear envelope. *PLoS One* 10: e0118698

Yatsenko AN, Georgiadis AP, Ropke A, Berman AJ, Jaffe T, Olszewska M, Westernstroer B, Sanfilippo J, Kurpisz M, Rajkovic A *et al* (2015) X-linked TEX11 mutations, meiotic arrest, and azoospermia in infertile men. *N Engl J Med* 372: 2097 – 2107

Zahn A, Furlong LI, Biancotti JC, Ghiringhelli PD, Marijn-Briggiler CI, Vazquez-Levin MH (2002) Evaluation of the proacrosin/acrosin system and its mechanism of activation in human sperm extracts. *J Reprod Immunol* 54: 43 – 63

Zhang T, Murphy MW, Gearhart MD, Bardwell VJ, Zarkower D (2014) The mammalian Doublesex homolog DMRT6 coordinates the transition between mitotic and meiotic developmental programs during spermatogenesis. *Development* 141: 3662 – 3671

Expanded View Figures

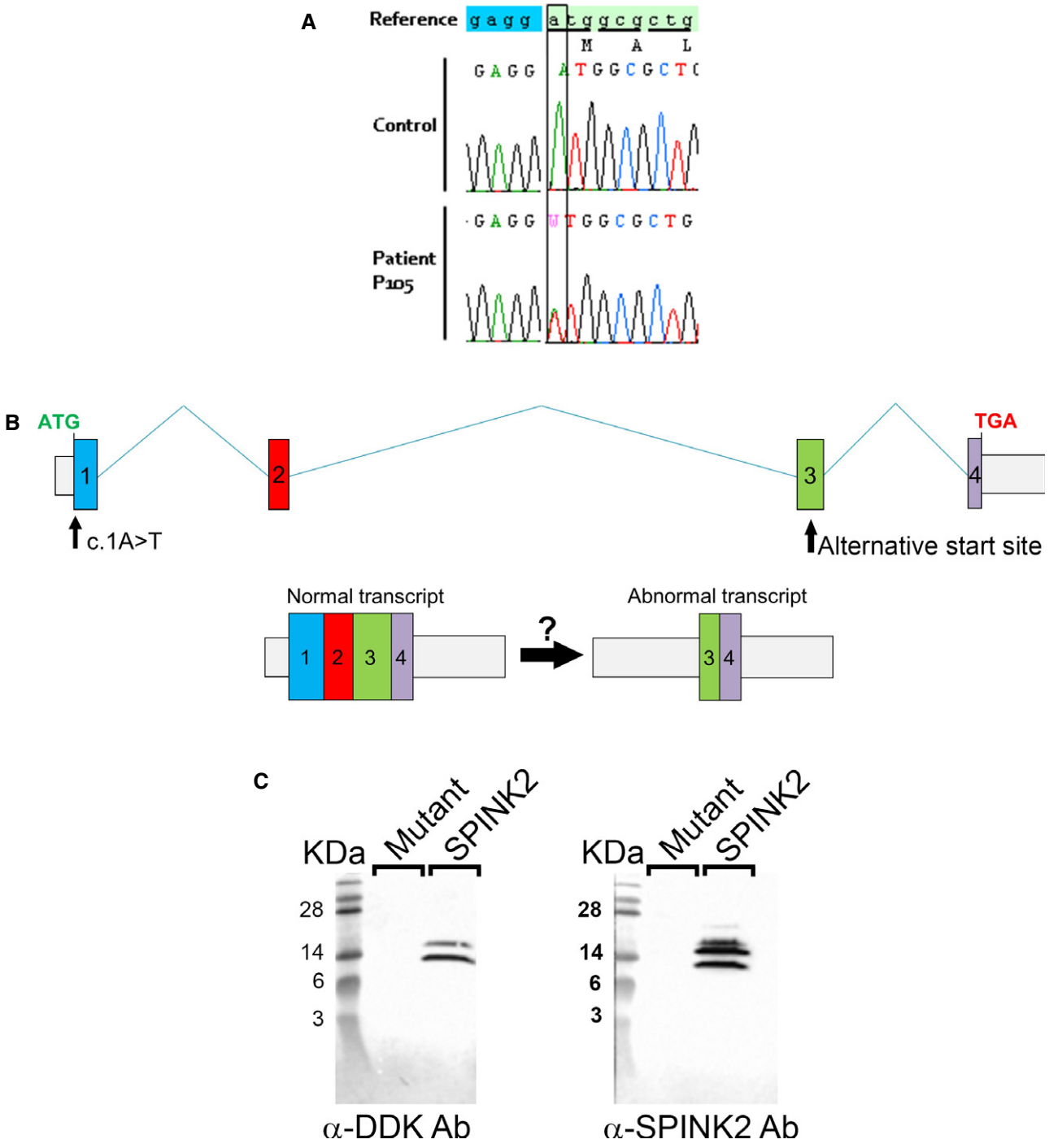

Figure EV1. Genetic analyses of the c.1A>T variant identified in patient P105.

A The c.1A>T variant, heterozygous in patient P105, abrogates the original start codon.

B An alternative start codon is present in the middle of exon 3 and may initiate translation to potentially produce a protein containing the last 27 amino acids of the wild-type protein.

C Western blot of HEK293 cell extracts transfected with C-terminus DDK-tagged SPINK2 or c.1A>T SPINK2 mutant and revealed by anti-DDK or anti-SPINK2 antibodies shows the absence of the putative truncated SPINK2 form.

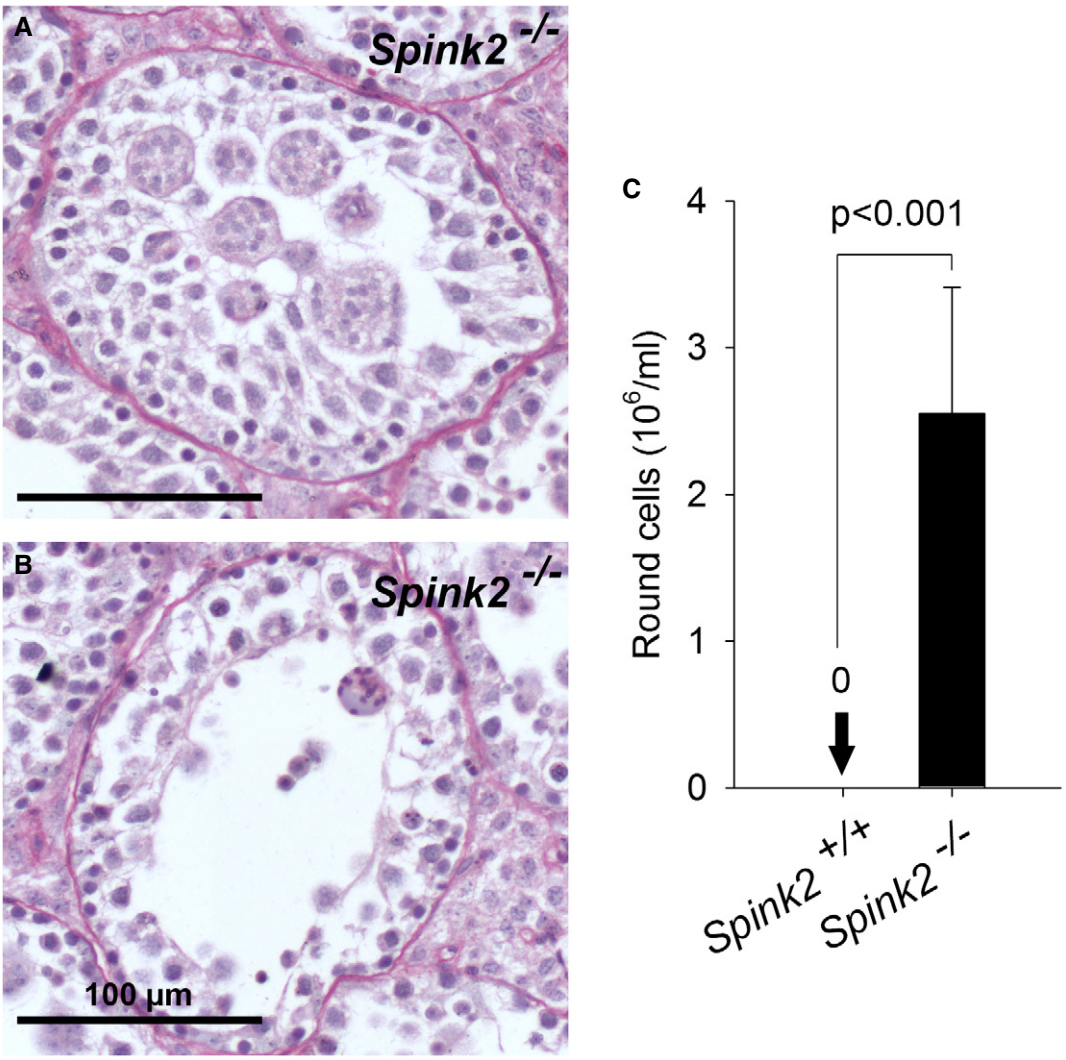

Figure EV2. Lack of Spink2 leads to germ cell desquamation and the presence of round cells in the cauda epididymis.

A, B Staining with hematoxylin and eosin of seminiferous tubule sections from *Spink2*$^{-/-}$ mice showed the presence of numerous round cells or symblasts within the lumen of tubules. Note that photograph (A) corresponds to a close-up of part of Fig 3C1 as it nicely illustrates the presence of symblasts in the tubule. Scale bar, 100 µm.

C Spermatocytograms of cauda epididymis extracts revealed the presence of only round cells at concentrations above 2 million/ml, whereas such cells were absent in WT extracts. Data are presented as mean ± SEM (n = 5).

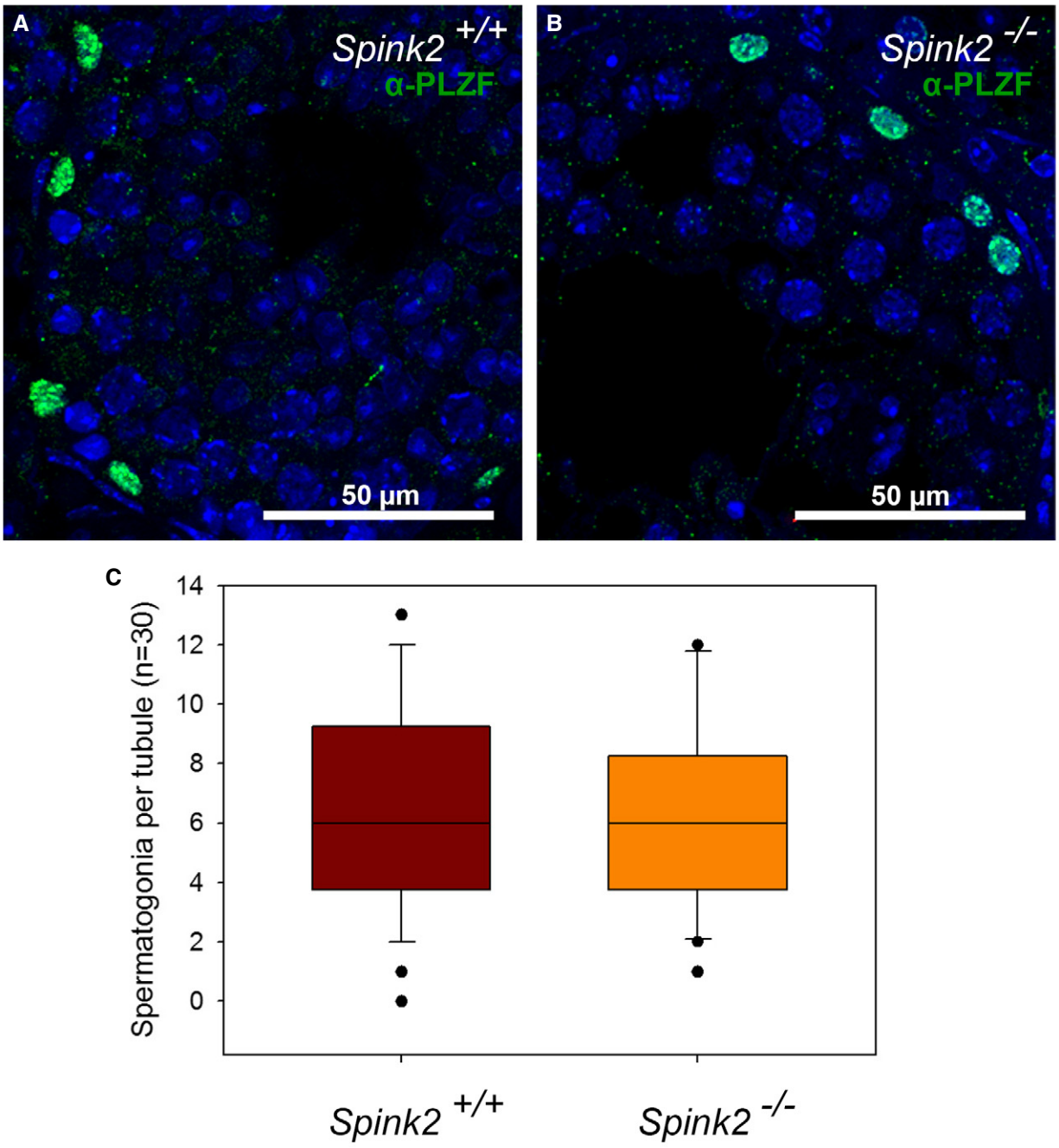

Figure EV3. Pool of non-differentiated spermatogonia is conserved in seminiferous tubules of *Spink2*$^{-/-}$ mice.

A, B Identification of spermatogonia by IF experiments using an anti-PLZF antibody in WT and *Spink2*$^{-/-}$ seminiferous tubule sections, respectively. Scale bars as indicated.

C Box plot showing the number of spermatogonia per seminiferous tubule section (n = 30 for each). No difference in the number of spermatogonia per seminiferous tubule section was observed. The line within the box marks the median, whiskers (error bars) above and below the box indicate the 90th and 10th percentiles, and black dots represent outliers.

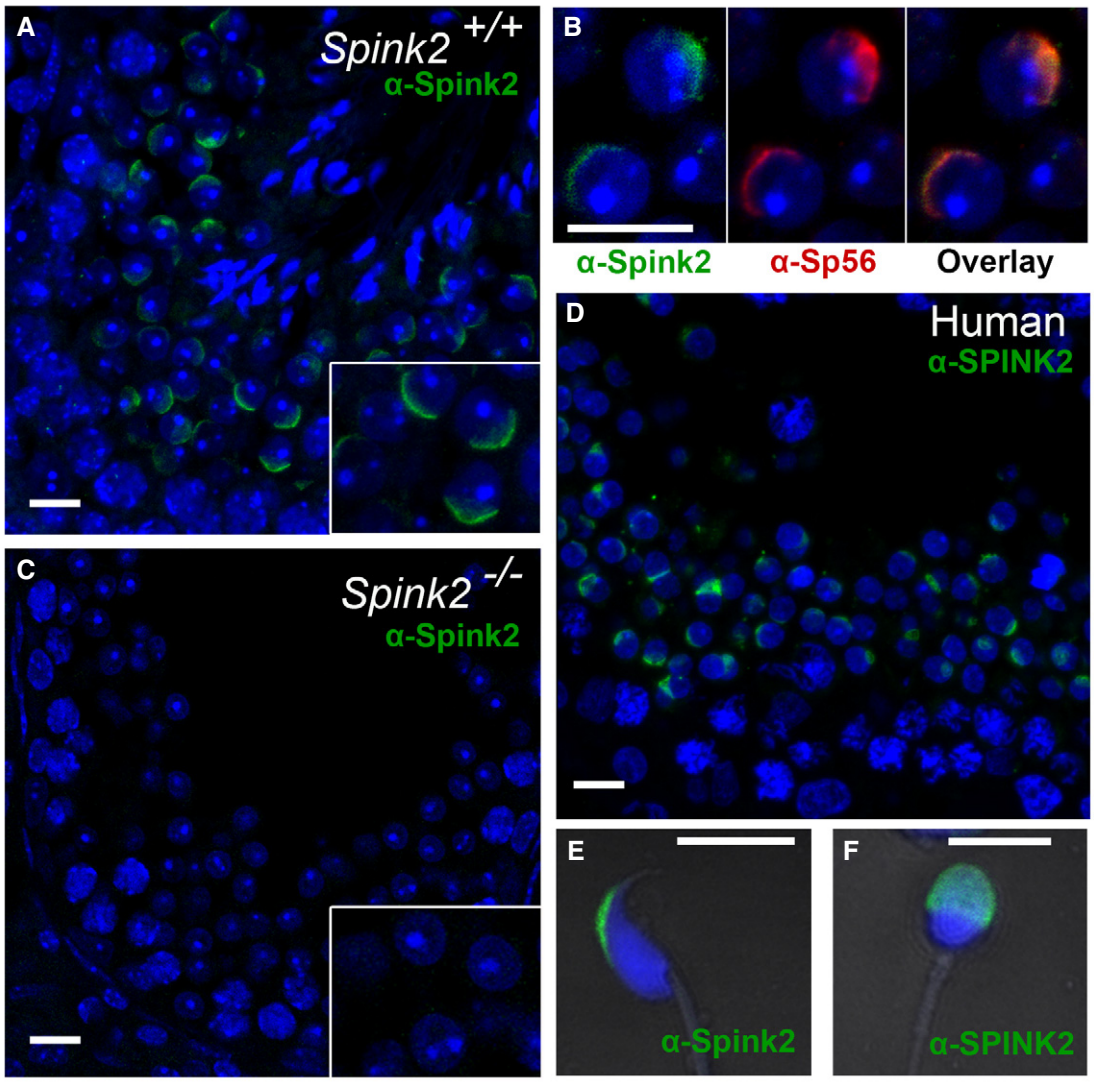

Figure EV4. SPINK2 is located in the acrosome of round spermatids and mature spermatozoa in mouse and human.

A Immunofluorescence experiments using an anti-SPINK2 antibody (green staining) reveals that Spink2 is located in the acrosome of WT mouse round spermatids. Scale bar, 10 μm.

B A double staining using an anti-SPINK2 antibody (green staining) and an anti-Sp56 antibody (red staining) shows that the two signals are colocalized. Scale bar, 10 μm.

C No Spink2 staining is observed in seminiferous tubule sections from *Spink2*$^{-/-}$ mice, stained with an anti-SPINK2 antibody. Scale bar, 10 μm.

D In sections of human seminiferous tubules, a similar localization of SPINK2 is observed in round spermatids, corresponding to the acrosome. Scale bar, 10 μm.

E IF experiments using an anti-SPINK2 antibody (green staining) reveal that Spink2 is located in the acrosome of WT epididymal mouse sperm. Scale bar, 10 μm.

F SPINK2 localization within the acrosome is conserved in ejaculated human sperm. No staining is observed in the midpiece or principle piece. Scale bar, 5 μm.

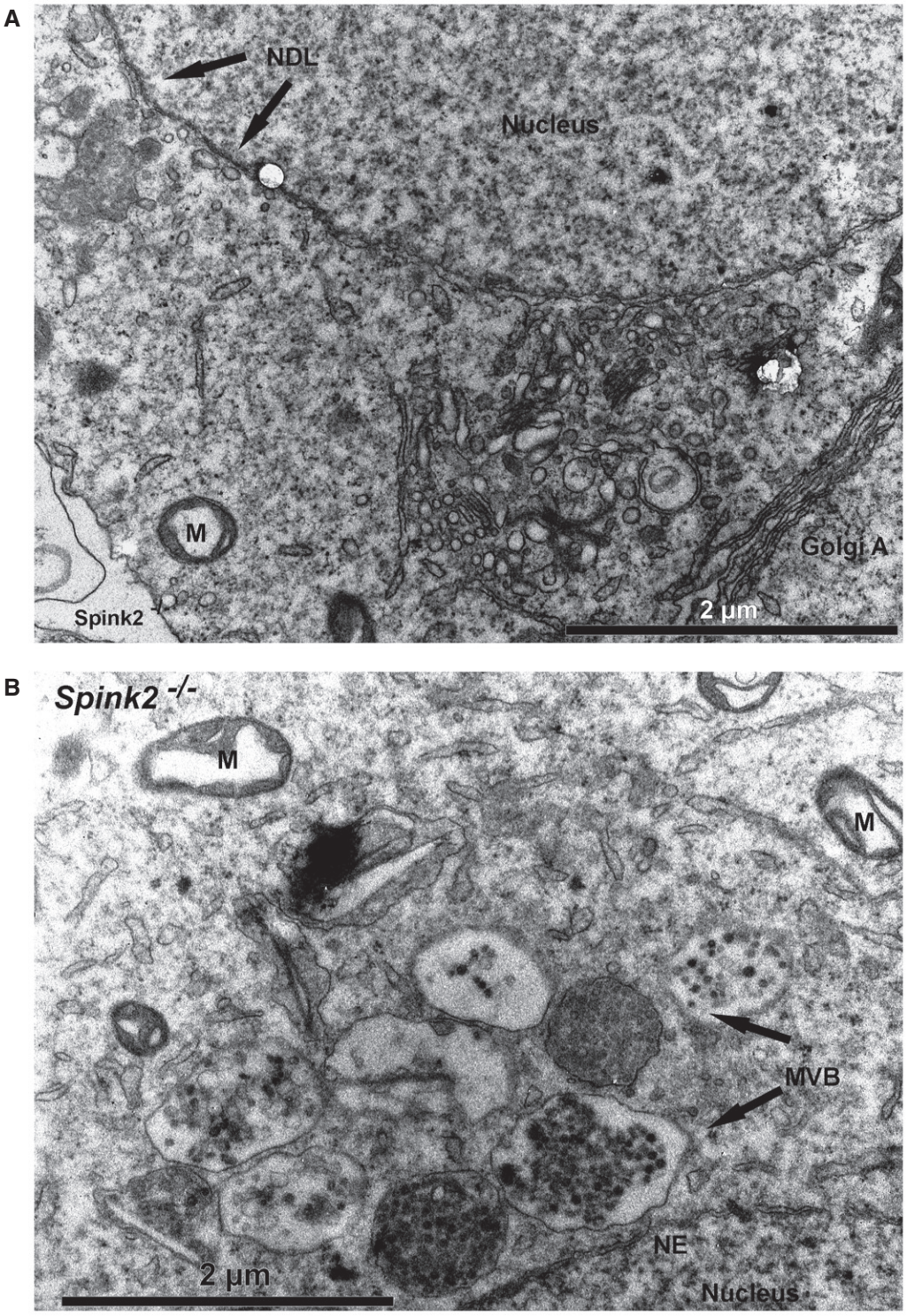

Figure EV5. Disjunction of the polarity of the Golgi apparatus and the nuclear dense lamina (NDL) in *Spink2*$^{-/-}$ round spermatids and presence of multivesicular bodies in the cytoplasm of *Spink2*$^{-/-}$ round spermatids.

A Partial section of a *Spink2*$^{-/-}$ round spermatid observed by EM showing the spatial disjunction of the Golgi apparatus and the NDL. NDL is evidenced by apposition of dense material on the nuclear side of the inner nuclear membrane. Another hallmark of this specialized area of the nuclear envelope is the tight apposition of both inner and outer nuclear membranes along the NDL. M, mitochondria. Scale bar, 2 µm.

B Partial section of a *Spink2*$^{-/-}$ round spermatid observed by EM showing structures corresponding to multivesicular bodies (MVB). M, mitochondria; NE, nuclear envelope; NDL, nuclear dense lamina. Scale bar, 2 µm.

Appendix - Table of content

Appendix Table S1. List of homozygous variants present in B1 and B2.
Coordinates of all variations are based on the UCSC GRCh37/hg19 assembly. [&] No RefSeq transcript accession number currently available. Nucleotidic references

Gene	Variant coordinates	Transcript	cDNA Variation	Amino acid variation	Prediction	Testis expression
SPINK2	Chr4:57686748G>C	NM_001271718.1 NM_001271720.1 NM_001271722.1 NM_021114.3	Splice acceptor site	-	Damaging	High and predominant
GUF1	Chr4:44683156G>T	NM_021927.2	c.637G>T	p.Ser148Ile	Damaging	Low
ZCCHC5	ChrX:77913158A>G	NM_152694.2	c.1056A>G	p.Phe254Leu	Damaging	Low
ARR3	ChrX:69498482C>G	NM_004312.2 ENST00000374495[&]	c. 947C>G c.994C>G	p.Ser299Cys	Damaging	Low
FTHL17	ChrX:31089629TC>AA	NM_031894.2	c.542C>A	p.Glu148Leu	Damaging	low

Appendix Table S2. List of *SPINK2* variants identified in azoo- and oligo- spermic patients (RefSeq : NM_021114**).**

Coordinates of all variations are based on the UCSC GRCh37/hg19 assembly. [&] No RefSeq transcript accession number currently available. The 5'UTR was only sequenced in 363 patients and the whole coding sequence was sequenced in all 611 patients . When the variant was not identified in ExAC the number of ExAC controls indicated corresponds to the number of subject analyzed in ExAC for the nearest described variant. We note that the beginning of *SPINK2* exon1 is particularly poorly covered.

Position	Localisation of the variation	cDNA reference	Consequences on the protein	Nb of homozygous patients (%)	Nb of ExAC homozygous controls (%)	Nb of heterozygous patients (%)	Nb of ExAC heterozygous controls (%)
4:57687851 (rs115163565)	5' UTR	c.1-23 A>T	-	2/363 (0,55)	307/4980 (6,2)	32/363 (8,8)	1816/4980 (36,5)
4:57687849 (rs114591157)	5' UTR	c.1-21 G>C	-	3/363 (0,83)	318/5065 (6,3)	30/363 (8,3)	1852/5065 (36,0)
4:57687828	Exon 1	c.1 A>T	p.M1L	0/611	0/6054	1/611	0/6054

Appendix Table S3. Sequence of the primer used for *SPINK2* sanger sequencing.

Primer name	Primer sequence	Size of amplicon
SPINK2-hSeq-Ex1-F	GAGTGGCGCAGGTAACAGAC	245 bp
SPINK2-hSeq-Ex1-R	CTGGGGAACCGCCAGTAAC	
SPINK2-hSeq-Ex2-F	TGGCTAATGCCTCAAATTCC	339 bp
SPINK2-hSeq-Ex2-R	ACGCAGTCCTCAATGGTTTC	
SPINK2-hSeq-Ex3-F	ACACGGTGAAACCCTGTCTC	552 bp
SPINK2-hSeq-Ex3-R	CAGAGGTTGCAGTGAACCAA	
SPINK2-hSeq-Ex4-F	GTGGGGACTTTCACCCTCTT	423 bp
SPINK2-hSeq-Ex4-R	GCAAAAGCCAAGAAACAAGG	

Appendix Table S4. Sequence of the primer used in RT-PCR and size of the amplified products

Primer name	Primer sequence	Size of amplicon
SPINK2-hRT-F	CTGCTCCTGGCAGTTACCTT	221 bp
SPINK2-hRT-R	CAGGGTCCATTTCGAATGAT	

Appendix Table S5. Sequence of the primer used in real time RT-PCR and size of the amplified products

Primer name	Primer sequence	Size of amplicon
SPINK2-hqRT-F	CACTTTAACCCTGTGTGTGG	117 bp
SPINK2-hqRT-R	TCAGCAGGGTCCATTTCGAA	
Spink2-mqRT-F	CTCATGAGACTCTCGACTCTTCC	150 bp
Spink2-mqRT-R	TACATTCATTGCTGTAAGTGTTCATATC	
ACTB-hqRT-F	CCAACCGCGAGAAGATGA	97 bp
ACTB-hqRT-R	CCAGAGGCGTACAGGGATAG	
Actb-mqRT-F	ACCAGAGGCATACAGGGACA	104 bp
Actb-mqRT-R	CTAAGGCCAACCGTGAAAAG	

Appendix Table S6. Sequence of the primer used for genotyping and size of the amplified products.

Primer name	Primer sequence	Size of amplicon
Spink2-WT-F	GCAATGGGCGTATCTCAAAT	174 bp
Spink2-WT-R	GGGACCTGATTTTCATGCAC	
Spink2-KO-F	CTCTTCCTCGCTCCCTTCTT	213 bp
Spink2-KO-R	GGGATTCTCCCAATCTCTCC	

Appendix Figure S1. Expression of *SPINK2* mRNA in different organs in human and mouse.
The expression pattern of SPINK2 transcript in various human **(A)** and mouse **(B)** tissues was determined by Quantitative real-time RT-PCR. Values were normalized to the expression level of beta-actin via the 2-ΔΔCT method. The 2-ΔΔCT value was set at 0 in heart, resulting in an arbitrary expression of 1. Data are presented as mean ± standard error mean (n=3). Statistical differences were assessed using t-test.

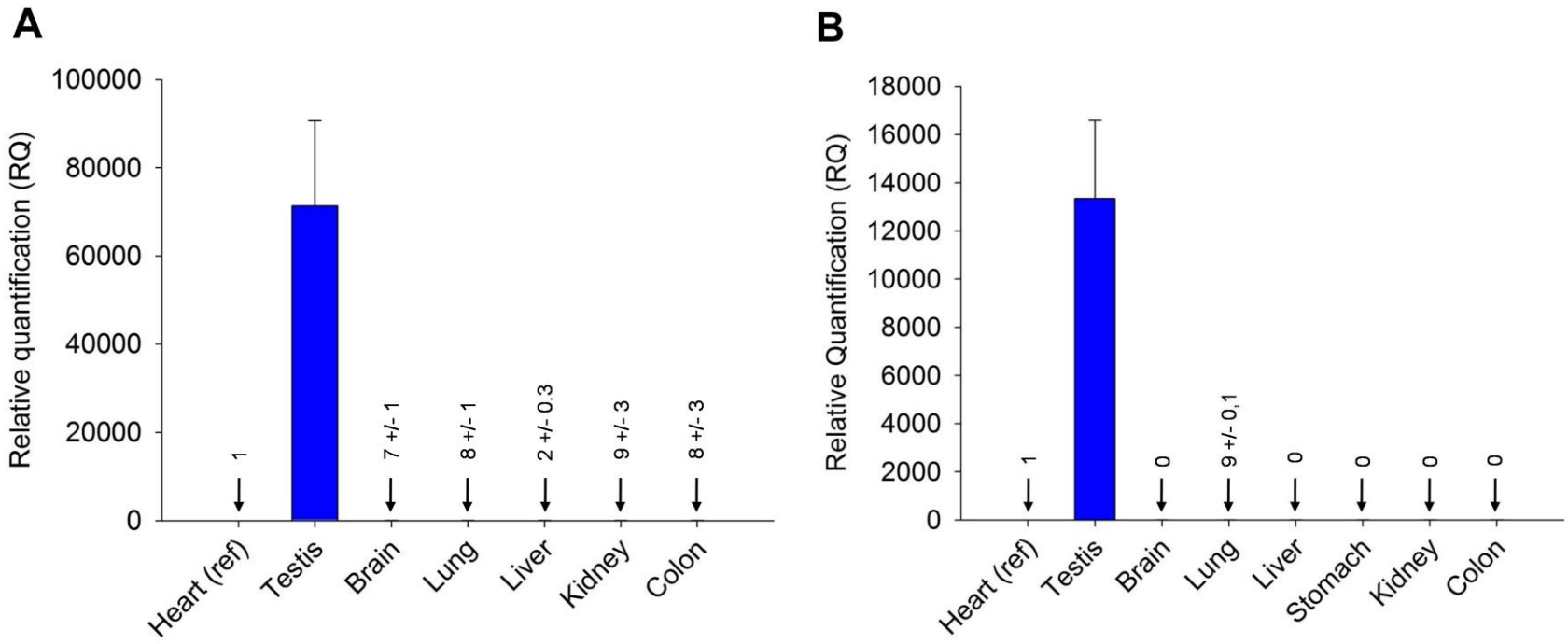

Appendix Figure S2. Impact on the protein structure of the c.206-3C>G *SPINK2* variant

(A) The normal transcript encodes for an 84 amino acids protein predicted to contain a signal peptide at the N-terminus region (blue) and a Kazal-type serine protease inhibitor domain at the C-terminus region (orange and red). UniProtKB accession number for human SPINK2 is P20155. **(B)** The c.206-3C>G splice variant generates two abnormal transcripts, T1 and T2 (see figure 2). Translation of these transcripts is predicted to produce truncated proteins lacking the Kazal-type serine protease inhibitor domain.

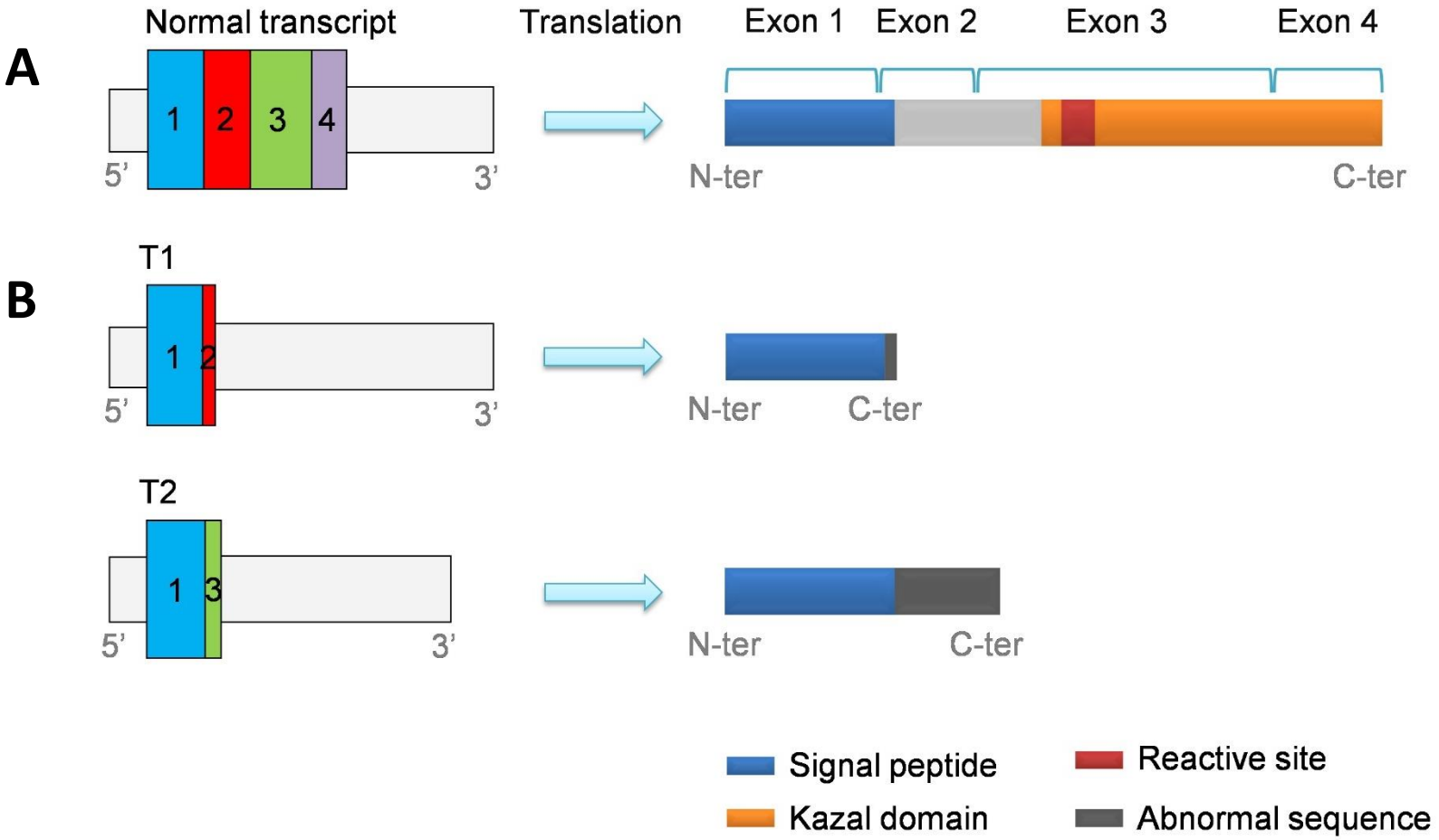

Appendix Figure S3. Absence of *Spink2* expression in testicular extracts from KO mice.

Relative quantification of *Spink2* transcript in testicular cells from **(A)** WT mice (n=3) and **(B)** *Spink2* $^{-/-}$ mice was determined by quantitative real-time RT-PCR. Values were normalized to the expression level of beta-actin via the 2-ΔΔCT method. The 2-ΔΔCT value was set at 0 in liver cells from WT mice (n=3), resulting in an arbitrary expression of 1. Data are presented as mean ± standard error mean. Statistical differences were assessed using t-test.

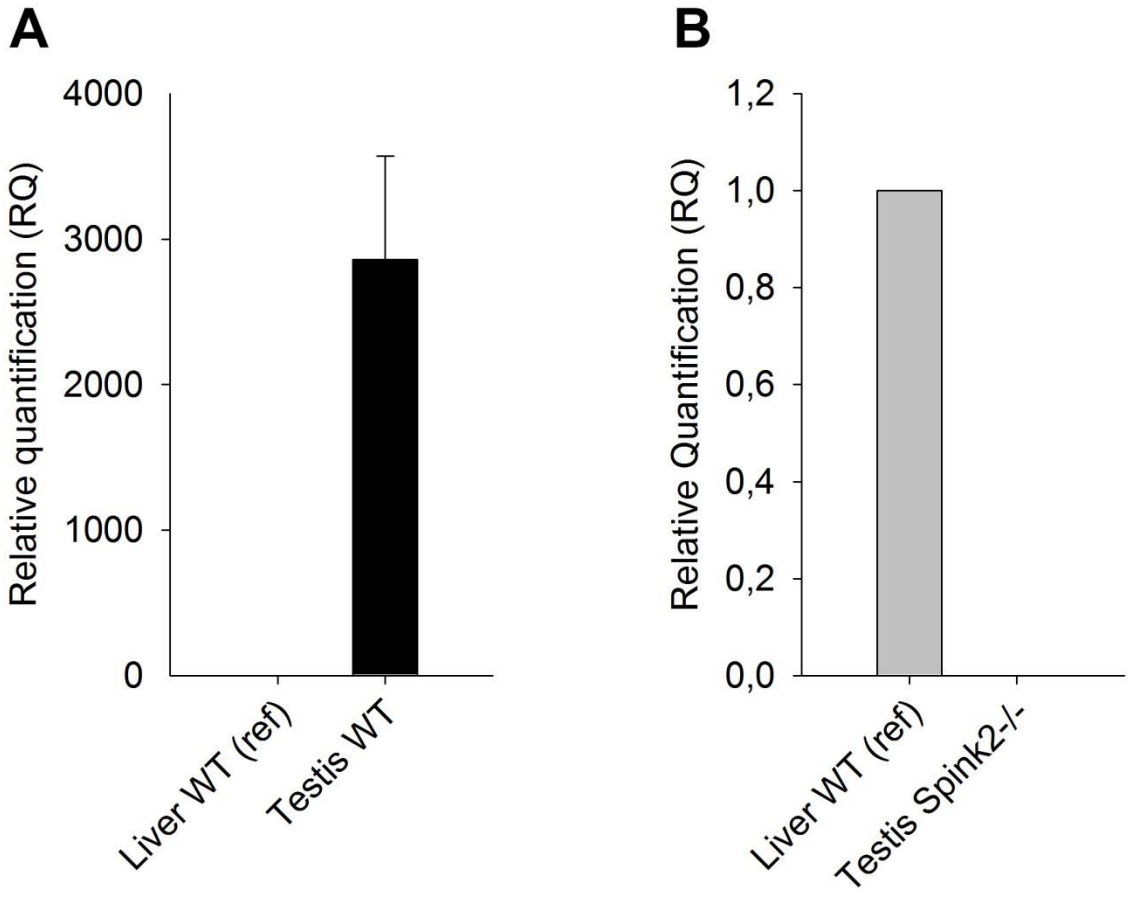

Appendix Figure S4. Specificity of antibodies targeting SPINK2.
(A) Western blot of protein extracts from HEK 293 cells heterologously transfected with or without a plasmid containing human isoform of SPINK2 tagged with DDK and revealed with an anti-SPINK2 antibody. **(B)** Similar experiment but revealed with an anti-DDK antibody. **(C)** Confocal images of HEK 293 cells transfected with human SPINK2-DDK and stained with an anti-SPINK2 antibodies (green) (top). All cells were counterstained with Hoechst (blue, staining) to mark the nuclei. Only transfected cells showed specific staining. Bottom, confoncal images of control non transfected cells showing no staining.

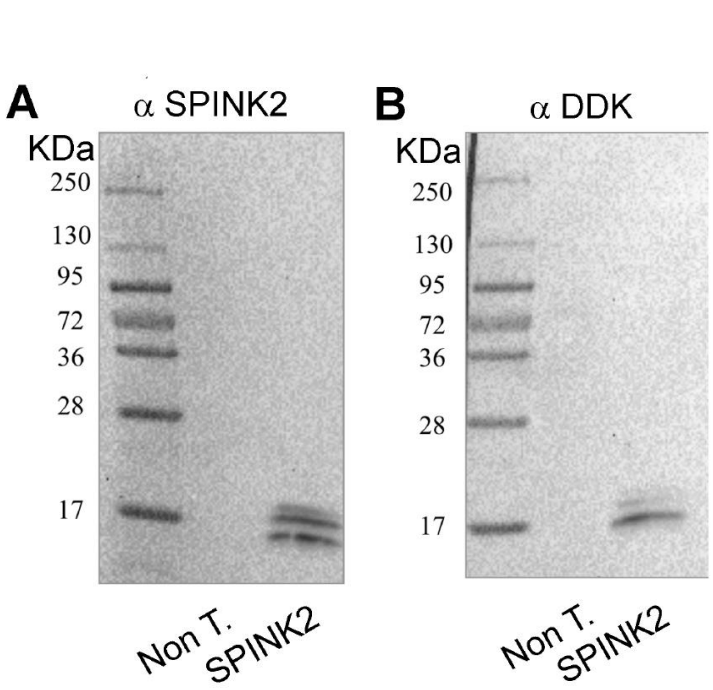

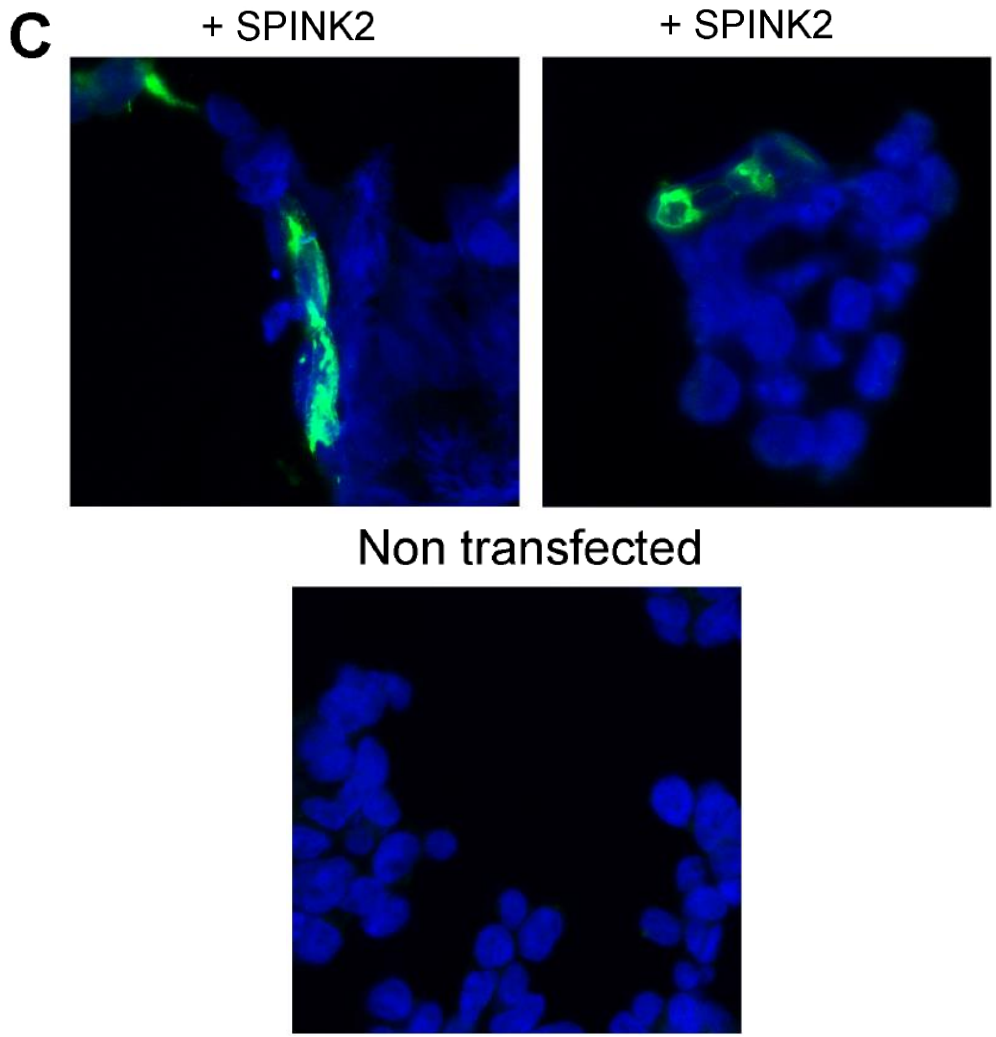

Appendix Figure S5. Absence of Spink2 does not lead to DNA fragmentation in spermatogenic cells.
(A) Representative images of TUNEL staining (green) counterstained with Hoechst (blue) of WT and *Spink2*$^{-/-}$ seminiferous tubule. Scale bar 70 µm. (**B**) Graph showing the % of cells with non fragmented DNA in WT (99.6 +/- 0.3 mean +/- SD, number of cells assessed 230-270 per biological replicate, n=3) and in *Spink2*$^{-/-}$ (99.6 +/- 0.1 mean +/- SD, number of cells assessed 300-380 per biological replicate, n=4) seminiferous tubules. NS "not statistically significant" (t-test) (**C**) Representative images of TUNEL staining (green) counterstained with Hoechst (blue) of fertile control and patient B1 seminiferous tubule. Scale bar 70 µm. (**D**) Graph showing the % of cells with non fragmented DNA in fertile control (number of cells assessed 812, n=1) and patient B1 control (number of cells assessed 789, n=1) seminiferous tubules.

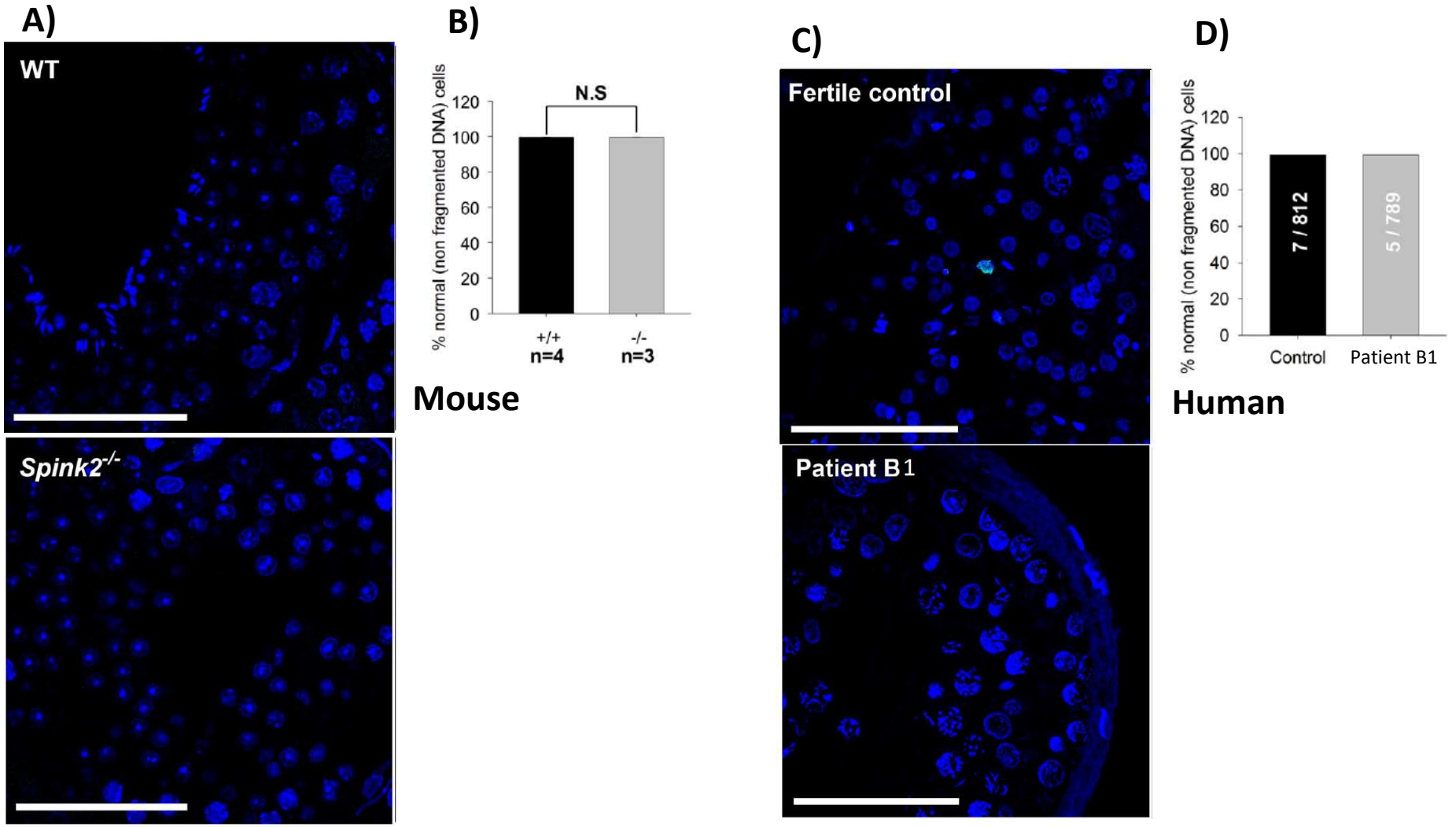

Appendix Figure S6. Equal protein loading was verified by stain-free gel technology and Western blots against house keeping protein (A) Stain-free™ technology was used to control protein loading levels. Left, activated gel showing loading of Western-blot of Fig 9D and right of Fig 9E (**B**) Identical loading as tested in figure 9D and 9D were revealed by anti-tubulin antibody and confirmed equal protein loading between different lanes.

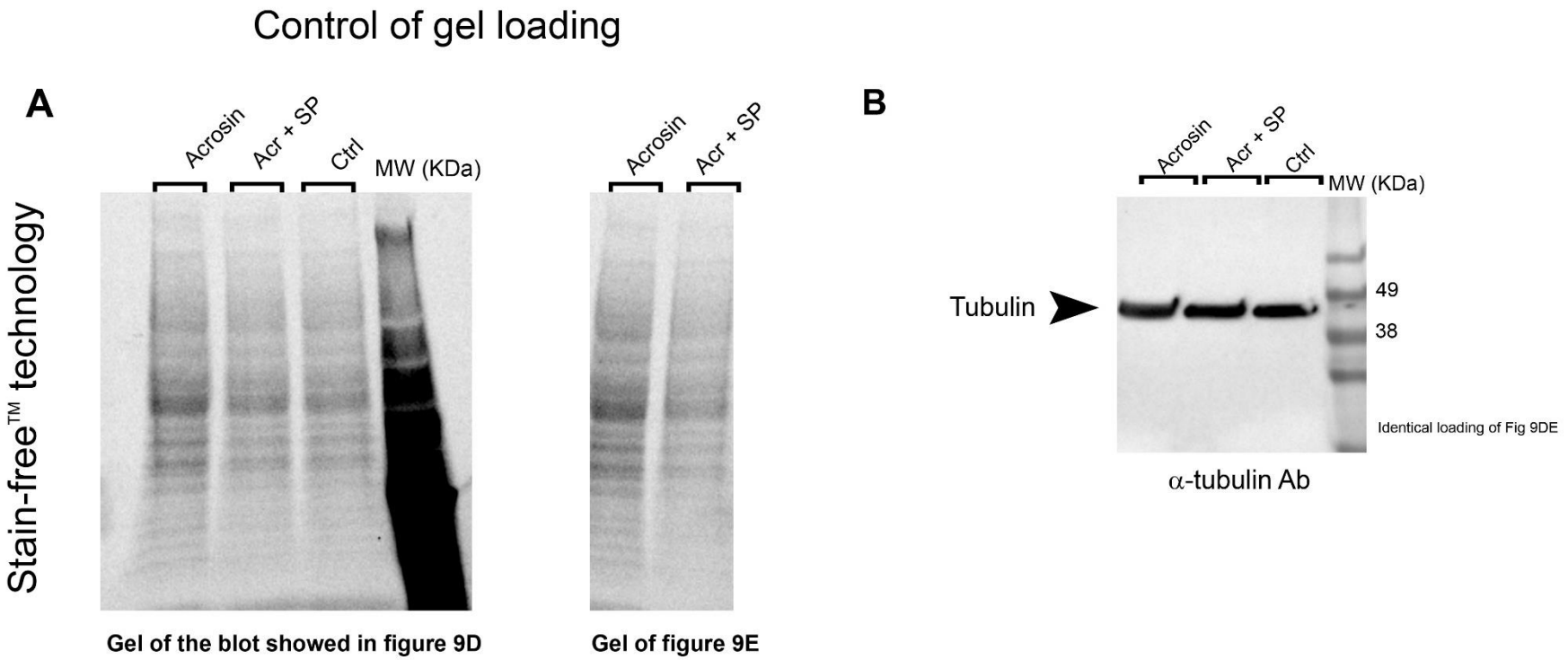

C: CRISPR as a tool for characterising human infertility

1. Article: Creation of knock out and knock in mice by CRISPR/Cas9 to validate candidate genes for human male infertility, interest, difficulties and feasibility

Kherraf Z-E, Conne B, Amiri-Yekta A, **Christou-Kent M**, Coutton C, Escoffier J, Nef S, Arnoult C, Ray PF. **Molecular and Cellular Endocrinology, March 2018.**

1.1. Context

The CRISPR/Cas9 technique has dramatically accelerated the process of generating transgenic mouse strains for the study of human infertility. Since its availability, the GETI Lab has made good use of this technique to rapidly generate lineages for candidate genes in collaboration with the University of Geneva. The following article gives details on technical aspects of this process based on the experience of generating four Knockout strains and one HA-tag knock-in strain for genes associated with a phenotype known as 'multiple morphological anomalies of the flagella' (MMAF). The article describes the experimental design and timeframe of the procedure, and shows the genetic results obtained as well as difficulties experienced.

The method described for the creation of the KI lineage is the same method used for the generation of the tagged PATL2-HA lineage. I was particularly involved in the processes of designing the guide RNA (gRNA) sequence and ssDNA repair template and selecting the method of delivery of these elements and the Cas9 expression plasmid into the mouse zygote. As evidenced in the article, this newly available method is a robust and efficient means of generating transgenic mouse lineages for the characterisation of genes associated with human infertility.

Molecular and Cellular Endocrinology 468 (2018) 70–80

Contents lists available at ScienceDirect

Molecular and Cellular Endocrinology

journal homepage: www.elsevier.com/locate/mce

Creation of knock out and knock in mice by CRISPR/Cas9 to validate candidate genes for human male infertility, interest, difficulties and feasibility

Zine-Eddine Kherraf [a, b], Beatrice Conne [c], Amir Amiri-Yekta [a, b, d], Marie Christou Kent [a], Charles Coutton [a, e], Jessica Escoffier [a], Serge Nef [c], Christophe Arnoult [a, 1], Pierre F. Ray [a, b, *, 1]

[a] Genetic Epigenetic and Therapies of Infertility, Institute for Advanced Biosciences, Inserm U1209, CNRS UMR 5309, Université Grenoble Alpes, F-38000, Grenoble, France
[b] UM GI-DPI, CHU Grenoble Alpes, Grenoble, F-38000, France
[c] Department of Genetic Medicine and Development University of Geneva Medical School, CH 1211, Geneva 4, Switzerland
[d] Reproductive Biomedicine Research Center, Royan Institute for Reproductive Biomedicine, ACECR, Tehran, PO Box 16635-148, Iran
[e] UM de Génétique Chromosomique, CHU de Grenoble, Grenoble, F-38000, France

ARTICLE INFO

Article history:
Received 12 October 2017
Received in revised form
2 March 2018
Accepted 3 March 2018
Available online 6 March 2018

Keywords:
High throughput sequencing
CRISPR/Cas9
Spermatogenesis
Sperm flagella
Knock out mice

ABSTRACT

High throughput sequencing (HTS) and CRISPR/Cas9 are two recent technologies that are currently revolutionizing biological and clinical research. Both techniques are complementary as HTS permits to identify new genetic variants and genes involved in various pathologies and CRISPR/Cas9 permits to create animals or cell models to validate the effect of the identified variants, to characterize the pathogeny of the identified variants and the function of the genes of interest and ultimately to provide ways of correcting the molecular defects.

We analyzed a cohort of 78 infertile men presenting with multiple morphological anomalies of the sperm flagella (MMAF), a severe form of male infertility. Using whole exome sequencing (WES), homozygous mutations in autosomal candidate genes were identified in 63% of the tested subjects. We decided to produce by CRISPR/cas9 four knock-out (KO) and one knock-in (KI) mouse lines to confirm these results and to increase our understanding of the physiopathology associated with these genetic variations. Overall 31% of the live pups obtained presented a mutational event in one of the targeted regions. All identified events were insertions or deletions localized near the PAM sequence. Surprisingly we observed a high rate of germline mosaicism as 30% of the F1 displayed a different mutation than the parental event characterized on somatic tissue (tail), indicating that CRISPR/Cas9 mutational events kept happening several cell divisions after the injection.

Overall, we created mouse models for 5 distinct loci and in each case homozygous animals could be obtained in approximately 6 months. These results demonstrate that the combined use of WES and CRISPR/Cas9 is an efficient and timely strategy to identify and validate mutations responsible for infertility phenotypes in human.

Contents

* Corresponding author. Genetics of Infertility and PGD, Institut de Biologie et Pathologie, R+2, CHU Grenoble Alpes 38 043, Grenoble Cedex 9, France.
E-mail address: pray@chu-grenoble.fr (P.F. Ray).
[1] Shared leadership.

https://doi.org/10.1016/j.mce.2018.03.002
0303-7207/

1. Introduction

Fertility disorders affect more than 15% of couples worldwide and are considered as a major health concern by the world health organization (WHO). Approximately half of these cases are related to male factors but despite the large number of genes specifically expressed in testes during spermatogenesis (Soumillon et al., 2013) and the multitude of KO infertile male mice described in the literature, only few genes have so far been associated with human male infertility and its molecular basis remains largely unknown (Coutton et al., 2015). The recent development of new high throughput sequencing (HTS) techniques and efficient targeted enrichment methods such as whole exome sequencing (WES) now allow the sequencing of all the coding sequences of any human being. The increased use of WES in human genetics allowed the identification of a large number of new Mendelian disease genes (Alkuraya, 2016) and the technique is now increasingly used in the field of male infertility (Ray et al., 2017). Using WES, the identification of plausible candidate genes for a particular phenotype is now relatively easy, quick and affordable. The difficulty comes from the large number of likely deleterious variants identified for each patient which renders difficult the identification of the causal mutation(s). For each candidate variant/gene, the main challenge is to validate the direct link between the identified variant and the patient's phenotype. Cellular or animal models are thus critical to confirm the link between a gene defect and a phenotype and to characterize the physiopathology associated with the identified genetic anomalies. Because of the high genetic homology between mice and men, the mouse model represents one of the best models for confirming and characterizing gene defects identified in human and this is particularly true for male reproductive disorders.

Mutant mice were traditionally generated using insertional mutagenesis or gene-targeting strategies (Wang et al., 2013). Using conventional gene targeted strategy, mutations are introduced by integrating exogenous repair templates through homologous recombination in embryonic stem (ES) cells. Injection of modified ES cells into blastocysts then allows the production of chimeric mice (Capecchi, 2005). This process is however laborious and expensive as the frequency of desired events was extremely rare (<0.01%) (Capecchi, 1989) and this is the reason why alternative technologies bypassing these difficulties were needed to accelerate this process. Recently, the use of artificial site-specific nucleases, such as zinc finger nuclease (ZFN) and transcriptional activator-like effector nucleases (TALENs) has enabled genome editing without the use of ES cells (Barman et al., 2017). However, difficulties associated with nucleases design and synthesis limited the widespread adoption of these technologies. The CRISPR (clustered regularly interspersed short palindromic repeats)/Cas9 (CRISPR-associated protein 9) technique which does not require the synthesis of target specific proteins has recently emerged as the method of choice for producing mutations in cells or animal models (Sapranauskas et al., 2011). The system requires the use of a single guide RNA (sgRNA) which will define the nucleotide sequence to be targeted and the Cas9 nuclease which will create a double strand break (DSB) underneath the RNA/DNA hybrid complex (Fig. 1A). The DSBs are usually repaired by the error-prone non-homologous end joining (NHEJ) mechanism that often creates small insertions and deletions (indels) thereby initiating truncating mutations (Fig. 1B). DSB can also be repaired by homology-directed repair (HDR) (Hsu et al., 2014) if a DNA template with homology to the sequence surrounding the DSB is found during the repair mechanism (Fig. 1C). The co-injection of a single stranded DNA (ssDNA) molecule homologous to the sequences flaking the targeted region will therefore favor HDR over NHEJ and will permit the replacement of the original sequence by the newly introduced sequence. Using a ssDNA slightly modified from the target genomic DNA permits to create a specific knock in (KI) or to insert a defined sequence that will be transcribed and translated. For the creation of mutant mice, the sgRNA and the Cas9 protein and potentially a ssDNA can be directly microinjected in a zygote to create a mutation at a predefined locus (Fig. 2). Homozygous mutant animals can be obtained after 1 or 2 back crossing permitting to create specific KO animals in only a few months (Fig. 2).

The recruitment of patients presenting with specific morphological anomalies of the spermatozoa enabled us to identify several genes associated with specific infertility phenotypes. We have demonstrated that approximately 80% of patients with large headed multiflagelled spermatozoa have a defective *AURKC* gene (Dieterich et al., 2009, 2007) and that in excess of 70% of men with round acrosomeless spermatozoa have a homozygous deletions of the *DPY19L2* gene (Coutton et al., 2012; Harbuz et al., 2011). The absence of spermatozoa in the ejaculate can also be caused by post meiotic defects and WES allowed to demonstrate that mutations in *SPINK2*, coding for a protease inhibitor targeting the acrosin could in fact prevent acrosome formation and block the spermiogenesis process (Kherraf et al., 2017). We now focus our research on

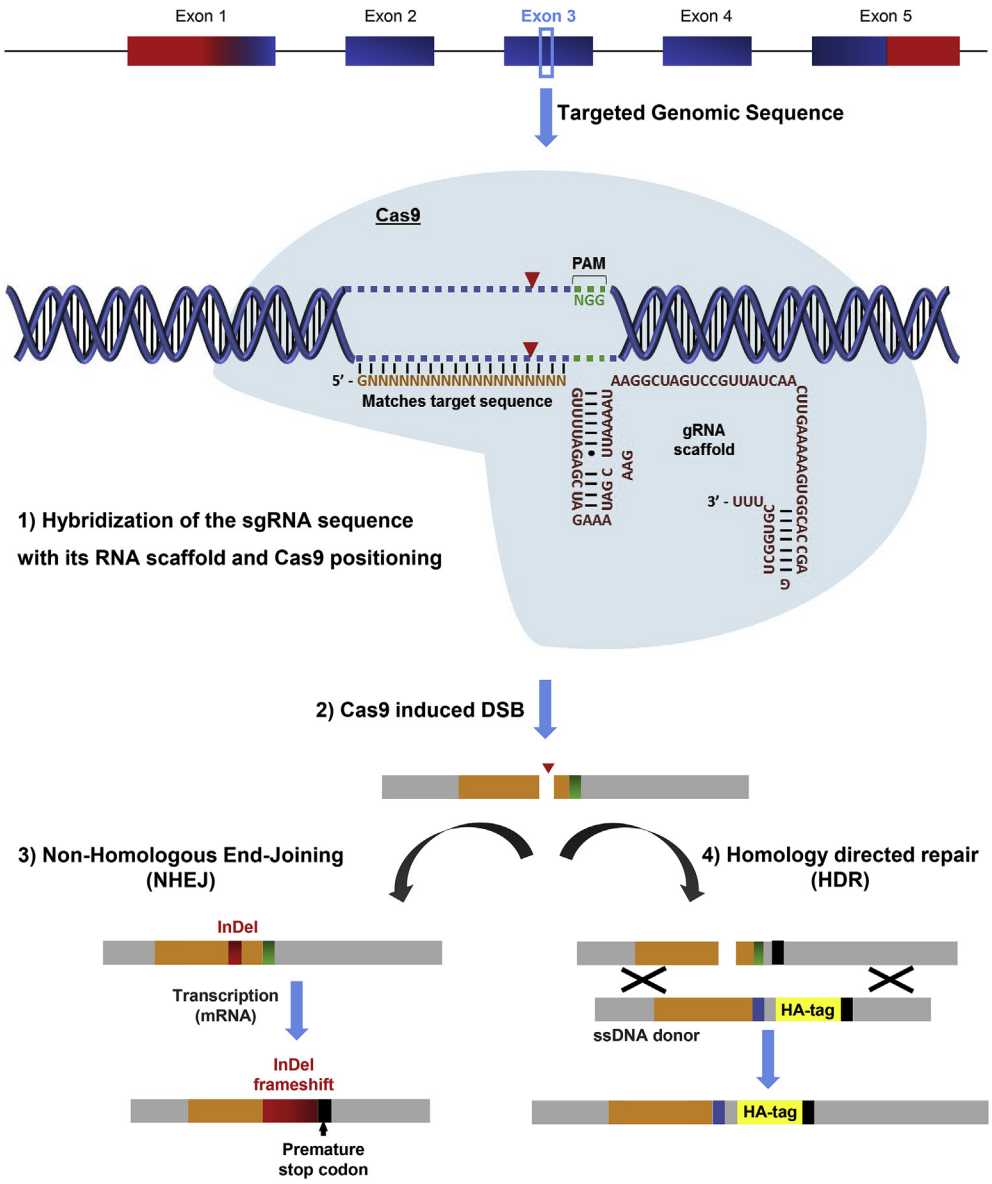

Fig. 1. The CRISPR/Cas9 system for genome editing.
1) The Cas9 endonuclease is directed to the targeted sequence by base pairing between the specific sgRNA (orange) and its target within the genomic DNA sequence. A "NGG" PAM sequence (Green NGG) located immediately downstream from the target sequence in the non-complementary strand is required for Cas9 recognition.
2) The Cas9 induces a DSB (red arrow-head) within the sgRNA targeted genomic DNA (orange box), normally between the third and the fourth bases from the PAM (orange box).
3) The error-prone NHEJ repair mechanism induces unpredictable insertions or deletions (InDels) represented by a red box, close to the initial DSB and usually within the sgRNA targeted sequence (orange box). The majority of InDels (which are not a multiple of 3 nucleotides) induce a frameshift that introduces a premature stop codon (black rectangle) which induces mRNA degradation (by non-sense mediated mRNA decay) and/or give a truncated non-functional protein. In most cases a null allele is obtained.
4) Co-injection of a ssDNA template homologous to the targeted sequence permits to repair the ds break by homology directed repair (HDR). Here the ssDNA template contains a small sequence (27 bp) coding for an HA-tag (yellow box) inserted immediately at the end of the protein of interest just before the stop codon (black box) to add a 9 amino acid tag to the targeted protein to facilitate its detection in-vivo. Compared to the targeted sequence, the ssDNA is also modified at the PAM sequence, the NGG (green box) is replaced by a TTG (blue box) to prevent new targeting by the sgDNA and ds breaks of the modified allele.

subjects presenting with Multiple Morphological Anomalies of the sperm Flagella (MMAF) characterized by the presence of short, bent, and coiled flagella and flagella of irregular width or absent mainly due to numerous ultrastructural defects of the axoneme leading to terato-asthenozoospermia. In 2014, we identified pathogenic mutations in the dynein axonemal heavy chain 1 (*DNAH1*) gene in 28% of the MMAF patients analyzed (Ben Khelifa et al., 2014). This result indicates that MMAF is genetically heterogeneous phenotype and that *DNAH1* is likely to be only one of the genes involved in this phenotype. Analysis of familial MMAF cases subsequently allowed us to confirm the implication of *DNAH1* in this syndrome (Amiri-Yekta et al., 2016). We then carried out WES analysis on 78 patients presenting with severe MMAF phenotype and identified *CFAP43* and *CFAP44* as two other genes involved in this phenotype (Coutton et al., 2018). Others have also reported mutations in *CFAP43* and *CFAP44* as important causes of MMAF in human (Tang et al., 2017; Sha et al., 2017). Further analysis of WES data allowed us to identify 9 other candidate genes which are currently being analyzed (data not published). To investigate the role of all these newly identified genes we performed gene

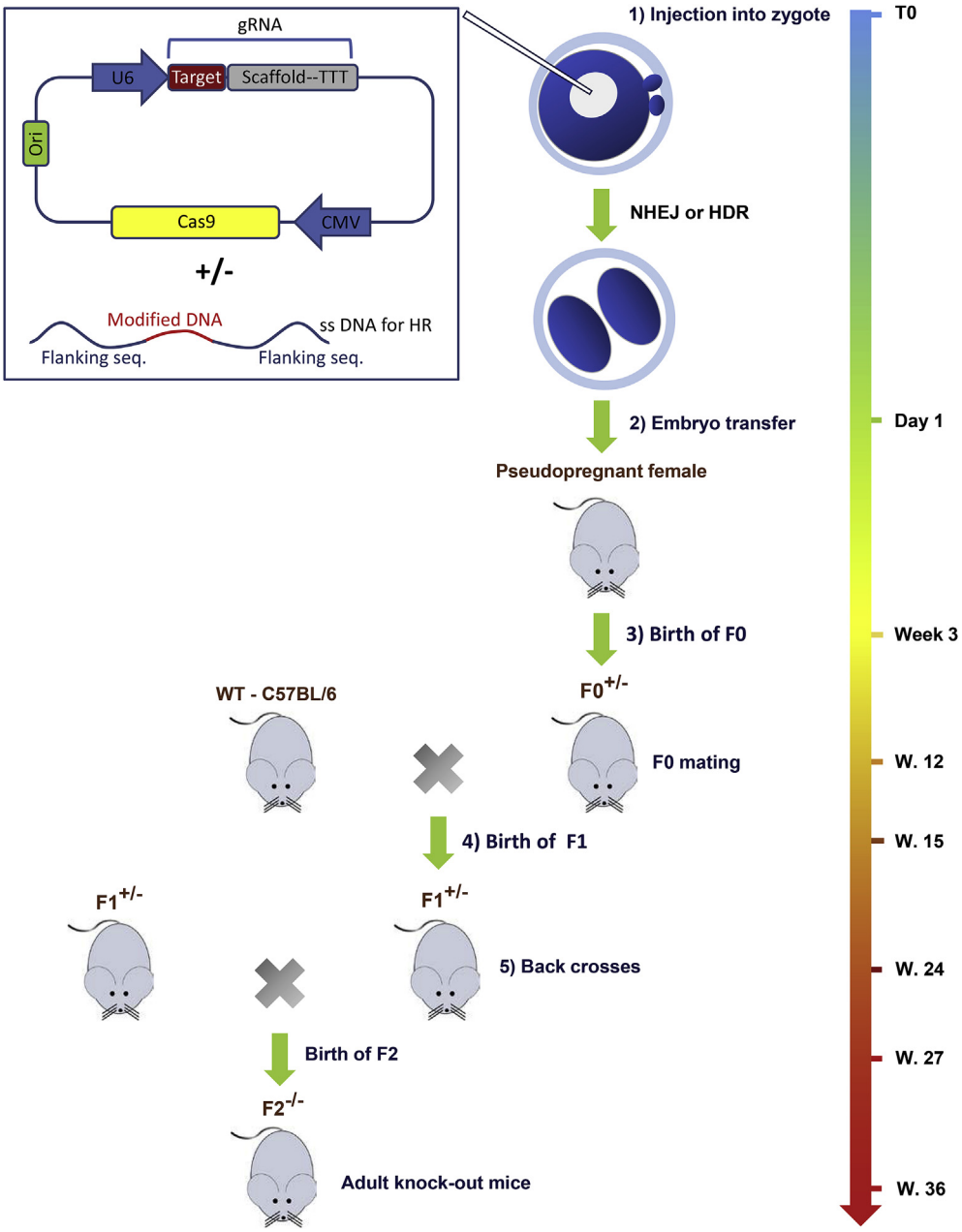

Fig. 2. Creation of KO/KI mice using the CRISPR/Cas9 system.
1) A minimal injection will contain a eukaryotic plasmid allowing the transcription of the sgRNA and the Cas9 (box on the left). The Cas9 protein will then be produced by the oocyte endogenous machinery. Knock in (KI) production can be achieved by the coinjection of a single stranded (ss) DNA for HDR. For insertion of a 5′ Tag, the sgRNA target (red line) is centered on the stop codon (TGA) marking the end of the coding sequence. The plasmid and, if necessary, the ssDNA are microinjected into the pronuclei of mice zygotes.
2) Obtained embryos are transferred into pseudopregnant females.
3) Genotyping of the obtained pups by Sanger sequencing allows the identification of founder mice (F0) carrying frameshift indels (or the correctly inserted sequence of choice). Because CRISPR/Cas9 system can remain active after several mitotic divisions founder mice can be mosaics carrying different mutations.
4) Breeding selected founder mice with wild-type (WT) C57BL/6J mice allows alleles segregation and transmission to the F1 mice generation. Sanger sequencing allows the identification of F1 mice with the same heterozygous frameshift indel.
5)Breeding these mice together leads to the production of F2 mice normally comprising 50% of heterozygotes, 25% of mutated homozygotes and 25% of WT mice. The mouse lineage is established and can be maintained for phenotypic characterization and further functional work.

invalidation in mouse using CRISPR/Cas9 technology for *Cfap43* and *Cfap44* and two of the 9 newly identified genes referred as *FlagC* and *FlagF*. Furthermore, as we could not obtain any specific antibodies for *FlagF* by conventional methods, we have generated a mouse lineage containing a HA-tagged *FlagF* gene. We describe here the techniques used and the results obtained to create these 5 transgenic mouse lines in a context of male infertility.

2. Material and methods

2.1. CRISPR/Cas9-mediated mice genome edition

The aim of this work was to generate 4 mouse lineages invalided for the *Cfap43, Cfap44, FlagC* and *FlagF* genes, respectively, to validate the candidate genes by assessing the spermatogenesis of the

corresponding knock-out mice. Additionally, the generation of a knock in (KI) was also carried out consisting of inserting 27 nucleotides coding for the HA tag at the end of the *FlagF* gene.

Generation of CRISPR/Cas9 edited mice was done at University of Geneva (UNIGE). All the procedures were done in Geneva until the birth of the modified litters. Mice were housed with unlimited access to food and water and were sacrificed by cervical dislocation after 8 weeks old, which means that they were pubescent and that their reproductive organs were fully established. All animal procedures were ran according to the Swiss and French guidelines on the use of animals in scientific investigations with the approval of the French local Ethical Committee (ComEth Grenoble N° 318, ministry agreement number #7128 UHTA-U1209-CA) and the Direction Générale de la Santé (DGS) for the State of Geneva.

All KO mice were created using the CRISPR/Cas9 technique as described in Figs. 1 and 2. To maximize the chances of generating deleterious mutations, two gRNA located in two distinct coding exons located at the beginning of the targeted genes were always used. For each gene the two gRNAs were inserted in two distinct plasmids, each plasmid also containing the Cas9 sequence. The Cas9 gene was driven by a CMV promoter and the gRNA and its RNA scaffold by an U6 promoter. Full plasmids (pSpCas9 BB-2A-GFP (PX458)) containing the specific sgRNA were ordered from Genescript (https://www.genscript.com/crispr-cas9-protein-crRNA.html). Both plasmids were co-injected in the zygotes' pronuclei as described in Fig. 2 at a concentration of 2.5 ng/μL. We note that we directly injected the plasmids as delivered by the supplier avoiding the *in vitro* production and purification of Cas9 proteins and sgRNA.

For the realization of the KI, one plasmid containing one sgRNA and the Cas9 was injected (5 ng/μL) with the single stranded DNA (50 ng/μL) for homology directed repair (Fig. 2). The single stranded DNA was 187 nt long and contained two 80 nucleotide-long arms homologous to the nucleotides located before and after *FlagF* stop codon, surrounding the 27 nucleotides encoding the HA Tag ending with a TAG stop codon (TAC CCA TAC GAT GTT CCA GAT TAC GCT TAG). The sgRNA sequence overlapped the native *Flagf* stop codon which was followed, 8 nucleotides further, by a TGG suitable as a Protospacer Adjacent Motif (PAM) sequence, which is an essential targeting component for efficient Cas9 binding and cleavage. PAM sequence consists of any nucleotide followed by two G (XGG). It is important to understand that if successful, the sgRNA will induce a double strand break near the site where the DNA modification is wanted (here at the end of the target gene to allow the insertion of a fusion HA Tag) and the break will either be repaired by HDR with the ssDNA and introduce the Tag, or, if unsuccessful by NHEJ. Due to the persistence of Cas9 and sgRNA several dsbreak can occur successively in the zygote or in early cleavage stage embryos. A successfully inserted Tag by HDR can therefore undergo a new DSB and repair by NHEJ thus altering the initial event and likely preventing the traduction of the Tag sequence. To limit this risk, in the ssDNA the TGG PAM sequence was changed to TTG. As the presence of a PAM sequence is necessary for DSB, this will normally prevent the occurrence of secondary events leading to the alteration of correctly inserted Tag. The synthetic ssDNA was purchased from IDT (https://www.idtdna.com/pages/products/dna-rna/ultramer-oligos). After the injection, zygotes were left for 4–6 h before being introduced into pseudopregnant host females and carried to term.

Edited founders were identified by Sanger sequencing from digit biopsies. Mice carrying the desired modification events (frameshift mutation or tag insertion) were crossed with C57BL6/J to ensure germline transmission and eliminate any possible mosaicism. Heterozygous animals with the same modification were then mated to generate homozygous offspring.

2.2. Mice genotyping strategy

DNA for genotyping was isolated from tail/digit biopsies. Tissues biopsies were digested in 200 μl of DirectPCR Lysis Reagent (Tail) (Viagen Biotech Inc, CA, USA) and 0.2 mg of proteinase K for 12–15 h at 55 °C followed by 1 h at 85 °C for proteinase K inactivation. The digested tissues were directly used for PCRs. Thirty-five cycles of PCR amplification were carried out with a hybridization temperature of 60 °C. Sequencing reactions were performed using BigDye Terminator v3.1 (Applied Biosystems). Sequence analyses were carried out on ABI 3130XL (Applied Biosystems). Sequences were analyzed using seqscape software (Applied Biosystems).

3. Results

3.1. Genetic results

WES had been performed on a total of 78 subjects with a MMAF phenotype (Coutton et al., 2018). After applying a series of computing filters permitting in particular to exclude all the non-rare variants (>1% in the ExAC database), we considered a gene to be a candidate gene if a homozygous loss of function variant was found in at least two subjects and if the gene was described to be highly expressed in the testis. A total of 11 genes corresponding to these criteria were identified (Table 1). Ten patients had a homozygous loss of function variant in *CFAP43*, six in *CFAP44* and six in *DNAH1*, three genes previously described as MMAF related genes (Coutton et al., 2018). Eight additional undisclosed autosomal genes were found to harbor homozygous mutations in at least two patients and are referred as *FLAG A-H*. *FLAGA* was mutated in 7 subjects, *FLAGB* in 4 subjects, *FLAG C and F* in 6 patients and *FLAG G* and *H* were found to be mutated in 4 patients. The variants localization and their respective impact on the FLAGC and FLAGF proteins are shown in Supp. Table 1. If all mutations are confirmed to be causal, a total of 49 subjects will have been diagnosed by WES with an overall efficiency of 63% (49/78).

To confirm the involvement of these genes in MMAF and to further characterize their function we decided to create KO animals for *Cfap43, Cfap44* (Coutton et al., 2018) and *FlagC and FlagF* (characterization still in progress). Seven subjects carried a homozygous *FlagA* deleterious variant but as this gene had already been described to be coding for an axonemal protein and the creation of KO animals was not undertaken for this gene. Finally, KO for the other genes (*FlagB, D, E, G, H*) may be done at a later stage.

Table 1
List of autosomal genes identified as candidate after exome sequencing of 78 MMAF patients and number of patients harboring a homozygous deleterious homozygous mutation.

Gene	Number of mutated subjects	% of tested subjects
CFAP43 [a]	10	12.8
FLAGA	7	9.0
CFAP44[a]	6	7.7
DNAH1	6	7.7
FLAGB	4	5.1
FLAGC[a]	3	3.8
FLAGD	3	3.8
FLAGE	3	3.8
FLAGF[a,b]	3	3.8
FLAGG	2	2.6
FLAGH	2	2.6
Total	49	62.8

[a] Indicates the genes for which KO mice were produced by CRISPR/Cas9.
[b] The gene for which a HA Tag was inserted. Identity of FLAG (for Flagellar gene) A-F is currently undisclosed.

3.2. Creation of F0 KO mice for Cfap43, Cfap44, FlagC, FlagF and of a HA tagged FlagF gene using the CRISPR/Cas9 technique

3.2.1. Creation of KO mice for Cfap43

Two separate series of injections were performed to generate mutated mice carrying frameshift indels. Data related to injected/transferred zygotes were not recorded for these first two experiments. The first injection allowed the production of 12 animals but none carried a mutation in either of the targeted exons (Supp. Table 2). The second injection resulted in 9 births with 5 mutated mice. Two mice had heterozygous complex indels, probably caused by the presence of two different variants on both alleles (not characterized) in the target region 1 (TR1), two mice had a heterozygous deletion (delAAGG or delTGTGAAGGGC) in the target region 2 (TR2) and a fifth mouse had a homozygous mutation delG in the TR2 (Supp. Tables 1 and 2). By chance, this latter mouse was a male and enabled us to analyze the morphology of the sperm of a KO *Cfap43* animal without further crossing. All the observed spermatozoa were immotile with very short flagella, typical of the MMAF phenotype (Coutton et al., 2018). Although it was impossible to generate a lineage from this infertile male, this first result strongly suggested that *CFAP43* was one of the genes responsible of the MMAF syndrome. Because we could not rule out an off target effect, a new colony was established by mating the F0 mouse carrying the delAAGG variant with a C57BL/6J WT animal for phenotype confirmation and further investigations. Of the 15 F1 pups obtained in two separate litters, 5 (33%) inherited the genotyped parental mutation (Supp. Table 3) and three additional F1 (20%) harbored a four nucleotides insertion (insTCCA) that had not been detected in the mutant parent (Supp. Tables 1 and 2). Homozygous *Cfap43*$^{-/-}$ delAAGG F2 males generated from F1 animals were infertile. All spermatozoa showed similar defects to those observed in the initial F0 homozygous delG mouse and were short (approximately 1/5th of the normal size) or absent and did not show any movement (Fig. 3).

3.2.2. Creation of KO mice for Cfap44

A total of three injections were performed in order to invalidate this gene. Despite the large number of pups obtained (n = 26), only one mouse was mutated and had an insertion (insTCAGATA) in the TR1 (Supp. Tables 1 and 2). Backcrossing of this mouse permitted to obtain three F1 litters (Supp. Table 3). Out of the 27 newborns, 8 mice (30%) had inherited the parental mutation (insTCAGATA). Two additional mutations (delTAC and delTATA in same target region, TR1) were found in a total of six mice (23%). Breeding were done for InsTCAGATA and delTATA animals and homozygous males were generated for both these *Cfap44* mutations. All *Cfap44*$^{-/-}$ male mice were infertile. Their sperm flagella were of normal size but often presented irregular caliber of the midpiece (Fig. 3). All spermatozoa were however immotile, often with a mild vibrating pulse.

3.2.3. Creation of KO mice for FlagC, FlagF and tagged mice FlagF-HA

A total of five injections were carried out for *FlagC, FlagF and FlagF-HA* (Supp. Table 2). An average of 139 zygotes were injected per session. Seventy percent of the zygotes survived the 1-cell stage and could be transferred into pseudopregnant females. On average 30 embryos were transferred per female. The transfer of 479 injected embryos permitted the birth of 65 pups indicating that only 14% of the embryos transferred led to a live birth (Supp. Table 2). Three of the five injections realized permitted to obtain >50% mutated live pups (Supp. Table 2). At least two mutated pups were obtained following each injection session.

Only one *FlagC* targeted injection was performed which permitted to obtain two F0 heterozygous animals. The first carried two uncharacterized events on TR1 and the second had a heterozygous delTAC on TR1 and a 12 nucleotide deletion in TR2 (delAAACCCGTTAGC). Following the backcrossing of the second mouse, 7 out of 19 (37%) newborn inherited the parental mutated allele (delTAC + delAAACCCGTTAGC) and 5 (26%) presented an insT in TR1. *FlagC*$^{-/-}$ animals have just been produced. Homozygous male are unfertile and we observed that all spermatozoa present a

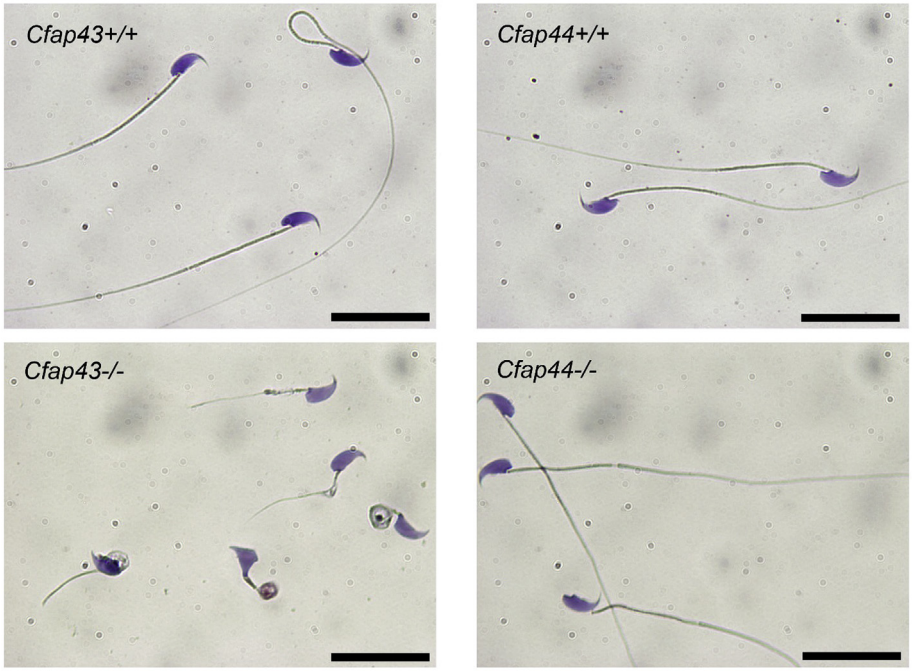

Fig. 3. Morphology of spermatozoa from *Cfap43* and *Cfap44* KO mice.
All spermatozoa from *Cfap43*$^{-/-}$ mice were short (approximately 1/5th of the normal size) or absent. Spermatozoa from *Cfap44*$^{-/-}$ mice were of normal size but often presented a kink at the end of the mid-piece. They did not show any progressive movement but sometimes a mild vibration. Scale bar 20 μm.

short flagella, a feature typical of the MMAF phenotype and very similar to what was observed on Cfap43$^{-/-}$ mice (data not shown). Creation of KO *FlagF* animals was also successful. Seventeen animals were created following two series of injections. A delG mutation was identified in one homozygous female mouse. Two animals carried a heterozygous event in TR1 (delTTCG, delCAGCTGGAA) and one had a complex event (uncharacterized) with the presence of a complex genomic rearrangement. Furthermore one F0 had a 12 nucletides insertion in TR2 (insAATGTACATAG). Generation of F1 animals carrying the delTTCG is still in progress.

Finally, we decided to insert an HA tag at the end of *FlagF* gene to compensate the lack of specific antibodies. The co-injection of the plasmid with the target RNA and the Cas9 gene along with the single stranded DNA for HDR was very successful in creating mutated pups. Six animals had the correct HA tag inserted by HDR, four of which had an indel on the other allele (Supp. Tables 1 and 2). Eight animals had a heterozygous indel created by NHEJ. In total 9 animals were compound heterozygotes (with two indels or one indel and one TAG insertion or perhaps sometimes a third event, possibly in mosaic. Due to the complexity of the events, we estimate that at least 12 events could not be characterized.

The two mice with only the HA tag insertion were bred with WT C57BL/6J animals to generate *FlagF* tagged mice. FlagF-HA homozygous males showed a normal fertility demonstrating that the tag does not interfere with the protein function. Studies of FlagF-HA localization and pulldown experiments are currently ongoing.

3.3. Size and position (in regards to the PAM) of the obtained mutations

Overall, following 10 series of injection targeting a total of 9 distinct sequences, we obtained (in F0 and F1) a total of 24 characterized individual *de novo* mutations (with a total of 20 different mutations). All the characterized mutations were indels and the HA tag was inserted correctly in 6 F0 animals. In addition, there were at least 18 bi-allelic heterozygous variants, often in mosaic that were not characterized. Deletions removed 1 to 21 nucleotides and insertions added 1 to 11 nucleotides. Approximately 80% of the indels were deletions. Half the events were small deletion of −1 to −4 nucleotides. The longest deletion and insertion were 15 and 11 nucleotides long respectively (Supp. Table 4 and Fig. 4).

All observed indels were located less than 20 nucleotides away from the PAM and the median point for indels was located 4 nucleotides before the PAM's first nucleotide. Only 4 events concerned some nucleotides located after the PAM (Supp. Table 4 and Fig. 5).

3.4. Overall results

Overall a total of 10 injection sessions were realized and all but three permitted to obtain at least one mutated pup. We can see that despite the three failures, we obtained an average of 3.4 mutated pups per injection session, highlighting the fact that the injections were very successful in producing mutated pups (Supp. Table 2).

Mutated animals were obtained for all genes investigated. Phenotypic characterization of the mutated animals has so far only been done for *Cfap43* and *Cfap44* genes. We obtained two independent mouse strains or homozygous animals for *Cfap43* and *Cfap44* with different insertions/deletions of a few nucleotides, all inducing a translational frameshift expected to lead to complete absence of the protein or production of a truncated protein. We observed in each case the same reproductive phenotype, so for *Cfap43* we restricted our study to a strain with a 4 bp deletion in the exon 21 (delAAGG) and for *Cfap44* we focused on a strain with a 7

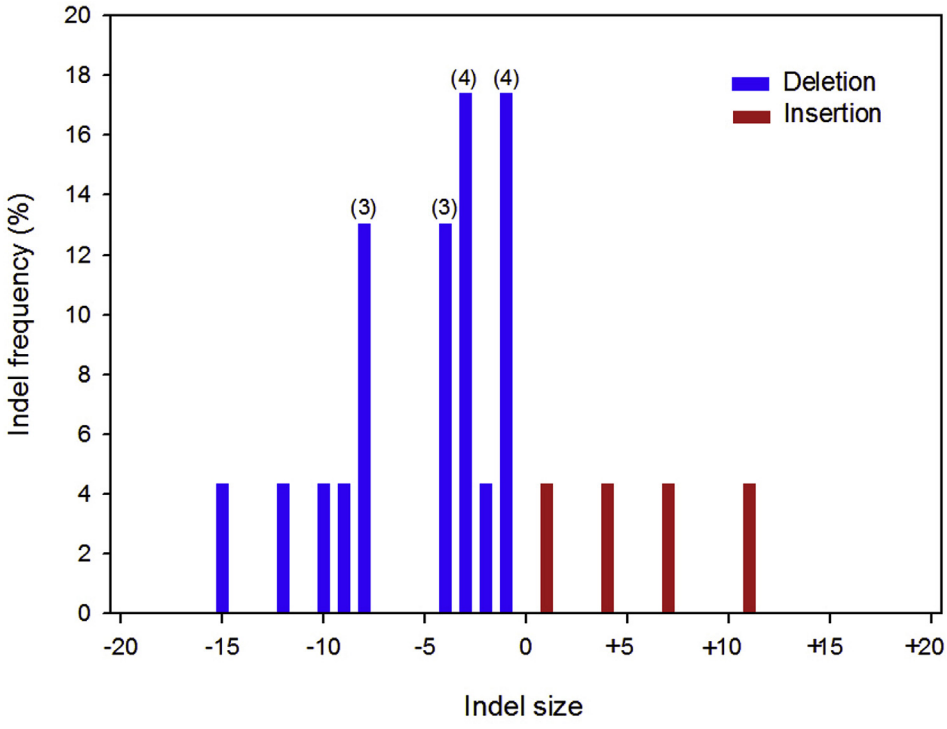

Fig. 4. Distribution of all *de novo* indels identified according to their size.
The graph shows the frequency of the indels according to their size in nucleotide. We counted all events observed in F0 animals as well as the new, non-parental events observed in F1. Identical indels identified in several F0 are independent mutational events and were all taken into consideration whereas identical non-parental indels transmitted by the same F0 parent were considered as a single event (due to parental germline mosaicism) and were counted only once.
As the HDR mechanism does not result in the production of indels, insertions of the HA tag which occurred during *FlagF-HA* production were not taken into consideration here. Are presented here all the observed NHEJ events (including those which took place following injections for *FlagF-HA* production). All indels are described in Supp. Table 2.

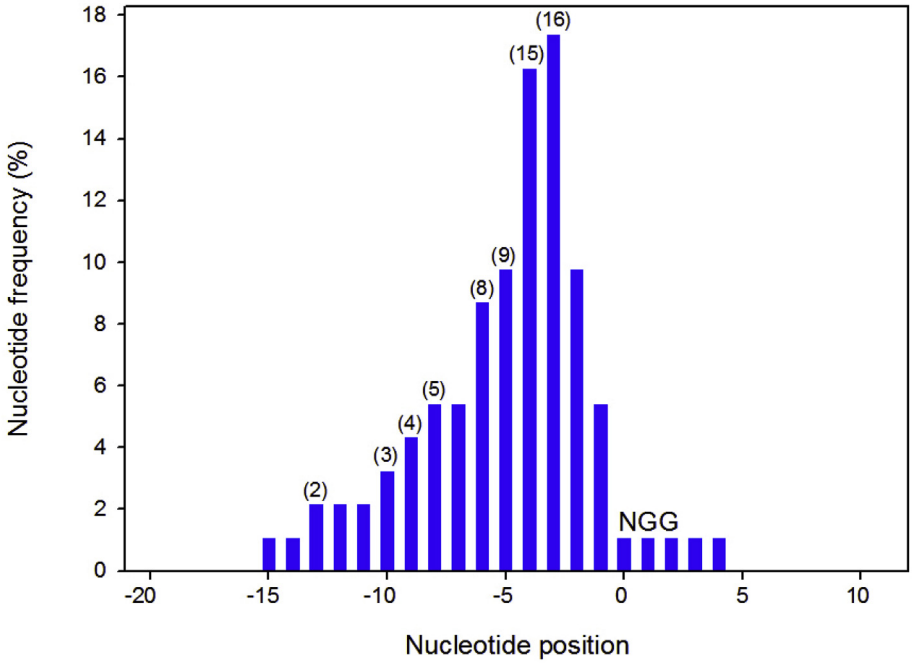

Fig. 5. Localization of NHEJ events on the sequence surrounding the PAM.
As in Fig. 4, all F0 and F1 *de novo* indels are taken into consideration. The plot indicates the number of times (frequency) a nucleotide was concerned by an indel. For the deletions, all deleted nucleotides were taken into account. For the insertions, both nucleotides located before and after the insertion were considered as affected by the NHEJ and counted. When an event occurred within a single nucleotide repeat, the most 5′ nucleotide was taken into consideration. All indels are described in Supp. Table 2. NGG corresponds to the PAM sequence.

bp insertion in exon 3 (InsTCAGATA). RT-PCR was performed on testis ARN from *Cfap43*$^{-/-}$ and *Cfap44*$^{-/-}$ mice which confirmed the production of abnormal transcripts in both mutants leading to a premature stop codon.

Reproductive phenotype was studied for both KO mice models. Homozygous KO males exhibited complete infertility when mated with WT females. Sperm concentrations fell within the normal values for mouse but all spermatozoa were immotile. For *Cfap43*$^{-/-}$, 100% of sperm had a short flagella whereas *Cfap44*$^{-/-}$ had a flagella of normal length with some moderate morphological abnormalities but with a complete absence of motility (Fig. 3). In both cases the axonemal structure was altered, often with an absence of the central microtubule pair. We note that the short flagella observed in *Cfap43*$^{-/-}$ animals is one of the hallmark of the MMAF phenotype in human, the KO model thus producing a faithful reproduction of the human anomalies. Sperm from *Cfap44*$^{-/-}$ animals do not present any obvious morphological anomalies of the flagella but are immotile and present the same ultrastructural defects observed in human. This confirms the human genetic results but highlights some slight differences between human and mouse flagellar growth (Coutton et al., 2018).

4. Discussion

Whole exome sequencing is a powerful technology that enables discovering new candidate genes implicated in different human disorders such as infertility. Validation of these genes through the study of transgenic animal models is important and enables to greatly improve our understanding of spermatogenesis and male reproduction. We observed here that CRISPR/Cas9 delivers its promises as mutated F0 animals were usually obtained in one month after the first injection and stable lineages producing homozygous animal could be obtained in approximately 6 months. Interestingly, we observed that the three KO models we have created (i.e. the *Cfap43*, *Cfap44 and FlagC* genes) reproduced the human phenotype. This confirms that mouse is a good model to study human male infertility and spermatogenesis. Furthermore, we have worked on several other models and have so far always observed a good correlation between the mouse and the human phenotype: we observed for instance that *Dpy19l2*$^{-/-}$ mice perfectly mimicked the globozoospermia phenotype (Pierre et al., 2012) and *Spink2*$^{-/-}$ mice had azoospermia, like our mutated patients (Kherraf et al., 2017).

4.1. Frequent occurrence of F0 mosaic

It has been reported that gRNA and Cas9 can be passed on through several successive mitoses initiating double strand break and NHEJ in different daughter cells thus producing mosaic animals carrying different mutations in different tissues (Inui et al., 2014; Midic et al., 2017; Yen et al., 2014). Here F0 animal were genotyped using tail/digit DNA, containing mostly bone, cartilage, muscle and skin tissues. We observed that all bred F0 animals did not only pass the initially identified mutation but that 23% of their offspring carried one of two different indels not present in the F0's tail. Most of these mutations were found in several siblings thus indicating that the analyzed F0 presented a germinal mosaic, often with three different mutations. As such variants were not detected in the tail/digit biopsies it seems that germ cell progenitors have been more subjected to CRISPR induced double strand breaks than the progenitors of the tested somatic cells. However, during the course of Sanger sequencing we observed a few abnormal electropherograms of very low intensity overlapping the normal sequence that could sign of the presence of low level mosaicism. When breeding these F0 animals we never obtained any mutations in the F1s, thus indicating that these abnormal sequences could have been the signs of low level somatic mosaicism.

The high rate of mosaicism observed here could be due in part to the fact that we chose to inject plasmids permitting the expression of the sgRNA and the Cas9 protein. It is likely that the plasmids will not be as quickly degraded than native RNA and protein thus permitting to induce some mutational even after several cell divisions. This can be an advantage as we could obtain some new mutations and an increased number of mutated animals. It however complicates the analysis and to limit the extent of mosaicism we can suggest to reduce the quantity of plasmid injected or to directly inject the protein and RNA. Interestingly, it was observed in human embryos that the rate of mosaicism was reduced when injecting the MI oocyte directly during the fertilization by ICSI rather than to inject the zygote (Ma et al., 2017) as is usually done and as was done here. Earlier injection of the CRISPR/Cas9 elements could therefore be an interesting alternative to reduce the occurrence of mosaicism.

4.2. Localization of the mutational events and off target mutations

The PAM, a short sequence motif adjacent to the gRNA-targeted sequence on the invading DNA, plays an essential role in Cas9 binding and DNA break (Shah et al., 2013). In our experience a suitable PAM sequence can always be found, especially if the objective is to create KO animals allowing great flexibility for choosing suitable target regions. For the creation of KI, gRNA has to be located near the target region leaving fewer choices and thus restricting the number of available gRNA sequences. We only have one experience with KI production but we had excellent results and could quickly obtain animals with the desired insertion, these results confirms that CRISPR/Cas9 is an efficient tool to generate KI animals (Seruggia and Montoliu, 2014). Double strand breaks normally occur 3 nucleotide prior the PAM sequence. As the breaks are repaired we cannot have a direct localization of the break. What can be observed is the localization of the modified nucleotide during the NHEJ repair process. We observed in Fig. 5 that the nucleotides that are most often modified are in fact the nucleotides located in positions 3 and 4 before the PAM. These results thus confirm that the DSB occurs most often between these two nucleotides and confirm that the obtained indels are located within the target sequence.

Many studies describe a relative high level of off-target mutagenesis induced by the CRISPR-Cas9 system when injected into cultured human cells (Fu et al., 2013; Kuscu et al., 2014) whereas many others showed a low incidence of this undesirable effect when this system is injected into mouse zygotes (Hryhorowicz et al., 2017; Iyer et al., 2015). Concerning our experience, we only sequenced the targeted sequences and have no way of assessing the frequency of such events. We therefore expect that Cas9 usage will slightly increase the overall rate of *de novo* indels. Simple statistic tell us that 90% of these events will not occur in coding sequence and an even greater percentage will have no deleterious effect. To be absolutely sure that the observed phenotype is due to the selected mutation, we used the following two strategies: 1) breeding with WT C57BL6/J animal and use F3-F5 animals. As off target events are unlikely to be allelic with the targeted sequence, the selection and backcrossing of the selected KO/KI will quickly eliminate the unwanted mutations. 2) Analyze several animals with different mutations. As we have seen here the CRISPR/Cas9 technique allows to obtain several animals with different indels. Furthermore, some F0 can have a homozygous mutation. An acceptable solution is to phenotype one or two F0 homozygous animal and to establish a stable line with a different mutation. The observation of the same phenotype in several animals with different indels rules out the possibility of a non-specific effect from an off target event.

4.3. Technical difficulties

The microinjection of Cas9-sgRNA into embryos requires a relatively high skill level. Recently, electroporation was used as an alternative to microinjection and demonstrated a high efficiency for introduction of Cas9-sgRNA into zygotes (Kaneko, 2017; Wefers et al., 2017). The injection can however be easily performed by any staff trained for mouse ICSI. As any highly technical gesture, there is a learning curve. We observed that our results improved with time (we had more births and mutations in the later injections). We believe that this might be partly related with skills improvement of the technical staff.

In our experience the use of “all in one” vectors (with the sgRNA and Cas9) and its direct injection into the male pronucleus saved much time and many operator dependent operations (such as RNA isolation and purification).

We note that some sgRNA did not permit to obtain any mutated animals (or very few) but the co-injection of two sgRNA always permitted to obtain several mutated pups. The use of two sgRNA located within the same gene has been described to mediate large deletions loosely delimited by the two sequences targeted by the sgRNAs (Chen et al., 2014; Han et al., 2014). In our experience such events are rare as we did evidenced them. Here, our main goal was to produce KO animals and the occurrence of such large deletion would be interesting as they would necessarily be deleterious and would have the added advantage of being easy to detect by a simple PCR. As we did not observe any disadvantage associated with the co-injection of two sgRNA we recommend this strategy.

4.4. Timing of CRISPR/Cas9 gene editing projects

Overall a CRISPR/Cas9 project can be divided into three steps: 1. target sequence selection, design of mutant alleles and preparation/ordering of plasmids/reagents, 2. microinjection or electroporation of zygotes and embryo transfer, and 3. genotyping of founder mice, back crossing and phenotyping. The first step only take a few hours of intellectual work and 2–3 weeks of production, usually by a service provider. In step 2 female mice are treated with hormones for superovulation starting three days before zygote microinjections. Upon the mating of superovulated females to males, zygotes are collected the next day, microinjected with CRISPR/Cas9 reagents and transferred into foster mothers, which give rise to birth after 3 weeks. Step 3 is the longest and usually takes approximately 6 months (Fig. 2). Biopsies can be taken from the pups derived from microinjected zygotes at the age of 10 days and used for genotyping. Initial genotyping will have to be done by double stranded sequencing of the target region, usually taking approximately 2 weeks. In many cases CRISPR/Cas9 microinjection permit the birth of mutant F0 founders that can be mated to WT animals when they reach fertility around 9 weeks. Considering that mice will reach reproductive age at 9 weeks, the expected timeframe to obtain the first mutated mature F1 animals is therefore of 24 weeks (2 gestation periods of 3 weeks and 2 periods of sexual maturation of 9 weeks) and mature F1 progeny will be available after 36 weeks (See Fig. 2). Mutated F0 pups recovered from manipulated zygotes are however not always successfully produced and a new series of injection must then be performed. It will usually take at least a month to reschedule the injection procedure.

5. Conclusion

Our genetic study on infertile subjects with flagellar defects (MMAF phenotype) permitted to identify some very plausible mutations located in 11 candidate genes in 63% of the analyzed subjects. This clearly confirms the interest of WES for both

pathological gene identification and diagnostic purpose in the context of male infertility. We also confirmed that the CRISPR/cas9 technique is very efficient to create KO and KI animals and is a promising strategy to study the function of candidate genes for infertility while permitting to convincingly confirm their pathogeny.

Conflicts of interest

The authors declare no conflict of interest.

Acknowledgments

This work was mainly supported by the following grants: The "MAS-Flagella" project financed by French ANR and the DGOS for the program PRTS 2014 to PR and CA and the Swiss National Science Foundation (Sinergia grant N° CRSII5_171007) to SN.

Appendix A. Supplementary data

Supplementary data related to this article can be found at https://doi.org/10.1016/j.mce.2018.03.002.

References

Alkuraya, F.S., 2016. Discovery of mutations for Mendelian disorders. Hum. Genet. 135, 615–623. https://doi.org/10.1007/s00439-016-1664-8.

Amiri-Yekta, A., Coutton, C., Kherraf, Z.-E., Karaouzène, T., Le Tanno, P., Sanati, M.H., Sabbaghian, M., Almadani, N., Gilani, S., Ali, M., Hosseini, S.H., Bahrami, S., Daneshipour, A., Bini, M., Arnoult, C., Colombo, R., Gourabi, H., Ray, P.F., 2016. Whole-exome sequencing of familial cases of multiple morphological abnormalities of the sperm flagella (MMAF) reveals new DNAH1 mutations. Hum. Reprod. 31, 2872–2880. https://doi.org/10.1093/humrep/dew262.

Barman, H.K., Rasal, K.D., Chakrapani, V., Ninawe, A.S., Vengayil, D.T., Asrafuzzaman, S., Sundaray, J.K., Jayasankar, P., October 2017. Gene editing tools: state-of-the-art and the road ahead for the model and non-model fishes. Transgenic Res. 26 (5), 577–589. https://doi.org/10.1007/s11248-017-0030-5.

Ben Khelifa, M., Coutton, C., Zouari, R., Karaouzène, T., E, D., Pernet-Gallay, K., Merdassi, G., Satre, V., Jouk, P.S., Hennebicq, S., Grunwald, D., Escalier, D., Pernet-Gallay, K., Jouk, P.S., Thierry-Mieg, N., Touré, A., Arnoult, C., Ray, P.F., 2014. Mutations in DNAH1, which encodes an inner arm heavy chain dynein, lead to male infertility due to multiple morphological abnormalities of the sperm flagella. Am. J. Hum. Genet. 94 (1), 94–104.

Capecchi, M.R., 1989. Altering the genome by homologous recombination. Science 244, 1288–1292.

Capecchi, M.R., 2005. Gene targeting in mice: functional analysis of the mammalian genome for the twenty-first century. Nat. Rev. Genet. 6, 507–512. https://doi.org/10.1038/nrg1619.

Chen, X., Xu, F., Zhu, C., Ji, J., Zhou, X., Feng, X., Guang, S., 2014. Dual sgRNA-directed gene knockout using CRISPR/Cas9 technology in Caenorhabditis elegans. Sci. Rep. 4. https://doi.org/10.1038/srep07581.

Coutton, C., Zouari, R., Abada, F., Khelifa, M.B., Merdassi, G., Triki, C., Escalier, D., Hesters, L., Mitchell, V., Levy, R., Sermondade, N., Boitrelle, F., Vialard, F., Satre, V., Hennebicq, S., Jouk, P.-S., Arnoult, C., Lunardi, J., Ray, P.F., 2012. MLPA and sequence analysis of DPY19L2 reveals point mutations causing globozoospermia. Hum. Reprod. 27, 2549–2558. https://doi.org/10.1093/humrep/des160.

Coutton, C., Escoffier, J., Martinez, G., Arnoult, C., Ray, P.F., 2015. Teratozoospermia: spotlight on the main genetic actors in the human. Hum. Reprod. Update 21, 455–485. https://doi.org/10.1093/humupd/dmv020.

Coutton, C., Vargas, A.S., Amiri-Yekta, A., Kherraf, Z.-E., Ben Mustapha, S.F., Le Tanno, P., Wambergue-Legrand, C., Karaouzène, T., Martinez, G., Crouzy, S., Daneshipour, A., Hosseini, S.H., Mitchell, V., Halouani, L., Marrakchi, O., Makni, M., Latrous, H., Kharouf, M., Deleuze, J.-F., Boland, A., Hennebicq, S., Satre, V., Jouk, P.-S., Thierry-Mieg, N., Conne, B., Dacheux, D., Landrein, N., Schmitt, A., Stouvenel, L., Lorès, P., El Khouri, E., Bottari, S.P., Fauré, J., Wolf, J.-P., Pernet-Gallay, K., Escoffier, J., Gourabi, H., Robinson, D.R., Nef, S., Duliouste, E., Zouari, R., Bonhivers, M., Touré, A., Arnoult, C., Ray, P.F., 2018. Mutations in CFAP43 and CFAP44 cause male infertility and flagellum defects in Trypanosoma and human. Nat. Commun. 9. https://doi.org/10.1038/s41467-017-02792-7.

Dieterich, K., Soto Rifo, R., Karen Faure, A., Hennebicq, S., Amar, B.B., Zahi, M., Perrin, J., Martinez, D., Sèle, B., Jouk, P.-S., Ohlmann, T., Rousseaux, S., Lunardi, J., Ray, P.F., 2007. Homozygous mutation of AURKC yields large-headed polyploid spermatozoa and causes male infertility. Nat. Genet. 39, 661–665. https://doi.org/10.1038/ng2027.

Dieterich, K., Zouari, R., Harbuz, R., Vialard, F., Martinez, D., Bellayou, H., Prisant, N., Zoghmar, A., Guichaoua, M.R., Koscinski, I., Kharouf, M., Noruzinia, M., Nadifi, S., Sefiani, A., Lornage, J., Zahi, M., Viville, S., Sele, B., Jouk, P.-S., Jacob, M.-C., Escalier, D., Nikas, Y., Hennebicq, S., Lunardi, J., Ray, P.F., 2009. The Aurora Kinase C c.144delC mutation causes meiosis I arrest in men and is frequent in the North African population. Hum. Mol. Genet. 18, 1301–1309. https://doi.org/10.1093/hmg/ddp029.

Fu, Y., Foden, J.A., Khayter, C., Maeder, M.L., Reyon, D., Joung, J.K., Sander, J.D., 2013. High-frequency off-target mutagenesis induced by CRISPR-Cas nucleases in human cells. Nat. Biotechnol. 31, 822–826. https://doi.org/10.1038/nbt.2623.

Han, J., Zhang, J., Chen, L., Shen, B., Zhou, J., Hu, B., Du, Y., Tate, P.H., Huang, X., Zhang, W., 2014. Efficient in vivo deletion of a large imprinted lncRNA by CRISPR/Cas9. RNA Biol. 11, 829–835. https://doi.org/10.4161/rna.29624.

Harbuz, R., Zouari, R., Pierre, V., Ben Khelifa, M., Kharouf, M., Coutton, C., Merdassi, G., Abada, F., Escoffier, J., Nikas, Y., Vialard, F., Koscinski, I., Triki, C., Sermondade, N., Schweitzer, T., Zhioua, A., Zhioua, F., Latrous, H., Halouani, L., Ouafi, M., Makni, M., Jouk, P.-S., Sèle, B., Hennebicq, S., Satre, V., Viville, S., Arnoult, C., Lunardi, J., Ray, P.F., 2011. A recurrent deletion of DPY19L2 causes infertility in man by blocking sperm head elongation and acrosome formation. Am. J. Hum. Genet. 88, 351–361. https://doi.org/10.1016/j.ajhg.2011.02.007.

Hryhorowicz, M., Lipiński, D., Zeyland, J., Słomski, R., 2017. CRISPR/Cas9 immune system as a tool for genome engineering. Arch. Immunol. Ther. Exp. 65, 233–240. https://doi.org/10.1007/s00005-016-0427-5.

Hsu, P.D., Lander, E.S., Zhang, F., 2014. Development and applications of CRISPR-Cas9 for genome engineering. Cell 157, 1262–1278. https://doi.org/10.1016/j.cell.2014.05.010.

Inui, M., Miyado, M., Igarashi, M., Tamano, M., Kubo, A., Yamashita, S., Asahara, H., Fukami, M., Takada, S., 2014. Rapid generation of mouse models with defined point mutations by the CRISPR/Cas9 system. Sci. Rep. 4, 5396. https://doi.org/10.1038/srep05396.

Iyer, V., Shen, B., Zhang, W., Hodgkins, A., Keane, T., Huang, X., Skarnes, W.C., 2015. Off-target mutations are rare in Cas9-modified mice. Br. J. Pharmacol. 12, 479, 479. https://doi.org/10.1038/nmeth.3408.

Kaneko, T., 2017. Genome editing in mouse and rat by electroporation. Methods Mol. Biol. Clifton NJ. 1630, 81–89. https://doi.org/10.1007/978-1-4939-7128-2_7.

Kherraf, Z.-E., Christou-Kent, M., Karaouzene, T., Amiri-Yekta, A., Martinez, G., Vargas, A.S., Lambert, E., Borel, C., Dorphin, B., Aknin-Seifer, I., Mitchell, M.J., Metzler-Guillemain, C., Escoffier, J., Nef, S., Grepillat, M., Thierry-Mieg, N., Satre, V., Bailly, M., Boitrelle, F., Pernet-Gallay, K., Hennebicq, S., Fauré, J., Bottari, S.P., Coutton, C., Ray, P.F., Arnoult, C., 2017. SPINK2 deficiency causes infertility by inducing sperm defects in heterozygotes and azoospermia in homozygotes. EMBO Mol. Med. 9, 1132–1149. https://doi.org/10.15252/emmm.201607461.

Kuscu, C., Arslan, S., Singh, R., Thorpe, J., Adli, M., 2014. Genome-wide analysis reveals characteristics of off-target sites bound by the Cas9 endonuclease. Nat. Biotechnol. 32, 677–683. https://doi.org/10.1038/nbt.2916.

Ma, H., Marti-Gutierrez, N., Park, S.-W., Wu, J., Lee, Y., Suzuki, K., Koski, A., Ji, D., Hayama, T., Ahmed, R., Darby, H., Dyken, C.V., Li, Y., Kang, E., Park, A.-R., Kim, D., Kim, S.-T., Gong, J., Gu, Y., Xu, X., Battaglia, D., Krieg, S.A., Lee, D.M., Wu, D.H., Wolf, D.P., Heitner, S.B., Belmonte, J.C.I., Amato, P., Kim, J.-S., Kaul, S., Mitalipov, S., 2017. Correction of a pathogenic gene mutation in human embryos. Nature 548, 413. https://doi.org/10.1038/nature23305.

Midic, U., Hung, P.-H., Vincent, K.A., Goheen, B., Schupp, P.G., Chen, D.D., Bauer, D.E., VandeVoort, C.A., Latham, K.E., 2017. Quantitative assessment of timing, efficiency, specificity and genetic mosaicism of CRISPR/Cas9-mediated gene editing of hemoglobin beta gene in rhesus monkey embryos. Hum. Mol. Genet. 26, 2678–2689. https://doi.org/10.1093/hmg/ddx154.

Pierre, V., Martinez, G., Coutton, C., Delaroche, J., Yassine, S., Novella, C., Pernet-Gallay, K., Hennebicq, S., Ray, P.F., Arnoult, C., 2012. Absence of Dpy19l2, a new inner nuclear membrane protein, causes globozoospermia in mice by preventing the anchoring of the acrosome to the nucleus. Dev. Camb. Engl. 139, 2955–2965. https://doi.org/10.1242/dev.077982.

Ray, P.F., Toure, A., Metzler-Guillemain, C., Mitchell, M.J., Arnoult, C., Coutton, C., 2017. Genetic abnormalities leading to qualitative defects of sperm morphology or function. Clin. Genet. 91, 217–232. https://doi.org/10.1111/cge.12905.

Sapranauskas, R., Gasiunas, G., Fremaux, C., Barrangou, R., Horvath, P., Siksnys, V., 2011. The Streptococcus thermophilus CRISPR/Cas system provides immunity in Escherichia coli. Nucleic Acids Res. 39, 9275–9282. https://doi.org/10.1093/nar/gkr606.

Seruggia, D., Montoliu, L., 2014. The new CRISPR-Cas system: RNA-guided genome engineering to efficiently produce any desired genetic alteration in animals. Transgenic Res. 23, 707–716. https://doi.org/10.1007/s11248-014-9823-y.

Sha, Yan-Wei, Wang, Xiong, Xu, Xiaohui, Su, Zhi-Ying, Cui, Yuanqing, Mei, Li-Bin, Huang, Xian-Jing, Chen, Jie, He, Xue-Mei, Ji, Zhi-Yong, Bao, Hongchu, Yang, Xiaoyu, Li, Ping, Li, Lin, 2017. Novel mutations in CFAP44 and CFAP43 cause multiple morphological abnormalities of the sperm flagella (MMAF). Reprod. Sci. 1933719117749756 https://doi.org/10.1177/1933719117749756.

Shah, S.A., Erdmann, S., Mojica, F.J.M., Garrett, R.A., 2013. Protospacer recognition motifs: mixed identities and functional diversity. RNA Biol. 10, 891–899. https://doi.org/10.4161/rna.23764.

Soumillon, M., Necsulea, A., Weier, M., Brawand, D., Zhang, X., Gu, H., Barthès, P., Kokkinaki, M., Nef, S., Gnirke, A., Dym, M., de Massy, B., Mikkelsen, T.S., Kaessmann, H., 2013. Cellular source and mechanisms of high transcriptome complexity in the mammalian testis. Cell Rep. 3, 2179–2190. https://doi.org/10.1016/j.celrep.2013.05.031.

Tang, S., Wang, X., Li, W., Yang, X., Li, Z., Liu, W., Li, C., Zhu, Z., Wang, L., Wang, J., Zhang, L., Sun, X., Zhi, E., Wang, H., Li, H., Jin, L., Luo, Y., Wang, J., Yang, S., Zhang, F., 2017. Biallelic mutations in CFAP43 and CFAP44 cause male infertility with multiple morphological abnormalities of the sperm flagella. Am. J. Hum. Genet. 100, 854–864. https://doi.org/10.1016/j.ajhg.2017.04.012.

Wang, H., Yang, H., Shivalila, C.S., Dawlaty, M.M., Cheng, A.W., Zhang, F., Jaenisch, R., 2013. One-step generation of mice carrying mutations in multiple genes by CRISPR/Cas-mediated genome engineering. Cell 153, 910–918. https://doi.org/10.1016/j.cell.2013.04.025.

Wefers, B., Bashir, S., Rossius, J., Wurst, W., Kühn, R., 2017. Gene editing in mouse zygotes using the CRISPR/Cas9 system. Methods San Diego Calif 121–122, 55–67. https://doi.org/10.1016/j.ymeth.2017.02.008.

Yen, S.-T., Zhang, M., Deng, J.M., Usman, S.J., Smith, C.N., Parker-Thornburg, J., Swinton, P.G., Martin, J.F., Behringer, R.R., 2014. Somatic mosaicism and allele complexity induced by CRISPR/Cas9 RNA injections in mouse zygotes. Dev. Biol. 393, 3–9. https://doi.org/10.1016/j.ydbio.2014.06.017.

Supplementary table 1: List of homozygous variants identified in FLAGC and FLAGF.

Gene	Nucleotide change	Amino-acid change	gnomAD frequency
FLAGC	c.2353_2354delTT	p.Leu785MetfsTer5 (p.L785X)	0
	c.1023+1G>A	Splicing variant	0
	c.2279T>A	p.Ile760Asn (p.I760N)	0
FLAGF	c.1084C>T	p.Arg362Ter (p.R362*)	$4.69x10^{-5}$
	c.2112delG	p.Arg704SerfsTer7 (R704X)	0
	c.2324A>T	p.Asp775Val (p.D775V)	0

Supplementary table 2: Generation of F0 mice after CRISPR/cas9 injection and number of homozygous (hmz) or heterozygous (htz) mutated (mut) pups in target region 1 (TR1) and target region 2 (TR2).

	Cfap43		*Cfap44*			*FlagC*	*FlagF*		*FlagF-HA*		Total	Av./Inj.
	Inj. 1	Inj. 2	Inj. 1	Inj. 2	Inj. 3	Inj. 1	Inj. 1	Inj. 2	Inj. 1	Inj. 2		
Injected zygotes						97	130	166	135	167	695	139
Transferred embryos						66	66	118	94	135	479	95.8
Newborns	12	9	7	10	9	8	3	14	10	20	102	10.2
Pups with 1 htz TR1 mut.	0	2	0	0	1	1	1	1	4	4	15	1.5
Pups with ≥2 TR1 mut.	0	0	0	0	0	1	0	1	1	8	10	1
Pups with 1 TR1 hmz mut.	0	0	0	0	0	0	1	0	0	0	1	0.1
Pups with 1 htz TR2 mut.	0	2	0	0	0	1	0	1	/	/	4	0.4
Pups with ≥ 2 TR2 mut.	0	0	0	0	0	0	0	0	/	/	0	0
Pups with 1 TR2 hmz mut	0	1	0	0	0	0	0	0	/	/	1	0.1
Total No of mut. pups	0	5	0	0	1	3	2	3	5	12	31	
% mut. Pups per live pup	0.0	55.6	0.0	0.0	11.1	37.5	66.7	21.4	50	60	30.4	
Total No of *de novo* indels	0	6	0	0	1	4	3	3	6	20	43	

Supplementary table 3: Generation of F1 mice from CRISPR/cas9 created F0 and number of pups presenting the parental mutation F0 or a new mutation Mut. 1 or Mut. 2.

Litter 1 and 2 for a same gene are generated with the same parents. The new mutations mut. 1 and mut.2 are identical from one litter to another. A maximum of two different "new" mutations (plus the parental mutation) were identified the 3 analyzed couples.

	Cfap43			*Cfap44*				*FlagC*			Total	% mut.
	Litter 1	Litter 2		Litter 1	Litter 2	Litter 3		Litter 1	Litter 2			
Newborn	3	12		6	11	10		9	10		61	
Pups with mut. F0	2	3		1	3	4		4	3		20	
% pups with F0 mut.	66,7	25,0		16,7	27,3	40,0		44,4	30,0			32,8
Pups with mut. 1	0	3		1	2	0		4	1		11	18,0
Pups with mut. 2	0	0		1	1	1		0	0		3	4,9
Total with non parental mut	0	3		2	3	1		4	1		14	
% pups with non parental mut	0,0	25,0		33,3	27,3	10,0		44,4	10,0			23,0
Total Nb mut. pups	2	6		3	6	5		8	4		34	
% overall mut. pups	66,7	50,0		50,0	54,5	50,0		88,9	40,0			55,7

Supplementary table 4: List of all mutations identified in F0 and F1 animals and position in regard to the PAM 1st nucleotide.

*indicates the mutations selected for generation of F1.†indicates the F0 homozygous mutations. Position refers to the position in regards to the PAM 1st nucleotide (**C**GG).ie: in "CAGCTGACTCA*TATA*CCGA**CGG"**delTATA (italic) is in position -5 in regards to the PAM (in bold). F0, F1 indicates if the mutation was first identified in F0 or F1 animals. "Target" indicates if the indels occurred in the first or second targeted region.

Gene Targeted	Position	Size	F0	F1	Mutation
Cfap43 Target1	NC	NC	2		Uncharacterized events
Cfap43 Target2	-4	-1	2		delG†
	-4	+4		1	insTCCA
	-6	-4	1		delAAGG*
	-10	-10	1		delTGTGAAGGGC
Cfap44 Target1	-4	+7	1		InsTCAGATA*
	-6	-3		1	delTAC
	-8	-4		1	delTATA*
Cfap44 Target2	/				
FlagC Target1	NC	NC	2		Uncharacterized events
	-4	+1		1	insT*
	-4	-3	1		delTAC
FlagC Target2	-13	-12	1		delAAACCCGTTAGC
FlagF Target1			2		Uncharacterized events
	-3	-1	2		delG†
	-6	-4	1		delTTCG
FlagF Target2	-4	+11	1		insAATGTACATAG
FlagF-HA	NC	NC	≥12		Uncharacterized events
		-	6		HA inserted
	-3	-2	1		delAG
	-3	-3	1		delAGC
	-4	-9	1		delCAGCTGGAA
	-5	-3	1		delGCA
	-9	-8	3		delTTCAGCAG
	-15	-15	1		delAATTAGTTCAGCAGC
Median	-4	-3			
Total			≥40	5	

Discussion

Scientific perspectives and future directions

1. PATL2

Our study is the first to characterise a mammalian PATL2 protein in its native cellular context. We have confirmed that mouse and human PATL2 are crucial for oocyte maturation. We have also demonstrated that murine PATL2 is strongly expressed in growing oocytes and that its absence leads to the dysregulation of specific key transcripts. Much remains to be learned regarding its specific mode of action and molecular interactions, especially in view of the differences that our results indicate between the murine and amphibian PATL2 orthologues and its role at multiple stages of oocyte/zygote development as suggested through study of our murine models.

Our mouse KO model showed a mixed arrest phenotype whereby a low rate of normal development was possible, however the majority of oocytes and early embryos arrested at various stages. This phenotype is likely linked to the diverse collection of dysregulated genes in Patl2 KO GV and MII oocytes brought to light through transcriptome analysis. These included a more than twofold downregulation of genes that are activated during oocyte maturation (such as *Gatsl3* of the mTORC1 pathway and *Pgrmc1*), genes involved in the MI-MII transition (such as *Fgf9* and *Cdc25a)* and numerous other factors important in the acquisition of meiotic/developmental competence (e.g. transcription factor *Sohlh2*, spindle assembly factors, secreted factors and stress/DNA damage response factors). It remains to be investigated how these dysregulations translate to the proteome level and which are direct/indirect consequences of PATL2 absence.

It is remarkable that, following *in vitro* fertilisation, the rate of embryo development continued to be inferior to the WT rate beyond EGA, until the blastocyst stage. This highlights the importance of oocyte factors and the necessity of correct meiotic maturation for true developmental competence. Surprisingly, a considerable number of genes expressed in the embryonic trophoblast were also found to be significantly downregulated in *Patl2* KO oocytes. These include three *Ephrin A* genes involved in implantation and maternally imprinted *Phlda2* involved in placental development. It would be pertinent to determine whether the

dysregulation of these genes, whose known functions are executed after EGA, are of consequence in the maturing oocyte or indeed in the early embryo.

We have evidence that murine PATL2 is detectable at weak levels until the zygote stage (through immunostaining and immunoblotting, unpublished), which is different to the system described in *Xenopus* oocytes whereby xPat1a is rapidly degraded upon GVBD [160,183]. Taking into account the human GV-arrest phenotype linked to PATL2 invalidation, we hypothesise that in mammals, PATL2 regulates groups of mRNAs that function in oocyte growth, meiotic maturation and after fertilisation, and that in humans PATL2 is indispensable for meiotic progression. A key objective for this project is now to clarify the role of PATL2 at each specific stage of oocyte maturation and post-fertilisation. Planned experiments include 1) transcriptome analyses on zygotes from WT and PATL2 KO mice at fixed time points 2) proteomic analyses at stages corresponding to those studied in the transcriptomic analyses and 3) Knock-down of PATL2 in GV and MII WT oocytes using the 'Trim-Away' method [307] followed by *in vitro* maturation, fertilisation and culture to the blastocyst stage to test developmental competence. It would also be of interest to investigate the expression profile of PATL1 in mammalian oocytes and zygotes and compare the transition from PATL2 to PATL1 expression to what has been demonstrated in *Xenopus*.

The variation in gene-invalidation phenotypes between mice and humans that we have described here is not unprecedented (another example is *CFAP44* [294]). Differences of this nature can perhaps be explained by variation in the *PATL2* N-terminal sequence, the possible existence of compensatory mechanisms in mice and differences in the respective reproductive systems. Indeed, major differences exist in the reproductive systems of humans and mice such as mono versus poly-ovulation and late versus early onset of major EGA. The timing of EGA is important since this determines the timeframe during which the dysregulations caused by the absence of PATL2 can have consequences for the developing embryo. It would be interesting to explore the PATL2-deficiency phenotype in species whose reproductive systems are closer to humans in these respects. In rabbits, for example, major EGA occurs at a similar stage to humans (8-cell stage). It would therefore be interesting to generate a PATL2 knockout rabbit model and to compare the severity of the OMD phenotype to that observed in humans and in mice.

In this study, we were unable to show colocalisation of Patl2-HA with either CPEB1, MSY2 or DDX6, whose orthologues have all been shown to interact with xPat1a in either a direct (Cpeb1

and Ddx6) or RNA-dependent (Msy2) manner in *Xenopus* oocytes. These differences could be due to variations in the N-terminal sequence, which shows poor conservation between the two vertebrate classes and is much shorter in mammals than *Xenopus* (733aa in *Xenopus*, 543aa in humans and 529aa in mice). The domain through which xPat1a interacts with Cpeb1 has not yet been specified, but it is known that the DDX6/Dhh1-binding peptide that is present in the N-terminal of xPat1a, xPat1b and yeast Pat1p is absent in mammalian PATL2 [176]. Lack of colocalisation with DDX6 is then perhaps not surprising. Furthermore, whereas xPat1a was shown to co-precipitate with c-Mos and cyclin B1 mRNA (whose translation is repressed by the CPEB1 complex) and its overexpression impacted the accumulation of both transcripts in *Xenopus* oocytes [160,183], neither were found to be altered in our *Patl2* KO oocyte transcriptome study.

It is an intriguing possibility that in mammals, the function of PATL2 may have evolved to control a different or more specific subset of mRNAs in a CPEB1-independent complex, and may repress their translation until after fertilisation or be inactivated through a different mechanism. In order to pinpoint the role of mammalian PATL2 more precisely, it would be necessary to characterise the PATL2 RNP complex, including protein partners and, if possible, bound mRNA. These techniques are challenging due to the large numbers of oocytes required to provide sufficient material, although throughout the course of my PhD I have made considerable progress refining a protocol for immunoprecipitation of the PATL2-HA complex for mass spectrometry analysis. Given these species-specific differences and the variety of functions and interactions that have been attributed to its various members, the Pat1 protein family would appear to be highly versatile and multi-functional.

2. SPINK2

We have successfully characterised the pathology associated with mutation of *Spink2* which is in line with the role of SPINK2 as an acrosin-inhibitor. *Spink2* invalidation in mice reproduces the human phenotype of azoospermia and revealed the cause of this to be degradation after the post-meiotic round spermatid stage. This stage corresponds to the stage of spermiogenesis during which the acrosome is formed, which is where we showed SPINK2 protein to be localised. Studying the consequences of SPINK2 inactivation in round spermatids, we observed signs of proteolytic damage, including to the Golgi apparatus, and microautophagy. We confirmed through HEK cell transfection that proacrosin is capable of autoactivation at neutral pH and that this unchecked activity leads to cell proliferation arrest and detachment: effects which are reversed by co-transfection of SPINK2. We therefore have strong evidence for the hypothesis that SPINK2 inhibits the activity of autoactivated proacrosin as it transits through the Golgi apparatus and thus preventing damage that otherwise leads to azoospermia.

This model could be of further value as a means to study and potentially treat acrosin-induced cell damage in spermatogenic cells. The particular mode of induced cell death is intriguing, since it apparently occurs by an apoptosis-independent pathway, and this could be of interest to further characterise. This murine model may also be used for the development and refinement of a novel form of therapy to treat this specific form of infertility through targeted delivery of SPINK2.

Clinical perspectives

In showing that *Patl2*-deficient mice have impaired fertility and oocyte meiotic deficiency, we have confirmed the causality of the *PATL2* mutation in the human OMD phenotype representing the second genetic cause of OMD to be confirmed after *TUBB8* [249]. During the course of my PhD, four additional reports were published describing a total of 21 *PATL2* variants in association with OMD in Chinese and Saudi Arabian cohorts [308–311]. The OMD-associated *PATL2* variants (including nonsense, missense, frameshift and splicing variants) all contained mutations before or within the PAT1 domain. One of the variants in the Saudi-Arabian cohort is the same variant reported in our study (Arg160*). Biallelic mutations gave rise to a GV-arrest phenotype and compound heterozygous mutations to a range of phenotypes from GV to early embryo arrest. These reports are in line with our findings and reinforce PATL2 invalidation as a cause of human infertility.

Mutation of *PATL2* was the cause of infertility for over a quarter of the patients in this cohort of 23. Combined with the other recent reports, this gives a total of 29 patients from 22 separate families across North African, West Asian and East Asian populations. The prevalence of PATL2-related OMD within the cohorts studied ranged from 2.8% in a large OMD cohort (180 patients [308]) to 44% in a cohort of uniquely GV-arrest OMD patients [310]. Whilst further such studies on larger cohorts would be needed to more accurately estimate the prevalence of PATL2-related OMD, these studies indicate mutation of PATL2 as a major cause of this rare pathology with a wide global spread. This finding makes PATL2 a good candidate for genetic screening in a clinical setting for patients with suspected OMD: information which would be invaluable in correctly diagnosing the cause of infertility and could avoid repeated cycles of ineffective ART procedures.

Regarding SPINK2: this familial case of azoospermia in association with homozygous SPINK2 mutation is the first to be reported. With increased accessibility of WES, further cases may be identified, and this gene could be a good candidate for genetic screening in azoospermia. The fact that we have also associated *SPINK2* mutation with the more common OATS phenotype with varying penetrance in the heterozygous state may be of wider clinical interest, adding to the list of genes that may contribute to this pathology in a dose-dependent manner. Currently, routine genetic screening for men in cases of infertility is limited to detection of numeric and structural chromosomal abnormalities and Y chromosome microdeletions, giving rise to a genetic diagnosis

for less than 5% of infertile couples [252]. If we were to widen this list to include genes with confirmed association to human infertility, such as *SPINK2* in men and *PATL2* in women, our diagnostic capacity for genetic-based infertility could be dramatically improved.

Studies such as these create a framework for the development of targeted therapies. Whereas it may not currently be possible to envisage a treatment for many genetic subtypes of infertility, it is reasonable to assume that with the advancement of ART techniques, certain subtypes may become treatable in the near future. In particular, infertility linked to a single gene mutation such as in the case of *PATL2* or *SPINK2,* in which the ovarian reserve/pool of spermatogonia is unaffected could feasibly become treatable (even more so if the gene is late-acting) by targeted delivery of the missing protein combined with *in vitro* maturation. Such potential treatment strategies would, of course, have to be carefully designed to respect ethical restrictions such as non-modification of the germline genome.

The importance of characterising actors of gametogenesis

1. Severe infertility as an opportunity to identify new actors

The GETI Lab has successfully identified a considerable number of gene mutations in association with severe human infertility through WES and the study of transgenic mice, proving this to be an efficient and robust methodology. WES is increasingly employed in clinical settings, and the fact that variants of the same genes with the same associated phenotype have been reported in geographically distant populations shows that our findings from this particular cohort are relevant to a wider population. Although this method may be limited to identifying single-gene causes for rare and severe types of infertility, it has proven to be a valuable method for uncovering important actors of human gametogenesis. The generation of transgenic mice permits not only validation of the genetic association but also characterisation of candidate genes in a mammalian system. This is important since the high degree of homology allows us to be more confident about the relevance of the conclusions drawn for the human system.

Despite high sequence homology, differences are occasionally revealed between human and mouse gene orthologues for reproductive functions, and this possibility must be taken into consideration when interpreting results and assessing the suitability of the mouse model. Such differences can be informative if the context of the particular reproductive system is taken into account when interpreting and comparing results. In the case of PATL2, the milder PATL2-deficiency-related infertility phenotype that appeared in the murine model made it possible to observe late-acting functional aspects of Patl2 in later stages of oocyte maturation and beyond fertilisation, which may otherwise have been masked.

2. Relevance for ART therapies

The elucidation of molecular pathways involved in gametogenesis generates knowledge that can be used to the benefit of patients in several ways. It is clear that if we are to attempt to develop personalised therapies for specific genetic subtypes of infertility, a detailed understanding of the corresponding protein function is indispensable. Beyond this, we hope that the knowledge generated can be used to inform the improvement of existing ART techniques such as *in vitro* gamete maturation, thus benefitting a larger number of patients.

In vitro maturation is a technique currently applied to immature retrieved oocytes for IVF or ICSI in which oocytes are cultured to induce oocyte maturation to make fertilisation possible. The success of this technique is intimately dependent on culture conditions, and its effectiveness is currently limited to oocytes derived from larger follicles. A better understanding of the processes that occur during oocyte growth and maturation could inform the optimisation of culture conditions and pave the way for expansion of this technique to the maturation of younger, more immature oocytes. This would have far-reaching applications, including creating the possibility for fertility preservation for young cancer patients whose oocytes may be cryopreserved ahead of reprotoxic therapy. As highlighted here, the oocyte growth phase is essential for correct meiotic maturation, response to fertilisation and subsequent development, and we must strive to understand the oocyte's exact requirements at this stage if we are to recreate conditions favourable to the acquisition of full developmental competence.

3. Wider applicability of findings

As well as informing the field of ART, the characterisation of actors of gametogenesis can have wider applications or relevance for other biological systems. As already mentioned, SPINK2 expression has been associated with certain cancers [210,211]. SPINK2 has also been found to be expressed in retinal ganglion cells and modulates their susceptibility to apoptosis after optic nerve damage [312]. Finally, very recently, an engineered form of SPINK2 was used as a scaffold structure in the targeted engineering of high affinity protease inhibitors [313].

The unique properties of the oocyte make it a model for translational regulation, cellular dormancy and reprogramming. Elements or paralogues of the specific mechanisms that exist to satisfy the particular requirements of the oocyte have been found to exist elsewhere in the body. Translational regulation for example plays an essential role in cell division and in the establishment of a body plan in embryogenesis. The RBP Musashi has recently been found to play a pivotal role in stem cell maintenance and was shown to repress translation by competing with eIF4G for binding of PABP in mammalian neural stem cells [135]. CPEB RNPs have been identified at neuronal synapses and implicated in synaptic plasticity and long-term memory consolidation as well as cellular senescence [120]. These examples illustrate how the findings from reproductive biology can be relevant to a wide range of medical fields.

References

1. Erickson GF. Follicle Growth and Development. *Glob. Libr. Women's Med.* 2009 ;.
2. Cordts EB, Christofolini DM, Santos AA dos, *et al.* Genetic aspects of premature ovarian failure: a literature review. *Arch. Gynecol. Obstet.* 2011 ; 283 : 635–643.
3. Piotrowska H, Kempisty B, Sosinska P, *et al. The role of TGF superfamily gene expression in the regulation of folliculogenesis and oogenesis in mammals: a review*. 2013 : 505–515 p.
4. Williams CJ, Erickson GF. *Morphology and Physiology of the Ovary*. MDText.com, Inc., 2012 : p.
5. Conti M, Chang RJ. *Folliculogenesis, Ovulation, and Luteogenesis*. Elsevier, 2016 : 2179-2191.e3 p.
6. Oktem O, Urman B. Understanding follicle growth in vivo. *Hum. Reprod.* 2010 ; 25 : 2944–2954.
7. Gougeon A. *Dynamics of follicular growth in the human: a model from preliminary results*. 1986 : 81–87 p.
8. Pepling ME. From primordial germ cell to primordial follicle: mammalian female germ cell development. *genesis* 2006 ; 44 : 622–632.
9. Kim M-R, Tilly JL. Current concepts in Bcl-2 family member regulation of female germ cell development and survival. *Biochim. Biophys. Acta - Mol. Cell Res.* 2004 ; 1644 : 205–210.
10. Anderson EL, Baltus AE, Roepers-Gajadien HL, *et al.* Stra8 and its inducer, retinoic acid, regulate meiotic initiation in both spermatogenesis and oogenesis in mice. *Proc. Natl. Acad. Sci. U. S. A.* 2008 ; 105 : 14976–80.
11. Chen C-L, Fu X-F, Wang L-Q, *et al.* Primordial follicle assembly was regulated by notch signaling pathway in the mice. *Mol. Biol. Rep.* 2014 ; 41 : 1891–1899.
12. Pangas SA, Choi Y, Ballow DJ, *et al.* Oogenesis requires germ cell-specific transcriptional regulators Sohlh1 and Lhx8. *Proc. Natl. Acad. Sci. U. S. A.* 2006 ; 103 : 8090–5.
13. Lim E-J, Choi Y. Transcription factors in the maintenance and survival of primordial follicles. *Clin. Exp. Reprod. Med.* 2012 ; 39 : 127.
14. Uda M, Ottolenghi C, Crisponi L, *et al.* Foxl2 disruption causes mouse ovarian failure by pervasive blockage of follicle development. *Hum. Mol. Genet.* 2004 ; 13 : 1171–1181.
15. Jagarlamudi K, Rajkovic A. Oogenesis: Transcriptional regulators and mouse models. *Mol. Cell. Endocrinol.* 2012 ; 356 : 31–39.
16. Eppig JJ, Wigglesworth K, Pendola FL. The mammalian oocyte orchestrates the rate of ovarian follicular development. *Proc. Natl. Acad. Sci.* 2002 ; 99 : 2890–2894.
17. Reddy P, Liu L, Adhikari D, *et al.* Oocyte-Specific Deletion of Pten Causes Premature Activation of the Primordial Follicle Pool. *Science (80-.).* 2008 ; 319 : 611–613.
18. Castrillon DH, Miao L, Kollipara R, *et al.* Suppression of Ovarian Follicle Activation in Mice by the Transcription Factor Foxo3a. *Science (80-.).* 2003 ; 301 : 215–218.
19. Adhikari D, Zheng W, Shen Y, *et al.* Tsc/mTORC1 signaling in oocytes governs the quiescence and activation of primordial follicles. *Hum. Mol. Genet.* 2010 ; 19 : 397–410.
20. Adhikari D, Flohr G, Gorre N, *et al.* Disruption of Tsc2 in oocytes leads to overactivation of the entire pool of primordial follicles. *Mol. Hum. Reprod.* 2009 ; 15 : 765–770.
21. Sánchez F, Smitz J. Molecular control of oogenesis. *Biochim. Biophys. Acta* 2012 ; 1822 : 1896–1912.
22. Adhikari D, Liu K. Molecular Mechanisms Underlying the Activation of Mammalian Primordial Follicles. *Endocr. Rev.* 2009 ; 30 : 438–464.
23. Vendola K, Zhou J, Wang J, *et al.* Androgens Promote Oocyte Insulin-Like Growth Factor I Expression and Initiation of Follicle Development in the Primate Ovary1. *Biol. Reprod.* 1999 ; 61 :

353–357.

24. Wassarman PM. Zona pellucida glycoproteins. *J. Biol. Chem.* 2008 ; 283 : 24285–9.

25. Nicholson SM, Bruzzone R. Gap junctions: getting the message through. *Curr. Biol.* 1997 ; 7 : R340-4.

26. Kumar NM, Gilula NB. The gap junction communication channel. *Cell* 1996 ; 84 : 381–8.

27. Simon AM, Goodenough DA, Li E, *et al.* Female infertility in mice lacking connexin 37. *Nature* 1997 ; 385 : 525–529.

28. Yamoto M, Shima K, Nakano R. Gonadotropin Receptors in Human Ovarian Follicles and Corpora lutea throughout the Menstrual Cycle. *Horm. Res.* 1992 ; 37 : 5–11.

29. Chang H, Brown CW, Matzuk MM. Genetic Analysis of the Mammalian Transforming Growth Factor-β Superfamily. *Endocr. Rev.* 2002 ; 23 : 787–823.

30. Eichenlaub-Ritter U, Peschke M. Expression in in-vivo and in-vitro growing and maturing oocytes: focus on regulation of expression at the translational level. *Hum. Reprod. Update* 2002 ; 8 : 21–41.

31. Fair T. Follicular oocyte growth and acquisition of developmental competence. *Anim. Reprod. Sci.* 2003 ; 78 : 203–16.

32. Liu K, Rajareddy S, Liu L, *et al.* Control of mammalian oocyte growth and early follicular development by the oocyte PI3 kinase pathway: New roles for an old timer. *Dev. Biol.* 2006 ; 299 : 1–11.

33. La Fuente R De. Chromatin modifications in the germinal vesicle (GV) of mammalian oocytes. *Dev. Biol.* 2006 ; 292 : 1–12.

34. Schultz RM, Letourneau GE, Wassarman PM. Program of early development in the mammal: changes in the patterns and absolute rates of tubulin and total protein synthesis during oocyte growth in the mouse. *Dev. Biol.* 1979 ; 73 : 120–33.

35. Sternlicht AL, Schultz RM. Biochemical studies of mammalian oogenesis: kinetics of accumulation of total and poly(A)-containing RNA during growth of the mouse oocyte. *J. Exp. Zool.* 1981 ; 215 : 191–200.

36. Sirard M-A. Factors Affecting Oocyte and Embryo Transcriptomes. *Reprod. Domest. Anim.* 2012 ; 47 : 148–155.

37. Clarke HJ. Post-transcriptional Control of Gene Expression During Mouse Oogenesis. 2012 ; 55 : 1–21.

38. Pincus G, Enzmann E V. The comparative behavior of mammalian eggs in vivo and in vitro: i. The activation of ovarian eggs. *J. Exp. Med.* 1935 ; 62 : 665–75.

39. Norris RP, Ratzan WJ, Freudzon M, *et al.* Cyclic GMP from the surrounding somatic cells regulates cyclic AMP and meiosis in the mouse oocyte. *Development* 2009 ; 136 : 1869–78.

40. Mehlmann LM. Oocyte-specific expression of Gpr3 is required for the maintenance of meiotic arrest in mouse oocytes. *Dev. Biol.* 2005 ; 288 : 397–404.

41. Jones KT. Turning it on and off: M-phase promoting factor during meiotic maturation and fertilization. *Mol. Hum. Reprod.* 2004 ; 10 : 1–5.

42. Edwards R. Follicular fluid. *J. Reprod. Fertil.* 1974 ; 37 : 189–219.

43. Yoshida H, Takakura N, Kataoka H, *et al.* Stepwise Requirement of c-kit Tyrosine Kinase in Mouse Ovarian Follicle Development. *Dev. Biol.* 1997 ; 184 : 122–137.

44. Otsuka F, McTavish KJ, Shimasaki S. Integral role of GDF-9 and BMP-15 in ovarian function. *Mol. Reprod. Dev.* 2011 ; 78 : 9–21.

45. Mihm M, Evans A. Mechanisms for Dominant Follicle Selection in Monovulatory Species: A Comparison of Morphological, Endocrine and Intraovarian Events in Cows, Mares and Women. *Reprod. Domest. Anim.* 2008 ; 43 : 48–56.

46. Dragovic RA, Ritter LJ, Schulz SJ, *et al.* Oocyte-Secreted Factor Activation of SMAD 2/3 Signaling Enables Initiation of Mouse Cumulus Cell Expansion1. *Biol. Reprod.* 2007 ; 76 : 848–857.

47. Russell DL, Robker RL. Molecular mechanisms of ovulation: co-ordination through the cumulus complex. *Hum. Reprod. Update* 2007 ; 13 : 289–312.

48. Mattson BA, Albertini DF. Oogenesis: Chromatin and microtubule dynamics during meiotic prophase. *Mol. Reprod. Dev.* 1990 ; 25 : 374–383.

49. La Fuente R De, Eppig JJ. Transcriptional Activity of the Mouse Oocyte Genome: Companion Granulosa Cells Modulate Transcription and Chromatin Remodeling. *Dev. Biol.* 2001 ; 229 : 224–236.

50. Conti M, Franciosi F. Acquisition of oocyte competence to develop as an embryo: integrated nuclear and cytoplasmic events. *Hum. Reprod. Update* 2018 ; 24 : 245–266.

51. Conti M, Hsieh M, Zamah AM, *et al.* Novel signaling mechanisms in the ovary during oocyte maturation and ovulation. *Mol. Cell. Endocrinol.* 2012 ; 356 : 65–73.

52. Beall S, Brenner C, Segars J. Oocyte maturation failure: a syndrome of bad eggs. *Fertil. Steril.* 2010 ; 94 : 2507–2513.

53. Schuh M, Ellenberg J. Self-Organization of MTOCs Replaces Centrosome Function during Acentrosomal Spindle Assembly in Live Mouse Oocytes. *Cell* 2007 ; 130 : 484–498.

54. Holubcová Z, Blayney M, Elder K, *et al.* Human oocytes. Error-prone chromosome-mediated spindle assembly favors chromosome segregation defects in human oocytes. *Science* 2015 ; 348 : 1143–7.

55. Jang JK, Rahman T, Kober VS, *et al.* Misregulation of the Kinesin-like Protein Subito Induces Meiotic Spindle Formation in the Absence of Chromosomes and Centrosomes. *Genetics* 2007 ; 177 : 267–280.

56. Lee J, Kitajima TS, Tanno Y, *et al.* Unified mode of centromeric protection by shugoshin in mammalian oocytes and somatic cells. *Nat. Cell Biol.* 2008 ; 10 : 42–52.

57. Coticchio G, Dal Canto M, Mignini Renzini M, *et al.* Oocyte maturation: gamete-somatic cells interactions, meiotic resumption, cytoskeletal dynamics and cytoplasmic reorganization. *Hum. Reprod. Update* 2015 ; 21 : 427–54.

58. Maro B, Verlhac M-H. Polar body formation: new rules for asymmetric divisions. *Nat. Cell Biol.* 2002 ; 4 : E281–E283.

59. Li R, Albertini DF. The road to maturation: somatic cell interaction and self-organization of the mammalian oocyte. *Nat. Rev. Mol. Cell Biol.* 2013 ; 14 : 141–152.

60. Blerkom J Van. Mitochondrial function in the human oocyte and embryo and their role in developmental competence. *Mitochondrion* 2011 ; 11 : 797–813.

61. Jégou A, Ziyyat A, Barraud-Lange V, *et al.* CD9 tetraspanin generates fusion competent sites on the egg membrane for mammalian fertilization. *Proc. Natl. Acad. Sci. U. S. A.* 2011 ; 108 : 10946.

62. Bianchi E, Doe B, Goulding D, *et al.* Juno is the egg Izumo receptor and is essential for mammalian fertilization. *Nature* 2014 ; 508 : 483–487.

63. Swain JE, Pool TB. ART failure: oocyte contributions to unsuccessful fertilization. *Hum. Reprod. Update* 2008 ; 14 : 431–446.

64. Georgadaki K, Khoury N, Spandidos DA, *et al.* The molecular basis of fertilization (Review). *Int. J. Mol. Med.* 2016 ; 38 : 979–86.

65. Liu M. The biology and dynamics of mammalian cortical granules. *Reprod. Biol. Endocrinol.* 2011 ; 9 : 149.

66. Avella MA, Xiong B, Dean J. The molecular basis of gamete recognition in mice and humans. *Mol. Hum. Reprod.* 2013 ; 19 : 279–289.

67. Gu T-P, Guo F, Yang H, *et al.* The role of Tet3 DNA dioxygenase in epigenetic reprogramming by oocytes. *Nature* 2011 ; 477 : 606–610.

68. Santos F, Hendrich B, Reik W, *et al.* Dynamic Reprogramming of DNA Methylation in the Early Mouse Embryo. *Dev. Biol.* 2002 ; 241 : 172–182.

69. Han L, Ren C, Zhang J, *et al.* Differential roles of Stella in the modulation of DNA methylation during oocyte and zygotic development. *Cell Discov.* 2019 ; 5 : 9.

70. Nakamura T, Arai Y, Umehara H, *et al.* PGC7/Stella protects against DNA demethylation in early embryogenesis. *Nat. Cell Biol.* 2007 ; 9 : 64–71.

71. Lin C-J, Koh FM, Wong P, *et al.* Hira-mediated H3.3 incorporation is required for DNA replication and ribosomal RNA transcription in the mouse zygote. *Dev. Cell* 2014 ; 30 : 268–79.

72. Fraser R, Lin C-J. Epigenetic reprogramming of the zygote in mice and men: on your marks, get set, go! *Reproduction* 2016 ; 152 : R211.

73. Lee MT, Bonneau AR, Giraldez AJ. Zygotic genome activation during the maternal-to-zygotic transition. *Annu. Rev. Cell Dev. Biol.* 2014 ; 30 : 581–613.

74. Lee MT, Bonneau AR, Takacs CM, *et al.* Nanog, Pou5f1 and SoxB1 activate zygotic gene expression during the maternal-to-zygotic transition. *Nature* 2013 ; 503 : 360–4.

75. Nothias JY, Majumder S, Kaneko KJ, *et al.* Regulation of gene expression at the beginning of mammalian development. *J. Biol. Chem.* 1995 ; 270 : 22077–80.

76. Alberts B, Johnson A, Lewis J, *et al. Molecular Biology of the Cell.* 4th Editio. New York : Garland Science, 2002 : p.

77. Yu J, Russell JE. Structural and functional analysis of an mRNP complex that mediates the high stability of human beta-globin mRNA. *Mol. Cell. Biol.* 2001 ; 21 : 5879–88.

78. Schwanhäusser B, Busse D, Li N, *et al.* Global quantification of mammalian gene expression control. *Nature* 2011 ; 473 : 337–342.

79. Carpenter S, Ricci EP, Mercier BC, *et al.* Post-transcriptional regulation of gene expression in innate immunity. *Nat. Rev. Immunol.* 2014 ; 14 : 361–376.

80. Luong XG, Conti M. RNA Binding Protein Networks and Translational Regulation in Oocytes. *Human Reproductive and Prenatal Genetics*. Elsevier, 2019 : 193–220.

81. Sutherland JM, Siddall NA, Hime GR, *et al.* RNA binding proteins in spermatogenesis: An in depth focus on the Musashi family. *Asian Journal of Andrology*. Medknow Publications, 2015 : 529–536.

82. Buratowski S. Transcription initiation unwrapped. *Nature* 2012 ; 483 : 286–287.

83. Richard P, Manley JL. Transcription termination by nuclear RNA polymerases. *Genes Dev.* 2009 ; 23 : 1247–69.

84. Katahira J. Nuclear export of messenger RNA. *Genes (Basel).* 2015 ; 6 : 163–84.

85. Maquat LE, Tarn W-Y, Isken O. The pioneer round of translation: features and functions. *Cell* 2010 ; 142 : 368–74.

86. López-Lastra M, Rivas A, Barría MI. Protein synthesis in eukaryotes: The growing biological relevance of cap-independent translation initiation. *Biol. Res.* 2005 ; 38 : 121–146.

87. Gebauer F, Hentze MW. Molecular mechanisms of translational control. *Nat. Rev.* 2004 ; 5 : 827–

835.

88. Wiederhold K, Passmore LA. Cytoplasmic deadenylation: regulation of mRNA fate. *Biochem. Soc. Trans.* 2010 ; 38 : 1531–6.

89. Tharun S, He W, Mayes AE, *et al.* Yeast Sm-like proteins function in mRNA decapping and decay. *Nature* 2000 ; 404 : 515–518.

90. Garneau NL, Wilusz J, Wilusz CJ. The highways and byways of mRNA decay. *Nat. Rev. Mol. Cell Biol.* 2007 ; 8 : 113–126.

91. Kulkarni M, Stoecklin G. On track with P-bodies. *Biochem. Soc. Trans.* 2010 ; 38 : 242–251.

92. Brengues M, Teixeira D, Parker R. Movement of Eukaryotic mRNAs Between Polysomes and Cytoplasmic Processing Bodies. *Science (80-.).* 2005 ; 310 : 486–489.

93. Standart N, Weil D. P-Bodies: Cytosolic Droplets for Coordinated mRNA Storage. *Trends Genet.* 2018 ; 34 : 612–626.

94. Hubstenberger A, Courel M, Bénard M, *et al.* P-Body Purification Reveals the Condensation of Repressed mRNA Regulons. *Mol. Cell* 2017 ; 68 : 144-157.e5.

95. Standart N, Minshall N. Translational control in early development: CPEB, P-bodies and germinal granules. *Biochem. Soc. Trans.* 2008 ; 36 : 671–676.

96. Svoboda P, Franke V, Schultz RM. Sculpting the Transcriptome During the Oocyte-to-Embryo Transition in Mouse. *Curr. Top. Dev. Biol.* 2015 ; 113 : 305–349.

97. Medvedev S, Pan H, Schultz RM. Absence of MSY2 in mouse oocytes perturbs oocyte growth and maturation, RNA stability, and the transcriptome. *Biol Reprod* 2011 ; 85 : 575–583.

98. Piqué M, López JM, Foissac S, *et al.* A Combinatorial Code for CPE-Mediated Translational Control. *Cell* 2008 ; 132 : 434–448.

99. Moore MJ. From Birth to Death: The Complex Lives of Eukaryotic mRNAs. *Science (80-.).* 2005 ; 309 : 1514–1518.

100. Mak W, Fang C, Holden T, *et al.* An Important Role of Pumilio 1 in Regulating the Development of the Mammalian Female Germline1. *Biol. Reprod.* 2016 ; 94 .

101. Sousa Martins JP, Liu X, Oke A, *et al.* DAZL and CPEB1 regulate mRNA translation synergistically during oocyte maturation. *J. Cell Sci.* 2016 ; 129 : 1271–1282.

102. Tay J, Richter JD. Germ cell differentiation and synaptonemal complex formation are disrupted in CPEB knockout mice. *Dev. Cell* 2001 ; 1 : 201–13.

103. Igea A, Méndez R. Meiosis requires a translational positive loop where CPEB1 ensues its replacement by CPEB4. *EMBO J.* 2010 ; 29 : 2182–93.

104. Chen J, Melton C, Suh N, *et al.* Genome-wide analysis of translation reveals a critical role for deleted in azoospermia-like (Dazl) at the oocyte-to-zygote transition. *Genes Dev.* 2011 ; 25 : 755–766.

105. Guzeloglu-Kayisli O, Lalioti MD, Aydiner F, *et al.* Embryonic poly(A)-binding protein (EPAB) is required for oocyte maturation and female fertility in mice. *Biochem. J.* 2012 ; 446 : 47–58.

106. Zhang T, Li Y, Li H, *et al.* RNA-associated protein LSM family member 14 controls oocyte meiotic maturation through regulating mRNA pools. *J. Reprod. Dev.* 2017 ; 63 : 383–388.

107. Sutherland JM, Sobinoff AP, Gunter KM, *et al.* Knockout of rna binding protein msi2 impairs follicle development in the mouse ovary: Characterization of msi1 and msi2 during folliculogenesis. *Biomolecules* 2015 ; 5 : 1228–1244.

108. Yang J, Medvedev S, Yu J, *et al.* Absence of the DNA-/RNA-binding protein MSY2 results in male and female infertility. *Proc. Natl. Acad. Sci. U. S. A.* 2005 ; 102 : 5755–5760.

109. Lin K, Zhang S, Chen J, *et al.* Generation and functional characterization of a conditional Pumilio2 null allele. *J. Biomed. Res.* 2018 ; 32 : 434–441.

110. Wu X, Viveiros MM, Eppig JJ, *et al.* Zygote arrest 1 (Zar1) is a novel maternal-effect gene critical for the oocyte-to-embryo transition. *Nat. Genet.* 2003 ; 33 : 187–191.

111. Hu J, Wang F, Zhu X, *et al.* Mouse ZAR1-like (XM_359149) colocalizes with mRNA processing components and its dominant-negative mutant caused two-cell-stage embryonic arrest. *Dev. Dyn.* 2010 ; 239 : 407–24.

112. Ramos SB V, Stumpo DJ, Kennington EA, *et al.* The CCCH tandem zinc-finger protein Zfp36l2 is crucial for female fertility and early embryonic development. *Development* 2004 ; 131 : 4883–93.

113. Ball CB, Rodriguez KF, Stumpo DJ, *et al.* The RNA-binding protein, ZFP36L2, influences ovulation and oocyte maturation. *PLoS One* 2014 ; 9 .

114. Voronina E, Seydoux G, Sassone-Corsi P, *et al.* RNA granules in germ cells. *Cold Spring Harb. Perspect. Biol.* 2011 ; 3 : a002774.

115. Swetloff A, Conne B, Huarte J, *et al.* Dcp1-bodies in mouse oocytes. *Mol. Biol. Cell* 2009 ; 20 : 4951–4961.

116. Flemr M, Ma J, Schultz RM, *et al.* P-Body Loss Is Concomitant with Formation of a Messenger RNA Storage Domain in Mouse Oocytes. *Biol. Reprod.* 2010 ; 82 : 1008–1017.

117. Boke E, Mitchison TJ. The balbiani body and the concept of physiological amyloids. *Cell Cycle* 2017 ; 16 : 153–154.

118. Pepling ME. A Novel Maternal mRNA Storage Compartment in Mouse Oocytes. *Biol. Reprod.* 2010 ; 82 : 807–808.

119. Udagawa T, Swanger SA, Takeuchi K, *et al.* Bidirectional control of mRNA translation and synaptic plasticity by the cytoplasmic polyadenylation complex. *Mol. Cell* 2012 ; 47 : 253–66.

120. Richter JD. CPEB: a life in translation. *Trends Biochem. Sci.* 2007 ; 32 : 279–285.

121. Nakanishi T, Kumagai S, Kimura M, *et al.* Disruption of mouse poly(A) polymerase mGLD-2 does not alter polyadenylation status in oocytes and somatic cells. *Biochem. Biophys. Res. Commun.* 2007 ; 364 : 14–19.

122. Kang MK, Han SJ. Post-transcriptional and post-translational regulation during mouse oocyte maturation. *BMB Rep.* 2011 ; 44 : 147–157.

123. Kozak M. Rethinking some mechanisms invoked to explain translational regulation in eukaryotes. *Gene* 2006 ; 382 : 1–11.

124. Villaescusa JC, Allard P, Carminati E, *et al.* Clast4, the murine homologue of human eIF4E-Transporter, is highly expressed in developing oocytes and post-translationally modified at meiotic maturation. *Gene* 2006 ; 367 : 101–109.

125. Minshall N, Reiter MH, Weil D, *et al.* CPEB interacts with an ovary-specific eIF4E and 4E-T in early Xenopus oocytes. *J. Biol. Chem.* 2007 ; 282 : 37389–37401.

126. Esencan E, Seli E. Translational Regulation of Gene Expression During Oogenesis and Preimplantation Embryo Development. *Human Reproductive and Prenatal Genetics*. Elsevier, 2019 : 221–239.

127. Nakahata S, Kotani T, Mita K, *et al.* Involvement of Xenopus Pumilio in the translational regulation that is specific to cyclin B1 mRNA during oocyte maturation. *Mech. Dev.* 2003 ; 120 : 865–80.

128. Padmanabhan K, Richter JD. Regulated Pumilio-2 binding controls RINGO/Spy mRNA translation and CPEB activation. *Genes Dev.* 2006 ; 20 : 199–209.

129. Collier B, Gorgoni B, Loveridge C, *et al.* The DAZL family proteins are PABP-binding proteins that

regulate translation in germ cells. *EMBO J.* 2005 ; 24 : 2656–2666.

130. Yu J, Hecht NB, Schultz RM. Expression of MSY2 in mouse oocytes and preimplantation embryos. *Biol. Reprod.* 2001 ; 65 : 1260–1270.

131. Ayache J, Bénard M, Ernoult-Lange M, *et al.* P-body assembly requires DDX6 repression complexes rather than decay or Ataxin2/2L complexes. *Mol. Biol. Cell* 2015 ; 26 : 2579–2595.

132. Smillie DA, Sommerville J. RNA helicase p54 (DDX6) is a shuttling protein involved in nuclear assembly of stored mRNP particles. *J. Cell Sci.* 2002 ; 115 : 395–407.

133. Minshall N, Kress M, Weil D, *et al.* Role of p54 RNA helicase activity and its c-terminal domain in translational repression, p-body localization and assembly. *Mol. Biol. Cell* 2009 ; 20 : 2464–2472.

134. Weston A, Sommerville J. Xp54 and related (DDX6-like) RNA helicases: Roles in messenger RNP assembly, translation regulation and RNA degradation. *Nucleic Acids Res.* 2006 ; 34 : 3082–3094.

135. Cragle CE, MacNicol MC, Byrum SD, *et al.* Musashi interaction with poly(A)-binding protein is required for activation of target mRNA translation. *J. Biol. Chem.* 2019 ; 294 : 10969–10986.

136. Tanaka KJ, Ogawa K, Takagi M, *et al.* RAP55, a cytoplasmic mRNP component, represses translation in Xenopus oocytes. *J. Biol. Chem.* 2006 ; 281 : 40096–40106.

137. Pepling ME, Wilhelm JE, O'Hara AL, *et al.* Mouse oocytes within germ cell cysts and primordial follicles contain a Balbiani body. *Proc. Natl. Acad. Sci. U. S. A.* 2007 ; 104 : 187–192.

138. Marnef A, Sommerville J, Ladomery MR. RAP55: Insights into an evolutionarily conserved protein family. *Int. J. Biochem. Cell Biol.* 2009 ; 41 : 977–981.

139. Susor A, Jansova D, Cerna R, *et al.* Temporal and spatial regulation of translation in the mammalian oocyte via the mTOR-eIF4F pathway. *Nat. Commun.* 2015 ; 6 .

140. Chen J, Torcia S, Xie F, *et al.* Somatic cells regulate maternal mRNA translation and developmental competence of mouse oocytes. *Nat. Cell Biol.* 2013 ; 15 : 1415–23.

141. Jansova D, Koncicka M, Tetkova A, *et al.* Regulation of 4E-BP1 activity in the mammalian oocyte. *Cell Cycle* 2017 ; 16 : 927–939.

142. Giraldez AJ, Mishima Y, Rihel J, *et al.* Zebrafish MiR-430 Promotes Deadenylation and Clearance of Maternal mRNAs. *Science (80-.).* 2006 ; 312 : 75–79.

143. Suh N, Baehner L, Moltzahn F, *et al.* MicroRNA function is globally suppressed in mouse oocytes and early embryos. *Curr. Biol.* 2010 ; 20 : 271–7.

144. Flemr M, Malik R, Franke V, *et al.* A Retrotransposon-Driven Dicer Isoform Directs Endogenous Small Interfering RNA Production in Mouse Oocytes. *Cell* 2013 ; 155 : 807–816.

145. Jong HK, Richter JD. RINGO/cdk1 and CPEB mediate poly(A) tail stabilization and translational regulation by ePAB. *Genes Dev.* 2007 ; 21 : 2571–2579.

146. Luong XG, Maria Daldello E, Rajkovic G, *et al.* Genome-wide analysis reveals a switch in the translational program upon oocyte meiotic resumption 2 3. *bioRxiv* 2019 ;.

147. Walser CB, Lipshitz HD. Transcript clearance during the maternal-to-zygotic transition. *Curr. Opin. Genet. Dev.* 2011 ; 21 : 431–443.

148. Bashirullah A, Halsell SR, Cooperstock RL, *et al.* Joint action of two RNA degradation pathways controls the timing of maternal transcript elimination at the midblastula transition in Drosophila melanogaster. *EMBO J.* 1999 ; 18 : 2610–2620.

149. Semotok JL, Cooperstock RL, Pinder BD, *et al.* Smaug recruits the CCR4/POP2/NOT deadenylase complex to trigger maternal transcript localization in the early Drosophila embryo. *Curr. Biol.* 2005 ; 15 : 284–94.

150. Medvedev S, Yang J, Hecht NB, *et al.* CDC2A (CDK1)-mediated phosphorylation of MSY2 triggers

maternal mRNA degradation during mouse oocyte maturation. 2008 ;.

151. DeRenzo C, Seydoux G. A clean start: Degradation of maternal proteins at the oocyte-to-embryo transition. *Trends Cell Biol.* 2004 ; 14 : 420–426.

152. Wyers F, Minet M, Dufour ME, *et al.* Deletion of the PAT1 gene affects translation initiation and suppresses a PAB1 gene deletion in yeast. *Mol. Cell. Biol.* 2000 ; 20 : 3538–49.

153. Dickinson ME, Flenniken AM, Ji X, *et al.* High-throughput discovery of novel developmental phenotypes. *Nature* 2016 ; 537 : 508–514.

154. Pradhan SJ, Nesler KR, Rosen SF, *et al.* The conserved p body component HPat/Pat1 negatively regulates synaptic terminal growth at the larval Drosophila neuromuscular junction. *J. Cell Sci.* 2012 ; 125 : 6105–6116.

155. Kamath RS, Fraser AG, Dong Y, *et al.* Systematic functional analysis of the Caenorhabditis elegans genome using RNAi. *Nature* 2003 ; 421 : 231–237.

156. Wang X, Watt PM, Louis EJ, *et al.* Pat1: a topoisomerase II-associated protein required for faithful chromosome transmission in Saccharomyces cerevisiae. *Nucleic Acids Res.* 1996 ; 24 : 4791–4797.

157. Standart N, Marnef A. Pat1 proteins: Regulating mRNAs from birth to death? *Biomol. Concepts* 2012 ; 3 : 295–306.

158. Marnef A, Weil D, Standart N. RNA-related nuclear functions of human Pat1b, the P-body mRNA decay factor. *Mol. Biol. Cell* 2012 ; 23 : 213–224.

159. Marnef A, Standart N. Pat1 proteins: a life in translation, translation repression and mRNA decay. *Biochem. Soc. Trans.* 2010 ; 38 VN-r : 1602–1607.

160. Marnef A, Maldonado M, Bugaut A, *et al.* Distinct functions of maternal and somatic Pat1 protein paralogs. *RNA* 2010 ; 16 : 2094–2107.

161. Castello A, Fischer B, Eichelbaum K, *et al.* Insights into RNA Biology from an Atlas of Mammalian mRNA-Binding Proteins. *Cell* 2012 ; 149 : 1393–1406.

162. Chowdhury A, Kalurupalle S, Tharun S. Pat1 contributes to the RNA binding activity of the Lsm1-7-Pat1 complex. *RNA* 2014 ; 20 : 1465–1475.

163. Braun JE, Tritschler F, Haas G, *et al.* The C-terminal alpha-alpha superhelix of Pat is required for mRNA decapping in metazoa. *EMBO J.* 2010 ; 29 : 2368–80.

164. Fourati Z, Kolesnikova O, Back R, *et al.* The C-terminal domain from S. cerevisiae Pat1 displays two conserved regions involved in decapping factor recruitment. *PLoS One* 2014 ; 9 .

165. Vindry C, Marnef A, Broomhead H, *et al.* Dual RNA Processing Roles of Pat1b via Cytoplasmic Lsm1-7 and Nuclear Lsm2-8 Complexes. *Cell Rep.* 2017 ; 20 : 1187–1200.

166. Bouveret E, Rigaut G, Shevchenko A, *et al.* A Sm-like protein complex that participates in mRNA degradation. *EMBO J.* 2000 ; 19 : 1661–71.

167. Pilkington GR, Parker R. Pat1 Contains Distinct Functional Domains That Promote P-Body Assembly and Activation of Decapping. *Mol. Cell. Biol.* 2008 ; 28 : 1298–1312.

168. Sharif H, Conti E. Architecture of the Lsm1-7-Pat1 complex: a conserved assembly in eukaryotic mRNA turnover. *Cell Rep.* 2013 ; 5 : 283–91.

169. Wu D, Muhlrad D, Bowler MW, *et al.* Lsm2 and Lsm3 bridge the interaction of the Lsm1-7 complex with Pat1 for decapping activation. *Cell Res.* 2014 ; 24 : 233–46.

170. Lobel JH, Tibble RW, Gross JD. Pat1 activates late steps in mRNA decay by multiple mechanisms. *bioRxiv* 2019 ; 594168.

171. Charenton C, Gaudon-Plesse C, Fourati Z, *et al.* A unique surface on Pat1 C-terminal domain directly interacts with Dcp2 decapping enzyme and Xrn1 5'-3' mRNA exonuclease in yeast. *Proc.*

Natl. Acad. Sci. U. S. A. 2017 ; 114 : E9493–E9501.

172. Scheller N, Resa-Infante P, la Luna S de, *et al.* Identification of PatL1, a human homolog to yeast P body component Pat1. *Biochim. Biophys. Acta - Mol. Cell Res.* 2007 ; 1773 : 1786–1792.

173. Ozgur S, Stoecklin G. Role of Rck-Pat1b binding in assembly of processing-bodies. *RNA Biol.* 2013 ; 10 : 528–39.

174. Ozgur S, Chekulaeva M, Stoecklin G. Human Pat1b Connects Deadenylation with mRNA Decapping and Controls the Assembly of Processing Bodies. *Mol. Cell. Biol.* 2010 ; 30 .

175. He F, Celik A, Wu C, *et al.* General decapping activators target different subsets of inefficiently translated mRNAs. *Elife* 2018 ; 7 .

176. Vindry C, Weil D, Standart N. Pat1 RNA-binding proteins: Multitasking shuttling proteins. *Wiley Interdiscip. Rev. RNA* 2019 ;.

177. Coller J, Parker R. General translational repression by activators of mRNA decapping. *Cell* 2005 ; 122 : 875–886.

178. Tharun S, Parker R. Targeting an mRNA for decapping: displacement of translation factors and association of the Lsm1p-7p complex on deadenylated yeast mRNAs. *Mol. Cell* 2001 ; 8 : 1075–83.

179. Nissan T, Rajyaguru P, She M, *et al.* Decapping Activators in Saccharomyces cerevisiae Act by Multiple Mechanisms. *Mol. Cell* 2010 ; 39 : 773–783.

180. Kamenska A, Lu WT, Kubacka D, *et al.* Human 4E-T represses translation of bound mRNAs and enhances microRNA-mediated silencing. *Nucleic Acids Res.* 2014 ; 42 : 3298–3313.

181. Murray MT, Schiller DL, Franke WW. Sequence analysis of cytoplasmic mRNA-binding proteins of Xenopus oocytes identifies a family of RNA-binding proteins. *Proc. Natl. Acad. Sci. U. S. A.* 1992 ; 89 : 11–15.

182. Rother RP, Frank MB, Thomas PS. Purification, primary structure, bacterial expression and subcellular distribution of an oocyte-specific protein in Xenopus. *Eur. J. Biochem.* 1992 ; 206 : 673–683.

183. Nakamura Y, Tanaka KJ, Miyauchi M, *et al.* Translational repression by the oocyte-specific protein P100 in Xenopus. *Dev. Biol.* 2010 ; 344 : 272–283.

184. Nakamura Y, Iwasaki T, Umei Y, *et al.* Molecular cloning and characterization of oocyte-specific Pat1a in Rana rugosa frogs. *J. Exp. Zool. Part A Ecol. Genet. Physiol.* 2015 ; 323 : 516–526.

185. Ramaswamy S, Weinbauer GF. Endocrine control of spermatogenesis: Role of FSH and LH/ testosterone. *Spermatogenesis* 2014 ; 4 : e996025.

186. Handel MA, Eppig JJ. *Sexual Dimorphism in the Regulation of Mammalian Meiosis*. Academic Press, 1997 : 333–358 p.

187. Lebelo SL, Horst G Van Der. Ultrastructural Changes Occurring During Spermiogenesis of the Vervet Monkey, Chlorocebus aethiops. *Asian J. Anim. Sci.* 2016 ; 10 : 247–254.

188. O'Donnell L. Mechanisms of spermiogenesis and spermiation and how they are disturbed. *Spermatogenesis* 2014 ; 4 : e979623.

189. Nakamura N. Ubiquitination Regulates the Morphogenesis and Function of Sperm Organelles. *Cells* 2013 ; 2 : 732–750.

190. Champroux A, Torres-Carreira J, Gharagozloo P, *et al.* Mammalian sperm nuclear organization: resiliencies and vulnerabilities. *Basic Clin. Androl.* 2016 ; 26 : 17.

191. Kierszenbaum AL, Rivkin E, Tres LL. Acroplaxome, an F-Actin–Keratin-containing Plate, Anchors the Acrosome to the Nucleus during Shaping of the Spermatid Head. *Mol. Biol. Cell* 2003 ; 14 : 4628–4640.

192. Zakrzewski P, Lenartowski R, Rędowicz MJ, *et al.* Expression and localization of myosin VI in developing mouse spermatids. *Histochem. Cell Biol.* 2017 ; 148 : 445–462.

193. Nasr-Esfahani MH, Razavi S, Javdan Z, *et al.* Artificial oocyte activation in severe teratozoospermia undergoing intracytoplasmic sperm injection. *Fertil. Steril.* 2008 ; 90 : 2231–2237.

194. Coutton C, Escoffier J, Martinez G, *et al.* Teratozoospermia: spotlight on the main genetic actors in the human. *Hum. Reprod. Update* 2015 ; 21 : 455–85.

195. Zahn A, Furlong LI, Biancotti JC, *et al.* Evaluation of the proacrosin/acrosin system and its mechanism of activation in human sperm extracts. *J. Reprod. Immunol.* 2002 ; 54 : 43–63.

196. Baba T, Azuma S, Kashiwabara S, *et al.* Sperm from mice carrying a targeted mutation of the acrosin gene can penetrate the oocyte zona pellucida and effect fertilization. *J. Biol. Chem.* 1994 ; 269 : 31845–9.

197. Polakoski KL, Zahler WL, Paulson JD. Demonstration of Proacrosin and Quantitation of Acrosin in Ejaculated Human Spermatozoa. *Fertil. Steril.* 1977 ; 28 : 668–670.

198. Vazquez-Levin MH, Furlong LI, Veaute C, *et al.* An overview of the proacrosin/acrosin system in human spermatozoa. *Endocrinol. Mol.* 2007 ;.

199. Kazal LA, Spicer DS, Brahinsky RA. Isolation of a Crystalline Trypsin Inhibitor-Anticoagulant Protein from Pancreas. *J. Am. Chem. Soc.* 1948 ; 70 : 3034–3040.

200. Wapenaar MC, Monsuur AJ, Poell J, *et al.* The SPINK gene family and celiac disease susceptibility. *Immunogenetics* 2007 ; 59 : 349–357.

201. Ma L, Yu H, Ni Z, *et al.* Spink13, an epididymis-specific gene of the Kazal-type serine protease inhibitor (SPINK) family, is essential for the acrosomal integrity and male fertility. *J. Biol. Chem.* 2013 ; 288 : 10154–65.

202. Witt H, Luck W, Hennies HC, *et al.* Mutations in the gene encoding the serine protease inhibitor, Kazal type 1 are associated with chronic pancreatitis. *Nat. Genet.* 2000 ; 25 : 213–6.

203. Furio L, Hovnanian A. Netherton syndrome: Defective kallikrein inhibition in the skin leads to skin inflammation and allergy. *Biological Chemistry*. Walter de Gruyter GmbH, 2014 : 945–958.

204. Zalazar L, Saez Lancellotti TE, Clementi M, *et al.* SPINK3 modulates mouse sperm physiology through the reduction of nitric oxide level independently of its trypsin inhibitory activity. *Reproduction* 2012 ; 143 : 281–95.

205. Lin M-H, Lee RK-K, Hwu Y-M, *et al.* SPINKL, a Kazal-type serine protease inhibitor-like protein purified from mouse seminal vesicle fluid, is able to inhibit sperm capacitation. *Reproduction* 2008 ; 136 : 559–71.

206. Jalkanen J, Kotimäki M, Huhtaniemi I, *et al.* Novel epididymal protease inhibitors with Kazal or WAP family domain. *Biochem. Biophys. Res. Commun.* 2006 ; 349 : 245–254.

207. Jeong J, Lee B, Kim J, *et al.* Expressional and functional analyses of epididymal SPINKs in mice. *Gene Expr. Patterns* 2019 ; 31 : 18–25.

208. Lee B, Park I, Jin S, *et al.* Impaired spermatogenesis and fertility in mice carrying a mutation in the Spink2 gene expressed predominantly in testes. *J. Biol. Chem.* 2011 ; 286 : 29108–29117.

209. Chen T, Lee T-R, Liang W-G, *et al.* Identification of trypsin-inhibitory site and structure determination of human SPINK2 serine proteinase inhibitor. *Proteins Struct. Funct. Bioinforma.* 2009 ; 77 : 209–219.

210. Hoefnagel JJ, Dijkman R, Basso K, *et al.* Distinct types of primary cutaneous large B-cell lymphoma identified by gene expression profiling. *Blood* 2005 ; 105 : 3671–8.

211. Xue C, Zhang J, Zhang G, *et al.* Elevated SPINK2 gene expression is a predictor of poor prognosis in acute myeloid leukemia. *Oncol. Lett.* 2019 ; 18 : 2877–2884.

212. Zegers-Hochschild F, Adamson GD, Mouzon J De, *et al.* International Committee for Monitoring Assisted Reproductive Technology (ICMART) and the World Health Organization (WHO) revised glossary of ART terminology, 2009∗. *Fertil. Steril.* 2009 ; 92 : 1520–1524.

213. Mascarenhas MN, Flaxman SR, Boerma T, *et al.* National, Regional, and Global Trends in Infertility Prevalence Since 1990: A Systematic Analysis of 277 Health Surveys. *PLoS Med.* 2012 ; 9 : e1001356.

214. Brugo-Olmedo S, Chillik C, Kopelman S. *Definition and causes of infertility.* 2001 : 41–53 p.

215. Weiss RV, Clapauch R. Female infertility of endocrine origin. *Arq. Bras. Endocrinol. Metabol.* 2014 ; 58 : 144–52.

216. Topaloğlu AK. Update on the Genetics of Idiopathic Hypogonadotropic Hypogonadism. *J. Clin. Res. Pediatr. Endocrinol.* 2017 ; 9 : 113–122.

217. Beate K, Joseph N, Nicolas de R, *et al.* Genetics of isolated hypogonadotropic hypogonadism: role of GnRH receptor and other genes. *Int. J. Endocrinol.* 2012 ; 2012 : 147893.

218. Salenave S, Trabado S, Maione L, *et al.* Male acquired hypogonadotropic hypogonadism: Diagnosis and treatment. *Ann. Endocrinol. (Paris).* 2012 ; 73 : 141–146.

219. Fraietta R, Zylberstejn DS, Esteves SC. Hypogonadotropic hypogonadism revisited. *Clinics (Sao Paulo).* 2013 ; 68 Suppl 1 : 81–8.

220. Haldeman-Englert CR, Hurst AC, Levine MA. *Disorders of GNAS Inactivation*. 1993 : p.

221. Carp HJA, Selmi C, Shoenfeld Y. The autoimmune bases of infertility and pregnancy loss. *J. Autoimmun.* 2012 ; 38 : J266–J274.

222. Unuane D, Tournaye H, Velkeniers B, *et al.* Endocrine disorders & female infertility. *Best Pract. Res. Clin. Endocrinol. Metab.* 2011 ; 25 : 861–873.

223. Vos M De, Devroey P, Fauser BCJ. Primary ovarian insufficiency. *Lancet* 2010 ; 376 : 911–921.

224. Nelson LM. Primary ovarian insufficiency. *N. Engl. J. Med.* 2009 ; 360 : 606–14.

225. Leo V De, Musacchio MC, Cappelli V, *et al.* Genetic, hormonal and metabolic aspects of PCOS: an update. *Reprod. Biol. Endocrinol.* 2016 ; 14 : 38.

226. Teede H, Deeks A, Moran L. Polycystic ovary syndrome: a complex condition with psychological, reproductive and metabolic manifestations that impacts on health across the lifespan. *BMC Med.* 2010 ; 8 : 41.

227. Qin K, Rosenfield RL. Role of cytochrome P450c17 in polycystic ovary syndrome. *Mol. Cell. Endocrinol.* 1998 ; 145 : 111–121.

228. Rosenfield RL, Ehrmann DA. The Pathogenesis of Polycystic Ovary Syndrome (PCOS): The Hypothesis of PCOS as Functional Ovarian Hyperandrogenism Revisited. *Endocr. Rev.* 2016 ; 37 : 467–520.

229. Viganò P, Parazzini F, Somigliana E, *et al.* Endometriosis: epidemiology and aetiological factors. *Best Pract. Res. Clin. Obstet. Gynaecol.* 2004 ; 18 : 177–200.

230. Bulletti C, Coccia ME, Battistoni S, *et al.* Endometriosis and infertility. *J. Assist. Reprod. Genet.* 2010 ; 27 : 441–7.

231. Hummelshoj L, Prentice A, Groothuis P. Update on Endometriosis. *Women's Heal.* 2006 ; 2 : 53–56.

232. Jayaprakasan K, Becker C, Mittal M, *et al.* The Effect of Surgery for Endometriomas on Fertility. Scientific Impact Paper No. 55. *BJOG An Int. J. Obstet. Gynaecol.* 2018 ; 125 : e19–e28.

233. Vercellini P, Viganò P, Somigliana E, *et al.* Endometriosis: pathogenesis and treatment. *Nat. Rev. Endocrinol.* 2014 ; 10 : 261–275.

234. Rolla E. Endometriosis: advances and controversies in classification, pathogenesis, diagnosis, and treatment. *F1000Research* 2019 ; 8 : 529.

235. Mrazek M, Fulka Jr J. Failure of oocyte maturation: possible mechanisms for oocyte maturation arrest. *Hum. Reprod.* 2003 ; 18 : 2249–52.

236. Bar-Ami S, Zlotkin E, Brandes JM, *et al.* Failure of meiotic competence in human oocytes. *Biol. Reprod.* 1994 ; 50 : 1100–7.

237. Christou-Kent M, Ray PF, Arnoult C. Échec de maturation ovocytaire Un rôle essentiel pour la protéine PATL2 dans l'ovogenèse. *médecine/sciences* 2018 ; 34 : 1042–1045.

238. Hartshorne G, Montgomery S, Klentzeris L. A case of failed oocyte maturation in vivo and in vitro. *Fertil. Steril.* 1999 ; 71 : 567–570.

239. Levran D, Farhi J, Nahum H, *et al.* Maturation arrest of human oocytes as a cause of infertility: case report. *Hum. Reprod.* 2002 ; 17 : 1604–1609.

240. Bergère M, Lombroso R, Gombault M, *et al. An idiopathic infertility with oocytes metaphase I maturation block*. 2001 : 2136–2138 p.

241. Neal MS, Cowan L, Louis JP, *et al.* Cytogenetic evaluation of human oocytes that failed to complete meiotic maturation in vitro. *Fertil. Steril.* 2002 ; 77 : 844–5.

242. Lincoln AJ, Wickramasinghe D, Stein P, *et al.* Cdc25b phosphatase is required for resumption of meiosis during oocyte maturation. *Nat Genet* 2002 ; 30 : 446–449.

243. Masciarelli S, Horner K, Liu C, *et al.* Cyclic nucleotide phosphodiesterase 3A-deficient mice as a model of female infertility. *J. Clin. Invest.* 2004 ; 114 : 196–205.

244. Libby BJ, La Fuente R De, O'Brien MJ, *et al.* The mouse meiotic mutation mei1 disrupts chromosome synapsis with sexually dimorphic consequences for meiotic progression. *Dev. Biol.* 2002 ; 242 : 174–187.

245. Spruck CH, Miguel MP De, Smith APL, *et al.* Requirement of Cks2 for the first metaphase/anaphase transition of mammalian meiosis. *Science (80-.).* 2003 ; 300 : 647–650.

246. Edelmann W, Cohen PE, Kane M, *et al.* Meiotic pachytene arrest in MLH1-deficient mice. *Cell* 1996 ; 85 : 1125–1134.

247. Hahn KL, Johnson J, Beres BJ, *et al.* Lunatic fringe null female mice are infertile due to defects in meiotic maturation. *Development* 2005 ; 132 : 817–828.

248. Revenkova E, Eijpe M, Heyting C, *et al.* Cohesin SMC1β is required for meiotic chromosome dynamics, sister chromatid cohesion and DNA recombination. *Nat. Cell Biol.* 2004 ; 6 : 555–562.

249. Feng R, Sang Q, Kuang Y, *et al.* Mutations in TUBB8 and Human Oocyte Meiotic Arrest. *N. Engl. J. Med.* 2016 ; 374 : 223–232.

250. Cooper TG, Noonan E, Eckardstein S von, *et al.* World Health Organization reference values for human semen characteristics*‡. *Hum. Reprod. Update* 2010 ; 16 : 231–245.

251. Tüttelmann F, Simoni M, Kliesch S, *et al.* Copy Number Variants in Patients with Severe Oligozoospermia and Sertoli-Cell-Only Syndrome. *PLoS One* 2011 ; 6 : e19426.

252. Tüttelmann F, Ruckert C, Röpke A. Disorders of spermatogenesis: Perspectives for novel genetic diagnostics after 20 years of unchanged routine. *Medizinische Genet. Mitteilungsblatt des Berufsverbandes Medizinische Genet. e.V* 2018 ; 30 : 12–20.

253. Patel AS, Leong JY, Ramasamy R. Prediction of male infertility by the World Health Organization laboratory manual for assessment of semen analysis: A systematic review. *Arab J. Urol.* 2018 ;.

254. Lindsay TJ, Vitrikas KR. Evaluation and treatment of infertility. *Am. Fam. Physician* 2015 ; 91 : 308–14.

255. Sakkas D, Ramalingam M, Garrido N, *et al.* Sperm selection in natural conception: What can we learn from Mother Nature to improve assisted reproduction outcomes? *Hum. Reprod. Update* 2015 ; 21 : 711–726.

256. National Collaborating Centre for Women's and Children's Health (UK). Fertility. *Fertility: Assessment and Treatment for People with Fertility Problems*. RCOG Press, 2004 : 1–63.

257. Palermo GD, O'Neill CL, Chow S, *et al.* Intracytoplasmic sperm injection: state of the art in humans. *Reproduction* 2017 ; 154 : F93–F110.

258. Tanaka A, Suzuki K, Nagayoshi M, *et al.* Ninety babies born after round spermatid injection into oocytes: survey of their development from fertilization to 2 years of age. *Fertil. Steril.* 2018 ; 110 : 443–451.

259. Tesarik J, Mendoza C, Testart J. Viable embryos from injection of round spermatids into oocytes. *N. Engl. J. Med.* 1995 ; 333 : 525.

260. Vaughan DA, Leung A, Resetkova N, *et al.* How many oocytes are optimal to achieve multiple live births with one stimulation cycle? The one-and-done approach. *Fertil. Steril.* 2017 ; 107 : 397-404.e3.

261. Hatırnaz Ş, Ata B, Hatırnaz ES, *et al.* Oocyte in vitro maturation: A sytematic review. *Turkish J. Obstet. Gynecol.* 2018 ; 15 : 112–125.

262. Dyer S, Chambers GM, Mouzon J de, *et al.* International Committee for Monitoring Assisted Reproductive Technologies world report: Assisted Reproductive Technology 2008, 2009 and 2010. *Hum. Reprod.* 2016 ; 31 : 1588–609.

263. Gnoth C, Maxrath B, Skonieczny T, *et al.* Final ART success rates: a 10 years survey. *Hum. Reprod.* 2011 ; 26 : 2239–2246.

264. Antonarakis SE. Carrier screening for recessive disorders. *Nat. Rev. Genet.* 2019 ; 20 : 549–561.

265. Patel B, Parets S, Akana M, *et al.* Comprehensive genetic testing for female and male infertility using next-generation sequencing. *J. Assist. Reprod. Genet.* 2018 ; 35 : 1489–1496.

266. Fukuda A, Tanino M, Matoba R, *et al.* Imbalance between the expression dosages of X-chromosome and autosomal genes in mammalian oocytes. *Sci. Rep.* 2015 ; 5 : 14101.

267. Sybert VP, McCauley E. Turner's syndrome. *N. Engl. J. Med.* 2004 ; 351 : 1227–38.

268. Garber K, Smith KT, Reines D, *et al.* Transcription, translation and fragile X syndrome. *Curr. Opin. Genet. Dev.* 2006 ; 16 : 270–5.

269. Pasquale E Di, Beck-Peccoz P, Persani L. Hypergonadotropic ovarian failure associated with an inherited mutation of human bone morphogenetic protein-15 (BMP15) gene. *Am. J. Hum. Genet.* 2004 ; 75 : 106–11.

270. Dixit H, Rao LK, Padmalatha V, *et al.* Mutational screening of the coding region of growth differentiation factor 9 gene in Indian women with ovarian failure. *Menopause* 2005 ; 12 : 749–54.

271. Zhao XX, Suzumori N, Yamaguchi M, *et al.* Mutational analysis of the homeobox region of the human NOBOX gene in Japanese women who exhibit premature ovarian failure. *Fertil. Steril.* 2005 ; 83 : 1843–4.

272. Zhao H, Chen Z-J, Qin Y, *et al.* Transcription factor FIGLA is mutated in patients with premature ovarian failure. *Am. J. Hum. Genet.* 2008 ; 82 : 1342–8.

273. Crisponi L, Deiana M, Loi A, *et al.* The putative forkhead transcription factor FOXL2 is mutated in blepharophimosis/ptosis/epicanthus inversus syndrome. *Nat. Genet.* 2001 ; 27 : 159–66.

274. Hyon C, Mansour-Hendili L, Chantot-Bastaraud S, *et al.* Deletion of CPEB1 Gene: A Rare but Recurrent Cause of Premature Ovarian Insufficiency. *J. Clin. Endocrinol. Metab.* 2016 ; 101 : 2099–

2104.

275. Tung JY, Rosen MP, Nelson LM, *et al.* Novel missense mutations of the Deleted-in-AZoospermia-Like (DAZL) gene in infertile women and men. *Reprod. Biol. Endocrinol.* 2006 ; 4 : 40.

276. Fogli A, Gauthier-Barichard F, Schiffmann R, *et al.* Screening for known mutations in EIF2B genes in a large panel of patients with premature ovarian failure. *BMC Womens. Health* 2004 ; 4 : 8.

277. Aittomäki K, Dieguez Lucena J, Pakarinen P, *et al.* Mutation in the follicle-stimulating hormone receptor gene causes hereditary hypergonadotropic ovarian failure. *Cell* 1995 ; 82 : 959–968.

278. Toledo SP, Brunner HG, Kraaij R, *et al.* An inactivating mutation of the luteinizing hormone receptor causes amenorrhea in a 46,XX female. *J. Clin. Endocrinol. Metab.* 1996 ; 81 : 3850–4.

279. Dixit H, Deendayal M, Singh L. Mutational analysis of the mature peptide region of inhibin genes in Indian women with ovarian failure. *Hum. Reprod.* 2004 ; 19 : 1760–4.

280. Qin Y, Jiao X, Simpson JL, *et al.* Genetics of primary ovarian insufficiency: new developments and opportunities. *Hum. Reprod. Update* 2015 ; 21 : 787–808.

281. Maiburg M, Repping S, Giltay J. The genetic origin of Klinefelter syndrome and its effect on spermatogenesis. *FNS* 2012 ; 98 : 253–260.

282. Plotton I, Brosse A, Cuzin B, *et al.* Klinefelter syndrome and TESE-ICSI. *Ann. Endocrinol. (Paris).* 2014 ; 75 : 118–125.

283. Jungwirth A, Giwercman A, Tournaye H, *et al.* European Association of Urology Guidelines on Male Infertility: The 2012 Update. *Eur. Urol.* 2012 ; 62 : 324–332.

284. Nuti F, Krausz C. Gene polymorphisms/mutations relevant to abnormal spermatogenesis. *Reprod. Biomed. Online* 2008 ; 16 : 504–513.

285. Massart A, Lissens W, Tournaye H, *et al.* Genetic causes of spermatogenic failure. *Asian J. Androl.* 2012 ; 14 : 40–8.

286. Reijo R, Lee T-Y, Salo P, *et al.* Diverse spermatogenic defects in humans caused by Y chromosome deletions encompassing a novel RNA–binding protein gene. *Nat. Genet.* 1995 ; 10 : 383–393.

287. Venkatesh T, Suresh PS, Tsutsumi R. New insights into the genetic basis of infertility. *Appl. Clin. Genet.* 2014 ; 7 : 235–43.

288. Coutton C, Martinez G, Kherraf Z-E, *et al.* Bi-allelic Mutations in ARMC2 Lead to Severe Astheno-Teratozoospermia Due to Sperm Flagellum Malformations in Humans and Mice. *Am. J. Hum. Genet.* 2019 ; 104 : 331–340.

289. Kherraf Z-E, Amiri-Yekta A, Dacheux D, *et al.* A Homozygous Ancestral SVA-Insertion-Mediated Deletion in WDR66 Induces Multiple Morphological Abnormalities of the Sperm Flagellum and Male Infertility. *Am. J. Hum. Genet.* 2018 ; 103 : 400–412.

290. Martinez G, Kherraf Z-E, Zouari R, *et al.* Whole-exome sequencing identifies mutations in FSIP2 as a recurrent cause of multiple morphological abnormalities of the sperm flagella. *Hum. Reprod.* 2018 ; 33 : 1973–1984.

291. Khelifa M Ben, Coutton C, Zouari R, *et al.* Mutations in DNAH1, which encodes an inner arm heavy chain dynein, lead to male infertility from multiple morphological abnormalities of the sperm flagella. *Am. J. Hum. Genet.* 2014 ; 94 : 95–104.

292. Liu C, Lv M, He X, *et al.* Homozygous mutations in SPEF2 induce multiple morphological abnormalities of the sperm flagella and male infertility. *J. Med. Genet.* 2019 ; jmedgenet-2019-106011.

293. Dong FN, Amiri-Yekta A, Martinez G, *et al.* Absence of CFAP69 Causes Male Infertility due to Multiple Morphological Abnormalities of the Flagella in Human and Mouse. *Am. J. Hum. Genet.* 2018 ; 102 : 636–648.

294. Coutton C, Vargas AS, Amiri-Yekta A, *et al.* Mutations in CFAP43 and CFAP44 cause male infertility and flagellum defects in Trypanosoma and human. *Nat. Commun.* 2018 ; 9 : 686.

295. Koscinski I, Elinati E, Fossard C, *et al.* DPY19L2 deletion as a major cause of globozoospermia. *Am. J. Hum. Genet.* 2011 ; 88 : 344–50.

296. Elinati E, Fossard C, Okutman O, *et al.* A new mutation identified in SPATA16 in two globozoospermic patients. *J. Assist. Reprod. Genet.* 2016 ; 33 : 815–820.

297. Dieterich K, Soto Rifo R, Faure AK, *et al.* Homozygous mutation of AURKC yields large-headed polyploid spermatozoa and causes male infertility. *Nat. Genet.* 2007 ; 39 : 661–665.

298. Chen S-R, Batool A, Wang Y-Q, *et al.* The control of male fertility by spermatid-specific factors: searching for contraceptive targets from spermatozoon's head to tail. *Cell Death Dis.* 2016 ; 7 : e2472–e2472.

299. Scacheri CA, Scacheri PC. Mutations in the noncoding genome. *Curr. Opin. Pediatr.* 2015 ; 27 : 659–64.

300. Goh G, Choi M. Application of whole exome sequencing to identify disease-causing variants in inherited human diseases. *Genomics Inform.* 2012 ; 10 : 214–9.

301. Tabor HK, Risch NJ, Myers RM. Candidate-gene approaches for studying complex genetic traits: practical considerations. *Nat. Rev. Genet.* 2002 ; 3 : 391–397.

302. Ding Y, Li H, Chen LL, *et al.* Recent advances in genome editing using CRISPR/Cas9. *Front. Plant Sci.* 2016 ; 7 .

303. Anwar WA, Khyatti M, Hemminki K. Consanguinity and genetic diseases in North Africa and immigrants to Europe. *Eur. J. Public Health* 2014 ; 24 : 57–63.

304. Escoffier J, Lee HC, Yassine S, *et al.* Homozygous mutation of PLCZ1 leads to defective human oocyte activation and infertility that is not rescued by the WW-binding protein PAWP. *Hum. Mol. Genet.* 2016 ; 25 : 878–891.

305. Amiri-Yekta A, Coutton C, Kherraf ZE, *et al.* Whole-exome sequencing of familial cases of multiple morphological abnormalities of the sperm flagella (MMAF) reveals new DNAH1 mutations. *Hum. Reprod.* 2016 ;.

306. Pierre V, Martinez G, Coutton C, *et al.* Absence of Dpy19l2, a new inner nuclear membrane protein, causes globozoospermia in mice by preventing the anchoring of the acrosome to the nucleus. *Development* 2012 ; 139 : 2955–65.

307. Clift D, So C, McEwan WA, *et al.* Acute and rapid degradation of endogenous proteins by Trim-Away. *Nat. Protoc.* 2018 ; 13 : 2149–2175.

308. Chen B, Zhang Z, Sun X, *et al.* Biallelic Mutations in PATL2 Cause Female Infertility Characterized by Oocyte Maturation Arrest. *Am. J. Hum. Genet.* 2017 ; 101 : 609–615.

309. Maddirevula S, Coskun S, Alhassan S, *et al.* Female Infertility Caused by Mutations in the Oocyte-Specific Translational Repressor PATL2. *Am. J. Hum. Genet.* 2017 ; 101 : 603–608.

310. Huang L, Tong X, Wang F, *et al.* Novel mutations in PATL2 cause female infertility with oocyte germinal vesicle arrest. *Hum. Reprod.* 2018 ; 33 : 1183–1190.

311. Wu L, Chen H, Li D, *et al.* Novel mutations in PATL2: expanding the mutational spectrum and corresponding phenotypic variability associated with female infertility. *J. Hum. Genet.* 2019 ; 64 : 379–385.

312. Dietz JA, Maes ME, Huang S, *et al.* Spink2 Modulates Apoptotic Susceptibility and Is a Candidate Gene in the Rgcs1 QTL That Affects Retinal Ganglion Cell Death after Optic Nerve Damage. *PLoS One* 2014 ; 9 : e93564.

313. Nishimiya D, Kawaguchi Y, Kodama S, *et al.* A protein scaffold, engineered SPINK2, for generation

of inhibitors with high affinity and specificity against target proteases. *Sci. Rep.* 2019 ; 9 : 11436.